Lifespan Brain Structural Trajectories and Individual Differences of Growth and Decline

Thesis (cumulative thesis)
Presented to the Faculty of Philosophy
of the
University of Zürich
for the degree of Doctor of Philosophy

by

Gabriel Ziegler

Accepted in the Autumn Term 2012
on the Recommendation of the Doctoral Committee:
Prof. Dr. rer. nat. L. Jäncke (main advisor)
Prof. Dr. Ch. Gaser

Zürich, 2014

Contents

Abstract **1**

Zusammenfassung **3**

1 General Introduction **5**
1.1 Biocultural Co-Constructivism 5
1.2 Voxel-based Brain Morphometry 6
1.2.1 Data Preparation 7
1.2.2 Segmentation 9
1.2.3 Normalization 9
1.2.4 Smoothing 10

2 Early Lifespan Individual Differences of Brain Structure **12**
2.1 Partial Least Squares Correlation of Multivariate Cognitive Abilities and Local Brain Morphology in Children and Adolescents 12
2.1.1 Abstract 13
2.1.2 Introduction 13
2.1.3 Materials and methods 16
2.1.4 Results and discussion 23
2.1.5 Supplemental Material 30

3 Structural Brain Trajectories in Adulthood and Later Life **36**
3.1 Models of Aging Brain Structure and Individual Decline - PART A Cross-sectional Methods 36
3.1.1 Abstract 37
3.1.2 Introduction 37
3.1.3 Age-related effects, trajectories and regression 39
3.2 Brain Structural Trajectories Over the Adult Lifespan 48
3.2.1 Abstract 49
3.2.2 Introduction 49
3.2.3 Materials and methods 51
3.2.4 Results 54

3.2.5 Discussion . . . 61
3.3 Detection of Pathological Aging on a Single Subject Level . . . 65
3.3.1 Abstract . . . 66
3.3.2 Introduction . . . 66
3.3.3 The Generative model of normative structural decline . . . 66
3.3.4 Gaussian confidence maps in untrained test cases . . . 68

4 Assessing Individual Decline Parameters 73
4.1 Models of Aging Brain Structure and Individual Decline - PART B Longitudinal Methods . . . 73
4.1.1 Analysis of inter-individual variability in aging brain structure . . . 74
4.1.2 Limitations . . . 82
4.1.3 Summary and perspectives . . . 85
4.2 Bayesian Decline Modelling . . . 87
4.2.1 Abstract . . . 88
4.2.2 Introduction . . . 88
4.2.3 Two level Bayesian models . . . 89
4.2.4 PLSC analysis of the covariance of decline parameters . . . 94

5 General Discussion 97
5.1 Covariance of Brain Structure and Cognitive Abilities in Early Lifespan . . . 97
5.1.1 Regional Distribution of Covariance . . . 98
5.1.2 Direction of Structure-Cognition Covariance . . . 99
5.1.3 Conclusion . . . 103
5.2 Structural Decline in Adulthood and Later Life . . . 104
5.2.1 Early Cognitive Reserve for Late Lifespan . . . 104
5.2.2 General Course of Age-Related Structural Decline . . . 105
5.2.3 Encoding and Decoding Model Nonlinearities . . . 107
5.2.4 Variance and Covariance of Decline Parameters . . . 109
5.3 Conclusions and Perspectives . . . 112

Acknowledgements 113

References 114

Curriculum Vitae 137

Abstract

This thesis, which is in the field of developmental neuroscience and psychology, was motivated and comprised by two streams of research. The first research stream is the framework for lifespan developmental psychology, that provides a general orientation for the study of behavioural development during ontogenesis. It is commonly accepted that development is a lifelong process with multiple dimensions, effect directions and adaptive changes to environmental demands. A key concept in the work of this thesis is that development is not limited to maturational or growth processes that conclude with a certain state of maturity during adulthood. Moreover, the framework of lifespan development assumes that age-related behavioural changes are centred in a complex and reciprocally interacting system, including the brain and the cultural environment of the individual; this interaction becomes manifest and measurable in the individual trajectories of development. Until recently variables of brain structure and function were often considered to be latent concepts within theoretical frameworks that are not possible to model quantitatively. Thus, many questions and hypotheses regarding the biological basis of lifespan changes of behaviour and cognition have not been sufficiently addressed to date.

The second research stream of work described in this thesis stems from the field of magnetic resonance-based neuroimaging and cognitive neuroscience. A large number of structural parameters and functional correlates of human brain networks have been established and explored in the last two decades. In particular, work on computational morphometry has developed methods for image segmentation, registration and intersubject normalisation, allowing researchers to explore the macroanatomical properties of the brains of individual subjects during different phases of their lifespan. This provides motivation to explore the classical concepts of lifespan development with regard to structural brain parameters, i.e., the multiple dimensions, effect directions and the individual differences between brains. Moreover, it raises questions regarding the relationships between brain, behaviour and environment, which comprise the individual differences between lifespan trajectories.

The thesis aims to bridge the gap between lifespan psychology and neuroimaging in order to support integrated lifespan neuroscience using computational methods. Due to the lack of established models and methods in this new field of research, this work clearly focusses on methodology. The thesis resulted in a series of published papers, manuscripts and conference proceedings that address basic and advanced computational methods in order to (a) analyse structural brain differences between individuals in relation to cognitive or behavioural predic-

tors (exemplified in the early lifespan), (b) estimate the general course of structural trajectories (in the adult lifespan) and (c) assess individual parameters of change using longitudinal data (illustrated for late-life structural decline). The chapters of the thesis firstly introduce the key questions, concepts and measures from a quantitative perspective, then describe useful statistical models and finally present applications of voxel-based morphometry on data from publicly available large-sample magnetic resonance imaging databases.

Using a multivariate partial least squares approach, it was observed that up to one-third of the individual differences in local grey matter volume in the early lifespan can be explained by profiles of cognitive abilities. Using parametric and nonparametric decline models, highly heterogeneous adult lifespan trajectories were found across brain regions that often exhibit accelerated volume loss in later life, for example in the medial temporal lobe. The normative variance in adult lifespan grey matter networks was calculated using Gaussian processes, presenting the potential for future diagnostic methods for the detection of pathologic brain changes in the elderly. Finally, Bayesian multilevel modelling revealed the extent of inter-individual differences of intra-individual grey matter volume shrinkage. The strongest reduction of volume with large individual differences was found to be in the subcortical grey matter regions of elderly individuals.

Zusammenfassung

Diese Arbeit im Bereich der Kognitiven Neurowissenschaft und Psychologie wurde durch zwei Forschungszweige motiviert. Der erste Zweig ist die Psychologie der Lebensspanne mit einer allgemeinen Orientierung auf die Analyse von Verhaltensänderungen während der Ontogenese. Ein Kerngedanke dieser wissenschaftlichen Strömung ist, dass Entwicklung nicht auf Reifungs- und Wachstumsprozesse beschränkt ist, welche zwangsläufig im Erwachsenenalter enden. Im Gegensatz dazu wird angenommen, dass Entwicklung ein lebenslanger Prozess mit multiplen Dimensionen und Richtungen ist, welcher kontinuierliche Anpassungsleistungen an Umweltanforderungen erforderlich macht. Darüberhinaus nimmt man an, dass alterskorrelierte Veränderungen des Verhaltens in ein komplexes und reziprok wechselwirkendes Systems aus biologischen Prozessen und individueller Umwelt eingebettet sind. Dieses System bezieht sowohl neurobiologische Parameter des Gehirns als auch die persönliche soziale Umwelt mit ein. Diese Interaktion von Biologie Verhalten und Umwelt manifestiert sich dann in messbaren individuellen Trajektorien der Entwicklung. Bis vor einigen Jahren waren funktionelle und strukturelle Hirnparameter zumeist theoretische Einheiten in Modellen der Ontogenese, ohne Möglichkeit diese anhand von Daten quantitativ zu testen. Viele Fragen und Hypothesen zur biologischen Basis der Verhaltens- und kognitiven Änderungen in der Lebensspanne konnten somit nicht hinreichend untersucht werden.

Die zweite Basis dieser Arbeit liegt in dem sich rasant entwickelnden Zweig der Magnetresonanz (MR)-basierten Hirnforschung. Eine Vielzahl von strukturellen Parametern und funktionellen Korrelaten von neuronalen Netzwerken wurden damit in den letzten zwei Dekaden etabliert. Neue Verfahren der computerunterstützten Hirnmorphometrie zur Segmentierung, Registrierung und Normalisierung erlauben die makroanatomischen Eigenschaften von Gehirnen in verschiedenen Phasen der Lebensspanne *in-vivo* zu beobachten. Dies ermöglicht erstmals die Konzepte der Lebensspannenpsychologie auch auf hirnparametrische Größen anzuwenden. Das heißt zum Beispiel die multiplen Dimension und Richtungen von struktureller Hirnentwicklung als auch die dabei auftretenden interindividuellen Unterschiede faßbar zu machen. Selbst grundlegende Fragen zu den Wechselbeziehungen von Gehirn- Verhalten- und Umweltparametern im Verlauf der Lebensspanne sind dabei noch ungeklärt.

Diese Arbeit zielt darauf ab die obigen Forschungszweige anzunähern und die Perspektive einer computer- und MR- gestützten Neurowissenschaft der Lebenspanne aufzuzeigen. Da es in diesem jungen Forschungsfeld noch wenig etablierte Modelle und Methoden gibt, ist diese Arbeit methodisch ausgerichtet. In einer Reihe von veröffentlichten und eingereichten Manuskripten

als auch Konferenzbeiträgen werden grundlegende als auch weiterführende Methoden entwickelt um (a) Kovarianzen von interindividuellen strukturellen Hirnunterschieden mit kognitiven und behavioralen Prädiktoren zu analysieren (ausgeführt in einer Stichprobe aus der frühen Lebensspanne) (b) den allgemeinen Verlauf der strukturellen Hirnentwicklung- und Alterung zu schätzen (anhand einer Stichprobe aus der Erwachsenenlebensspanne) und um (c) die individuellen Trajektorien mit Hilfe von Längsschnittsdaten messbar zu machen (illustriert in einer Stichprobe aus der späten Lebensspanne). Die entsprechenden Kapitel führen zunächst die Fragen und Grundgrößen formalisiert ein, danach werden die zentralen statistischen Modelle beschrieben und anhand von Hirndaten der Voxel-basierten Morphometrie (VBM) von frei verfügbaren Stichproben angewandt.

Unter Verwendung eines Partial Least Squares (PLS) Ansatzes konnte gezeigt werden, dass bis zu einem Drittel der lokalen interindividuellen Unterschiede der Volumina grauer Substanz durch individuelle kognitive Fähigkeiten erklärt werden kann. Mit parametrischen und nichtparametrischen Modellen wurden weiterhin regionenspezifische Unterschiede der Trajektorien über die adulte Lebensspanne herausgearbeitet. Dabei zeigte sich eine Beschleunigung des strukturellen Abbaus in hohem Alter in medial temporalen Hirnregionen. Mit Hilfe von Gauss Prozessen wurde ein Ansatz verfolgt um die normative Variabilität von gesunder Hirnalterung der grauen Substanz zu modellieren. Dies stellt eine Vorarbeit für diagnostische Verfahren zur MR-basierten Detektion von pathologischen Alterungsvorgängen dar. Schließlich wurden Bayesche Multilevelmodelle zur Analyse von inter-individuellen Unterschieden der lokalen Abbauraten grauer Substanz verwendet. Die stärksten Atrophieraten im hohen Erwachsenenalter und auch die größten interindividuellen Unterschiede wurden in den subkortikalen Kernbereichen identifiziert.

Chapter 1

General Introduction

Biocultural co-constructivism will be outlined briefly, providing a meta-theoretical framework for the remainder of this thesis in the context of lifespan neuroscience. After introducing variables, processes and levels of analysis in the broader perspective of co-constructivism, an empirical approach to measure macroanatomical properties of individual brains will be described.

1.1 Biocultural Co-Constructivism

An important achievement of contemporary lifespan neuroscience has been to overcome binary simplifications of either pure nativism or empiricism to explain the development of stable differences in individual behaviours. In so doing, developmental scientists have proposed the concept of biocultural co-constructivism, which extends beyond the ideas of interactionism and constructivism (see e.g. Baltes et al., 2006; Li, 2003). This co-constructivism emphasises the complexity and reciprocity of interactions between biological and environmental factors that collaboratively produce or *co-construct* differences at the level of the brain, behaviour and culture. The proposed framework interrelates processes taken from neurobiology, psychology and sociology, all of which undergo changes during human ontogenesis from conception to old age. This conceptual framework involves changes in biochemical, experiential, physical and societal variables and aims to identify joint operations and interfaces between these levels of analysis.

At the micro-level 'biocultural' refers to the neurochemistry of genetic and metabolic processes that maintain the correct homeostasis, neuronal function and neuroanatomical properties of the brain (Lindenberger et al., 2006, 2008). At the meso-level these aspects of the brain are deeply involved in the generation of individual behaviour, whether it is stable (in the sense of personality or traits) or time-varying (in the sense of learning and memory). On the macro-level the framework emphasises cultural and environmental inputs to the individual subject; these include shared cultural norms, social incentives and also unshared environments during socialisation. Irrespective of the particular level of analysis, a central aspect of biocultural co-constructivism is developmental change or *constant flux* during ontogenesis. Thus, it is supposed that there is considerable age-related change in the 'homeostatic states' at the level of the brain, behaviour

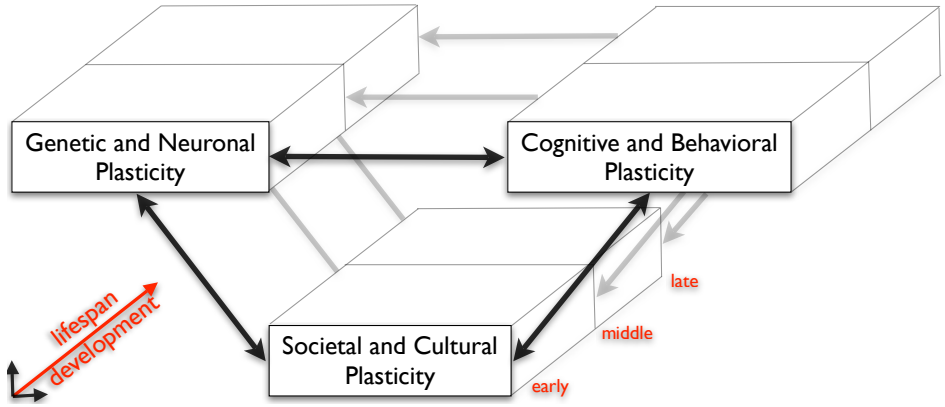

Figure 1.1: Schematic illustration of the Biocultural Co-Constructivism. There are reciprocal interactions between processes on the neurobiological, the behavioural and the cultural level during the human ontogeny. The adaptive and interactive change of variables in each of these levels is referred to as plasticity.

and culture. Li (2003) emphasised that lifespan dynamics at different levels might have different time constants, e.g., the high stability of the genome, the decade-lasting generation cycles of cultural change or the short-term changes in behavioural patterns.

Expanding the perspective to the human lifespan, the interdependent changes of state generate what often is referred to as *developmental plasticity*. Plasticity is a core concept of the co-constructivism framework and lifespan neuroscience (Baltes et al., 1980; Baltes, 1987; Magnusson, 1996), referring to the notion of constrained modifiability and constructability of variables at the level of the brain, behaviour and culture dependent of each other (Figure 1.1). For example, the currently prevailing microstructure at the neuronal level depends on the subjects' individual learning experience (Quartz and Sejnowski, 1997). Notably, although plasticity refers primarily to intra-individual adaptive processes at different levels of analysis, it simultaneously affects the variability which is observed across subjects. Due to the uniqueness of individual states at the level of the brain, behaviour and culture, one might expect considerable inter-individual differences in changes throughout the human lifespan. More specifically, the framework implies that plasticity induces differences in the functional and structural organisation of the brain; this allows exploration of the implications of biocultural co-constructivism at specific neuronal levels using contemporary neuroimaging techniques.

1.2 Voxel-based Brain Morphometry

Magnetic resonance imaging (MRI) provides a powerful technique to quantify, *in-vivo*, structural brain differences and changes throughout the human lifespan (Mietchen and Gaser, 2009; Toga and Thompson, 2003). While brain morphometry often focusses on clinically relevant changes, there is increasing interest in applying this method to study healthy brain development, plasticity and age-related brain decline. From this perspective, the T1-weighted MRI image contrast is of particular interest, since it provides insights into macroanatomical properties of the cerebral

cortex and the subcortical grey matter (GM), the white matter (WM) and the cerebrospinal fluid (CSF) of the brain.

Voxel-based morphometry (VBM) is a semi-automated framework to analyse local brain volume differences among human populations and individuals (Ashburner and Friston, 2000, 2001; Davatzikos et al., 2001; Salmond et al., 2002). For the purpose of analysis of individual differences, a critical assumption of a one-to-one anatomical mapping between different brains is made. That is, it is assumed that there are homologous points in different brains (Ashburner, 2009). Early VBM approaches aimed to quantify *mesoscopic* anatomical differences after removing *macroscopic* differences using spatial normalisation. However, a formal definition of these concepts has still not been agreed upon and is a topic of contemporary debate (e.g. Bookstein, 2001; Ashburner and Friston, 2001; Davatzikos, 2004).

1.2.1 Data Preparation

Generally, VBM requires high quality MRI data for the successful application of each of the following pre-processing steps. Firstly, appropriate MRI data acquisition methods must be chosen in order to optimise the image contrast between GM, WM and CSF (Deichmann et al., 2000). MRI image processing is often conceptualised as a series of pipeline procedures. Firstly, *de-noising* of the T1-weighted images is essential and can be realised using non-spatially localised (*non-local*) algorithms (Buades et al., 2005). Usually, at this early stage of pre-processing, an automated method for segmentation of the head images into brain and non-brain tissue is applied, known as *skull-stripping* (e.g. the BET algorithm, Smith, 2002). Secondly, a *bias-field correction* is used to eliminate the dependence of image intensity on non-uniformities in the magnetic field B0 (e.g. the N3 algorithm, Sled et al., 1998). These magnetic field inhomogeneities are caused by a variety of factors including inhomogeneities in the applied radiofrequency pulses, gradient-driven eddy currents and the anatomy of the individual being imaged. The effects of non-local de-noising and bias-field correction are illustrated in Figure 1.2. The sequence of the preprocessing steps often varies substantially for different VBM pipelines, e.g., FSL (Centre for Functional Magnetic Resonance Imaging of the Brain (FMRIB), Oxford, UK, http://fsl.fmrib.ox.ac.uk), SPM8 (Wellcome Trust Centre for Neuroimaging, London, UK, http://www.fil.ion.ucl.ac.uk/spm), or the VBM8 toolbox (http://dbm.neuro.uni-jena.de/vbm). It is worth mentioning that all processing steps are expected to interact with each other, also resulting in slightly different preprocessing results after application of certain pipeline sequences (Ashburner and Friston, 2009). This has led to a paradigm shift away from simple sequential techniques, towards more integrated generative modelling approaches, e.g., unified segmentation (Ashburner and Friston, 2005). These approaches often take advantage of Bayesian generative modelling of anatomy to obtain posterior densities of pre-processing parameters.

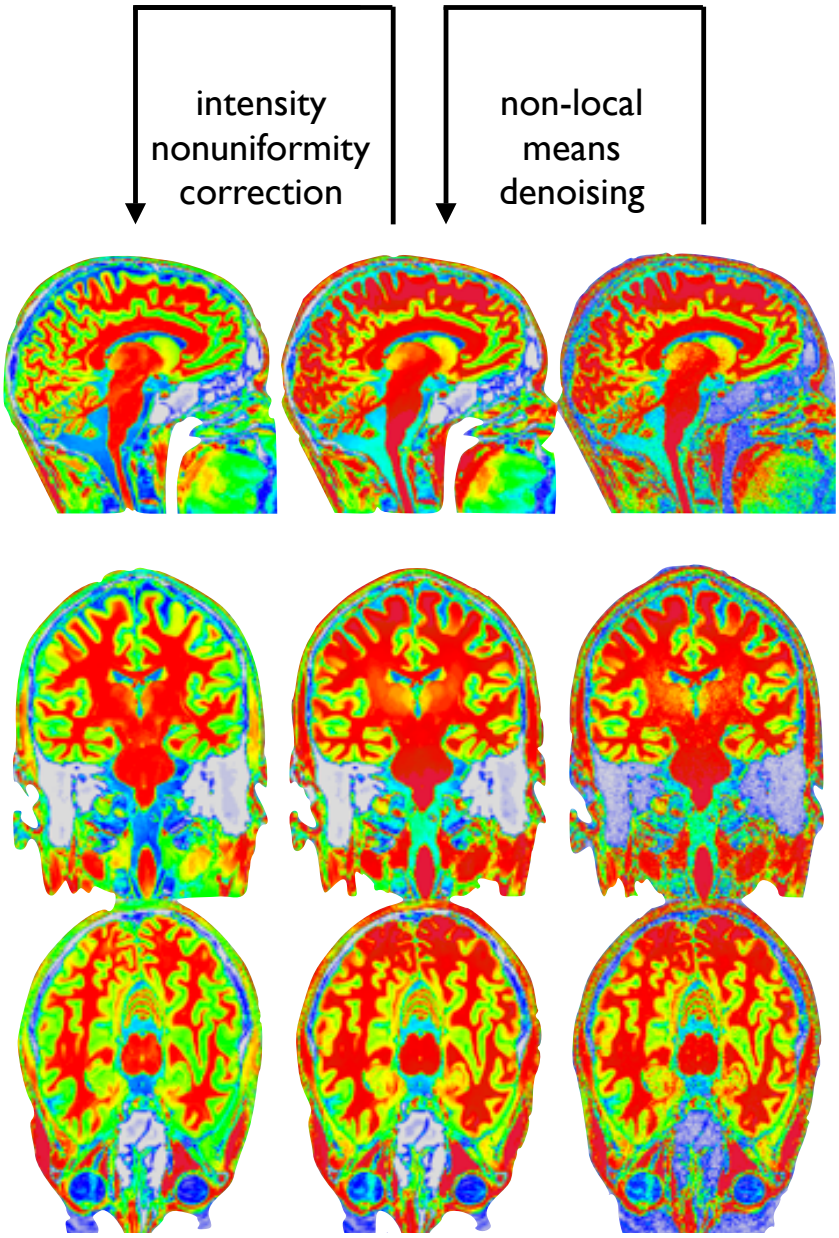

Figure 1.2: Effects of non-local means de-noising and bias-field correction are depicted for three sections of a T1 weighted anatomical MRI image.

Figure 1.3: Segmentation of a T1-weighted image into grey matter (GM), white matter (WM), and cerebrospinal fluid (CSF) tissue classes.

1.2.2 Segmentation

As described by Ashburner and Friston (2005), probabilistic frameworks enable image registration, tissue classification and bias-field correction to be combined within the same generative model. In particular, *unified segmentation* assumes every voxel to be an unknown mixture of four distinct tissue classes: GM, WM, CSF and a 'remainder' class (see Figure 1.3). For this purpose, a model known as 'mixture of Gaussians' (MOG) is used. More complex approaches to segmentation, with additional tissue classes, are sometimes applied (see e.g. Fischl et al., 2002). Due to the finite spatial resolution of MRI, a single image voxel may be composed of a mixture of tissue types; this is known as the partial volume effect (PVE). The estimation of the amount of each tissue type within each voxel can be obtained from a trimmed minimum covariance determinant (TMCD) method, using a mixel PVE model (Tohka et al., 2004). Moreover, the generative model of unified segmentation incorporates a smooth intensity variation (for bias-field correction) and a nonlinear registration (using cosine transform basis functions) with tissue priors. By optimising an objective function, an accurate solution for the whole interactive problem can be found. Further sources of image artefacts, e.g., spatial distortions in the magnetic field $B1$ of the MR scanner, are not modelled in the segmentation and, therefore, have the potential to influence the segmentation results. Multicentre studies are vulnerable to such artefacts since they vary from scanner to scanner and can only be reduced by strict quality control procedures, which should include regular scanning of standardised phantoms.

1.2.3 Normalization

In order to analyse individual differences of lifespan brain morphology with VBM, intersubject registration or *normalisation* to a reference template is required. In contrast to earlier approaches to normalisation (Ashburner and Friston, 1999), the work presented in this thesis focussed on the DARTEL approach ('Diffeomorphic Anatomical Registration Through Exponentiated Lie' algebra) (Ashburner, 2007). A diffeomorphism is a globally one-to-one smooth and continuous mapping with invertible derivatives, i.e. with non-zero Jacobian determinants. If brain mapping is not diffeomorphic, then the topology of the brain is not necessarily preserved. DARTEL creates a 'flow field' using a sophisticated nonlinear registration model, with approximately 6.000.000 parameters; it has proven to be highly accurate with respect to the degree of overlap achieved for manually defined regions and has outperformed alternative intersubject registration algorithms

(Klein et al., 2009). The core of DARTEL is an iterative procedure which relies on GM and WM tissue class images for the individual subjects of a sample, which are first rigid-body aligned with each other (see Figure 1.4A). DARTEL then computes a template, based on the average tissue probability maps across all subjects and warps all individual tissue maps onto this temporary reference template, thus providing a new template based on the averaged warped tissue probability maps and so on. With each subsequent iteration the average becomes increasingly sharp (see Figure 1.4B). The image registration steps are based on Bayesian model optimisation of an objective function that implements a trade-off of achieved similarity to the reference template and the parsimony of the applied nonlinear deformation. Ashburner and Friston (2009) proposed a general framework to generate tissue probability maps that represent average shapes across subjects in samples of interest. In particular, early lifespan paediatric samples are challenging due to the morphological changes that occur in the human brain during normal development (Wilke et al., 2008; Altaye et al., 2008). Notably, the average tissue template has to be further aligned to the MNI reference space (for introduction of MNI see Evans et al., 1993) to enable intra-study comparisons of explored effects (Eickhoff et al., 2007). It is worth mentioning that the applied deformations of DARTEL's nonlinear warping induce volumetric changes of the image voxels; these changes are reflected by the Jacobian determinants of the deformations. In order to preserve individual differences of local brain volumes after normalisation on the reference template, a *modulation* of local volumes by multiplication with these Jacobian determinants can be applied.

1.2.4 Smoothing

The final step of VBM is low-pass filtering of the segmented and normalised images obtained by the previous steps. This is usually achieved by convolving the images with isotropic Gaussian kernels with a full width at half maximum (FWHM) of 4 to 16 mm. Smoothing (or blurring) removes fine-scale structure from the data and, at the same time, substantially increases the sensitivity to detect larger-scale differences. The kernel size determines the minimum size of detectable differences and should, therefore, match the minimum size of differences in question. Moreover, by the central limit theorem, Gaussian kernel smoothing increases the 'Gaussianity' of voxelwise observations, which is often required for subsequent statistical parametric testing.

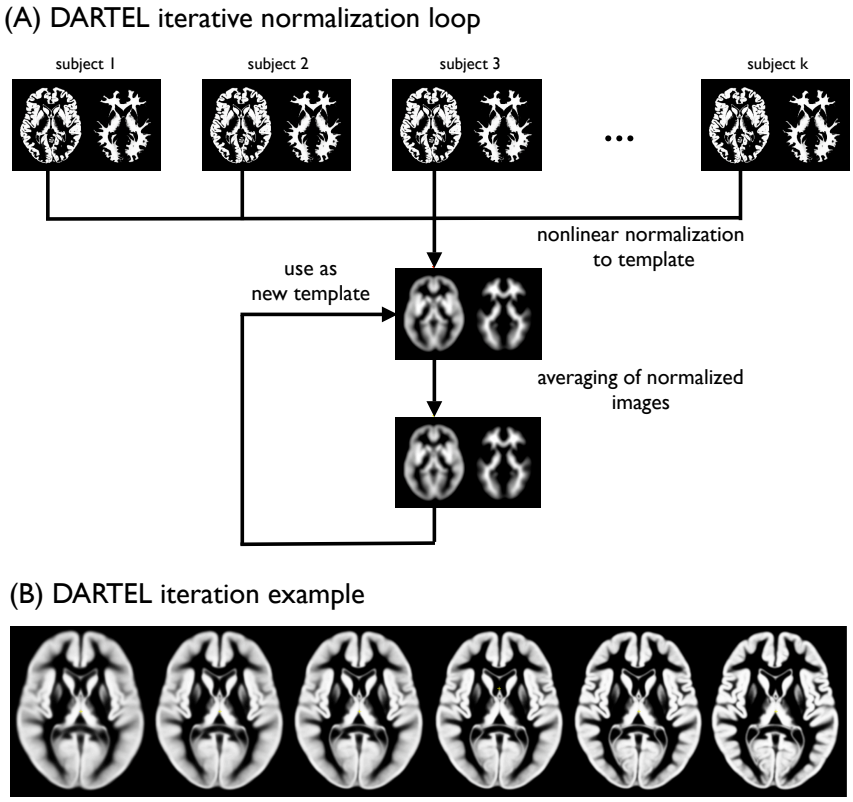

Figure 1.4: DARTEL Normalisation: (A) DARTEL's iterative template generation using nonlinear warped individual grey and white matter tissue classes. The average of the normalised images serves as a new template for the next iteration. (B) An example of DARTEL's template iteration shows increasing morphological details.

Chapter 2

Early Lifespan Individual Differences of Brain Structure

2.1 Partial Least Squares Correlation of Multivariate Cognitive Abilities and Local Brain Morphology in Children and Adolescents

Gabriel Ziegler[1], **Robert Dahnke**[1], **Alissa D. Winkler**[1], **Christian Gaser**[1,2]
1 Structural Brain Mapping Group, Department of Psychiatry, Jena University Hospital, Jena, Germany.
2 Department of Neurology, Jena University Hospital, Jena, Germany.

Type of contribution Research article (published in Ziegler et al., 2013)

Personal contribution G.Z. conceived and developed study, adapted and implemented 3 PLSC algorithms, factor analysis, partialling models, analyzed the MRI data, interpreted the data and wrote the paper. R.D., C.G. preprocessed the data, C.G. corrected the manuscript.

2.1.1 Abstract

Intelligent behavior is not a one-dimensional phenomenon. Individual differences in human cognitive abilities might be therefore described by a 'cognitive manifold' of intercorrelated tests from partially independent domains of general intelligence and executive functions. However, the relationship between these individual differences and brain morphology is not yet fully understood. Here we take a multivariate approach to analyzing covariations across individuals in two feature spaces: the low-dimensional space of cognitive ability subtests and the high-dimensional space of local grey matter volume obtained from voxel-based morphometry. By exploiting a partial least squares correlation framework in a large sample of 286 healthy children and adolescents we identify directions of maximum covariance between both spaces in terms of latent variable modelling. We obtain an orthogonal set of latent variables representing commonalities in the brain-behavior system which emphasize specific neuronal networks involved in cognitive abilities differences. We further explore the early lifespan maturation of the covariance of cognitive abilities and local grey matter volume. The dominant latent variable revealed positive weights across widespread grey matter regions (in the brain domain) and the strongest weights for parents ratings of childrens' executive function (in the cognitive domain). The obtained latent variables for brain and cognitive abilities exhibited moderate correlations of 0.46-0.6. Moreover, the multivariate modelling revealed indications for a heterochronic formation of the association as a process of brain maturation across different age groups.

2.1.2 Introduction

A major goal of human development research is to identify the functional and structural processes that are predictive of individual cognitive skills (Tau and Peterson, 2010). Magnetic Resonance Imaging (MRI) and computational morphometry have become invaluable tools for *in-vivo* exploration of the underlying changes in healthy brain maturation (Mietchen and Gaser, 2009; Toga and Thompson, 2003). On the one hand, research focused on commonalities shared by children with typical pediatric development has revealed that the general course of brain structure development is distinct in different brain regions and tissue types (Lenroot and Giedd, 2006; Giedd and Rapoport, 2010). Studies observed inverted-U shaped and curvilinear trajectories in grey matter volume (GMV) (Gogtay et al., 2004; Lenroot et al., 2007) and cortical thickness (CT) (Shaw et al., 2006; Shaw, 2008; Sowell et al., 2004), and rather continuous increases in white matter volume (WMV) into early adulthood (Ostby et al., 2009; Tamnes et al., 2010c). In addition trajectories of brain maturation exhibited a substantial sexual dimorphism with delayed peaks in male GMV (Lenroot et al., 2007) and CT (Shaw, 2008) development. On the other hand, there is a growing interest in the individual variability of structural maturational patterns and their relation to differences in cognitive abilities and behavior during adulthood (Kanai and Rees, 2011; Deary et al., 2010). The general intelligence factor, i.e. the g-factor, possesses impressive predictive validity for lifespan educational and occupational success as well as social mobility (Deary, 2012). However, the causes and neurodevelopmental mechanisms underlying individual

differences of stable cognitive abilities in adults are still unresolved. Studies exploring general intelligence in relation to brain morphology have been conducted in children and adolescents (Luders et al., 2011; Shaw et al., 2006; Karama et al., 2009, 2011; Lange et al., 2010; Tamnes et al., 2011; Wilke et al., 2003) and younger and middle-aged adults (Narr et al., 2007; Luders et al., 2007, 2008, 2009b; Tamnes et al., 2011; Haier et al., 2004). In addition, recent studies have focused on more specific cognitive abilities and skills in the verbal domain (Porter et al., 2011; Ramsden et al., 2011), working memory (Østby et al., 2011, 2012), and executive functions (Tamnes et al., 2010c). A broad set of cognitive processes contributes to what is commonly referred to as executive functions. Among others this includes planning, working memory, problem solving and inhibition of responses (Chan et al., 2008). There is neuropsychological and non-clinical evidence for a relation of executive functions and general intelligence (Friedman et al., 2008; Ackerman et al., 2005; Salthouse et al., 2003; Shelton et al., 2009; Ardila et al., 2000), but as suggested by Friedman et al. (2006) the current intelligence measures do not sufficiently assess these executive control abilities as a contributing factor to 'intelligent behavior'. Thus, in order to capture the complexity of individual differences in cognitive abilities, tests should assess both domains of intelligence and executive function.

Partial least squares framework

Recent studies have emphasized the potential of multivariate analyses for brain development data in general (Bray et al., 2009) and brain maturation in particular (Lerch et al., 2006; Dosenbach et al., 2010; Hoeft et al., 2011; Misaki et al., 2012). The partial least squares (PLS) approach is a class of latent variable algorithms initially originated by Herman Wold (Wold, 1975, 1982) to model associations between two or more blocks of indicators of a system by means of latent variables (Wegelin, 2000; Geladi, 1988; Hoeskuldsson, 1988). PLS has proven to be particularly useful when the number of observations is much smaller than the number of indicators. In addition to applications in psychology, economics, chemometrics and medicine, PLS was successfully introduced to identify associations between multiple behavioral predictors and whole brain activity correlates derived from PET and fMRI (McIntosh et al., 1996, 2004; McIntosh and Lobaugh, 2004; Krishnan et al., 2011; Koutsouleris et al., 2010). There are several advantages of PLS for the purpose of modelling the relationship among local brain structure and multivariate cognitive abilities:

Firstly, the PLS framework naturally extends the classical latent variable approach to cognitive abilities tests (Spearman, 1904; Bartholomew, 2004; Carroll, 1993; Jensen, 1998) in a way that directly includes structural properties of brains in the very process of modelling individual differences. In particular, neuroimaging studies that investigate multivariate aspects of individual differences of cognitive abilities (e.g. Barbey et al., 2012; Colom et al., 2007, 2006, 2010; Ebisch et al., 2012; Gläscher et al., 2010; Karama et al., 2011) often apply an analysis procedure with the following two *separate* steps. (A) At first a measurement model of multiple cognitive tests is used to obtain valid estimates of specific cognitive domains or to extract higher order

intelligence factors. (B) Afterwards the obtained domain- or factor scores are related to the structural brain data using the general linear model in a mass-univariate manner. Using (A) and (B) basically corresponds to decomposing the unknown multivariate mapping F: $C \rightarrow B$ of the 'cognitive abilities space' to the 'brain structure space' into separate univariate mappings mappings for each voxel/vertex and cognitive domain/factor. By applying PLS we propose a fundamentally different approach that jointly models individual differences in both multivariate spaces in a single generative model of latent variables. Instead of exploring neuronal correlates of *a-priori* fixed cognitive constructs this generalizes the covariance to a multivariate problem with free weightings in both spaces. Moreover, the major difference is that the optimal feature weighting in both spaces is driven by the maximum covariances (see e.g. Shawe-Taylor and Cristianini, 2004) instead of maximizing (error-free) variance in factor analysis or latent variable modelling of cognitive tests.

Secondly, the PLS approach is an exploratory method that affords the analysis of structural patterns through the entire brain. PLS overcomes the limitation of the numbers of observed variables in Structural Equation Modelling (SEM) and thus allows the analysis of MR-based images with tens or hundreds of thousands of voxels or vertices without *a-priori* selection of certain ROIs.

Thirdly, PLS models overcome a limitation of mass-univariate approaches by increasing the sensitivity to detect subtle or spatially distributed effects in brain signals (McIntosh and Lobaugh, 2004). Unlike the general linear model (Monti, 2011, for review), PLS explicitly allows modelling effects of numerous strongly collinear or near-linear dependent indicators (Wegelin, 2000), which is especially true for cognitive abilities tests (Jensen, 1998).

Fourthly, in contrast to the alternative and very similar canonical correlation analysis (CCA) (Borga M., 1992, for a unified framework of PLS and CCA), the coefficients derived from PLS modelling were found to be easier to interpret and more stable (Wegelin, 2000). This is mainly because the coefficients in PLS models express the bivariate contribution of each indicator to the latent variables which is in contrast to the mutually dependent coefficients derived from CCA that 'behave' more like multiple linear regression coefficients.

The aim of the current study was to identify latent variables underlying multiple cognitive abilities and local brain structure in a large sample of 286 healthy children and adolescents from the NIH study of normal brain development. By using Partial Least Squares Correlation (PLSC) and Voxel-Based Morphometry (VBM) we explored grey matter networks that covaried with a broad set of 19 abilities tests in the domains of intelligence, processing speed, and executive functioning. Finally, we explored age-related maturational differences of the covariance in age groups of younger and older children, and adolescents.

2.1.3 Materials and methods

Modelling cognitive abilities and local brain structure in the PLS framework

Though the PLS framework is much more general we here only focus on the two-block case and use it to jointly analyze individual differences in a set of behavioral predictors and spatial brain variables. We assume the cognitive data and the brain data is represented in two matrices (or blocks) $\mathbf{X}$ and $\mathbf{Y}$, respectively $l \times m$ and $l \times n$. The columns of $\mathbf{X}$ correspond to cognitive test data, e.g. total IQ scores or verbal span. The columns of $\mathbf{Y}$ contain voxelwise structural brain features after normalization and registration, in particular local grey matter volume maps obtained from VBM. In order to avoid variance differences that may bias the PLS modelling steps, we assume the columns of $\mathbf{X}$ and $\mathbf{Y}$ to be standardized features, e.g. z-scores. The main idea here is that individual differences observed in $\mathbf{X}$ and $\mathbf{Y}$ are generated by two latent variables, say $\boldsymbol{\zeta}$ and $\boldsymbol{\xi}$, respectively. In other words, the columns in $\mathbf{X}$ and $\mathbf{Y}$ are assumed to be indicators for the *a-priori* unknown variables $\boldsymbol{\zeta}$ and $\boldsymbol{\xi}$ which we estimate from the data. Importantly, $\boldsymbol{\zeta}$ and $\boldsymbol{\xi}$ are assumed to covary, in order to represent the cross-covariance of the indicators $\mathbf{X}^T\mathbf{Y}$ at the level (of error free) latent variables, which makes PLSC a special case of Structural Equation Modelling (SEM). A graphical path model representation of the above outlined idea is depicted in Figure 2.1A. Our goal to identify directions of maximum covariance in the multivariate observations $\mathbf{X}$ and $\mathbf{Y}$ can be further formalized:

$$\sigma_1 = Cov(\boldsymbol{\zeta_1}, \boldsymbol{\xi_1}) = \max_{||u||=||v||=1} Cov(\mathbf{Xu}, \mathbf{Yv}) \tag{2.1}$$

The desired solution for weightings (or often called saliences) $\mathbf{u}$ and $\mathbf{v}$ are the first left and right singular vectors of the cross-block covariance matrix $\mathbf{X}^T\mathbf{Y}$. We here applied the SVD approach to implement the criteria (2.3) that directly calculates the left and right singular vectors of the covariance matrix $\mathbf{X}^T\mathbf{Y}$. Thus, the main results of this paper further exploit the PLS-SVD algorithm. However, the readers particularly interested in other iterative and kernel-based approaches to PLSC are referred to supplemental material presented in section 2.1.5. This also includes the comparison of the underlying orthogonality constraints for PLS-SVD and PLS-NIPALS and the similarity of analysis results of particular PLSC implementations in our NIH dataset.

Application to the NIH study of healthy brain development

Sample We used a subsample of the NIH MRI study of normal brain development available in the NIH MRI Pediatric MRI Data Repository, (https://nihpd.crbs.ucsd.edu). The NIH MRI Pediatric project focuses on brain development in healthy typically developing infants, children and adolescents from a demographically balanced population based sampling (Evans and Group, 2006, for overview). The neuroimaging data was acquired in multiple pediatric centers and included a variety of MR-based sequences and protocols. Moreover, apart from exploring the general course of normal brain development an important part of the project is to reveal

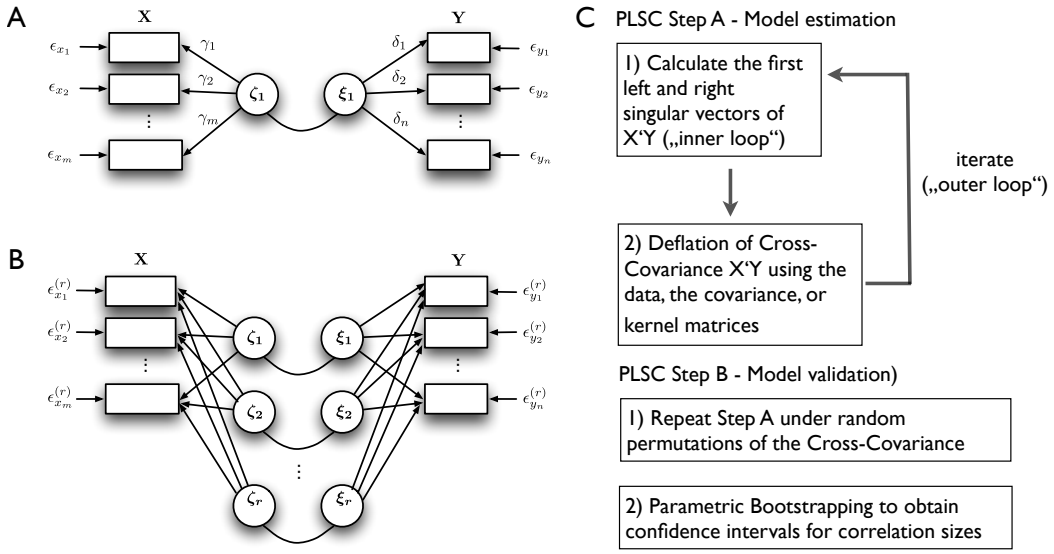

Figure 2.1: **An overview of the applied PLSC methodology.** (A) A single latent variable model is used to explain the covariance of the cognitive variables $\mathbf{X}$ and brain variables $\mathbf{Y}$. The latent variables $\boldsymbol{\zeta}_1$ and $\boldsymbol{\xi}_1$ reflect the corresponding covariance. The loadings $\boldsymbol{\gamma}$ and $\boldsymbol{\delta}$ are obtained from regression of the latent variables on the data. The resulting residual variances ϵ_{x_i} and ϵ_{y_i} might be correlated and can be analyzed using deflation. (B) The multiple latent variable model after r deflation steps is shown. This results in a sequence of latent variables $\boldsymbol{\zeta}_i$ and $\boldsymbol{\xi}_i, i = 1, \ldots, r$ and new regression residuals $\epsilon_{x_i}^{(r)}$ and $\epsilon_{y_i}^{(r)}$. (C top). (PLSC Step A) Algorithmic structure of the PLSC analysis to analyze covariance structure of data X and Y. The outer loop is used to deflate either the data, the covariance (for PLS-SVD) or the kernel matrices, and the inner loop calculates the corresponding first left and right singular vectors of the covariance $\mathbf{X}^T\mathbf{Y}$. (C bottom) (PLSC Step B) Model selection and validation is performed using permutations testing and bootstrapping respectively. Permutation testing reveals the covariances σ_i under random permutations of rows of $\mathbf{X}$ leaving $\mathbf{Y}$ unchanged. Parametric bootstrapping is used to assess the stability of the latent variable model parameters by providing confidence intervals. Figure from Ziegler et al. (2013).

Table 2.1: **Demographical description of the sample**

Age group (years)	Subjects	Subjects from site (1/2/3/4/5/6)	Females (%)	FSIQ mean (std)
6-9.5	94	17/16/12/14/12/23	45 (54)	113 (14.3)
9.5-13.5	101	9/24/13/24/10/21	55 (54)	112 (11.1)
13.5-18.5	91	12/14/24/17/10/14	51 (49)	109 (11.2)
Total	286	38/54/49/55/32/58	151 (53)	111 (12.3)

Age groups with number of subjects, gender, as well as mean and standard deviation of general intelligence of the analyzed subsample from the NIH MRI repository. The scanning sites from 1-6 are the Children's Hospital Boston, Cincinnati Children's Hospital Medical Center, University of Texas Health Science Center at Houston, University of California in LA, Children's Hospital of Philadelphia, Washington University in St. Louis, respecitvely. FSIQ denotes the full scale IQ obtained from Wechsler Abbreviated Scale of Intelligence (WASI).

the correlation to cognitive and behavioral measures. The screening procedures excluded subjects with a family history of inherited neurological disorders or a lifetime history of Axis I psychiatric disorders, abnormalities during perinatal development, birth complications, physical growth problems, neurological or specific psychiatric disorders. In order to study subjects with normal pediatric development, the behavioral screening excluded subjects with child behavior checklist (CBCL) T-scores < 70, full scale WASI IQ < 70, or Woodcock - Johnson III Achievement Battery subtest scores < 70. A detailed description of the sample acquisition and exclusion criteria can be found in Evans et al. (Evans and Group, 2006) and here (https://nihpd.crbs.ucsd.edu/nihpd/info/Documents/). We started with a sample from release 4 of the NIH MRI study objective 1 (Evans and Group, 2006; Almli et al., 2007) of the children and adolescents. The full sample included 433 subjects with ages 4.5-18 years. However, due to our focus on cognitive abilities, the sample was reduced to 394 subjects between 6-18 years of age with comparable protocols of cognitive testing (see below for details). After checking the completeness of the explicitly rich cognitive test battery, the sample strongly reduced to 307 fully available datasets. We observed variations in raw data slice resolution of the images. These differences strongly influenced the quality of the image preprocessing results. Thus we discarded further 21 scans due to substantial artifacts in segmentation, registration, or nonlinear between-subjects normalization. Finally, the accepted sample consisted of 286 children (151 females, 135 males) with ages 6-18.5 years ($M = 11.6$, $SD = 3.5$,). The demographic details and descriptive statistics of the analyzed sample are presented in Table 2.1.

Cognitive abilities space and factor analysis In addition to the MR imaging data, the NIH study of normal brain development included approximately three hours of neuropsychological assessments of individual's cognition and behavior using multiple psychometric instruments (Waber et al., 2007). In order to cover a broad spectrum of children's and adolescents' intellectual abilities, we here included a rich set of psychometric measures from the domains of intelligence, processing speed and executive function. All analyzed test scores stem from reliable and validated instruments that were applied using age appropriate test forms. Firstly, we included vocabulary,

similarities, matrix reasoning, and block design subtests from the Wechsler Abbreviated Scale of Intelligence (Wechsler, 1999). These measures are typically applied to obtain a brief general intelligence assessment. Additionally, we used measures of processing speed and verbal working memory using the coding task and the digit span task of the Wechsler Intelligence Scale for Children (WISC-III) and the corresponding score form the Wechsler Adult Intelligence Scale (WAIS-III) for the older adolescents (Wechsler, 1991, 1997). Secondly, Cambridge Neuropsychological Test Battery (CANTAB) is a collection of computerized, non-verbal touchscreen tests for cognitive assessment. Originally developed for diagnosis of cognitive deficits in dementia (Fray and Robbins, 1996), it also became a valid tool for testing children (Luciana, 2003). We included the executive function errors and stages of the Intra-Extra Dimensional Set Shift task (IED) (a computerized version of the Wisconsin Card Sorting test), the Spatial Span (SSP), and Spatial Working Memory (SWM) strategy and responses scores. Thirdly, the Behavior Rating Inventory of Executive Function (BRIEF) was developed to capture the real-world behavioral manifestations of executive dysfunction (Gioia et al., 2002a,b; Gioia and Isquith, 2004; Gioia et al., 2010). In contrast to the above performance tests BRIEF uses parents' ratings of their children's everyday executive task performance. We included the metacognition subtests monitor, organization of materials, plan/organize, working memory, initiate as well as the behavioral regulation subtests emotional control, shift, and inhibition. The resulting set of 19 cognitive ability measures (6 WASI/WISC, 5 CANTAB, 8 BRIEF) were raw test scores, i.e. usually obtained from sums over items. As the explicit aim of this paper is to estimate the loadings within the cognitive abilities space in a single model with the brain data, no separate measurement model was applied. Notably, all BRIEF subtest scores, the CANTAB IED number of errors and both CANTAB SWM scores are originally inverted, i.e. higher values originally indicated deficits. In order to simplify interpretation of results in terms of a cognitive manifold of abilities, the sign of all inverted variables was switched. The resulting 19 cognitive measures are positive correlates of intellectual ability and executive function. Before subsequent statistical analysis, an outlier detection procedure was applied, replacing extreme values (i.e. more than 3σ) by regression imputation using the highest correlating covariate of the remaining data. The descriptive statistics and the correlation matrix of the recoded cognitive abilities parameters is provided in Table 2.2.

Local brain structure space A detailed overview of the acquisition protocols of the NIH MRI Pediatric study can be found here (http://pediatricmri.nih.gov/nihpd/info/protocols.html). The available sample included data from both primary protocols and fallback protocols with either 1 mm or 3 mm slice thickness, respectively. The preprocessing and analysis steps were done in SPM8 (Wellcome Trust Centre for Neuroimaging, London, UK, http://www.fil.ion.ucl.ac.uk/spm) using the VBM8 toolbox (http://dbm.neuro.uni-jena.e/vbm). During preprocessing the images were interpolated to an isotropic resolution of 1.5 mm. The images were (1) corrected for bias-field inhomogeneities, (2) registered using a linear (i.e. 12-parameter affine) and a nonlinear diffeomorphic transformation (Ashburner, 2007), and (3) stripped of non-brain

Table 2.2: **Cognitive test descriptive statistics and correlation matrix**

Mean	56.27	55.14	10.67	56.32	56.04	10.78	6.05	-174.59	-32.72	8.2	-22.41	-45.95	-49.24	-16.65	-47.04	47.97	-45.29	-45.74	-46.61
std	7.84	9.39	2.90	8.65	9.39	2.64	1.68	26.96	6.55	0.94	13.86	8.84	8.69	3.96	8.26	8.31	8.02	7.78	7.11
min	30	31	4	28	28	3	2	-233	-45	5	-73	-78	-71	-28	-71	-74	-73	-70	-72
max	80	80	19	79	80	19	9	-82	-10	9	0	-28	-33	-11	-36	-35	-36	-36	-36
	reasoning	block	processing speed	vocabu--lary	simila-rities	verbal WM span	SSP span	SWM responses	SWM strategy	IED shift stages	IED shift error	monitor	organize material	plan/ organize	working-memory	initiate	emotional control	shift	inhibit
reasoning	1.00	0.41	0.13	0.42	0.34	0.13	0.22	0.22	0.18	0.11	0.24	0.05	-0.07	0.03	0.07	-0.05	-0.02	-0.01	-0.01
block	0.41	1.00	0.25	0.31	0.31	0.12	0.31	0.18	0.16	0.19	0.23	0.11	-0.08	0.02	0.08	0.03	0.04	0.07	0.08
processing speed	0.13	0.25	1.00	0.21	0.23	0.15	0.15	0.09	0.10	0.15	0.25	0.14	0.04	0.19	0.17	0.07	0.09	0.12	0.14
vocabulary	0.42	0.31	0.21	1.00	0.54	0.29	0.19	0.15	0.14	0.23	0.32	0.06	-0.05	0.09	0.14	0.14	-0.01	0.01	0.08
similarities	0.34	0.31	0.23	0.54	1.00	0.24	0.14	0.13	0.13	0.16	0.31	0.08	-0.09	0.04	0.08	0.00	-0.08	-0.08	0.12
verbal WM span	0.13	0.12	0.15	0.29	0.24	1.00	0.18	0.13	0.06	-0.04	0.04	0.09	-0.01	0.06	0.13	0.08	0.00	0.01	0.10
SSP span	0.22	0.31	0.15	0.19	0.14	0.18	1.00	0.08	0.06	0.05	0.14	0.05	-0.02	0.04	0.08	-0.04	0.00	0.00	0.03
SWM responses	0.22	0.18	0.09	0.15	0.13	0.13	0.08	1.00	0.81	-0.14	0.21	0.03	0.02	0.08	0.14	0.02	0.07	0.06	0.10
SWM strategy	0.18	0.16	0.10	0.14	0.13	0.06	0.06	0.81	1.00	-0.10	0.22	0.01	-0.04	0.04	0.07	0.02	0.02	-0.02	0.02
IED shift stages	0.11	0.19	0.15	0.23	0.16	-0.04	0.05	-0.14	-0.10	1.00	0.54	0.07	-0.04	0.06	-0.04	0.05	-0.04	0.08	0.05
IED shift error	0.24	0.23	0.25	0.32	0.31	0.04	0.14	0.21	0.22	0.54	1.00	0.18	-0.03	0.14	0.10	0.12	0.01	0.13	0.20
monitor	0.05	0.11	0.14	0.06	0.08	0.09	0.05	0.03	0.01	0.07	0.18	1.00	0.48	0.72	0.63	0.61	0.59	0.57	0.65
organize material	-0.07	-0.08	0.04	-0.05	-0.09	-0.01	-0.02	0.02	-0.04	-0.04	-0.03	0.48	1.00	0.57	0.51	0.50	0.35	0.29	0.36
plan/organize	0.03	0.02	0.19	0.09	0.04	0.06	0.04	0.08	0.04	0.06	0.14	0.72	0.57	1.00	0.74	0.68	0.51	0.53	0.54
working-memory	0.07	0.08	0.17	0.14	0.08	0.13	0.08	0.14	0.07	-0.04	0.10	0.63	0.51	0.74	1.00	0.59	0.45	0.49	0.58
initiate	-0.05	0.03	0.07	0.14	0.00	0.08	-0.04	0.02	0.02	0.05	0.12	0.61	0.50	0.68	0.59	1.00	0.55	0.51	0.50
emotional control	-0.02	0.04	0.09	-0.01	-0.08	0.00	0.00	0.07	0.02	-0.04	0.01	0.59	0.35	0.51	0.45	0.55	1.00	0.64	0.59
shift	-0.01	0.07	0.12	0.01	-0.08	0.01	0.00	0.06	-0.02	0.08	0.13	0.57	0.29	0.53	0.49	0.51	0.64	1.00	0.55
inhibit	-0.01	0.08	0.14	0.08	0.12	0.10	0.03	0.10	0.02	0.05	0.20	0.65	0.36	0.54	0.58	0.50	0.59	0.55	1.00

Mean, standard deviation, and range of the analyzed subtest raw scores (top). Pearson correlation matrix of 19 cognitive ability test scores included in the PLSC analysis (bottom). Reasoning, block, processing speed, vocabulary, similarities and verbal WM span are subtests from the WASI/WISC battery. SSP span, SWM responses, SWM strategy, IED shift stages, and IED shift error refer to CANTAB's computerized testing subtests of executive functions. Monitor, organize material, plan/organize, working-memory, initiate, emotional control, shift, and inhibit are BRIEF's subtest for executive dysfunction.

tissue in the T1-weighted images. Thereafter, some results from the SPM8 unified segmentation package (Ashburner and Friston, 2005) were used to initialize a VBM8 algorithm that classifies brain tissue in grey matter (GM), white matter (WM), and cerebrospinal fluid (CSF). In order to avoid introducing a systematic bias into the segmentation routine by using the standard adult reference data (Wilke et al., 2003) the Template-O-Matic toolbox (Wilke et al., 2008) was used to generate a sample-specific template. The VBM8 segmentation contains partial volume estimation (PVE) to account for mixed voxels with two tissue types (Tohka et al., 2004). The algorithm uses an adaptive maximum a posteriori (AMAP) approach (Rajapakse et al., 1997) and a subsequent application of a hidden Markov random field model (Cuadra et al., 2005). Within the AMAP estimation the local variations of the parameters (means and variance) are modeled as slowly varying spatial functions. This accounts for intensity inhomogeneities and other local variations. We also included a further quality check using covariance-based inhomogeneity measures of the sample as implemented in the VBM8 toolbox. Thereafter, the resulting grey matter volume images were multiplied voxelwise by the determinants of Jacobian matrices from SPM's nonlinear transformations before subsequent statistical analysis on local volumes. This modulation is done to adjust for local volume changes introduced by the nonlinear normalization. Finally, a smoothing step was performed using a Gaussian kernel of 8 mm full width at half maximum (FWHM). In order to analyze brain regions that have a high probability to contain grey matter tissue, the images were masked by a binary image indicating voxelwise sample mean of grey matter volume (GMV) exceeding absolute threshold of 0.2. All analyses were performed on GMV images obtained using the above steps. After thresholding 315004 grey matter voxels entered the PLSC modelling. Thus, the voxels served as potentially correlated indicators of structural grey matter network properties in a 315004 dimensional local brain structure space. The spatial adjacency of voxels was not explicitly used for feature construction but is implicitly reflected by their covariance structure. The brain data will be further denoted with $\mathbf{Y}$.

Effects of confounding variables Using an observational design to investigate the covariance of brain structure and cognitive abilities, we had to limit the potential influences of covariates. In contrast to a cross-sectional analysis of age-related effects, the analysis of the ability-brain covariation sets a different focus and potentially allows indirect statistical effects between the triplet of age, brain structure, and the cognitive abilities (Salthouse, 2011b). A crucial point for neuroanatomic correlates of intelligence is that they might be influenced by confounds, e.g. brain size (Taki et al., 2012; Rushton and Ankney, 2009; McDaniel, 2005), global brain parameters (Peelle et al., 2012), gender (Schmithorst, 2009; Luders et al., 2006, 2009a; Narr et al., 2007), and particularly chronological age. This is especially true for studies on early lifespan cognitive abilities, because the size of the expected effects due to individual maturational differences is substantial (Gogtay et al., 2004; Lenroot et al., 2007). In order to focus on individual differences in the local grey matter networks that are independent of age and global brain differences, we applied partialling models to increase the specificity of observed covariations. Global variance removal also decorrelates the local structural features, avoiding the global parameter differences

to dominate the regional brain-behavior covariance patterns (see also supplemental material Figure 2.2). This increases the sensitivity to detect local network differences related to cognitive

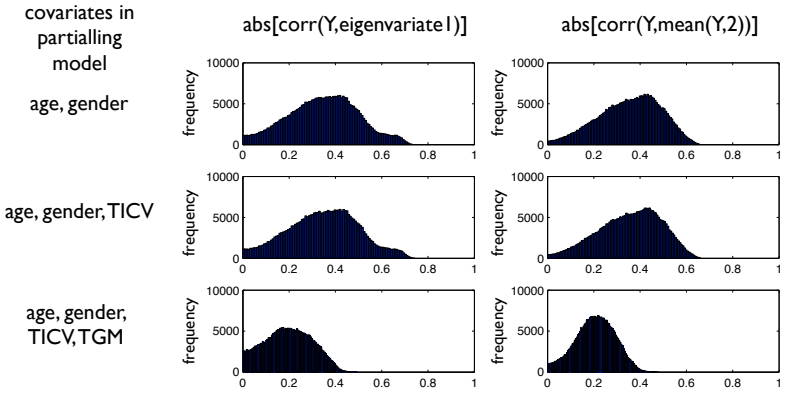

Figure 2.2: **Illustration of decorrelation of spatial brain features by including TGM in partialling models.** Histogram of absolute correlations of voxelwise grey matter volume with the first eigenvariate (left) and mean (right) across all voxels of 286 children and adolescents from our NIH sample. Including TICV does not reduce intercorrelations of features (top to middle row). In contrast, removing confounding effects of total grey matter volume (TGM) using partialling substantially reduces intercorrelations (middle to bottom row). Figure from supplemental material S1 in Ziegler et al. (2013).

abilities. In addition to obtain the local grey matter segments, VBM8 was used to estimate the absolute tissue volumes in subject's native space. We then corrected the data for cubic age, linear gender, total intracranial volume (using TICV=TGM+TWM+TCSF), and total grey matter volume (TGM) effects using multiple linear regression. Cognitive data $\mathbf{X}$ and also the brain data $\mathbf{Y}$ will denote the corrected data after application of a partialling model including age, age^2, age^3, gender, and TICV, and TGM.

PLSC procedure, model selection and validity After preprocessing and correcting the NIH sample data for confounds, the above introduced PLS-SVD algorithm was applied to the 19 cognitive tests scores $\mathbf{X}$ with the VBM grey matter images $\mathbf{Y}$. An important issue for appropriate PLSC modelling of the brain-behavior covariance is model selection and statistical inference. Full deflation of the cross-block covariance using the above methods results in a saturated PLSC model, i.e. some of the higher-degree latent variables simply fit random covariations of the errors of the blocks. Therefore, nonparametric permutation testing was suggested to assess the significance of the latent variables contribution to the brain-behavior covariance (McIntosh and Lobaugh, 2004). We repeated the PLSC algorithm under 2000 random permutations of the individual cognitive ability data with respect to the brain data. To account for biases due to flipping, reordering and rotations in the resampled data, the observed weightings were transformed to the initial PLSC solution using procrustes transformations (Milan and Whittaker, 1995). P-values were calculated estimating the probability of observing equal or higher covariances $\sigma_r = Cov(\boldsymbol{\zeta_r}, \boldsymbol{\xi_r})$ for each of the corresponding latent variables under permutations of the data. Finally, unless stated otherwise the subset of latent variables with $p < 0.05$ was considered

to significantly contribute to the covariance. A related issue of PLSC modelling is the validation and confidence in the observed model parameters (Krishnan et al., 2011). PLSC weights and scores imply a covariance of cognitive ability and brain structure which is sensitive to sampling variability and thus requires a cross-validation technique (Efron and Tibshirani, 1994). As suggested by McIntosh et al. (McIntosh and Lobaugh, 2004) we applied parametric bootstrapping to obtain standard errors for the cognitive ability correlations with the latent scores $\boldsymbol{\zeta}_r$ and $\boldsymbol{\xi}_r$. We used 500 bootstrap samples by sampling with replacement and further assessed symmetric 95% confidence intervals, i.e. $\mu \pm 1.96\sigma$ of the correlation parameter distributions.

Analysis of effects of maturation In order to realize a group PLSC to analyze age-related differences of the structure-cognition covariance we first reordered rows in the cognitive abilities scores and brain data matrices according to 3 age groups with 6-9.5 (n_1=94), 9.5-13.5 (n_2=101), and 13.5-18 (n_3=91) years, and also obtained: $\mathbf{X}_i$ and $\mathbf{Y}_i, i = 1, \ldots, 3$. The aim was to use age specific cognitive weightings and age independent brain network weightings (which might improve interpretation), we adapted the above maximum covariance criterion (2.3):

$$\sigma_1 = \max_{||u||=||v||=1} Cov(\begin{bmatrix} \mathbf{X}_1\mathbf{u}_1 \\ \mathbf{X}_2\mathbf{u}_2 \\ \mathbf{X}_3\mathbf{u}_3 \end{bmatrix} , \begin{bmatrix} \mathbf{Y}_1 \\ \mathbf{Y}_2 \\ \mathbf{Y}_3 \end{bmatrix} \mathbf{v}) \tag{2.2}$$

This corresponds to searching for first left and right singular vectors of the covariance matrix obtained from row-wise concatenation of age group covariance matrices.

$$\mathbf{C}_{gr} = \begin{bmatrix} \mathbf{X}_1^T\mathbf{Y}_1 \\ \mathbf{X}_2^T\mathbf{Y}_2 \\ \mathbf{X}_3^T\mathbf{Y}_3 \end{bmatrix} = \mathbf{U}\boldsymbol{\Sigma}\mathbf{V}^T = \sum_{r=1}^{R} \sigma_r \begin{bmatrix} \mathbf{u}_{1r} \\ \mathbf{u}_{2r} \\ \mathbf{u}_{3r} \end{bmatrix} \mathbf{v}_r^T$$

This favours the application of the above PLS-SVD algorithm with extended behavioral data vectors. Thus, for our purpose of age-group covariance analysis we applied the PLS-SVD algorithm and model validation procedures to the above covariance matrix $\mathbf{C}$. Separation of the extended cognitive weights, and recalculation of loadings revealed the group specific results.

2.1.4 Results and discussion

Whole group PLSC analysis

We first focused on the PLSC analysis of the whole group of 286 children and adolescents after removing age effects and confounding influences. We directly analyzed the 19 test scores in relation to voxel-based grey matter segments. Figure 2.3 shows the obtained PLSC model with latent variable 1 (LV1), (p=0.003, 29.6%), LV2 (p=0.03, 18.0%), and LV5 (p=0.02, 5.5%) showing a significant contribution to the covariance. The dominant LV1 exhibited widespread positive weightings in bilateral medial and superior temporal gyri (including the IPC), frontome-

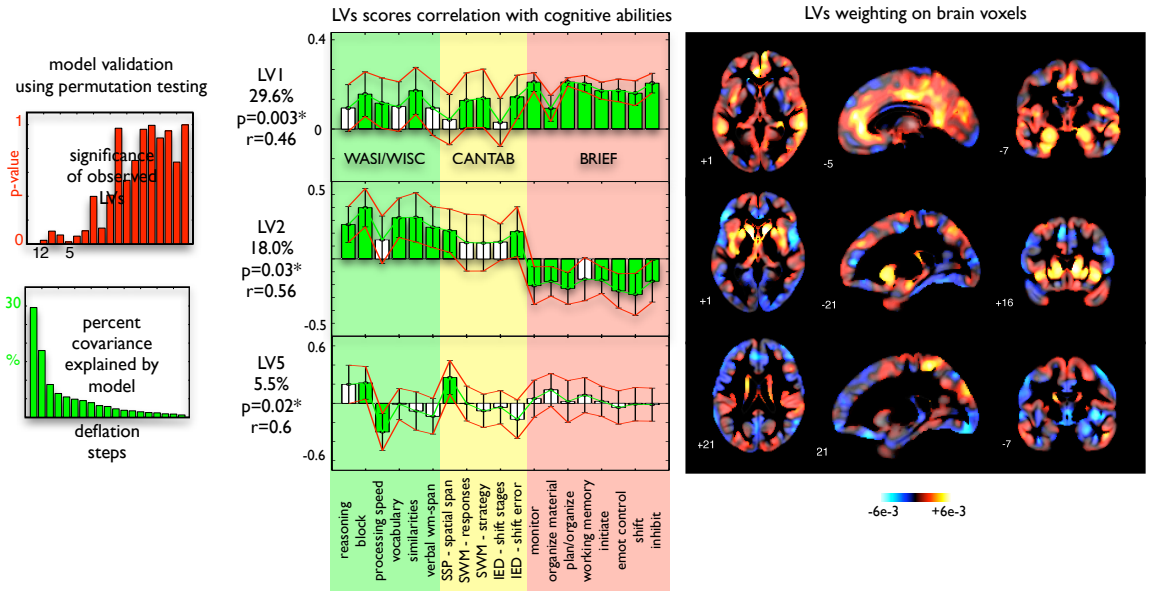

Figure 2.3: **Partial least squares correlation (PLSC) analysis of 19 cognitive ability scores and local grey matter volume obtained from VBM in 286 children and adolescents, ages 6-18.** The brain and cognitive data was first corrected using an appropriate partialling model with age, age^2, age^3, gender, and TICV, TGM then the PLSC estimation was performed using a PLS-SVD approach. Permutation testing revealed the significance of the latent variables. All latent variables with $p<0.05$ are presented. The cognitive and brain weighting patterns from the PLSC analysis are shown for latent variables 1, 2 and 5. The cognitive ability subtest weightings are standardized in terms of correlations with the corresponding PLSC's brain scores. The red error bars indicate confidence intervals for each subtest's correlations to latent brain scores using 500 parametric bootstrap samples. The observed correlations of latent brain and cognitive scores (i.e. $corr(\boldsymbol{\zeta}_i, \boldsymbol{\xi}_i)$) ranged from 0.46 to 0.6. Figure and legend modified from Ziegler et al. (2013).

dial, anterior and posterior cingulate regions, the precuneus, and early visual areas. In addition the frontal area 10, the left inferior and middle frontal gyrus, the insular cortex, the medial temporal lobe and the left fusiform gyrus showed high weightings. The corresponding cognitive profile revealed more emphasized correlations of LV1 to BRIEF's executive function scores and minor correlations to intelligence subtests block, similarities, and CANTAB's IED errors. The observed pattern of grey matter volume correlations to multiple cognitive performance scores is in line with observed abilities differences in the large study of Shaw et al. (2006) that revealed peaking positive IQ correlations to fronto-temporal cortical thickness measures in the late childhood around age 11. Although the investigated set of tests did not exclusively focus on general intelligence or IQ, LV1 supports findings of early lifespan studies on morphometric correlates of cognitive abilities in the anterior cingulate cortex (Frangou et al., 2004; Wilke et al., 2003; Karama et al., 2011) in frontal (Frangou et al., 2004; Shaw et al., 2006; Karama et al., 2011; Pangelinan et al., 2011) and temporo-parietal cortex (Shaw et al., 2006; Karama et al., 2011; Lange et al., 2010). Notably, in contrast to classical paper pencil tests the BRIEF scores represent parents' rating of childrens' day to day executive function, organization, planing, working memory skills etc. BRIEF's intercorrelations with WASI test scores were found to be low and

thus both represent rather independent aspects of abilities differences (see Table 2.2).

According to a prevailing theoretical network model for human cognitive abilities differences in adults, the Parieto-Frontal Integration Theory (P-FIT), neuronal processing of intelligent behavior is distributed over a wide network of brain regions that are involved in different stages of information processing, i.e. recognition, abstraction, problem-solving, and response selection (Jung and Haier, 2007, for review). Although LV1 stronger emphasizes BRIEF compared to WASI, the cortical grey matter regions exhibit a considerable overlap with the proposed set of P-FIT brain regions or modules. We additionally observed a substantial contribution of the hippocampus and the medial temporal lobe grey matter to the dominant LV1. However, the P-FIT theory clearly focuses on higher-level cognitive processes and thus the existing studies on neuronal substrates of general intelligence measures in the early lifespan (in contrast to studies on elderly subjects) often restrict their analysis to cortical grey matter. A few studies have also suggested the significance of medial temporal lobe regions for childhood cognitive ability in terms of IQ (Schumann et al., 2007; Deboer et al., 2007) and working memory (Østby et al., 2012). The study by Østby et al. (2012) implicated individual differences in children's hippocampal volume and their long term recall performance after 1 week. We speculate that these effects might be involved in BRIEF's real world planning and metacognition skills that were found to be highly weighted in LV1.

After projection in the orthogonal subspace from the dominant LV1, the second latent variable LV2 indicated a more mixed pattern including both positive and negative weightings. In particular LV2 was found to have positive weightings in subcortical grey matter, especially the caudate nucleus, putamen, and adjacent insular regions, the inferior and superior parietal cortex, precentral area 6, and parts of the superior and middle frontal gyrus. However, the remaining cortical regions also showed negative weightings especially in the left prefrontal cortex and the temporo-parietal regions. Thus, after accounting for the covariance explained by the dominant LV1, those subjects more similar to this mixed pattern tend to have higher scores in WASI intelligence scores and slightly lower BRIEF skills in everyday executive function. LV2 exemplifies that interpretation of multivariate analysis across several cognitive domains and brain regions is more complex than for univariate analysis, because the effects only make sense using the whole pattern, i.e. the cognitive profile and the spatial map. However, LV2's pattern might indicate a different role of striatal and most cortical regional volumes for individual differences in cognitive ability. Notably, the intercorrelations of WASI, and CANTAB with BRIEF's test scores are small. Therefore although both CANTAB and BRIEF focus on executive functions, they represent rather independent sources of variance in our cognitive ability space (see also cognitive tests correlation matrix in Table 2.2). We suppose LV2's pattern is likely to be driven by two effects that are almost independent in the cognition block: (a) subjects with higher WASI and CANTAB test scores tended to have higher striatum grey matter volume, and (b) subjects with higher BRIEF scores seemed to have more widespread cortical grey matter and slightly less striatal volume. Recent neuroimaging evidence suggests, that the basal ganglia, and particularly the dorsal striatum might be directly involved in higher-level cognitive processes,

executive functions and decision making (Cools, 2011, 2008; Balleine et al., 2007; van Schouwenburg et al., 2012). In this line of research van Schouwenburg et al. (2010) used Dynamic Causal Modelling (DCM) (Friston et al., 2003) to demonstrate the functional involvement of striatal circuits in high-level cognitive control. In addition, striatum's association with cognitive ability is supported by structural MRI studies on macroanatomy. Dorsal striatum volume was found to be positively associated with, and additionally predicted, individual differences in children's cognitive control task performance (Chaddock et al., 2010, 2012). Moreover, young adults' initial dorsal striatum volume predicted performance improvement and skills transfer in a video game that explicitly focused on cognitive flexibility (Erickson et al., 2010). These studies support our observation of a positive LV2 weighting for WASI and CANTABs with the basal ganglia volume, i.e. (a). The observed pattern of a slightly negative association between local striatum volume and BRIEF's scores, i.e. (b), is suggested by one recent study by Lange et al. (2010).

Finally, we also observed the higher order LV5 ($p<0.05$). The observed LV5 indicates higher values of parietal and lateral temporal grey matter networks are associated with individual differences in the block design score, spatial span and processing speed. These regions have been implicated in the P-FIT networks for intelligence differences (Jung and Haier, 2007). However, LV5's contribution to the whole cross-block covariance should be interpreted keeping in mind the much stronger exploratory power of dominant LV1, i.e. (5.5% for LV5 vs. 29.6% for LV1). Taken together, our PLSC analysis revealed generalizable (spatial and cognitive) patterns and latent variables that contribute to stable individual differences in brain morphology and cognitive ability in the early lifespan. The PLSC models of VBM data revealed latent variable correlations of moderate size 0.46-0.6, which exceeds correlation sizes observed in common univariate analysis models (e.g. with IQ Shaw et al., 2006) and supports pattern based analysis in future studies.

Age group PLSC analysis

Individual differences in a cross-sectional observational design might be confounded with age differences. We did account for this possibility by applying appropriate partialling before PLSC modelling, removing the cubic effects of age. Consequently, the above whole group PLSC model approximated a residualized 'average structure-cognition covariance'. However, the developmental processes that cause individual differences in macroanatomy and cognition to covary, are likely to undergo changes across developmental stages. Studies using univariate analysis of grey matter networks have provided evidence for maturational changes of the structure-cognition covariance (Wilke et al., 2003; Karama et al., 2009). Thus, a further focus of this work was how the multivariate structure-cognition covariance evolves as a function of age. In order to reintroduce age differences we extended the above PLSC approach to estimate the covariance separately for ages 6-9.5 years (young), 9.5-13.5 years (middle), 13.5-18 years (old) in one model (see also Table 2.1). Firstly, we applied within age group partialling to avoid biased estimates due to the remaining age differences. Secondly, a modified age-group PLSC model was applied that explicitly allowed group specific cognitive scores and weightings exhibiting the maximal covariance to

local grey matter volumes for each group separately. In order to make latent variables and the corresponding grey matter networks comparable, the LV's brain weightings were assumed to be identical across the age groups. Notably, this is not restrictive because each age group can vary with respect to its contribution to a certain LV, i.e. which can be strong with high weightings or low with weightings around zero. Consequently, if there are group invariant brain patterns we would obtain the age-specific cognitive weightings as intended and otherwise the age group variant brain patterns are simply captured by other LVs.

Permutation testing revealed an increased number of contributing LVs compared to the above whole group model (LV1-3 and LV7-10, $p<0.05$). It indicates that by allowing some age differences to be modeled (or parameterized), more complex models of the multivariate structure-cognition covariance seem to be appropriate. For reasons of space, simplicity, and explained covariance the first four significant LVs are shown in Figure 2.4. Notably, all LVs were

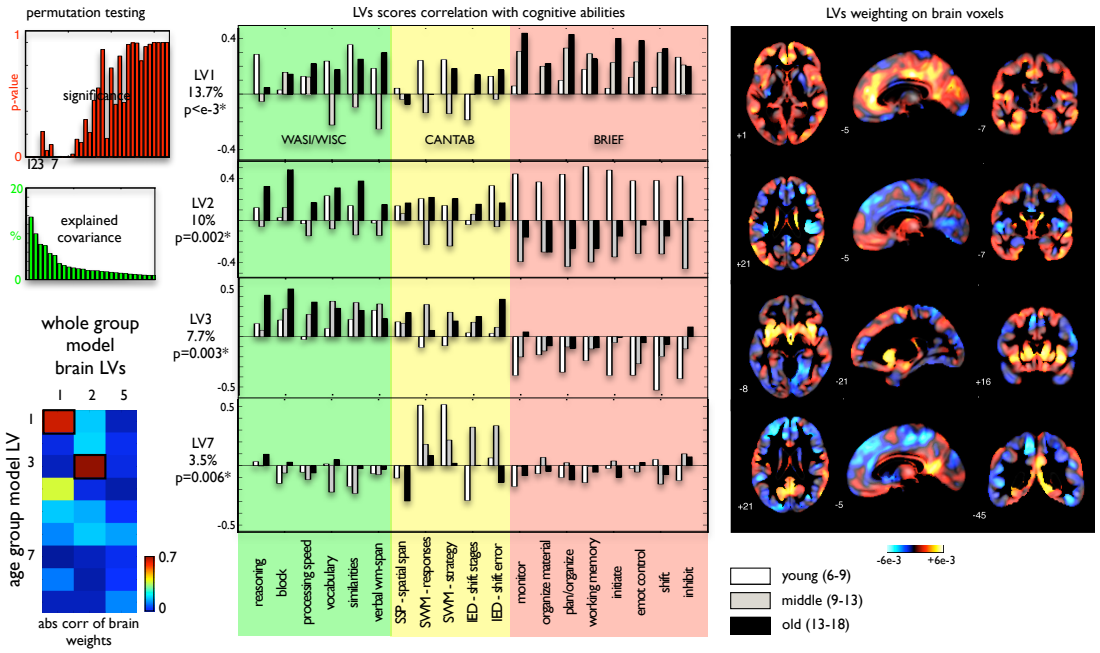

Figure 2.4: **Analysis of maturation of the structure-cognition covariance in 286 children and adolescents using age groups with 6-9, 9-13.5, and 13.5-18 years respectively.** The data was processed using a within age group partialling model with confounders age, age^2, age^3, gender, TICV, and TGM. The PLSC model was used to estimate group specific cognitive weighting profiles (see methods section for details). Permutation testing revealed significance of LVs. Shown are LVs 1, 2, 3 and 7 with $p<0.05$. The similarity to LVs in the whole group PLSC model was identified using absolute correlations of the brain weighting patterns. Each age group can vary with respect to its contribution to a certain LV, i.e. strong with high weightings or low with weightings around zero. Figure and legend modified from Ziegler et al. (2013).

found to exhibit group differences, especially comparing the young and middle-aged groups to the adolescents. The inter-correlations of brain weightings from latent variables LV1 ($p<0.001$, 13%) and LV3 ($p=0.003$, 7.7%) indicated similarity to the LV1 and LV2 of the whole group PLSC model respectively. The corresponding grey matter networks were thus consistently observed in

our PLSC analyses.

LV1 revealed a late increasing relationship of individual differences in grey matter networks and everyday executive functions as measured by BRIEF. This is in line with the hypothesis of a protracted development of executive functions that continues through childhood into adolescence and early adulthood (Blakemore and Choudhury, 2006; Jurado and Rosselli, 2007, for review). However, the widespread pattern of LV1 does not support a exclusively high relevance of frontal lobe regions for these task and also suggests an important role of posterior parts of the brain (Tamnes et al., 2010c, for discussion of this point).

LV2 exhibited a reversal of the estimated covariance between the younger and middle age groups. That means, the pattern of 'more is more' with respect to local grey matter volumes and BRIEF scores switched to a 'more is less' pattern in between both groups. Similar childhood changes of the direction of the covariance were also observed for measures of general intelligence in univariate analysis of cortical thickness (see e.g. Figure 1 in Shaw et al., 2006). We speculate that this might be related to the onset of cortical fine tuning of networks in terms of cellular processes, e.g. pruning, dendritic changes, myelination. LV3, similar to LV2 in the whole group PLSC model, showed strong positive weightings in the striatum and mixed postive and negative weightings in other cortical networks. The childhood behavioral correlations seemed to 'move' from BRIEF to WASI and CANTAB during early adolescence. As discussed for the whole group PLSC model, this variable might indicate a mixture of effects. Inspecting the results of the age-group model, we thus additionally observed indications for a developmental change of the role of basal ganglia and cortical volumes for cognitive ability.

Interestingly, the posterior grey matter network of LV7 showed specific association to CANTAB's spatial working memory and set shifting tests (see also Tamnes et al., 2010c). In particular, this latent variable was positively associated with grey matter volume in the precuneus, the posterior cingulate (PCC) and retrosplenial (RSC) cortices, the lingual gyrus, the inferior and superior parietal cortex, the left fusiform and parahippocampal gyri. As recently reviewed by Kravitz et al. (2011), human visuo-spatial processing in the 'dorsal stream' is likely to be driven by three complex subsystems of anatomical and functional connectivity relating the parietal cortex to either prefrontal, premotor or medial temporal lobe regions respectively (Margulies et al., 2009). The observed brain pattern emphasizes individual grey matter volume differences in the latter subsystem of medial pathways (via PCC and RSC) that are supposed to relay and integrate spatial information from the occipito-parietal system to the hippocampal formation and the parahippocampal cortex (Kravitz et al., 2011). The contribution of these regions to SWM performance differences is also supported by human functional MRI studies of navigation (Maguire et al., 1998; Grön et al., 2000), visual motion (Antal et al., 2008), and visual short-term memory (Todd and Marois, 2004; Mitchell and Cusack, 2008). In contrast to the above LVs, the LV7 covariance here exhibits a 'fade out' pattern with higher covariance in children compared to adolescent subjects. This early childhood covariance to posterior networks would be in line with the anterior posterior gradient of structural maturation (e.g. shown for cortical thickness in Shaw, 2008). Occipito-parietal visual systems are found to mature earlier compared to more

fronto-temporal networks.

There are limitations of the current study that could be addressed in future work. Firstly, the available cognitive tests WASI/WISC, CANTAB and BRIEF in the NIH data repository have been applied assuming the reliability and validity of the psychometric tools (see also Waber et al., 2007). When using PLSC as an exploratory tool for brain analysis with multiple cognitive scores, there are no assumptions about the measurement model in the age groups. However, we can not exclude that observed age group differences are also related to inherent limitations of the cognitive assessments tools, e.g. variability of sensitivity and validity between age groups. Artifacts from test invariance would be rather likely to occur in single subtests and not influence the whole observed pattern across the 19 scores. This is supported by the inspection of the correlation matrices of the cognitive scores, which indicated no substantial age-related changes. Secondly, the applied PLSC scheme is cross-sectional and uses cubic age models for residualized analysis of individual differences. We thus can not separate brain-cognition covariance that is due to already existing differences (from earlier maturation periods) and brain-cognition covariance due to ongoing structural changes, e.g. pruning in adolescents. Further studies might disentangle these contributions to our findings by using analysis of individual structural trajectories obtained from longitudinal data. Thirdly, the spatial brain features in our PLSC model were restricted to local grey matter segments obtained from VBM. Additionally, efficiency of cognitive processing is expected to require a fast communication between these grey matter regions (Tamnes et al., 2010a,b). It would be promising to also include other modalities, e.g. local white matter volumes (WMV) and diffusion tensor imaging (DTI) data. Along with this idea, a recent unsupervised learning method called Link Independent Component Analysis (Link ICA) was suggested to jointly analyze individual and age-related differences across MRI modalities (Groves et al., 2011, 2012). The PLSC deflations result in orthogonal latent variables while ICA aims at finding spatially-independent non-gaussian sources, which might be less restrictive. Finally, in analogy to basic factor analytic methods, maximizing the covariance in PLSC comes at the cost of having most cognitive test scores load on all latent variables. Future studies might also focus on appropriate 'non-oblique' rotation techniques within the PLSC framework which transform the observed pattern of brain-behavior covariance weights into a 'simple structure'.

Conclusion

Here we considered multivariate PLSC models to explore the relationship between cognitive ability patterns and the fine-grained differences in local brain anatomy measured with MRI. We investigated these joint variations in healthy children and adolescents and observed that cognitive patterns explain substantial amounts of structural differences in the maturing brain. The multivariate approach revealed latent variable correlations between morphological patterns and cognitive profiles suggesting more complex brain-behavior models. Moreover, the findings suggest dynamic changes of the multivariate structure-cognition covariance as a process of brain maturation.

2.1.5 Supplemental Material S1: Modelling cognitive abilities and local brain structure using different PLSC algorithms

The main results of the paper are based on the effective PLS-SVD implementation of PLSC. However, the PLS framework is much more general and powerful with several alternative algorithms to obtain latent variables of the covariance. Thus we further explored the results of different PLSC algorithms in the same NIH dataset. We suppose the cognitive data and the brain data is represented in two matrices (or blocks) $\mathbf{X}$ and $\mathbf{Y}$, respectively $l \times m$ and $l \times n$. The columns of $\mathbf{X}$ correspond to cognitive test data, e.g. total IQ scores or verbal span. The columns of $\mathbf{Y}$ contain voxelwise structural brain features after normalization and registration, e.g. local grey matter volume. In order to avoid variance differences to bias the PLS modelling steps, we suppose the columns of $\mathbf{X}$ and $\mathbf{Y}$ to be standardized features, e.g. z-scores. The main idea here is that individual differences observed in $\mathbf{X}$ and $\mathbf{Y}$ are generated by two latent variables, say $\boldsymbol{\zeta}$ and $\boldsymbol{\xi}$, respectively. In other words, the columns in $\mathbf{X}$ and $\mathbf{Y}$ are assumed to be indicators for the *a-priori* unknown variables $\boldsymbol{\zeta}$ and $\boldsymbol{\xi}$ which we aim to estimate from the data. Importantly, $\boldsymbol{\zeta}$ and $\boldsymbol{\xi}$ are supposed to covary, in order to represent the cross-covariance of the indicators $\mathbf{X}^T\mathbf{Y}$ at the level (of error free) latent variables, which makes PLSC a special case of structural equation modelling (SEM). A graphical path model representation of the above outlined idea is depicted in Figure 2.1A. Our goal to identify directions of maximum covariance in the multivariate observations $\mathbf{X}$ and $\mathbf{Y}$ can be further formalized:

$$\sigma_1 = Cov(\boldsymbol{\zeta_1}, \boldsymbol{\xi_1}) = \max_{||u||=||v||=1} Cov(\mathbf{Xu}, \mathbf{Yv}) \tag{2.3}$$

The desired solution for weightings (or often called saliences) $\mathbf{u}$ and $\mathbf{v}$ are the first left and right singular vectors of the cross-block covariance matrix $\mathbf{X}^T\mathbf{Y}$. Wold (1975) introduced the classical form of PLS as a nonlinear iterative partial least squares (NIPALS) algorithm to obtain the optimal normalized weightings $\mathbf{u}^*$ and $\mathbf{v}^*$ and the corresponding latent variable scores $\boldsymbol{\zeta}^* = \mathbf{Xu}^*$ and $\boldsymbol{\xi}^* = \mathbf{Yv}^*$. This part of the algorithm forms the 'inner loop' of PLS-NIPALS, which uses data matrices $\mathbf{X}$ and $\mathbf{Y}$ as inputs and repeats the following steps until convergence (see also Figure 2.1C):

1) $\mathbf{u} = \mathbf{X^T}\boldsymbol{\xi}/(\boldsymbol{\xi}^\mathbf{T}\boldsymbol{\xi})$
2) $||\mathbf{u}|| \rightarrow \mathbf{1}$
3) $\boldsymbol{\zeta} = \mathbf{Xu}$
4) $\mathbf{v} = \mathbf{Y^T}\boldsymbol{\zeta}/(\boldsymbol{\zeta}^\mathbf{T}\boldsymbol{\zeta})$
5) $||\mathbf{v}|| \rightarrow \mathbf{1}$
6) $\boldsymbol{\xi} = \mathbf{Yv}$

The obtained normalized weightings of the indicators are proportional to its covariance with the other block's latent variable, i.e. $u_j \propto Cov(\mathbf{X}_{.j}, \boldsymbol{\xi}), j = 1, \ldots, m$ and $v_k \propto Cov(\mathbf{Y}_{.k}, \boldsymbol{\zeta}), k =$

$1, \ldots, n$. In addition, with converged weighting vectors $\mathbf{u}$ and $\mathbf{v}$, $s_1\mathbf{u}\mathbf{v}^T$ forms a least-squares-optimal rank-one approximation of the covariance matrix $\mathbf{X}^T\mathbf{Y}$ (Seber, 2007). Subsequently, loadings $\boldsymbol{\gamma}$ and $\boldsymbol{\delta}$ for paths depicted in Figure 1A are obtained via linear regression of the $\mathbf{X}$ and $\mathbf{Y}$ on the scores $\boldsymbol{\zeta}$ and $\boldsymbol{\xi}$:

$$\boldsymbol{\gamma} = \mathbf{X}^T\boldsymbol{\zeta}/(\boldsymbol{\zeta}^T\boldsymbol{\zeta}) \quad \text{and} \quad \boldsymbol{\delta} = \mathbf{Y}^T\boldsymbol{\xi}/(\boldsymbol{\xi}^T\boldsymbol{\xi}) \tag{2.4}$$

The inner loop of PLS-NIPALS is closely related to the power method for fast iterative calculation of singular vectors and might be replaced by it (Shawe-Taylor and Cristianini, 2004). Therefore an alternative approach address the criteria in equation (2.3) is to directly calculate the left and right singular vectors of the covariance matrix $\mathbf{X}^T\mathbf{Y}$. This second PLSC algorithm will be further referred to as PLS-SVD (i.e. applied to obtain the main results of the paper). Moreover, the introduction of the theories of statistical learning and regularization (Schölkopf and Smola, 2002; Shawe-Taylor and Cristianini, 2004) later resulted in the kernel-based approach to the PLS algorithms (Rosipal, 2001; Rosipal R, 2006). To illustrate we first suppose an arbitrary mapping of the input vectors $\mathbf{x}$, e.g. the cognitive profiles, into a potentially high-dimensional feature space: $\Phi : \mathcal{X} \to \mathcal{F}$. Individual differences of subject's data are now reflected by the distributions of mapped points $\Phi(\mathbf{x})$ in $\mathcal{F}$. An important theoretical result is that all dot products or relationships of subjects in $\mathcal{F}$ can be replaced by a symmetric positive definite mapping k, i.e. $\langle \Phi(\mathbf{x}), \Phi(\mathbf{y}) \rangle = k(\mathbf{x}, \mathbf{y})$ (Schölkopf and Smola, 2002; Shawe-Taylor and Cristianini, 2004). Therefore, selection and construction of particular kernel functions k allows studying individual differences of subjects input features under high-dimensional mappings Φ without using the mapping explicitly. In the general case of feature mappings Φ_x and Φ_y we obtain kernel matrices that reflect all scalar products of subjects mapped input data for cognitive tests $\mathbf{K}_x = \Phi_x(\mathbf{X})\Phi_x(\mathbf{X})^T$ and brain images $\mathbf{K}_y = \Phi_y(\mathbf{Y})\Phi_y(\mathbf{Y})^T$. The following inner loop of kernel PLS forms a dual representation of the above given PLS-NIPALS algorithm. Notably, the normalization of weightings was replaced by a normalization of scores which produces linearly transformed latent variables:

$$\begin{aligned} &1) \quad \boldsymbol{\zeta} = \mathbf{K}_x\boldsymbol{\xi} \\ &2) \quad ||\boldsymbol{\zeta}|| \to 1 \\ &3) \quad \boldsymbol{\xi} = \mathbf{K}_y\boldsymbol{\zeta} \\ &4) \quad ||\boldsymbol{\xi}|| \to 1 \end{aligned}$$

The weightings are further computed using $\mathbf{u} = \mathbf{X}^T\boldsymbol{\xi}$, and $\mathbf{v} = \mathbf{Y}^T\boldsymbol{\zeta}$. For reasons of simplicity, visualization and to favour comparisons to the above algorithms we further used the linear kernel mapping $k(\mathbf{x}, \mathbf{y}) = \langle \mathbf{x}, \mathbf{y} \rangle = \mathbf{x}^T\mathbf{y}$ for the brain and the cognitive input data. Therefore, the following kernel matrices $\mathbf{K}_x = \mathbf{X}\mathbf{X}^T$ and $\mathbf{K}_y = \mathbf{Y}\mathbf{Y}^T$ and the mapping $\Phi_x(\mathbf{X}) = \mathbf{X}$ and $\Phi_y(\mathbf{Y}) = \mathbf{Y}$ were used for comparisons of weightings. Using this linear kernel-based approach to obtain directions defined by equation (2.3) will further be referred to as PLS-K-LIN.

Projection schemes: deflation of the data, covariance and kernel matrices

After initial convergence of one of the inner loops we obtained weightings, scores, and the path coefficients (or loadings) of the model in Figure 2.1B. This first latent variable thus reveals the most simple model of the covariance $\mathbf{X}^T\mathbf{Y}$ of both blocks of data. However, because this rank-one approximation with $n+m$ parameters is not a saturated model, there might be unexplained covariations in the residuals. Therefore PLSC includes an outer loop to deflate the data, the covariance or the kernel matrices, by projection in the orthogonal subspace defined by the first latent variable. This outer loop is iterated for up to $R = rank(\mathbf{X}^T\mathbf{Y})$ steps which reveals latent variable scores $\zeta_1, \ldots, \zeta_R$ and $\xi_1, \ldots, \xi_R$ with nonzero covariances $s_1, \ldots, s_r$. The here applied PLS-NIPALS approach uses the following iterative rank-one approximations of the data matrices separately, resulting in a sequence of residual data matrices $\mathbf{X}^{(r)}, \mathbf{Y}^{(r)}, r = 1, \ldots, R, \mathbf{X}^{(1)} = \mathbf{X}, \mathbf{Y}^{(1)} = \mathbf{Y}$:

$$\mathbf{X}^{(r+1)} = \mathbf{X}^{(r)} - \boldsymbol{\zeta}_r\boldsymbol{\gamma}_r^T \tag{2.5}$$

$$\mathbf{Y}^{(r+1)} = \mathbf{Y}^{(r)} - \boldsymbol{\xi}_r\boldsymbol{\delta}_r^T, \tag{2.6}$$

with loadings $\boldsymbol{\gamma}_r$ and $\boldsymbol{\delta}_r$ derived from regression (via equation (2.4)) of $\mathbf{X}^{(r)}$ and $\mathbf{Y}^{(r)}$ on the scores $\boldsymbol{\zeta}_r$ and $\boldsymbol{\xi}_r$ obtained from the inner loop of PLS-NIPALS (with inputs $\mathbf{X}^{(r)}$ and $\mathbf{Y}^{(r)}$). Note that this step corresponds to a deflation mapping using the scores, i.e. $\mathbf{X}^{(r)} \rightarrow (\mathbb{I} - c\boldsymbol{\zeta}_r\boldsymbol{\zeta}_r^T)\mathbf{X}^{(r)}$ and $\mathbf{Y}^{(r)} \rightarrow (\mathbb{I} - c\boldsymbol{\xi}_r\boldsymbol{\xi}_r^T)\mathbf{Y}^{(r)}$ with $c = 1$ for normalized scores. After r deflation steps, PLS-NIPALS revealed the following PLS model:

$$\mathbf{X} = \boldsymbol{\zeta}_1\boldsymbol{\gamma}_1^T + \cdots + \boldsymbol{\zeta}_r\boldsymbol{\gamma}_r^T + \epsilon_x^{(r)} = \mathbf{Z}\boldsymbol{\Gamma}^T + \epsilon_x^{(r)} \tag{2.7}$$

$$\mathbf{Y} = \boldsymbol{\xi}_1\boldsymbol{\delta}_1^T + \cdots + \boldsymbol{\xi}_r\boldsymbol{\delta}_r^T + \epsilon_y^{(r)} = \boldsymbol{\Xi}\boldsymbol{\Delta}^T + \epsilon_y^{(r)} \tag{2.8}$$

In contrast PLS-SVD uses an iterative rank-one approximation of the cross-block covariance $\mathbf{C}^{(1)} = \mathbf{X}^T\mathbf{Y}$ with the sequence of left and right singular vectors $\mathbf{u}_r$ and $\mathbf{v}_r$, r=1, . . . , R obtained from either the power method or efficient algorithms for complete singular value decomposition, i.e. $\mathbf{C} = \mathbf{USV}$:

$$\mathbf{C}^{(r+1)} = \mathbf{C}^{(r)} - \sigma_r\mathbf{u}_r\mathbf{v}_r^T \tag{2.9}$$

The latent scores matrices are revealed by projection of the data on the corrsponding singular vector (or weighting) matrices $\mathbf{U}$ and $\mathbf{V}$, i.e. $\mathbf{Z} = \mathbf{XU}$ and $\boldsymbol{\Xi} = \mathbf{YV}$. In addition, the linear path coefficients or loadings for PLS-SVD were obtained from equation (2.4) using projections on the (undeflated) data $\mathbf{X}$ and $\mathbf{Y}$ respectively. Finally, a kernel-based alternative for the above deflations of the data and the covariance was implemented. The PLS-K-LIN algorithm thus instead used deflation of the kernel matrices $\mathbf{K}_x$ and $\mathbf{K}_y$ to estimate higher order latent variables of brain-behavior covariance. We implicitly used the mappings of the data in the high-dimensional features space $\Phi_x : \mathcal{X} \rightarrow \mathcal{F}_1$, and $\Phi_y : \mathcal{Y} \rightarrow \mathcal{F}_2$ and aimed at deflating the kernel matrices of the

data $\mathbf{K}_x = \Phi_x(\mathbf{X})\Phi_x(\mathbf{X})^T$ and $\mathbf{K}_y = \Phi_y(\mathbf{Y})\Phi_y(\mathbf{Y})^T$. If we suppose normalized latent variables scores, the deflation of the mapped data would be accomplished by:

$$\Phi_x(\mathbf{X}) \rightarrow (\mathbb{I} - \boldsymbol{\zeta}\boldsymbol{\zeta}^T)\Phi_x(\mathbf{X}) \tag{2.10}$$

$$\Phi_y(\mathbf{Y}) \rightarrow (\mathbb{I} - \boldsymbol{\xi}\boldsymbol{\xi}^T)\Phi_y(\mathbf{Y}) \tag{2.11}$$

Thus, the corresponding kernel matrix deflations in the outer loop of the kernel PLS algorithm are:

$$\mathbf{K}_x \rightarrow (\mathbb{I} - \boldsymbol{\zeta}\boldsymbol{\zeta}^T)\mathbf{K}_x(\mathbb{I} - \boldsymbol{\zeta}\boldsymbol{\zeta}^T) \tag{2.12}$$

$$\mathbf{K}_y \rightarrow (\mathbb{I} - \boldsymbol{\xi}\boldsymbol{\xi}^T)\mathbf{K}_y(\mathbb{I} - \boldsymbol{\xi}\boldsymbol{\xi}^T) \tag{2.13}$$

This general formulation allows application to diverse forms of kernel mappings, e.g. linear, polynomial, squared exponential (Shawe-Taylor and Cristianini, 2004, for kernel construction). However, as stated above, for practical application to the neuroimaging dataset with PLS-K-LIN, linear kernel mappings were used for both the $\mathbf{X}$ and $\mathbf{Y}$ data.

Orthogonality in different PLSC algorithms

After preprocessing and correcting the NIH sample data for confounders as outlined in the main paper, the above introduced PLS-NIPALS, PLS-SVD and PLS-K-LIN algorithms were applied to data. This involved using either the data, the covariance or the kernel as inputs and revealed latent variable scores $\mathbf{Z}$ and $\boldsymbol{\Xi}$, weightings $\mathbf{U}$ and $\mathbf{V}$, and loadings $\boldsymbol{\Delta}$ and $\boldsymbol{\Gamma}$ for each algorithm. The number of inner-loop iterations for PLS-NIPALS and PLS-K-LIN were set to 50, which provided very good convergent results for the singular vectors. The number of outer-loop iteration steps were choosen R=19, i.e., $R = rank(\mathbf{X^T Y})$. Note, that the normalized weightings $\mathbf{U}$ and $\mathbf{V}$ are pairwise orthogonal for all algorithms, i.e., $\mathbf{U}\mathbf{U}^T = \mathbb{I}$, and $\mathbf{V}\mathbf{V}^T = \mathbb{I}$. However, PLSC models with more than one latent variable are only applicable due to certain orthogonality constraints for the model paramters of different LVs, i.e., the latent scores and weightings. Thus, the obtained weightings from different PLSC deflation schemes are orthogonal, but PLS-NIPALS and PLS-SVD differ with respect to their constraints for the latent scores. The normalized scores are orhogonal for PLS-NIPALS, i.e., $\mathbf{Z}\mathbf{Z}^T = \mathbb{I}$ and $\boldsymbol{\Xi}\boldsymbol{\Xi}^T = \mathbb{I}$, which is not necessarily true for PLS-SVD. Figure 2.5A shows that PLS-NIPALS produced linear independent latent variables for the same block and at the same time allowed cross-block scores to correlate. The situation for PLS-SVD is exactly the opposite, while we expected them to reveal different models of the structure-cognition covariance. Moreover, this implies the additivity across latent variables of the explained data variances of $\mathbf{X}$ and $\mathbf{Y}$ in PLS-NIPALS (but not for PLS-SVD) and the additivity of covariances across latent variables for PLS-SVD (but not for PLS-NIPALS).

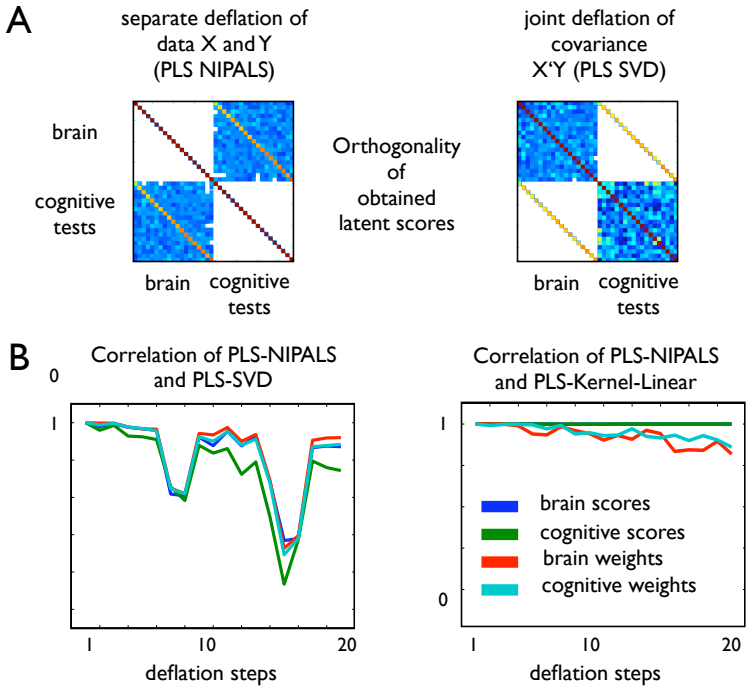

Figure 2.5: Similarities and differences using PLS with deflation of either the data (PLS-NIPALS), the covariance (PLS-SVD), and the kernel matrices (PLS-K-LIN). (A) Different orthogonality constraints of PLS-NIPALS and PLS-SVD are shown in terms of obtained correlations of brain and cognitive scores in our whole group NIH dataset with 286 children and adolescents. (B) The obtained correlation of brain scores, cognitive scores, brain weights, and cognitive weights is shown for 19 deflation steps of PLS-NIPALS and PLS-SVD in the whole group NIH data. The same comparison is also shown for PLS-NIPALS and PLS-Kernel-Linear. Figure and legend from supplemental material in Ziegler et al. (2013).

Applying different PLSC algorithms to the NIH dataset

After obtaining PLSC's dominant latent variable guided by the maximum covariance principle, higher order LVs might differ due to the particular applied deflation method. Thus, we explored these effects of PLS-NIPALS, PLS-SVD and the kernel-based PLS-K-LIN on the above NIH dataset. PLS-NIPALS, which was initially introduced by Herman Wold (Wold, 1975) was used as a reference for the comparisons. Figure 2.5B depicts the correlation of the obtained scores and weightings using 19 deflation steps of PLS-NIPALS and PLS-SVD. The observed first 6 latent variables' scores and weightings produced by PLS-NIPALS and PLS-SVD were found to be highly similar with increasing fluctuating deviations for higher degree LVs. Thus, although the orthogonality constraints of the algorithms substantially differ, this did not affect the neuroimaging application results significantly. However, the deviations should be taken into account for further studies with a high number of significant LVs. A related issue is that we observed a pattern of slightly alternating lower and higher p-values in the investigated PLSC models. This systematic finding might be influenced by the supposed orthogonality assumption for the successive latent variables and reduces the flexibility of the modelled covariance. Moreover, it supports further exploration of models with partially intercorrelated latent variables for the

structure-cognition covariances in further studies.

In addition, we explored a kernel-based mapping of the brain and cognitive data, which in principle compresses all individual differences of the features into two kernel matrices (Shawe-Taylor and Cristianini, 2004). Thus, kernels might serve as effective information bottlenecks for high-dimensional subject specific data. This is particularly useful for neuroimaging data, where the number of observations (or subjects) is much smaller than the numbers of voxels or brain features. Using PLS-NIPALS and PLS-K-LIN we observed almost identical results for the scores and only small deviations of the weighting vectors. At the same time this dual implementation was found to be highly efficient with respect to memory and running time due to much less computational load with calculations run on kernel matrices. Therefore, future PLSC application studies might take the advantages of kernel-based instead of traditional PLSC implementations. In addition, it is promising that the kernel mapping also allows exploration of more general relationships between cognitive abilities and neuranatomical correlates. In contrast to the above presented results, this involves non-linear modelling of the brain-behavior covariance (Rosipal R, 2006; Rosipal, 2003) and the integration of spatial models in the very process of kernel construction.

Acknowledgments

This work was supported in part by BMBF grants (01EV0709 and 01GW0740). Data used in the preparation of this article were obtained from the NIH Pediatric MRI Data Repository created by the NIH MRI Study of Normal Brain Development. This is a multisite, longitudinal study of typically developing children from ages newborn through young adulthood conducted by the Brain Development Cooperative Group and supported by the National Institute of Child Health and Human Development, the National Institute on Drug Abuse, the National Institute of Mental Health, and the National Institute of Neurological Disorders and Stroke (Contract #s N01-HD02-3343, N01-MH9-0002, and N01-NS-9-2314, -2315, -2316, -2317, -2319 and -2320). A listing of the participating sites and a complete listing of the study investigators can be found at http://www.bic.mni.mcgill.ca/nihpd/info/participating_centers.html. Notably, this manuscript reflects the views of the authors and may not reflect the opinions or views of the NIH.

Chapter 3

Structural Brain Trajectories in Adulthood and Later Life

3.1 Models of Aging Brain Structure and Individual Decline - PART A Cross-sectional Methods

Gabriel Ziegler[1], Robert Dahnke[1], Christian Gaser[1,2], and the Alzheimers Disease Neuroimaging Initiative[3]

1 Structural Brain Mapping Group, Department of Psychiatry, Jena University Hospital, Jena, Germany.

2 Department of Neurology, Jena University Hospital, Jena, Germany.

3 Data used in the preparation of this article were obtained from the Alzheimer's Disease Neuroimaging Initiative (ADNI) database (www.loni.ucla.edu/ADNI). As such, the investigators within the ADNI contributed to the design and implementation of ADNI and/or provided data but did not participate in analysis or writing of this report. Complete listing of ADNI investigators available at http://adni.loni.ucla.edu/wp-content/uploads/how_to_apply/ADNI_Authorship_List.pdf.

Type of contribution Research article[1], (published in Ziegler et al., 2012a)

Personal contribution G.Z. conceived and designed the overview framework, adapted and implemented the algorithms for polynomial models, spline models, longitudinal models, preprocessed the data, analyzed the MRI data, and wrote the paper. R.D., C.G. helped to preprocess the data, R.D. photoshopped some figures, C.G. corrected the paper.

[1] In order to improve the structure of this thesis, the original overview article is divided in PART A describing cross-sectional models and PART B describing longitudinal models. PART A is included as introduction to chapter 3 and PART B is included as introduction to chapter 4

3.1.1 Abstract

The aging brain's structural development constitutes a spatiotemporal process that is accessible by MR-based computational morphometry. Here we introduce basic concepts and analytical approaches to quantify age-related differences and changes in neuroanatomical images of the human brain. The presented models first address the estimation of age trajectories, then we consider inter-individual variations of structural decline, using a repeated measures design. We concentrate our overview on preprocessed neuroanatomical images of the human brain to facilitate practical applications to diverse voxel- and surface-based structural markers. Together these methods afford analysis of aging brain structure in relation to behavioral, health or cognitive parameters.

3.1.2 Introduction

There is a growing interest in the neuroscience of aging. Magnetic Resonance Imaging (MRI) has become a promising and versatile technique for noninvasive *in-vivo* measurement of the morphological changes the brain undergoes in aging and dementia. The fast emerging field of computational morphometry offers imaging methods that quantify a variety of anatomical features of aging brains (Toga and Thompson, 2003; Mietchen and Gaser, 2009). In addition, semi-automated voxel- and surface-based processing techniques afford developmental studies of large representative samples of healthy or clinical populations with high economy of time, no rater bias and high sensitivity. The field of lifespan psychology (LP) provides a conceptual framework to describe the changes of brain and behavior during human ontogenesis (Baltes and Staudinger, 1999). The core assumption is that the brain and behavior keep on developing during the entire lifespan. Moreover, it emphasizes that development and aging can be studied with respect to the following aspects:

(i) Multidimensionality

(ii) Multidirectionality

(iii) Inter-individual differences.

For our purposes, multidimensionality (i) states that examining brain structural development and aging using MR morphometry is a high-dimensional problem in modalities and space (i.e., brain regions). Application of different MR pulse sequences, segmentation techniques, voxel- or surface-based processing, and fibre tracking afford the acquisition of a large variety of structural brain markers (Toga and Thompson, 2003; Assaf and Pasternak, 2008; Mietchen and Gaser, 2009). Thus, age effects can be studied in local grey matter volume using Voxel-Based Morphometry (VBM), cortical thickness by Surface-Based Morphometry (SBM), white matter properties by magnetization transfer (MT) imaging and multi-echo T2-weighted sequences, and the integrity of fibre connections by Diffusion Tensor Imaging (DTI) (for review see Raz and Rodrigue, 2006; Gunning-Dixon et al., 2009; Fjell and Walhovd, 2010). In addition, there is an

increasing number of studies that aim at combining information from different modalities in order to explore the underlying processes of age-related brain structural changes (Westlye et al., 2010; Draganski et al., 2011). At the same time, most computational and semi-automated methods provide anatomical markers in 3D volume- or 2D surface space that obtain resolutions in the range of millimeters. The advantage of this 'quasi-continuous' measurement is the sensitive detection of age-related effects without the restriction of any *a-priori* assumptions regarding location and spatial extent. The existing studies reveal a heterogeneous regional pattern of age effects over the lifespan (Raz and Rodrigue, 2006; Raz and Kennedy, 2009; Walhovd et al., 2011; Fjell and Walhovd, 2010) indicating region specific processes in structural brain aging.

Modelling the trajectories of neuroanatomical marker's growth and/or decline as a function of age, studies have observed substantial variation in directions of change (Raz and Kennedy, 2009; Fjell and Walhovd, 2010). This multidirectionality (ii) of brain aging is expressed by annual rates of decline in structural aspects of a region such as local grey matter volume, cortical thickness, etc. In addition, the local rates of decline allow to estimate the extrapolated loss of brain structural integrity across the adult lifespan. A related question is whether structural aging accelerates with advancing ages. There is evidence that annual rates of decline may exhibit substantial changes over decades (Ziegler et al., 2012b). Consequently, an age trajectory's functional form could potentially contain information about qualitatively different phases (e.g., increase, plateau, decline) and the timing of structural development and degradation (Raz et al., 2005; Fjell and Walhovd, 2010).

The third aspect of development across the lifespan is related to the ongoing reciprocal interaction between the individual ontogeny and its surrounding biocultural context (for a conceptual framework see Baltes et al., 2006). It is assumed that structure and function of a subject's brain (at a certain age) depends on the individual genetic code, its unique learning experience and the past and currently prevailing inner- and extraorganismic environment. As a consequence of cumulative effects over the lifespan, one would expect substantial inter-individual differences (iii) in the micro- and macrostructural architecture in the brains of elderly people even at the same age. Exploring these individual differences in healthy, prodromal and pathological forms of age-related change is a major challenge for neuroimaging studies. An important research issue still is the identification of protective and risk-inducing factors. That is, which contributors and modifiers do protect or harm integrity of brain structure, function and cognitive abilities into an advanced age. This perspective has motivated a large number of studies addressing the specific role of structural brain markers for normative age-related cognitive decline observed in healthy elderly people (Raz and Kennedy, 2009; Salthouse, 2011c). However, there is still a lack of longitudinal studies that relate intra-individual changes of whole brain morphology at a local level to covariates and predictors, such as cognitive abilities (Raz and Lindenberger, 2011; Salthouse, 2011a). There is also a potential for improvement by applying multivariate models to analyze age differences and intra-individual change (Bray et al., 2009; Salthouse, 2011c).

In this paper we overview basic analytical approaches to study core aspects of age-related differences and individual changes in MR-based morphometry. This suggests practical appli-

cation to a multitude of voxel- and surface-based markers that reveal structural dynamics in the temporal range of months to several decades of the lifespan. We close with a discussion of limitations and opportunities for further improvement.

3.1.3 Age-related effects, trajectories and regression

Much of the research on aging cognition and brain structure uses a cross-sectional study design. Usually this refers to single MRI acquisitions of individuals, covering a certain age range over the lifespan. Organization, collection, preprocessing and analysis costs are comparably moderate, which makes it generally attractive for many research settings and also substantially increases available sample sizes. In this section we further discuss analysis of a single cross-sectionally sampled and preprocessed MR-based neuroanatomical marker (e.g., grey matter volume or cortical thickness) that has been normalized (or warped) to either a voxel- or surface-based reference template respectively and smoothed afterwards (Mietchen and Gaser, 2009). For making inferences about age effects it is important to assume that all applied preprocessing techniques are completely age-unbiased. We take m subjects' morphometry datasets, each having n structural features that correspond to voxels or vertices of a reference template. We arrange this dataset to the $m \times n$ brain structure matrix $\mathbf{Y}$ with entries y_{ij} (using observations in rows and voxels- or vertices in columns) and the corresponding subject ages in the $m \times 1$ column vector $\mathbf{age} = [age_1, age_2, \ldots, age_m]^T$. Unless otherwise specified bold face letters denote either matrices (e.g., $\mathbf{M}$) or column vectors (e.g., $\mathbf{m}$) of observed or estimated deterministic data. The corresponding non-boldface letters denote stochastic random vectors (e.g., Y) or random variables (e.g., y).

Generative and recognition models of age

Regarding the modelling of an aging brain structure, we would first like to emphasize a valuable distinction of applied techniques into generative and recognition models (see Figure 3.1) (Friston and Ashburner, 2004; Friston et al., 2008). Both quantify how causes or experimental factors (e.g., pathology, mental states, developmental stage etc.) can be related to differences in brain measures (e.g., MRI/fMRI). Importantly, they strongly differ in the directions of prediction and inference, and modelling of errors. Thus generative and recognition models yield to specific applications in structural brain aging research.

Generative Models: A generative (or forward) model predicts the brain structural differences Y as some parametric function G of age, i.e., $Y = G(age, \beta)$. We apply parameters β that perform best in prediction of sample brain data based on subjects' ages. Building a generative model of Y requires *a-priori* information and assumptions regarding how the brain structure is explicitly related to age. For instance one assumes whether G contains linear, polynomial, or more complex functions of age. Then, by testing significance of these parameters β and differences of model performance one is able to infer about age effects and different shapes of age trajectories, non-linear terms, etc.

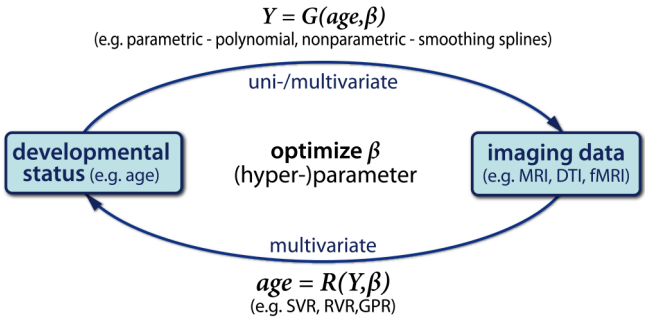

Figure 3.1: Schematic illustration of generative and recognition models of age. A generative model G predicts the brain structural differences Y as a univariate or multivariate parametric function of age (top). Conversely, recognition models R predict individual's age or age-group based on brain differences Y (bottom). According to the multidirectionality, age trajectories are not assumed to be strictly increasing or decreasing functions of age, e.g., inverted-U shaped. Consequently, in case of continuous age, these univariate recognition models are not reasonable (see also Friston and Ashburner, 2004). Figure modified from Ziegler et al. (2012a).

Recognition Models: Conversely to generative models, by applying recognition models in neuroimaging we make inferences regarding experimental factors (e.g., stimulus category, disease groups, or subjects' developmental status) from the brain differences. In the special case of aging research, a recognition model uses some parametric function R of brain structural differences Y to optimally predict subjects age group (via classification) or the exact biological age (via regression), i.e., $age = R(Y, \beta)$. Such an inference regarding brain age might be useful for diagnosis of dementia and pathological aging. Alternatively, recognition models can be applied directely to separate healthy aging, prodromal stages and pathological changes in the aging brain.

Mass-univariate generative models of age

The application of generative models is valuable to obtain insights into the multidirectionality of brain development and age-related differences. At the same time, these models can provide information about the regional variability of age effects. Both aims can be achieved by arranging G in a 'mass-univariate' manner, i.e., modelling the structural marker Y with independent functions for each voxel- or vertex in the brain separately: $G = (g^{(1)}(age, \beta_1), \ldots, g^{(n)}(age, \beta_n))^T$ (see also Friston et al., 1995). Although G provides more flexibility, the local age trajectories $g^{(k)}(age, \beta_k)$ (of different voxels- or vertices k) are often chosen from the same class of parametric functions, e.g., linear, quadratic, etc. Then the general linear model (GLM) provides a powerful and flexible framework to implement various types of cross-sectional age trajectories, which are linear in the parameters. Under the assumptions of the Gauss-Markov theorem, ordinary least squares (OLS) minimization provides 'optimal' unbiased estimators of voxel- or vertex-wise statistical parametric maps (SPMs) for each parameter (for review see Monti, 2011). After estimation, the SPMs can be easily tested against null hypothesis, which affords classical inference about region specific effects of age. It is important to note that generative models of age are not necessarily univariate and thus G can also be implemented using a multivariate spatial model, e.g., using

spatial prior modelling, canonical variates analysis (CVA), etc. (Kherif et al., 2002).

Polynomial model of age: In order to explore multidirectionality of brain development across the lifespan, many studies assume a linear age trajectory due to its conceptual simplicity, straightforward interpretation and robustness. However, this linearity assumption may be questioned due to the complex interactions taking place in the aging cellular systems that underlie neuroanatomy. It is therefore reasonable to suppose that the true structural age trajectories $g(age)$ are arbitrarily continuous and differentiable functions of age. Hence, the annual rate of decline is given by its derivative, i.e., $\dot{g}(age)$. Apparently, a linear approximation (as applied in many studies) is not necessarily valid if the sampled age range increases and $g(age)$ is highly nonlinear, e.g., inverted-U shaped. This might have led to contradictory results in structural aging literature (see Walhovd et al., 2011; Fjell and Walhovd, 2010) and thus motivates the application of more flexible models. A more general model for local age trajectories uses the pth degree polynomial expansion of age in all voxels- or vertices k:

$$y_{ik} = \sum_{r=0}^{p} \beta_{rk}(age_i)^r + \epsilon_{ik}, \quad \epsilon_{ik} \sim \mathcal{N}(0, \sigma^2_{\epsilon_k}) \tag{3.1}$$

This can be easily rewritten in the GLM matrix form $\mathbf{Y} = \mathbf{XB} + \mathbf{E}$, using the design matrix $\mathbf{X} = [\mathbf{age}_0, \mathbf{age}_1, \ldots, \mathbf{age}_p]$ containing column-wise ascending powers of subject ages, the parameter matrix $\mathbf{B}$ with entries $\beta_{r+1,k}$, and matrix $\mathbf{E}$ with errors ϵ_{ik}. We further suppose that Gaussian errors are independent of the deterministic and pairwise linear independent predictors (Monti, 2011). For $p = 1$, this results in a linear approximation of the age trajectory. It is important to note that for higher degrees the GLM model estimation would be seriously affected due to the problem of multicollinearity, i.e., substantial correlations of predictors (Andrade et al., 1999). The multicollinearity of the design matrix increases the variance of parameter estimates of all correlated predictors and thus reduces the sensitivity to identify and separate specific age effects of degree p. It therefore is recommended to orthogonalize the age predictors $\mathbf{X}$ using either Gram-Schmidt algorithm or QR-decomposition.

A crucial point of the polynomial model is the *a-priori* selection of an appropriate degree for the age range and structural marker of interest. Many studies report the existence of linear and quadratic age effects while cubic effects are often not investigated (Raz and Rodrigue, 2006; Raz and Kennedy, 2009; Walhovd et al., 2011; Fjell and Walhovd, 2010). Using the GLM and a sufficiently high degree, e.g., $p = 4$, different models can be tested via F-statistics comparing explained variances or t-statistics of a particular parameter of interest (e.g., β_{2k} for quadratic effects). Therefore, the polynomial model allows addressing two aspects of multidirectionality of structural brain aging. Firstly, it affords inference about region specific age effects and provides estimates of local annual rates of decline using a linear approximation. Secondly, it enables the detection of changes in the annual rates of decline by rejection of the linearity assumption via significant terms of higher degrees. Figure 3.2 depicts the application of a 2nd degree polynomial

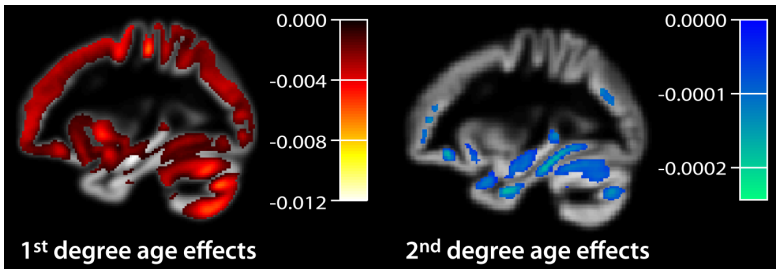

Figure 3.2: Application of a polynomial age model in a large cross-sectional healthy subjects sample of voxel-based morphometry data ($n = 1094$, 18-94 years, normalized grey matter volume segment). Here we depict the estimates of 1st and 2nd degree beta coefficients. We applied a voxel threshold of $t = 5.097, p < 0.05$, FWE corrected. Figure and legend from from Ziegler et al. (2012a).

age model to a large database of voxel-based morphometry data. Notably, there are severe limitations of using polynomial models to represent brain structural trajectories as a function of age (Fjell et al., 2010b). Firstly, the shape, the extreme values, and the inflection points of lower degree models are highly restrictive, imposing strong constraints on the unknown developmental process. This might reveal biased estimates of characteristic points (e.g. the maximum values) and the corresponding ages. Secondly, the polynomial model is a global regression method, i.e., each part of the trajectory strongly depends on all data points irrespective of their age difference. For instance the estimated trajectory at the age of 20 is also influenced by subjects with ages of 90 which is not a desired behavior of the model. Finally, the parameter estimates obtained by OLS minimization would be seriously affected by uneven sample distributions, often observed in research practice.

Nonparametric regression methods Alternatively, rather than finding the parameters with respect to some fixed set of basis functions, nonparametric regression techniques might provide a more unbiased estimation of the true developmental trajectory. Thus applied to a cross-sectional dataset they directly aim at finding an 'optimal' generative model that predicts the local structure in voxel- or vertex k as a function of age:

$$y_{ik} \quad = \quad g^{(k)}(age_i) + \epsilon_{ik}, \quad \epsilon_{ik} \sim \mathcal{N}(0, \sigma^2_{\epsilon_k}) \tag{3.2}$$

After performing the nonparametric regression, the estimated function $g^{(k)}$ itself contains the information about age-related differences and thus we here leave out the parameters. Nevertheless, nonparametric regression methods often use parameters or hyperparameters concerning priors. Notably, the optimization takes place without forcing the age trajectories $g^{(k)}$ into a rigidly defined parametric class of functions (Fox, 2008). The trajectories are only supposed to be smooth continuous functions of age. Here, we briefly outline three methods to obtain age trajectories nonparametrically, which are called linear smoothers. Local regression (LOESS): This nonparametric method provides a local approximation of the age trajectory $g^{(k)}$ using linear or quadratic functions (Cleveland, 1979; Cleveland et al., 1988). It is local in the sense that

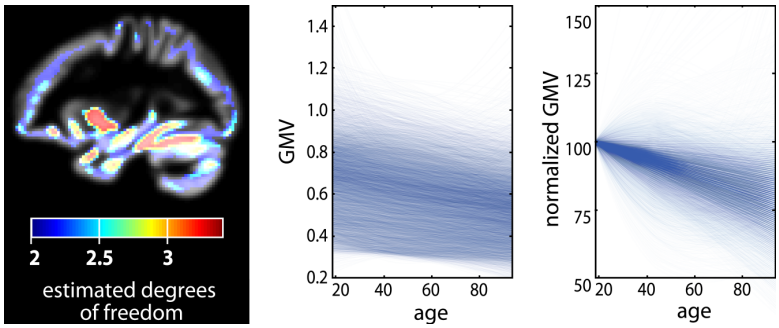

Figure 3.3: Application of a nonparametric age model in a large cross-sectional healthy subjects sample of voxel-based morphometry data ($n = 1094$, 18-94 years, normalized grey matter volume segment). The voxel-wise age trajectories were achieved using a smoothing spline regression technique with generalized cross-validation to identify the optimal smoothing parameter from the interval $[1, 1.5]$. The effective degrees of freedom of the estimated local spline trajectories are depicted (left). The plot shows obtained age trajectories in 10000 randomly selected grey matter voxels (middle). We also show a normalized version of age trajectories using grey matter volume at age 18 as a reference for further lifespan development (right). Figure and legend from Ziegler et al. (2012a).

the estimated structural value at a specific age is more strongly influenced by subjects with similar ages. In contrast to the above polynomial model, it uses weighted least squares (WLS) optimization to estimate the trajectory at a certain age. The smoothness of the resulting loess-fit strongly depends on the bandwidth of the local weighting function which has to be chosen in advance. Smoothing spline regression (SSR): The idea of spline regression is to determine an 'optimal' age trajectory that maximizes its goodness of fit and the smoothness at the same time (Craven and Wahba, 1978; Silverman, 1985; Wahba, 1990). In particular, it optimizes a modified version of the sum of squares that additionally includes a roughness penalty term and a smoothing parameter λ that balances both desired properties of $g^{(k)}$:

$$S(g^{(k)}) \quad = \quad \sum_{i=1}^{m} \left(y_{ik} - g^{(k)}(age_i) \right)^2 + \lambda \int [\frac{d^2}{dx^2} g^{(k)}(x)]^2 dx \tag{3.3}$$

Then, the minimization of S specifies the age trajectory in the form of a piecewise cubic spline. According to the choice of λ, the 'optimal' trajectory can exhibit strong overfitting (i.e., $\lambda = 0$) or even a linear approximation (i.e., $\lambda \to \infty$) of the data. Favorably, Generalized Cross-Validation (GCV) has been suggested for automatic determination of the smoothness parameter (Craven and Wahba, 1978) using a tradeoff of goodness of fit and model complexity (in terms of estimated degrees of freedom). For a further discussion of model selection criteria see also (Fjell et al., 2010b). Figure 3.3 depicts the application of a nonparametric smoothing spline regression to estimate local age trajectories in a large sample of voxel-based morphometry data. Gaussian process regression (GPR): Nonparametric regression is also discussed from the perspective of Bayesian inference (Silverman, 1985). Thus it is reasonable to consider the whole structural age trajectory as a probabilistic entity. Instead of focussing on fixed estimates of age trajectories $g^{(k)}(age)$, a probabilistic perspective accounts for the substantial shape uncertainty of resulting

fits using cross-sectional MR data with between-subject variability and errors. GPR is a framework which directly allows modelling of trajectories as distributions with a mean and spread (Rasmussen and Williams, 2006). To put it simply, one can think of GPR as an equivalent to regression analysis using an infinite number of basis functions. In general, a Gaussian Process (GP) is a distribution of functions that is fully specified in terms of a mean function and a covariance function (or kernel). For our purpose, we define the mean and covariance function using the expectation and the covariance of the unknown true local age trajectory $g^{(k)}(age)$:

$$m^{(k)}(age) = \mathbb{E}[g^{(k)}(age)] \tag{3.4}$$

$$cov^{(k)}(age_1, age_2) = \mathbb{E}[(g^{(k)}(age_1) - m^{(k)}(age_1))(g^{(k)}(age_2) - m^{(k)}(age_2))] \tag{3.5}$$

Using this mean and covariance function allows us to consider the local structural differences (of voxel- or vertex k) in terms of Gaussian Processes (for details see Rasmussen and Williams, 2006):

$$g^{(k)}(age) \sim \mathcal{GP}(m^{(k)}, cov^{(k)}) \tag{3.6}$$

In order to build nonparametric generative models of age, GPs may be useful in the following ways: Firstly, specific constructions of mean and covariance functions allow the definition of priors over neuroanatomically plausible age trajectories including trends or smoothness constraints. Secondly, the priors can be conditioned on Gaussian MR-based structural data. This results in posterior distributions which characterize the local structural age trajectories given observations. Similar to loess and spline regression, GPR also requires the estimation of free (hyper-) parameters of the covariance and mean function.

In order to obtain estimates of the local age trajectories, the nonparametric regression methods have some drawbacks. Firstly, it is important to note that different nonparametric methods and implementations may vary with respect to the applied criteria for their optimization, i.e., what does 'optimal' mean quantitatively? This favors the application of free, publicly available tools with a high level of transparency such as the statistical package R R Project page and the Gaussian Processes for machine learning package Gaussian Process page. Secondly, the optimization of the hyperparameters (e.g. smoothness parameter of smoothing splines and covariance parameters of GPs) is computationally intensive and can be time consuming in a 'mass-univariate' application to local brain data. Alternatively, spatial generative models of age using smoothness priors might provide a promising alternative (Penny et al., 2005; Groves et al., 2009). Thirdly, inferences about trajectory shape are not accessible by simple test statistics. Thus, application studies often draw the nonparametric estimates of age-related trajectories without measures of confidence, irrespective of the substantial variability around the mean. However, LOESS and GPR also provide confidence intervals and variances, which might be useful for trajectory plots and formal inference about regional variability of age-related decline and comparisons of clinical groups in future studies (Cleveland and Grosse, 1991; Rasmussen and Williams, 2006). A

related issue is the inference about characteristic points of the timing of decline, e.g., ages of maximal acceleration of decline. Permutation testing or bootstrap resampling might be used to yield significance of regional differences and confidence intervals on estimates.

Multivariate recognition model: pattern-based estimation of individual's brain age

The recognition model class was predominantly motivated and developed in the field of machine learning and pattern analysis. Many approaches to classification and regression in high-dimensional datasets have evolved, often using kernel methods or Bayesian learning. Recognition models have also been successfully applied in developmental neuroimaging research (Bray et al., 2009; Franke et al., 2010). Only a few studies have aimed at finding a function that performs best in predicting the individual ages given a MR-based morphological marker:

$$age_i \quad = R(\mathbf{y_i}, \beta) + \epsilon_i, \quad \epsilon_i \sim \mathcal{N}(0, \sigma_\epsilon^2) \tag{3.7}$$

Here we use $\mathbf{y}_i$ to denote the whole preprocessed image of subject i (i.e., the ith row of $\mathbf{Y}$) and $\boldsymbol{\beta}$ is a vector of hyperparameters. In order to predict the age of individuals, we do not simply invert the local generative age trajectories $g^{(k)}(age, \boldsymbol{\beta}_k)$ because of two reasons. Firstly, according to the multidirectionality age trajectories are not assumed to be strictly increasing or decreasing functions of age. Conversely, lifespan trajectories are often expected to be three-phasic with increase, plateau and decrease, e.g., inverted-U shape (Fjell et al., 2010a). Secondly, according to Davatzikos (2004) and (Friston and Ashburner, 2004) a 'mass-univariate' approach is advantageous for the analysis of region specifc age effects, but it seems insufficient for predictions and clinical classification tasks. In particular, to optimally predict ages of individual subjects, the inter-regional dependencies of the local age effects should be taken into account. Using a 'mass-univarate' approach, these dependencies are expressed by correlated model errors over voxels- or vertices (Friston and Ashburner, 2004). In contrast, a multivariate model is able to account for correlations and redundancies in the high-dimensional structural images. This suggests using the whole preprocessed image as a multivariate input to a single prediction function R. In addition to univariate regression, the framework of Gaussian Processes is also capable of making predictions based on high-dimensional input-spaces (Rasmussen and Williams, 2006), e.g., morphological images. There is a large variety of covariance functions that can be applied, e.g., the squared exponential or rational quadratic, etc. In order to implement the age estimation model including prediction errors, one might apply the Gaussian Process regression with the following choice of a covariance function (see also Franke et al., 2010):

$$cov(age_i, age_j) \quad = \quad k(\mathbf{y_i}, \mathbf{y_j}) + \sigma_\epsilon^2 \delta_{ij}, \tag{3.8}$$

$$k(\mathbf{y_i}, \mathbf{y_j}) \quad = \quad \sum_{r=1}^{m} \frac{1}{\alpha_r} \phi_r(\mathbf{y_i}) \phi_r(\mathbf{y_j}), \tag{3.9}$$

$$\phi_r(\mathbf{y}) \quad = \quad exp(-\frac{1}{2l^2} |\mathbf{y} - \mathbf{y}_r|^2) \tag{3.10}$$

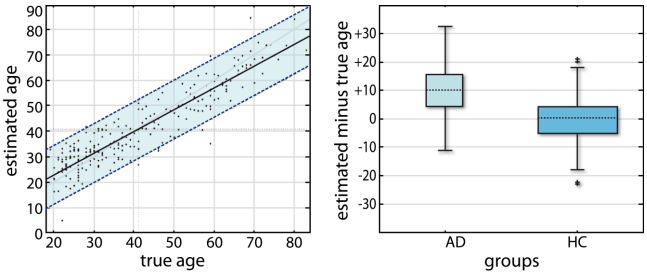

Figure 3.4: Application of a recognition model of age to cross-sectional voxel-based morphometry (VBM) data (modified from Franke et al., 2010). The recognition model was implemented using a relevance vector machine (RVR) which afterwards was trained on 410 healthy subject's grey matter segments after VBM preprocessing. Brain-based age estimation results in an independent test sample of $n = 245$ (left). The overall correlation between estimated and the true age is $r = 0.92$, and the overall mean absolute error is 4.98 years. Boxplots of estimation residuals, i.e., estimated age minus true age is shown for two subsamples from the ADNI database (AD with $CDR = 1$, NO with $CDR = 0$) (right). The gray boxes contain the values between the 25th and 75th percentiles of the samples, including the median (dashed line). The width of the boxes depends on the sample size. Figure and legend modified from Ziegler et al. (2012a)

Due to its particular structure, performing regression with kernel k is also called Relevance Vector Regression (RVR) (Tipping, 2001). The fundamental idea of GPR age estimation with relevance vector covariance is as follows: Firstly, we place basis functions ϕ_i on all m input images in the dataset. Secondly, we optimize the hyperparameters $\boldsymbol{\beta} = (\alpha_1, \ldots, \alpha_m, l, \sigma_\epsilon^2)$ (via marginal likelihood) which increases some α_i and therefore removes the contribution of the corresponding basis function ϕ_i to the covariance function. The remainders of the contributing images, $\mathbf{y}_i$, are called relevance vectors which constitute a sparse representation of the training images $\mathbf{Y}$. The covariance function with optimized hyperparameters β then specifies a Gaussian prior distribution. Third, if we condition the prior distribution on a given dataset of images, we obtain the posterior and the predictive distribution including estimated ages. Finally, in order to estimate the generalization error of the framework, the performance of the age estimator $R(\mathbf{y}, \beta)$ can be tested in an independent dataset or applying other cross-validation techniques (Schölkopf and Smola, 2002). Figure 3.4 depicts the application of the above presented multivariate recognition model to perform MR-based age estimation in healthy and clinical subjects (for details see Franke et al., 2010). A critical issue of multivariate recognition of age-related differences is the 'curse of dimensionality', i.e., the necessity of precedent feature selection or dimensionality reduction in the image space. Apart from multivariate dimensionality reduction techniques (der Maaten et al., 2008) downsampling might also be useful (Franke et al., 2010). Secondly, multivariate recognition of the aging brain structure is restricted to comparable large training samples obtained from semi-automated processing. Thirdly, after training there is low transparency of the fitted age model, i.e., it only contains implicit knowledge about the process of structural aging. Consequently, the strength of this approach lies in its ability to make predictions in unseen cases and applied clinical research.

Limitation of cross-sectional methods

There are substantial limitations of cross-sectional designs in brain aging research. Firstly, in order to analyze multidirectionality of local neuroanatomical development, one cannot exclude the effects of different birth cohorts and secular trends. In addition, the sampling may be age-biased resulting in an unrepresentative composition over ages (Raz and Rodrigue, 2006). Secondly, the sensitivity of detection of polynomial effects of age is expected to vary substantially with the sample distribution (e.g., range and size) and the true amount of between-subjects differences. Thirdly, the major concern here is that the presented models do not explicitly account for inter-individual variability of brain structure for fixed ages. All introduced generative models aim at estimating the average population brain structure as a process of age. However, this 'moving average' would simply overlook any subgroup with a more successful structural aging pattern (see Fjell et al., 2006). Consequently, by applying the above models, the obtained residuals represent an unknown mixture of the measurement and preprocessing errors and the true inter-individual variability of local brain structure. At least in part, repeated measures MRI allows these influences to be disentangled and provides valuable measures of reliability of MR-based morphometry.

3.2 Brain Structural Trajectories Over the Adult Lifespan

Gabriel Ziegler[1], **Robert Dahnke**[1], **Lutz Jäncke**[3], **Arne May**[4], **Rachel Aine Yotter**[1], **Christian Gaser**[1,2]

1 Structural Brain Mapping Group, Department of Psychiatry, Jena University Hospital, Jena, Germany.
2 Department of Neurology, Jena University Hospital, Jena, Germany.
3 Division Neuropsychology, Institute for Psychology, University of Zürich, Zürich, Switzerland
4 Department of Systems Neuroscience, Universitaets-Krankenhaus Eppendorf, Hamburg, Germany

Type of contribution Research article (published in Ziegler et al., 2012b)

Personal contribution G.Z. conceived and designed the study, adapted and implemented the algorithms for polynomial models and spline models, analyzed the MRI data, and wrote the paper. C.G. helped to conceive the study, preprocessed the data, generated the surface projections. R.D. helped to work with CARET, generated the surface figure, additionally photoshoped some plots, C.G, L.J., A.M., R.Y. corrected the paper.

3.2.1 Abstract

The aim of this large-sample cross-sectional voxel-based morphometry (VBM) study of anatomical brain data was to investigate linear and nonlinear age-related trajectories of grey matter volume in the human brain during the adult lifespan. To date, there are only a few structural brain studies investigating local nonlinear aspects at the voxel level, i.e., without using anatomical ROIs as a priori hypothesis. Therefore, we analyzed 547 T1-weighted MR images of healthy adult brains with an age range of 19 to 86 years, including 161 scans of subjects with ages 60 and older. We found that the gray matter volume in some regions did not linearly decrease over time, but rather exhibited a delayed decline. Nonlinear age trajectories were observed in the medial temporal lobe regions, the basal ganglia, and parts of the cerebellum. Their trajectories indicated a preservation of grey matter volume during the early adult lifespan. Interestingly, we found nonlinear grey matter structural dynamics specifically in parts of the brain that have been extensively discussed in the context of learning and memory. We propose a hypothesis in relation to the functional role of these brain regions that may explain these results.

3.2.2 Introduction

A major question in lifespan developmental neuroscience is how the brain changes as a function of aging. Previous neuroimaging studies have given some insight into the complexity of age-related grey matter changes (Raz and Rodrigue, 2006; Sowell et al., 2004). Methods employed included voxel-based morphometry (VBM) (Ashburner and Friston, 2000), estimates of cortical thickness across the brain surface (Dale et al., 1999; Fischl et al., 1999) or manual volume tracing. Longitudinal studies are able to measure true intra-subject age-related changes (Dotson et al., 2009; Driscoll et al., 2009; Fjell et al., 2009a; Marcus et al., 2010; Raz et al., 2005, 2004b; Resnick et al., 2003; Scahill et al., 2003; Thambisetty et al., 2010) and allow assessments of contributing factors and intersubject differences in aging (Raz et al., 2010, 2005). Unfortunately, these studies, although valuable, are rare and not yet capable of addressing age-related brain differences spanning several decades. To address the latter point, cross-sectional studies have been conducted to estimate the (population) mean trajectories of local grey matter changes over the entire adult lifespan. Age-associated volume differences during adulthood were found for manually (Allen et al., 2005; Lupien et al., 2007; Raz et al., 2004b; Sullivan et al., 1995, 2005, 2004) and automatically (Cherubini et al., 2009; Walhovd et al., 2005a, 2011) segmented brain regions of interest (ROI). Recent studies explored more spatially fine-grained age-related differences of adult brain structure by using surface-based (Fjell et al., 2009b,c; Salat et al., 2004; Sowell et al., 2007; Westlye et al., 2011) or voxel-based (Giorgio et al., 2010; Good et al., 2001; Grieve et al., 2005; Kennedy et al., 2009) analysis of cortical thickness, T1-intensity, or grey matter volume.

In order to focus on the question of how brain grey matter changes over an individual's lifetime, the lifespan perspective enables the discrimination of qualitatively different age trajectories, e.g., linear, quadratic, or more complex functions of age (see also Fjell et al., 2010a;

Jernigan and Gamst, 2005; Walhovd et al., 2011). From this point of view, aging of the brain is considered as a developmental process with certain inherent dynamics that can be studied via trajectories showing growth/decline, extreme values, and acceleration of the rates of change. Initial approaches investigating structural development during adulthood on the global level revealed linear trajectories of the total grey matter volume (Allen et al., 2005; Giorgio et al., 2010; Good et al., 2001; Grieve et al., 2005; Hasan et al., 2007) also, cortical grey matter volume (Sullivan et al., 2004; Walhovd et al., 2005a) was reported to be a linear function over adulthood. By introducing quadratic terms, two recent studies on large healthy adult samples demonstrated small significant improvements of the cerebral cortex volume model fit (Walhovd et al., 2011), at least for women (Fjell et al., 2009c). On the local level, ROI-based (i.e., region-wise) analysis revealed significant nonlinearities of volume trajectories during adulthood for medial temporal lobe, especially for the hippocampal region (Allen et al., 2005; Fjell et al., 2009c; Jernigan and Gamst, 2005; Kennedy et al., 2009; Lupien et al., 2007; Raz et al., 2004a; Walhovd et al., 2005a, 2011) and subcortical nuclei (Walhovd et al., 2011). However, these studies are limited by their a priori selection of anatomical ROIs, leaving the nonlinearity of other grey matter regions unexplored. Moreover, neuroanatomical subregions of larger ROIs can show nonlinear (i.e., qualitatively different) trajectories than the whole region in total, which would be completely overlooked by ROI-based analysis. Irrespective of their vital importance for research on lifespan development, plasticity, and aging, there are only a few structural brain studies investigating nonlinear aspects on the spatially fine-grained vertex- or voxel-wise level. Using VBM overcomes the [limitations of] existing ROI-based approaches, because it allows identification of unpredicted cortical or subcortical grey matter (sub)regions that exhibit a nonlinear volume function. In the large VBM study by Good et al. (2001), no local quadratic age effects on grey matter volume were observed. However, a nonlinear trend could be missed due to lack of subjects in the higher ages, since visual inspection of the published results revealed only 20 subjects with ages of 60 and older.

The purpose of the study proposed here is to illuminate previously unexplored areas of the brain with local nonlinear grey matter volume age trajectories for a large sample that includes a high proportion of subjects of advanced age. To accomplish this, we measured voxel-wise nonlinear age-related grey matter volume differences over the adult lifespan in a sample of 547 healthy adults ranging from 19-86 years. The large sample size included 161 datasets from subjects with ages 60 and older, providing increased estimation accuracy of estimated late-life grey matter differences. We used a two-step approach for (1) voxel-wise detection of quadratic age effects in grey matter volume and (2) estimation of local nonlinear age-related trajectories in the regions found to have significant quadratic age effects. In addition, we further elucidated at which age that age-related grey matter volume decreases start?

Table 3.1: **Demographical description of the sample**

Age group (years)	Subjects	Subjects from site[a] (1/2/3)	Females (%)	Ethnicity[b] (%)	Education[c] mean (SD)
19-29	88	30/40/18	40(45)	69/1/18/12	4.56 (0.97)
30-39	103	58/24/21	59(57)	76/3/15/6	4.76 (0.61)
40-49	88	49/28/11	44(50)	85/1/9/5	4.14 (1.15)
50-59	83	55/25/3	31(37)	83/4/7/6	3.81 (1.27)
60-69	123	77/39/7	45(37)	83/3/10/4	3.51 (1.54)
70-79	54	31/17/6	18(33)	89/2/6/3	3.46 (1.55)
80-86	8	6/1/1	5(63)	100/0/0/0	3.50 (2.07)
Total	547	306/174/67	242(44)	81/2/11/6	4.05 (1.03)

[a]Three separate subsamples from different scanning sites in London: Guys Hospital Philips 1.5T/Institute of Psychiatry General Electric 1.5T/Hammersmith Hospital with a Philips 3T scanner. [b]Percentage ratio of different ethnic groups in the whole IXI sample: Caucasian/Black/Asian/Other. [c]Education levels: 1 - no qualifications; 2 - O-levels, GCSEs, or CSE; 3 - A-levels; 4 - further education; 5 - university or polytechnic degrees. SD, standard deviation.

3.2.3 Materials and methods

Subjects

The publicly accessible IXI database includes T1, T2, and diffusion-weighted protocols of MR brain data from normal, healthy subjects with a wide age distribution (IXI Webpage). In order to investigate voxel-based morphometric differences in grey matter, the analysis was restricted to T1-weighted MR images. After selecting for completeness of imaging and demographic data, the full sample consisted of 547 T1-weighted standard anatomical brain images with corresponding ages from 19 to 86 years (mean age: 48.1 ± 16.6 years; 242 male/305 female). The data has been acquired at three separate institutions in London: Guys Hospital using a Philips 1.5T system, the Institute of Psychiatry using a General Electric 1.5T, and the Hammersmith Hospital with a Philips 3T scanner. These subsamples consisted of 306, 174, and 67 subjects, respectively. The T1-weighted imaging protocols with MP-RAGE sequence provided 150, 150, and 146 sagittal slices for the 3 scanners, respectively, with the same acquisition matrix 256×256 and in-plane resolution of $0.93 \times 0.93 \times 1.2mm^3$. The age distribution and demographic details of the IXI sample are presented in Table 3.1. 80.6 percent of the sample encompassed Caucasian subjects and 79.9 percent achieved advanced or even higher educational levels and certificates. The mean ages in subsamples of respective scanning sites were different (mean ages: 50.26/46.69/42.06 years, ANOVA site effect: $p < 0.0003$) but there was no interaction of gender and site with respect to age.

MR Image Processing

The major preprocessing and analysis steps were done in SPM8 (Wellcome Trust Centre for Neuroimaging, London, UK, SPM Webpage) using the VBM8 toolbox (VBM Webpage). The images were (1) corrected for bias-field inhomogeneities, (2) registered using a linear (i.e., 12-parameter

affine) and a nonlinear transformation, and (3) stripped of non-brain tissue in the T1-weighted images. Afterwards, some results from the SPM8 unified segmentation package (Ashburner and Friston, 2005) were used to initialize a VBM8 algorithm that classifies brain tissue in grey matter (GM), white matter (WM), and cerebrospinal fluid (CSF). This VBM8 segmentation procedure contains partial volume estimation (PVE) to account for mixed voxels with two tissue types (Tohka et al., 2004). The algorithm is based on an adaptive maximum a posteriori (AMAP) approach (Rajapakse et al., 1997) and subsequent application of a hidden Markov random field model (Cuadra et al., 2005). The AMAP estimation is adaptive in the sense that local variations of the parameters (means and variance) are modeled as slowly varying spatial functions. This accounts for intensity inhomogeneities and other local variations of intensity. Usually, the problem of normalization over a large age range is solved by generation of age-specific templates and priors (Wilke et al., 2008). However, our applied AMAP estimation does not rely on tissue priors, i.e., it overcomes segmentation bias that occurs due to the application of inappropriate tissue priors in elderly subjects with high atrophy. Therefore, the usual age-specific adaption of segmentation was not necessary. It is still possible that normalization errors occurred in brains showing stronger atrophy. In order to detect these deviations, we additionally included a further quality check based on inhomogeneity measures of the sample as implemented in the VBM8 toolbox. The covariance of voxel-based data was used to exclude subjects with extremal values and/or artifacts. Afterwards, resulting individual grey matter volume images were multiplied voxel-wise by the determinants of Jacobian matrices from SPM's nonlinear transformations before subsequent statistical analysis on local grey matter volumes. This modulation is done to adjust for local volume changes introduced by the nonlinear normalization. A final smoothing step was performed using Gaussian smoothing with a kernel of 4 mm full width at half maximum (FWHM). All analyses were performed on grey matter volume (GMV) images obtained using the above steps.

Analysis of linear age-related effects

To compare the total amount of age-related GMV differences in selected functional systems in the major lobes, we used a collection of bilateral regions of interest (ROI) as provided by the SPM Anatomy Toolbox v1.6 (Amunts et al., 2000; Eickhoff et al., 2005, 2006c,a; Geyer et al., 1999; Malikovic et al., 2007; Morosan et al., 2001; Rottschy et al., 2007; Scheperjans et al., 2008), based on cytoarchitectonic probabilistic maps (Eickhoff et al., 2007). ROI names and accordant functional systems from higher motor function, speech production and sensory systems are listed in Table S2. Prefrontal cortical areas 10, 46, and 24, and the ventral visual stream areas inferior temporal gyrus (ITG) and fusiform gyrus were added from SPM toolbox WFU PickAtlas 2.3 (Maldjian et al., 2003). In order to detect linear age-related differences in GMV, a single GLM with site factor and site-by-age interactions was used. To achieve a region-specific age-related trajectory, the voxel-wise estimated GLM parameters (for each site separately) were averaged and a mean trajectory was calculated by a subsample-size weighted mean. The resulting slopes

were used to estimate the annualized and total GMV loss from age 20 to 80 years. Due to the assumed linearity of GMV trajectories in this analysis, the choice of an interval spanning six decades is arbitrary and can be replaced by linear scaling of the estimated total GMV atrophy.

Analysis of nonlinear age-related effects

The key issue of this study is the voxel-wise identification of nonlinear age-related effects over adult lifespan. An appropriate model for nonlinear age-related GMV differences in a cross-sectional study (i.e., with large intersubject differences) must balance complexity such that it sufficiently maps inherent aging dynamics but also reduces degrees of freedom (Fjell et al., 2010b). Recent studies on structural brain aging that included nonlinearities support the usage of polynomial models up to degree 3 (Walhovd et al., 2011). Polynomials with higher degrees or exponential functions can be more accurate but at the same time introduce the danger of overfitting. Consequently, for the scope of this study, the detection of nonlinearities was performed by rejection of the linearity assumption via identification of significant second order (i.e., quadratic) age-related dynamics. A general linear model (GLM) was used to identify voxels in which quadratic functions of age significantly better explained the variance in GMV than linear models. To account for effects of different scanning sites, our full model included a site factor (with 3 levels and unequal variances) and age (as linear and quadratic covariates for each level). Model estimation was done via restricted maximum likelihood (ReML). Analysis of linear age-related effects was performed using all brain voxels in the grey matter region. In order to avoid detection of GMV nonlinearities due to processes in the adjacent white matter, the analysis of quadratic age-related effects included whole brain GMV values above an absolute threshold of 0.2. The site-by-age interactions were weighted and averaged per subsample to achieve mean effects. Weighted means of GLM parameters were corrected for multiple comparisons by a family-wise-error (FWE) method, resulting in voxel-wise thresholds of $t = 5.18$ ($p < 0.05$) for linear and $t = 4.83$ ($p < 0.05$) for quadratic effects.

Furthermore, our method contained a second step, which addressed the estimation of the adult lifespan trajectories in identified clusters with linear and nonlinear age-related effects. As recently suggested for model-free analysis of cross-sectional volumetric data, we used a non-parametric smoothing spline technique (Fjell et al., 2010b). According to Fjell et al. (2010b), using a quadratic model to detect nonlinearities by rejection of the linearity assumption is a valid approach. However, significance of the quadratic terms does not imply that the investigated development takes a quadratic course. That is, a parametric model is not necessary correctly specified without a priori knowledge about the true developmental model. Nonparametric smoothing splines are a local regression method that overcomes this limitation by only making assumptions about the smoothness of the model, which can be chosen by use of certain optimality criteria. Importantly, Fjell, et al. demonstrated that due to the locality of estimation, the nonparametric smoothing spline was less vulnerable to variations in the range of the sample than a quadratic model. In our study, the estimation of smoothing splines was performed in

the free software environment for statistical computing R (version 2.12) by using the function sreg of the fields package (R Webpage). After intra-cluster averaging of GMV, the data was approximated by cubic smoothing spline functions with a smoothness parameter minimizing the generalized cross-validation (GCV) criterion (for details see also Wahba, 1990). Furthermore, the ages with strongest acceleration of decline and estimated total GMV loss over the adult lifespan were calculated for all clusters and ROIs showing significant nonlinear age-related trajectories. An analysis of maximum GMV was performed on both approaches, i.e., the second order models and the smoothing spline estimations of adult trajectories. Notably, the nonparametric estimation of trajectories in clusters with significant quadratic age-related effects is provided in an explorative manner, i.e., not focussed on aspects of formal inference. For sake of readability we prefer using the notion 'nonlinear' to refer to the quadratic model used for detection and also for the smoothing spline model used for estimation of the developmental trajectories.

As outlined in (Eickhoff et al., 2006b, 2007), cytoarchitectonic maps obtained from post-mortem brains provide objective a priori ROIs to test anatomical hypotheses in functional and structural neuroimaging. The cytoarchitectonically verified maps were proposed to precisely analyze anatomical MR scans, also in the comparably small subdivisions of the MTL network (Amunts et al., 2005). In order to differentiate age-related trajectories in MTL subregions, we estimated developmental trajectories in bilateral a priori ROIs of the amygdala and hippocampal subregions, as provided by SPM Anatomy Toolbox (Amunts et al., 2005). The used ROIs (with labels) included the cornu ammonis 1-3 (CA), the dentate gyrus including fascia dentata and CA4 (FD), the subicular complex (SUB), the entorhinal cortex (EC), and the amygdala (AMG).

3.2.4 Results

Linear trajectories and estimates of total GMV loss during adulthood

Cortical surface projections of linear age-dependent t-values and slope parameters are depicted in Figure 3.5. The large sample reveals significant negative linear age-related GMV differences in almost all areas of the cerebral cortex. By inspection of the regression slopes (corresponding to annualized rates of atrophy) of voxels with linear age effects (threshold: $t = 5.18, p < 0.05$, FWE-corrected), age-related decreases are most pronounced in the frontal and parietal lobes and less pronounced in the temporal and occipital lobes. The frontomedial and insular regions, the inferior frontal gyrus, and the inferior parietal lobe show stronger age effects on GMV during adulthood while the middle and inferior temporal gyrus and the occipital brain regions are either less affected or unaffected. The results of the linear ROI analysis for specialized sensory, motor, and selected prefrontal cortex regions are summarized in Table 3.2. Furthermore, Figure 3.6 visualizes differential estimates of lifespan GMV atrophy in selected extrastriate regions of the ventral and dorsal visual processing streams. The ventral stream areas human V3v (hOC3v) and inferior temporal gyrus revealed low estimated GMV atrophy with 0.37% and 0.32% p.a., respectively (total: 22% and 19%). The fusiform gyrus exhibited the lowest estimate of analyzed

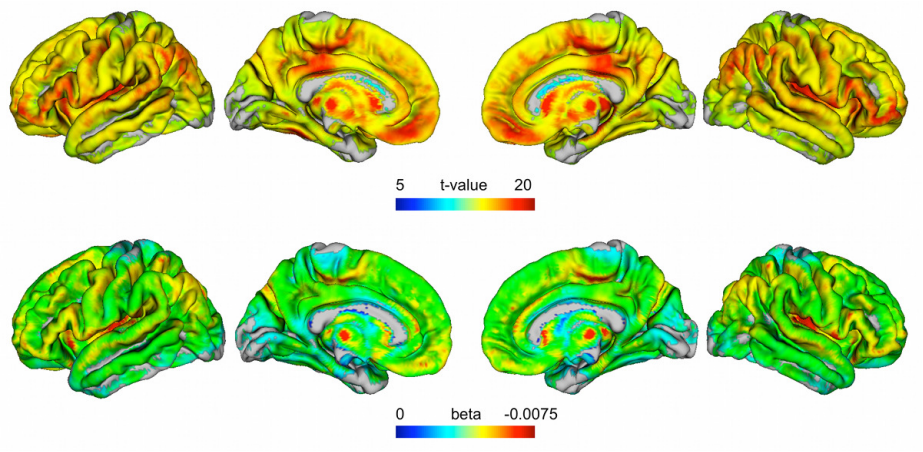

Figure 3.5: Shown are cortical projections of linear age regression parameters on a central surface template from FreeSurfer. The projection method searches for the maximum t-value from the linear age model within ± 5 mm of the surface normal. The t-values (upper row) indicate brain regions of significant linear age-related decreases in the GLM. Non-colored (gray) areas were not significant. The results were corrected for multiple comparisons by FWE (voxel threshold $t = 5.18, p < 0.05$). The color-coded beta values (or regression slopes) (lower row) of the same (maximum t-value) voxel indicate the rate of age-related changes in the linear cross-sectional model of GMV. Figure and legend from Ziegler et al. (2012b)

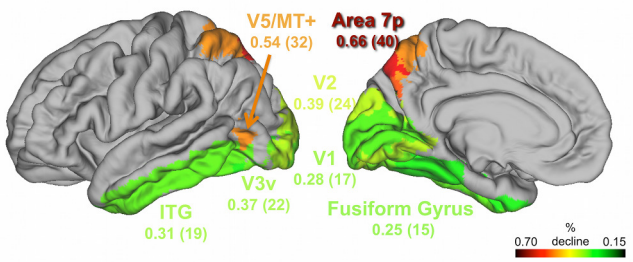

Figure 3.6: Differential pattern of annualized (total adult lifespan) GMV atrophy in analyzed ROIs of the dorsal and ventral visual streams in 547 healthy subjects. Ventral stream: hOC3v (V3v), inferior temporal gyrus (ITG), fusiform gyrus. Dorsal stream: V5/MT+, area 7. Annualized rates are given in terms of percentage reduction of GMV per anno. Total adult lifespan GMV atrophy is estimated by percentage reduction of GMV from age 20 to 80. GMV is modeled as a linear function of age. All analyzed grey matter voxels are significant with respect to threshold $t = 5.18$ ($p < 0.05$) using FWE correction for multiple comparison. Figure and legend modified from Ziegler et al. (2012b)

Table 3.2: **Annual rates of decline in linear ROI models**

brain region of interest	size of region in voxel (bilateral)	annualised GMV loss in % p.a. (total % from age 20 to 80)
visual system		
Area 17 (V1)	10622	0.28 (17.1)
Area 18 (V2)	7595	0.39 (23.6)
dorsal		
V5/MT+	375	0.54 (31.9)
Area 7a	6911	0.57 (34.2)
Area 7m	711	0.60 (35.8)
Area 7p	2798	0.66 (39.7)
Area 7pc	1315	0.54 (32.4)
ventral		
hOC3v (V3v)	3013	0.37 (22.1)
hOC4v (V4v)	3038	0.33 (19.6)
inferior temporal gyrus	16292	0.31 (18.6)
fusiform gyrus	11422	0.25 (14.8)
auditory system		
TE1.0	1015	0.64 (38.2)
TE1.1	790	0.57 (33.9)
TE1.2	462	0.60 (35.7)
TE3	1981	0.63 (37.8)
somatosensory system		
Area 1	4155	0.60 (35.8)
Area 2	4362	0.57 (33.8)
Area 3a	2405	0.46 (27.7)
Area 3b	3609	0.57 (33.9)
OP1	2590	0.58 (35.0)
prefrontal cortex		
Area 10	8676	0.54 (32.6)
Area 46 (DLPFC)	2798	0.60 (35.8)
Area 24 (dMCC)	2728	0.36 (21.5)
Area 44 (Broca's area)	4901	0.63 (37.8)
Area 45 (Broca's area)	4774	0.66 (39.7)
motor cortex		
Area 6 (premotor/SMA)	21064	0.58 (34.9)
Area 4a	5580	0.50 (30.1)
Area 4p	2431	0.63 (37.6)
parietal cortex		
hP1 (aIPS)	1618	0.37 (22.1)
hP2 (aIPS)	916	0.44 (26.2)
hP3 (aIPS)	1311	0.52 (31.2)
PF (IPC)	4495	0.53 (31.7)
PGa (IPC)	4300	0.60 (35.8)
PGb (IPC)	5354	0.64 (38.1)

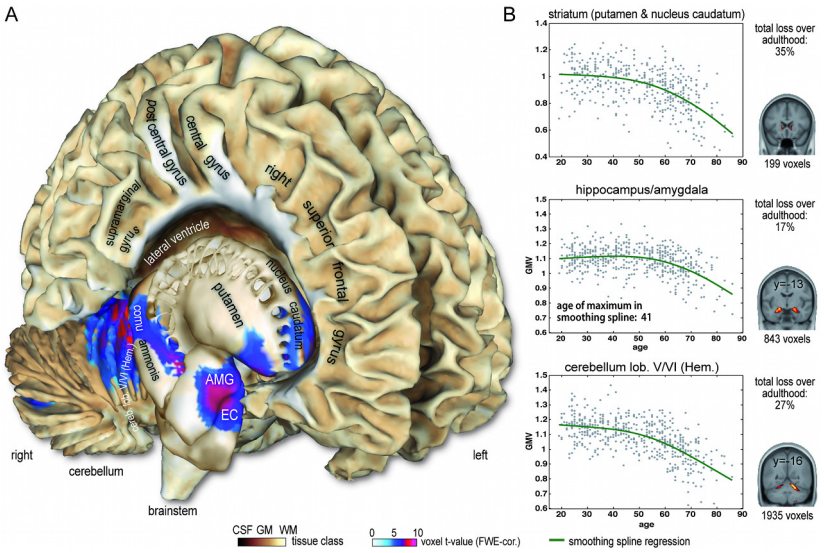

Figure 3.7: (A) Significant quadratic age effects on human GMV over adult lifespan are projected on the right hemisphere of Colin's brain. The results were corrected for multiple comparisons by FWE (voxel threshold $t = 4.83$ ($p < 0.05$); extent threshold $k = 50$ voxels ($p < 0.0001$)). Parietal operculum cluster is not depicted. (B) Estimated developmental trajectories of mean GMV for right hemisphere clusters in the striatum, hippocampus-amygdala complex, and cerebellum. A mean trajectory is calculated using sample size weighted means of subsample trajectories for different scanning sites to remove between-scanner variance. The given values of total loss over adulthood are percentage reductions of GMV from age 20 to 80. Figure and legend from Ziegler et al. (2012b)

neocortical ROIs with 0.25% p.a. (total: 15%). In contrast the dorsal stream areas V5/MT+ and area 7 showed strong age-related effects with up to 0.67% GMV reduction p.a. (total: 40%).

Nonlinear trajectories of local grey matter volume

On global level, our sample did not exhibit lifespan nonlinearities of normalized total grey matter and white matter volume. In contrast, local voxel-based GLM analysis revealed brain clusters having nonlinear age effects in the medial temporal lobe, the basal ganglia, and the cerebellum (see Table 3.3). Figure 3.7A depicts the right hemisphere clusters exhibiting nonlinear age-related GMV, projected on an anatomical T1 template surface. Strong nonlinear age effects were observed in the left and right anterior hippocampus, as well as further voxels in the adjacent parahippocampal and amygdala regions. For the polynomial model, inclusion of a quadratic age predictor increased the explained variance of mean cluster GMV by 11% and 14% for left and right hippocampus respectively. Furthermore, we identified right cerebellar, nucleus caudate, and putamen clusters, as well as nonlinear age effects in the posterior insula (in a subregion of parietal operculum 2 (OP2)) and left ventral orbitofrontal cortex. The data plots and estimated age-related trajectories for clusters in the right hippocampus, cerebellum, and striatum are shown in Figure 3.7B. To further quantify characteristics of brain regions with nonlinear trajectories, the age of maximum GMV (for both quadratic and non-monotonic spline trajectories) and estimated total GMV loss over the adult lifespan were calculated. All clusters

Table 3.3: **Local wholebrain results for nonlinear age effects on grey matter volume.**

brain region	hemi-sphere	clustersize in voxels	voxel t-value (FWE-corr.)	peak MNI MNI coord. (mm)			explained variance gain	age of max. GMV in quadratic model	age of max. change of slope of spline model
				x	y	z			
hippocampus/amygdala	left	1003	8.99	-28	-15	-18	14	41.3	59
cerebellum lob. V/VI (Hem.)	right	1935	8.61	15	-54	-17	7	30.8	54
hippocampus/amygdala	right	843	7.76	30	-13	-20	11	40.2	59
cerebellum lob. VII (Hem.)	right	1014	7.09	20	-61	-57	7	33.2	57
cerebellum lob. VI/VII (Hem.)	left	880	7.05	-20	-55	-18	6	31.8	55
striatum	right	199	7.03	18	10	-9	6	32.5	56
parietal operculum	left	91	6.86	-36	-19	16	5	26.6	55
parietal operculum	right	91	6.64	36	-16	16	4	23.1	50
orbitofrontal cortex	left	64	6.57	-27	35	-17	7	34.5	59
nucleus caudate	left	66	6.40	-12	20	0	4	30.5	55
cerebellum lob. VII (Hem.)	left	212	6.26	-20	-79	-35	5	33.3	54
putamen	left	93	6.23	-16	8	-12	5	30.2	52
cerebellum lob. VIII (Vermis)	right	72	5.99	6	-72	-44	5	33.4	57

Listed are cluster size, peak t-values with coordinates, percentage increase of explained variance of GMV by inclusion of a quadratic age predictor, ages of maximum GMV in quadratic model, and the ages of maximum change of slope in the smoothing spline model. All reported brain regions are significant with voxel threshold t=4.83 (P ¡ 0.05) and extent threshold k=50 voxels (p ¡ 0.0001) using FWE correction.

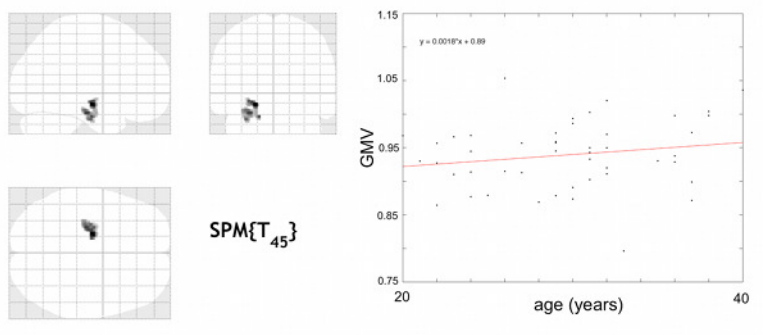

Figure 3.8: Voxel-wise test for linearly increasing GMV in 47 young adult subjects (GROUP1, ages 20 to 40), with voxel threshold $t = 1.69$ ($p < 0.05$, uncorrected) and cluster threshold $k = 215$ voxels ($p < 0.05$, uncorrected). There was a 4% GMV increase of mean cluster linear regression during early adulthood (estimated in GROUP2, $n = 47$, ages 20 to 40). Figure from Ziegler et al. (2012b).

exhibiting nonlinear age-related volumetric effects revealed strongest negative acceleration of GMV in middle or late adult lifespan. Furthermore, the cluster-specific parameters suggested the exceptionality of the hippocampus-amygdala complex, with the latest onset of age-related structural decline (estimated maximum GMV at about 40 years for quadratic and also non-parametric models) and small total loss during adult lifespan (17% for right hemisphere). The observed non-monotone trajectory in the hippocampus-amygdala complex raised the question whether there are indications for positive age associations of grey matter volume in this particular cluster. Therefore, we conducted a post hoc analysis on a subsample of 94 adult subjects with ages 20 to 40. We used a split-half approach in order to (a) detect clusters with linearly increasing GMV in half of the subsample (GROUP1, $n = 47$, ages 20-40 years) and to (b) study the cluster-specific GMV differences in the second half of the subsample (GROUP2, $n = 47$, ages 20-40 years). This technique avoids the risk of inferential errors about the size of local age-related increases in GMV due to double-dipping (Kriegeskorte et al., 2009). For low thresholds (primary: $t = 1.69, p < 0.05$, unc., extent: $k = 215, p < 0.05$), we observed a coherent cluster restricted to the left hippocampus (see Figure 3.8) in GROUP1. Within this cluster, the linear trajectory indicated an early adult GMV volume increase of 4% in GROUP2.

In order to summarize the age-related dynamics in grey matter regions with and without nonlinear age effects, Figure 3.9A shows estimates of the GMV trajectories of analyzed regions. GMV is normalized by volume at age 20 to make development between brain regions comparable. For the striatum and the cerebellum, we observed small negative age effects on GMV during early adulthood. After early adulthood, the estimated trajectory shows a stronger decline, reaching the mean neocortical volume trajectory at older ages. The results of our ROI-based test for nonlinear age effects in medial temporal lobe volume trajectories are summarized in Figure 3.9C and D. In contrast to all other analyzed MTL regions, the trajectory in the subicular complex ROI exhibited no nonlinear age effect. Figure 3.9C shows the estimated spline trajectories (relative to GMV at age 20) of the MTL subregions. All subregions exhibited the strongest adult acceleration of GMV decline during the ages 55 to 65 (see Figure 3.9D). Notably, the estimated spline

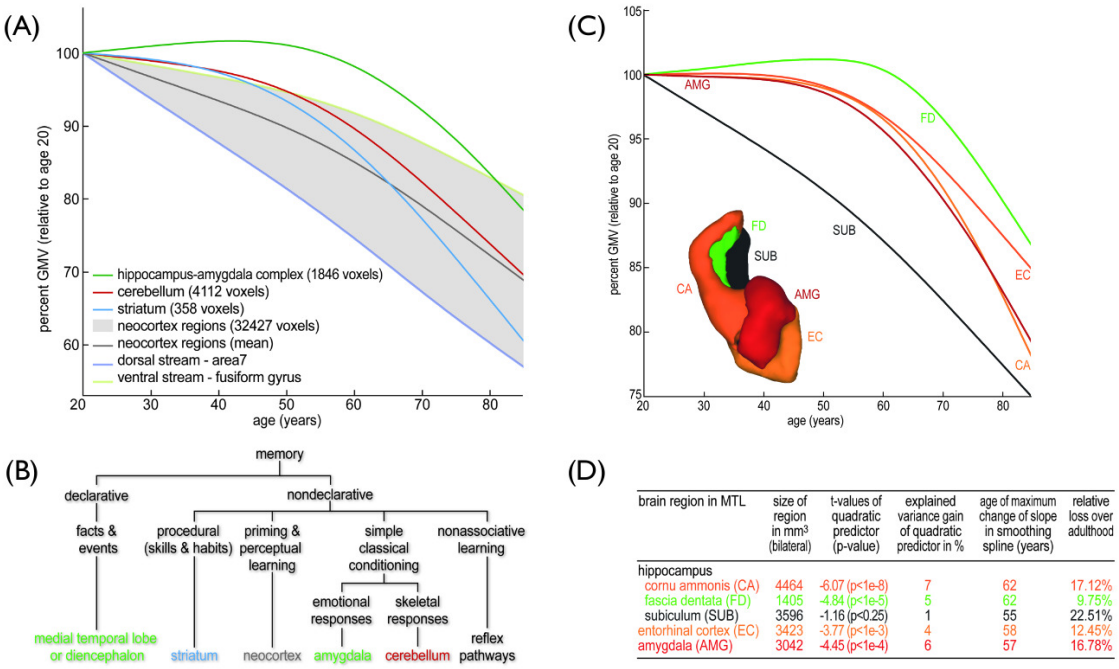

brain region in MTL	size of region in mm³ (bilateral)	t-values of quadratic predictor (p-value)	explained variance gain of quadratic predictor in %	age of maximum change of slope in smoothing spline (years)	relative loss over adulthood
hippocampus					
cornu ammonis (CA)	4464	-6.07 (p<1e-8)	7	62	17.12%
fascia dentata (FD)	1405	-4.84 (p<1e-5)	5	62	9.75%
subiculum (SUB)	3596	-1.16 (p<0.25)	1	55	22.51%
entorhinal cortex (EC)	3423	-3.77 (p<1e-3)	4	58	12.45%
amygdala (AMG)	3042	-4.45 (p<1e-4)	6	57	16.78%

Figure 3.9: (A) Estimated GMV trajectories are plotted for identified brain regions in cerebellum, striatum, and MTL that revealed significant nonlinear age-related differences. Blue, red, and green lines represent the mean smoothing spline trajectory over all clusters in the same (bilateral) brain region. The grey background area represents the range of trajectories from 34 a priori defined neocortical ROIs, which exhibited no quadratic age effects. The ventral stream - fusiform gyrus and dorsal stream - area 7 were found to be the upper and lower boundary of all 34 analyzed ROIs. Mean neocortex smoothing spline regression was added for comparison (grey line). Development is delineated in units of relative GMV with respect to GMV at age of 20. (B) A taxonomy of long-term memory systems by Squire (2004) lists the brain structures thought to be especially important for each form of declarative and non-declarative memory. Color-coding illustrates that significant clusters of whole-brain voxel-wise tests for nonlinearity were mainly observed within brain structures that are associated with learning and memory. (C) Aging trajectories are plotted for a priori defined medial temporal lobe subregions. Regression plots within ROIs were achieved by subsample size weighting of site mean spline regressions (over all voxels in ROI). For comparison of regressions between analyzed subregions, the modeled GMV is depicted in units of GMV relative to age of 20. Also shown is a surface reconstruction of used ROI masks in 3D voxel space. Subregions: CA - cornu ammonis 1-3, EC - entorhinal cortex, FG - dentate gyrus inc. fascia dentata and CA4, SUB - subicular complex. AMG - amygdala. (D) Test of lifespan nonlinearity of MTL subregion age trajectories using quadratic age predictors in a second-order polynomial model. Percentage gain of explained variance of GMV data included the quadratic age predictor. Estimation of ages with the strongest change in slope was obtained from the smoothing spline model for the medial temporal lobe subregions during the adult lifespan. The estimated GMV loss is the reduction of GMV at age of 80 (as modeled by smoothing splines) relative to age of 20. Figure and legend from Ziegler et al. (2012b).

trajectory of the FD region (including the dentate gyrus) shows the lowest estimated total GMV loss over adult lifespan to be about 10%.

3.2.5 Discussion

Previous studies investigating age-related effects have already suggested a nonlinear progression of grey matter volume dynamics in a priori hypothesized regions of the brain, especially in the MTL (Raz et al., 2004a). However, the preference for linear approximation of a continuously changing process (DeFelipe, 2006) may be one reason for some contradictory results in aging literature (for review see Walhovd et al., 2011). To address this problem, here we used a framework for detection and estimation of voxel-wise nonlinear developmental trajectories in order to quantify local trajectories of age-related differences in grey matter volume during the adult lifespan. We conducted a large-sample VBM analysis to reliably identify networks or small brain regions showing nonlinear grey matter volume dynamics, which denote changes in the annual rate of atrophy. Specific nonlinearities of structural trajectories might be related to the preservation of local brain volume during the early years of adult lifespan and a late acceleration of age-related decline.

Linear age-related differences of grey matter volume

First, we successfully replicated earlier VBM findings that showed stronger age-related effects in the frontal and parietal lobes compared to the temporal and occipital lobes in cross-sectional (Good et al., 2001; Smith et al., 2007) and longitudinal (Resnick et al., 2003) studies. The ROI analysis points out that primary and secondary visual regions and especially the ventral visual stream areas show much smaller age-related differences than dorsal visual stream regions, prefrontal cortex regions, motor areas, and primary/secondary cortices of other sensory modalities. This is in line with manual (Raz et al., 2004a, 2005) and automated volumetric (Good et al., 2001) findings. Interestingly, research on brain maturation has provided information about differential preservation and vulnerability patterns in visual processing streams. Particularly, fusiform regions seem to continue maturing into late adolescence and some authors also suggest high experience dependency of its development (Golarai et al., 2010; Grill-Spector et al., 2008). In our cross-sectional study, we observed eminently low estimates of adult lifespan atrophy of grey matter volume in the fusiform gyrus. However, we can only speculate that the observed low annualized rates of GMV loss in the fusiform gyrus may be related to its (adaptive) role in visual processing and functional plasticity (Bukach et al., 2006; Tarr and Gauthier, 2000). Moreover, the above reported strong effects of age on GMV in the dorsal stream areas are in line with the recently observed vulnerability for developmental disorders of visual motion processing (Braddick et al., 2003; Gunn et al., 2002; Mendes et al., 2005). Finally, stronger age-related GMV differences in the dorsal part of the highly interconnected visual system network might be considered in studies about functional dedifferentiation within (Chen et al., 2002; Park et al., 2004) and between (Haxby et al., 1991; Grady et al., 1994) visual processing streams.

Nonlinear trajectories over the adult lifespan

In order to address local nonlinear age-related differences in adult GMV, we applied a framework for detection and nonparametric estimation of the mean cross-sectional trajectories with quadratic age-related components. In contrast to ROI-based methods, our voxel-based approach is able to detect even very small grey matter regions that exhibit nonlinear age-related differences. The 547 healthy subjects revealed nonlinear GMV development in the bilateral anterior hippocampus-amygdala complex, the cerebellum, the striatum, and moreover small portions of the parietal operculum and the left ventral orbitofrontal gyrus. Therefore, this large cross-sectional VBM study supports previous manual (Allen et al., 2005; Kennedy et al., 2009; Raz et al., 2004a) and automated (Walhovd et al., 2005b,a, 2011) volumetric studies, suggesting nonlinear development in the human hippocampus during the adult lifespan. Moreover, the finding of a nonlinear developmental trajectory in hippocampus-amygdala complex may be related to cross-sectional (Good et al., 2001; Grieve et al., 2005; Sullivan et al., 2005; Walhovd et al., 2005a) and longitudinal (Fjell et al., 2009a; Raz et al., 2004a) evidence, indicating the preservation of hippocampal volume during the early and middle adult lifespans and a more pronounced late decrease of volume. As further support, recent work showed slightly increasing grey matter volume in the hippocampus-amygdala complex in adolescents and early adults (Ostby et al., 2009). Interestingly, our post hoc analysis suggested small positive age effects of local volume in parts of the hippocampus, which continue to the age of about 40. This question should be further addressed by carefully selected longitudinal studies about healthy brain aging that include demographic, behavioral, and cognitive data. Our whole brain voxel-wise analysis also shows nonlinear adult volume trajectories in parts of the cerebellum and the basal ganglia. The local GMV within these clusters exhibits rather small GMV differences with respect to age during early adult lifespan, while volumes in many neocortical regions already seemed to decline (see Figure 3.9A). However, this study was concerned with voxel-based local detection and estimation of nonlinear trajectories of GMV during the adult lifespan, which did not include specific tests for between-trajectory comparisons.

Structural trajectories in the medial temporal lobe

Recent large sample cross-sectional MRI studies gave some insights into the complexity of adult lifespan volume trajectories in several subcortical structures, including the hippocampus and the amygdala (Fjell et al., 2009c). There is also a growing interest to differentiate hippocampal subfields with respect to age-related effects. In a recent study of La Joie et al. (2010), VBM with millimeter resolution appeared as a reliable automated technique to distinguish cornu ammonis and subicular complex regions of the hippocampus for cross-sectional estimation of age-related differences over adulthood. Therefore, we tested for nonlinearity of grey matter volume trajectories in the MTL network by ROI-based analysis of the bilateral amygdala, subicular complex, entorhinal cortex, cornu ammonis 1-3, and dentate gyrus (including fascia dentata and CA4). The applied ROIs are based on cytoarchitectonic analysis of human brains and take into

account the intersubject variability of brain structures by maximum probability maps (Amunts et al., 2005; Eickhoff et al., 2006b, 2007). We observed significant nonlinear age effects on GMV in all MTL subregions except for the subicular complex. Therefore, this large sample VBM analysis supports recent results about differential age-related effects within hippocampal subregions and the subicular complex (La Joie et al., 2010). Post hoc analysis of the nonlinear developmental trajectories in the MTL subregions indicated an acceleration of volume loss around the age of 60.

Research on age-related changes in cellular morphology gave insights in the developmental processes that may be related to the local volume trajectories of the cerebrum and MTL (Baumann and Pham-Dinh, 2001; Burke and Barnes, 2006; Flood, 1991; Flood et al., 1985, 1987b,a; Hof and Morrison, 2004; Mora et al., 2007; Peters et al., 1998). Based on recent research on cellular plasticity, Klempin and Kempermann (2007) hypothesized that hippocampal neurogenesis is related to demand- and experience-dependent optimization of DG-CA3 connections for adult processes of learning and memory (see also Pereira et al., 2007). Interestingly, we observed the lowest (10%) estimates of total adult GMV atrophy in the hippocampal FD region, which includes the dentate gyrus and the CA4 region. But we have to admit that our study lacks the resolution to obtain a reliable segmentation of the separate dentate gyrus subregion. Therefore, this result needs further investigation using high resolution MRI over a wide age-range. Notably, earlier studies suggested focal cell death in the human subicular complex due to aging, which might be related to our finding of the early adult decline of GMV trajectories in this particular region (Simić et al., 1997; West et al., 1994). Future multimodal studies on hippocampal cellular plasticity are needed to clarify the complex relation of volumetric changes in MTL (as measured by MRI) and focal changes of neuronal and glial density or dendritic extent. One could argue that an important issue to the observation of nonlinear trajectories in parts of cerebrum and MTL is myelination. The latter is known to be a late developmental process, specifically in humans (Baumann and Pham-Dinh, 2001). Our MRI-based approach contained a segmentation algorithm that included partial volume estimation (Tohka et al., 2004). In order to reduce influences due to adult formation of myelin, we applied an absolute voxel-wise GMV threshold of 0.2. Thus our analysis of GMV nonlinearities was restricted to all grey matter voxels with explicitly high grey matter volume content. Therefore, the presented nonlinear volumetric trajectories are most likely due to processes within grey matter tissue.

In order to interpret the spatial pattern of local deviations from linearity, we speculate that it might be related to a localized delay of declining structural brain integrity during the adult lifespan. According to theories about aging, the nonlinear trajectories may indicate a localized altered interaction of progressive and regressive neurobiological changes as a process of normal aging (Sowell et al., 2004). Recent studies emphasize the reciprocal dynamics of biological, genetic, and environmental factors contributing to brain development over the lifespan (Baltes et al., 2006). Even though it is still unknown to what extent these factors drive local GMV dynamics, the pattern of delayed decline in MTL, basal ganglia, and cerebellum might not be completely independent of their functional role for adaptive behavior. Interestingly, we observed

nonlinear age-related trajectories of local grey matter volumes in parts of the brain that have been extensively studied in the context of learning and memory (Squire, 2009). In our whole brain local analysis of grey matter volume, more than 96% of brain voxels that exhibited nonlinear age-related effects over the adult lifespan were found within systems that have been associated with declarative and procedural memory or classical conditioning (Figure 3.9B). Unfortunately, due to a lack of psychometric data, we were not able to relate observed structural dynamics to cognitive or behavioral factors. However, recent longitudinal studies on training-induced neuroanatomic correlates demonstrated substantial GMV increases in the adult MTL due to acquisition of abstract knowledge (Draganski et al., 2006) and also motor skills (Boyke et al., 2008). It is tempting to consider the hypothetical construct of a "cognitive or brain reserve" (Stern, 2009) for maintenance of cognitive performance in face of neurodegenerative changes due to aging and dementia. According to Stern (2009), a reserve could be also expressed by inter-subject differences of regional brain volumes, and this would also apply to temporal shifts of their decline.

However, the limitation of this study is that a cross-sectional design is incapable of separating intersubject differences (e.g., birth cohorts) and true intrasubject changes as a process of aging. On the one hand, the large intersubject differences reduce the sensitivity for the detection of age-related changes in cross-sectional designs (Du et al., 2006) and may therefore underestimate the real effects. Certain regions with nonlinear age-related trajectories could have been missed. On the other hand, a large sample size is known to increase the sensitivity for detection of linear and nonlinear age-related effects. Unfortunately, for age-related brain changes over the adult lifespan, there is still a lack of appropriate longitudinal data. Another critical issue is related to the GLM-based detection of nonlinearities, which could be further extended to assess higher order effects of age. However, future correlational studies and behavioral paradigms may help to elucidate the potential of active cognitive and/or behavioral training for structural preservation of MTL and learning related structures.

3.3 Detection of Pathological Aging on a Single Subject Level

Gabriel Ziegler[1], **Robert Dahnke**[1], **Christian Gaser**[1,2]

1 Structural Brain Mapping Group, Department of Psychiatry, Jena University Hospital, Jena, Germany.
2 Department of Neurology, Jena University Hospital, Jena, Germany.

Type of contribution Manuscript based on conference abstract, presented at the Annual Meeting of Human Brain Mapping, 2012, Beijing, China.

Personal contribution G.Z. conceived and designed the framework, adapted and implemented algorithms for Gaussian process confidence maps, analyzed the MRI data, and wrote the manuscript. R.D., C.G. preprocessed the data, R.D. calculated global brain parameters and supported server administration for calculations.

3.3.1 Abstract

In order to support the very process of clinical decision making on healthy vs. pathological aging in single cases, we here propose a computerized knowledge-based system. This is realized by a transparent quantitative assessment of patient's regional brain alterations, termed local confidence maps. The approach is twofold. Firstly, we built a generative (or encoding) model of the normative structural decline of local grey matter volume. It accounts for the general course of age-related decline and its variability in normal aging. Secondly, the single patient's brain structure is compared to this normative reference, resulting in probabilistic expressions of the regional brain alterations, i.e., the confidence maps. These maps are introduced to serve as a valuable and accurate extension of the diagnostic information for subsequent clinical decisions.

3.3.2 Introduction

There is a consensus that local grey matter volume exhibits a substantial decline as a process of healthy aging (Fjell and Walhovd, 2010). In addition the individual decline parameters often exhibit large variations across subjects (Raz et al., 2010). Therefore, visual assessment of healthy vs. pathological regional atrophy is a challenging task even for experienced radiologists. Recent studies emphasized the potential of computerized methods and multivariate classification technique to support diagnosis and treatment of Alzheimer's disease and dementia (Klöppel et al., 2008; Westman et al., 2011). In particular the MR-based detection of early stage AD and later conversion in patients with mild cognitive impairment (MCI) revealed promising results (Davatzikos et al., 2011; Misra et al., 2009). Unfortunately, the existing whole brain image classification techniques strongly lack transparency of the underlying process of clinical decision making. Consequently, the results of computerized black box decisions are highly accurate but not yet sufficient for the clinical practice. We here aim at bridging this gap between multivariate classifiers and visual local analysis of single patient's brain who is at risk developing dementia or another form of pathological brain aging. In order to directly support the conclusions made by medical experts, we propose a computerized system that quantifies and visualizes the single patients local brain alterations under examination, termed confidence maps. Then multivariate classification indices *combined* with the highly transparent confidence maps provide a valid and useful information basis for subsequent clinical decisions made by medial experts instead of computers.

3.3.3 The Generative model of normative structural decline

For the purpose of a reference for valid single case decisions we used Voxel-Based Morphometry (VBM) in a large healthy aging brain database (n = 1338, ages 18-94, mean 47.42, std 19.7) which has been pooled using healthy subjects from the freely available MRI sample of ADNI (n=216), OASIS (n=316), IXI (n=561), and the INDI (n=245) research projects. A nonlinear spatial normalization transformed all subjects images to a reference template in order to afford

between-subjects comparisons (Ashburner, 2007). The obtained database was expected to reflect the aging-related differences as well as normative individual variability in terms of fine-grained maps of local grey matter volume (GMV) content. At first, we focused on the estimation of the age-specific normative reference distributions of the local grey matter volume contents. In particular, Gaussian Process Regression (GPR) (Rasmussen and Williams, 2006) was applied to built a generative (or encoding) model of the normative structural aging process on the local voxelwise level. In order to account for additional age-independent sources of variance, the generative model supposes local grey matter volume measures y across adulthood to be a function of multiple person specific and acquisition specific factors. In particular, we focussed on the person specific variables age, the global grey matter volume, and the total intracranial volume, i.e., denoted by $\mathbf{x}_{sub} = [age, TGM, TICV]$. Moreover acquisition specific variables, in particular the signal-to-noise ratio and the MR image non-uniformity histogram entropy (see e.g. Belaroussi et al., 2006) were also included as potential sources of variance across multiple imaging centers, i.e., denoted by $\mathbf{x}_{meth} = [snr, h]$. Then the lifespan generative model of local grey matter follows

$$y = g(\mathbf{x}, \boldsymbol{\theta}) + \epsilon, \quad \epsilon \sim \mathcal{N}(0, \sigma_\epsilon^2) \tag{3.11}$$

with multiparameter input $\mathbf{x} = [\mathbf{x}_{sub}, \mathbf{x}_{meth}] = [age, TGM, TICV, snr, h]$, hyperparamter $\boldsymbol{\theta}$, and independent identical distributed gaussian noise ϵ. A Gaussian process (GP) is a distribution of functions, which is fully specified by its mean and its covariance function. To realize the local multiparameter GPR, a simple zero mean model and a covariance with noisy observations was applied:

$$m(\mathbf{y}) = \mathbf{0} \tag{3.12}$$

$$Cov(\mathbf{y}) = \mathbf{K}(\mathbf{X}, \mathbf{X}) + \sigma_\epsilon^2 \mathbf{I} \tag{3.13}$$

with full sample local grey matter volume data $\mathbf{y}$ and multiparameter input data $\mathbf{X}$. The basic idea here is to suppose the between-subjects covariance of local grey matter observations y to be a function of the similarities of individual input parameters $\mathbf{x}$ and an additional noise term. In particular, because of the *a-priori* unknown contributions of age and other parameters to the variability of y, the covariance (or kernel) matrix $\mathbf{K}$ is realized using a squared exponential function with automatic relevance determination (ARD):

$$Cov(g(\mathbf{x_i}), g(\mathbf{x_j})) = k(\mathbf{x_i}, \mathbf{x_j}) = \sigma_f^2 exp(-\frac{1}{2}(\mathbf{x_i} - \mathbf{x_j})^T diag(\boldsymbol{\ell})^{-2}(\mathbf{x_i} - \mathbf{x_j})), \tag{3.14}$$

with additional covariance hyperparameter σ_f^2, and input parameter length scales $\ell_1, \ldots, \ell_5$. Consequently, subjects with more similar age and global parameters are expected to reveal more similar local grey matter observations. The final covariance hyperparamters $\boldsymbol{\theta} = [\sigma_\epsilon, \sigma_f, \ell_1, \ldots, \ell_5]$ for the lifespan generative model were obtained from maximization of the log marginal likeli-

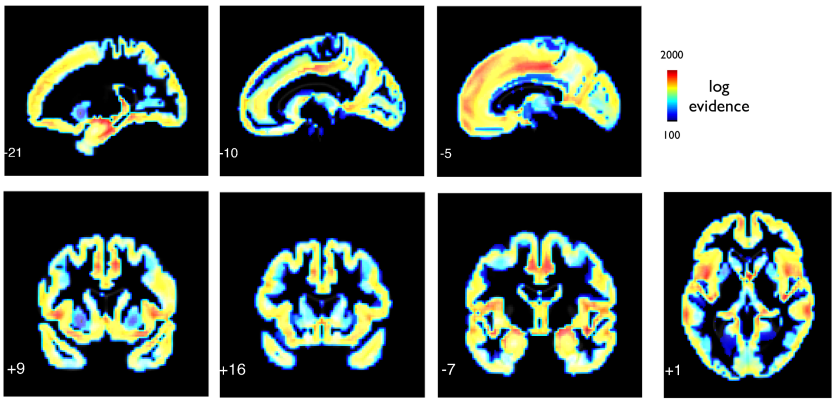

Figure 3.10: Gaussian process (GP) age regression of local grey matter volume using a large healthy adult brain database of 1338 subjects with ages 18-94 years. The multiparameter GP model uses a squared exponential covariance function with automatic relevance determination (ARD) and a zero mean function. Depicted are slice overlays of the log marginal likelihood (or evidence) $log\ p(\mathbf{y}|\mathbf{X}, \boldsymbol{\theta})$ of the local GP models after optimization of hyperparameters $\boldsymbol{\theta}$.

hood (or log evidence) $log\ p(\mathbf{y}|\mathbf{X}, \boldsymbol{\theta})$. (Rasmussen and Williams, 2006). This Bayesian model optimization for the GPR is assumed to optimal balance data-fit and model parsimony.

The resulting log evidence of the generative model is depicted in Figure 3.10. The cortical regions generally provided higher evidences compared to subcortical regions especially putamen. Frontal regions were found to have higher evidence than more posterior parts of the brain. These regional differences in the GPR models might be due to effects of segmentation, nonlinear normalization, the total explained variance by age effects and true intersubject differences in local grey matter volume. Notably, the multiparameter generative model cannot be displayed without fixing a few parameters. Figure 3.11 shows the general course (or expectation) of the model for two voxels in the prefrontal cortex and the hippocampus respectively, holding the TICV, snr, and h constant on their mean. Obviously, the hippocampus grey matter volume exhibited substantial nonlinear effects in relation to both total grey matter volume and chronological age. Additionally, the applied GPR approach aimed at estimating the regional grey matter variability across-subjects. Although the cross-sectional design basically confounds regional errors due to measurement and normalization with true individual variability of local grey matter volume, the model error variance σ_ϵ^2 might be informative about the distribution of measured between-subjects differences (Figure 3.12). The regional distribution of σ_ϵ^2 is shown in Figure 3.13 and provides insights into the local variability of the obtained voxelwise grey matter volume across subjects.

3.3.4 Gaussian confidence maps in untrained test cases

The generative lifespan model based on the voxelwise training database $\{\mathbf{y}, \mathbf{X}\}$ also affords predictions for untrained test subjects with person and aquisition specific predictors $\mathbf{X}_*$. For this purpose the predictive distribution $p(g_*|\mathbf{y}, \mathbf{X}, \boldsymbol{\theta}, \mathbf{X}_*)$ given the 'knowledge' of the lifespan

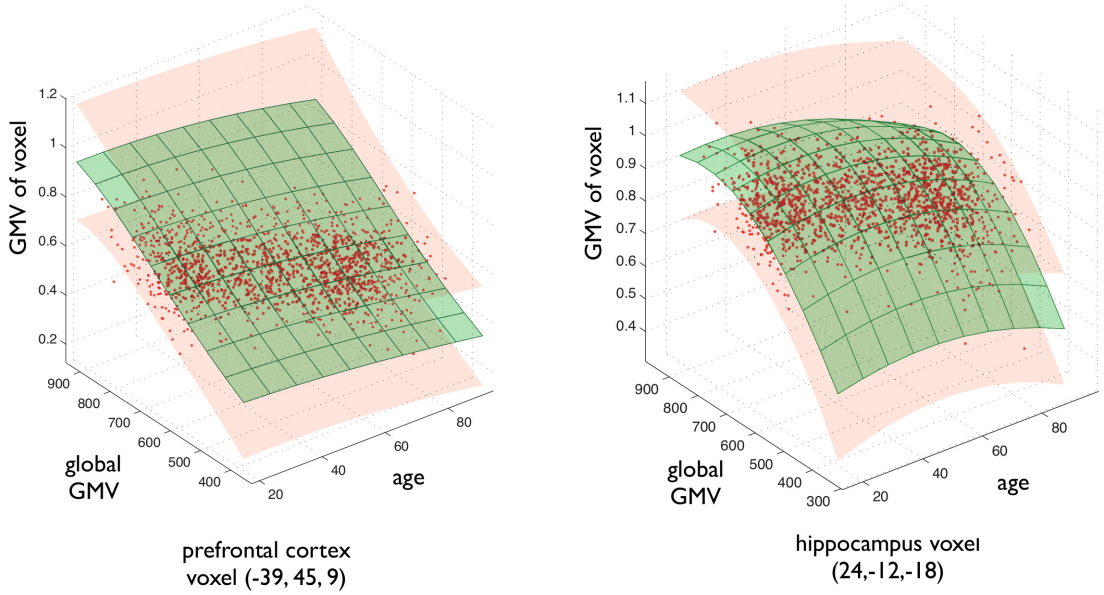

Figure 3.11: Gaussian process (GP) age regression of local grey matter volume using a large healthy adult brain database of 1338 subjects with ages 18-94 years. The multiparameter GP model uses a squared exponential covariance function with automatic relevance determination (ARD) and a zero mean function. The regression results are shown with local grey matter volume $\mathbf{y}$ as a function of global grey matter volume and subject's age. On the left we show a prefrontal cortex (-39,45,9) mm MNI voxel compared to a hippocampus voxel (24,-12,-18) mm MNI on the right. The age specific expectation is shown in green and the $\mu \pm 1.96\sigma_\epsilon$ confidence intervals for the error variance σ_ϵ^2 is shown in orange.

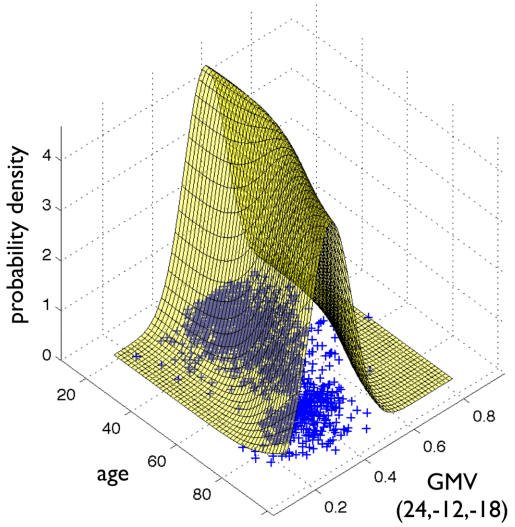

Figure 3.12: Gaussian process (GP) age regression of local grey matter volume using a large healthy adult brain database of 1338 subjects with ages 18-94 years. The multiparameter GP model uses a squared exponential covariance function with automatic relevance determination (ARD) and a zero mean function. Depicted is the gaussian distribution of the residual effects in a single frontal cortex voxel (24,-12,-18) mm MNI. It captures the uncertainty of the lifespan trajectory due to individual differences and measurement errors.

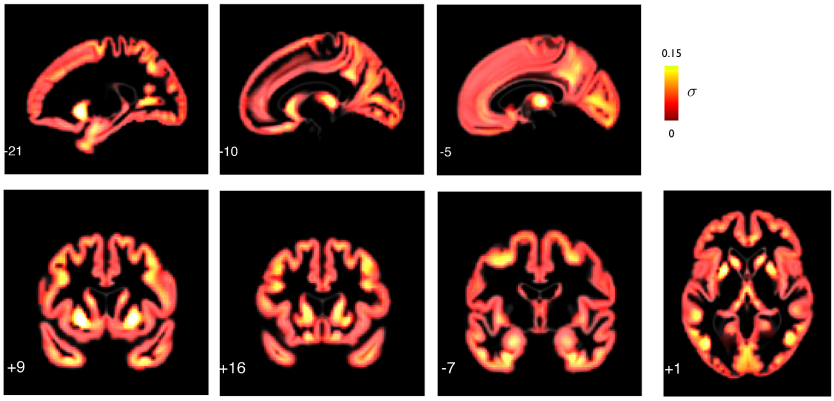

Figure 3.13: Gaussian process (GP) age regression of local grey matter volume using a large healthy adult brain database of 1338 subjects with ages 18-94 years. The multiparameter GP model uses a squared exponential covariance function with automatic relevance determination (ARD) and a zero mean function. Depicted is the regional standard deviation, i.e., σ_ϵ of the error variable ϵ. It measures the local variability due to individual differences or measurement and preprocessing errors of the applied VBM pipeline.

database, the optimized hyperparamters $\boldsymbol{\theta}$, and the test subjects' predictors $\mathbf{X}_*$ is obtained by conditioning on the observations (for details see Rasmussen and Williams, 2006). The predictive distribution is also gaussian and specified by the following expectation and covariance:

$$E(g_*|\mathbf{y}, \mathbf{X}, \boldsymbol{\theta}, \mathbf{X}_*) = \mathbf{K}(\mathbf{X}_*, \mathbf{X})[\mathbf{K}(\mathbf{X}, \mathbf{X}) + \sigma_\epsilon^2 \mathbf{I}]^{-1}\mathbf{y} \quad (3.15)$$

$$Cov(g_*|\mathbf{y}, \mathbf{X}, \boldsymbol{\theta}, \mathbf{X}_*) = \mathbf{K}(\mathbf{X}_*, \mathbf{X}_*) - \mathbf{K}(\mathbf{X}_*, \mathbf{X})[\mathbf{K}(\mathbf{X}, \mathbf{X}) + \sigma_\epsilon^2 \mathbf{I}]^{-1}\mathbf{K}(\mathbf{X}, \mathbf{X}_*), \quad (3.16)$$

with the above specified k and optimized $\sigma_f, \ell_1, \ldots, \ell_5$. In case of additionally available MRI brain scan of test subjects, we denote the preprocessed, normalized data of local grey matter volume $\mathbf{y}_*$. Then using the predictive distribution $p(g_*|\mathbf{y}, \mathbf{X}, \boldsymbol{\theta}, \mathbf{X}_*)$ allows evaluating each subject's local voxelwise predictive probabilities in terms of a cumulative distribution, further denoted with gaussian confidence maps. The resulting maps range from 0 to 1 providing a probabilistic map for observing the particular subject's grey matter pattern given the knowledge of a healthy lifespan structural aging database (Figure 3.14A). Moreover, inspecting subject's voxelwise lower or higher quantiles directly allows to assess regions with highly unlikely grey matter volume content from a normative reference perspective (Figure 3.14B). For instance, significantly reduced grey matter volume in medial temporal lobe regions was observed in subjects with mild cognitive impairment (MCI) and Alzheimer's Disease (AD) (Figure 3.14B left and middle). Moreover, visualization of the gaussian confidence maps, thresholding maps, and local quantile plots might provide a valuable extension of the information basis in clinical case scenarios with subjects at risk to convert to pathological aging.

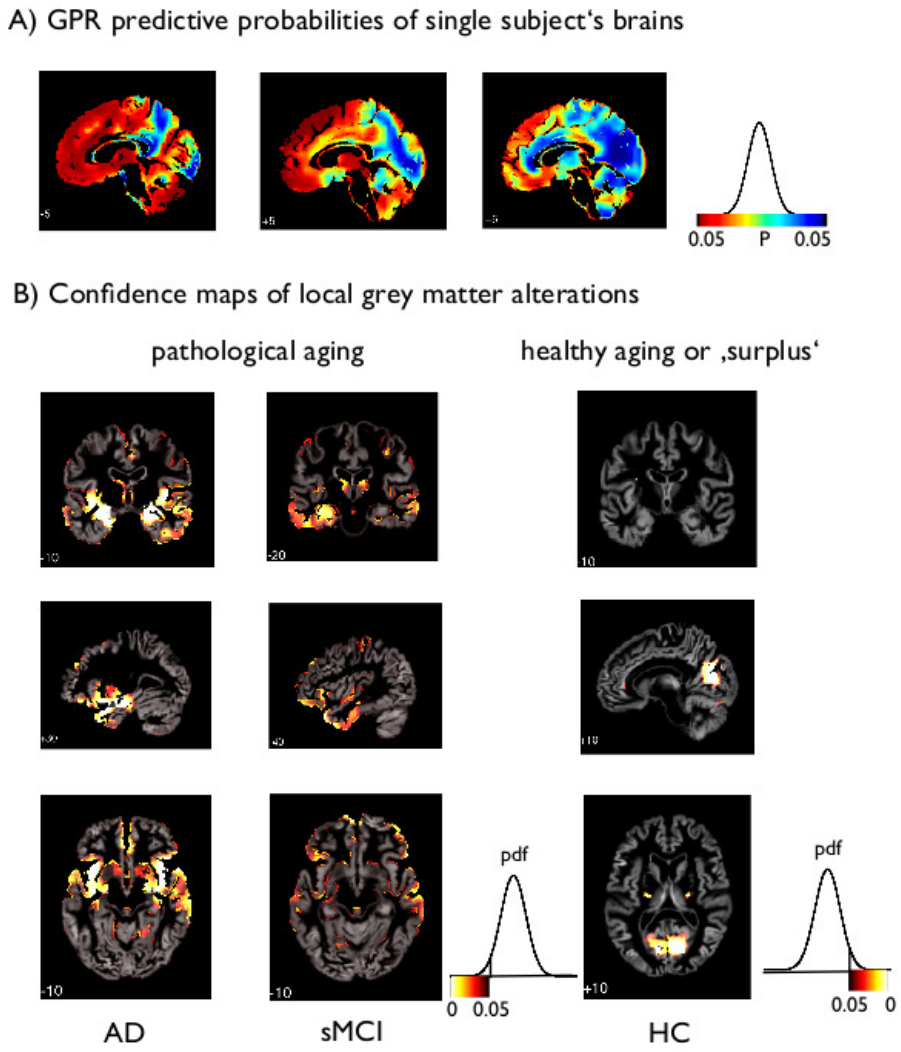

Figure 3.14: Gaussian confidence maps using Gaussian process (GP) age regression from large healthy adult brain database of 1338 subjects with ages 18-94 years. (A) Confidence maps of local grey matter volume in a single subject with Alzheimer's disease. The maps are obtained from evaluation of the predictive distribution given the patients input data $\mathbf{x}_* = [age_*, TGM_*, TICV_*, snr_*, h_*]$, the healthy adults database $\{\mathbf{y},\mathbf{X}\}$, and the optimized GP parameters $\boldsymbol{\theta}$, i.e., $p(g_*|\mathbf{y}, \mathbf{X}, \boldsymbol{\theta}, \mathbf{x}_*)$. The patients map is further obtained from assessing the likelihood to observe his brain image $\mathbf{y}$ given the Bayesian knowledge about normal age-related differences. Lower to higher cumulative probabilities range from red to blue. (B) Confidence maps after thresholding highlight local brain alterations of individual grey matter volume in pathological and healthy elderly. 3 Subjects are shown with either MCI, AD and without clinical diagnose.

Acknowledgments

This work was supported by the BMBF grant 01EV0709. Data collection and sharing for this project was funded by the Alzheimer's Disease Neuroimaging Initiative (ADNI) (National Institutes of Health Grant U01 AG024904). ADNI is funded by the National Institute on Aging, the National Institute of Biomedical Imaging and Bioengineering, and through generous contributions from the following: Abbott; Alzheimer's Association; Alzheimer's Drug Discovery Foundation; Amorfix Life Sciences Ltd.; AstraZeneca; Bayer HealthCare; BioClinica, Inc.; Biogen Idec Inc.; Bristol-Myers Squibb Company; Eisai Inc.; Elan Pharmaceuticals Inc.; Eli Lilly and Company; F. Hoffmann-La Roche Ltd and its affiliated company Genentech, Inc.; GE Healthcare; Innogenetics, N.V.; Janssen Alzheimer Immunotherapy Research & Development, LLC.; Johnson & Johnson Pharmaceutical Research & Development LLC.; Medpace, Inc.; Merck & Co., Inc.; Meso Scale Diagnostics, LLC.; Novartis Pharmaceuticals Corporation; Pfizer Inc.; Servier; Synarc Inc.; and Takeda Pharmaceutical Company. The Canadian Institutes of Health Research is providing funds to support ADNI clinical sites in Canada. Private sector contributions are facilitated by the Foundation for the National Institutes of Health (www.fnih.org). The grantee organization is the Northern California Institute for Research and Education, and the study is coordinated by the Alzheimer's Disease Cooperative Study at the University of California, San Diego. ADNI data are disseminated by the Laboratory for Neuro Imaging at the University of California, Los Angeles. The Open Access Series of Imaging Studies (OASIS) is supported by grants P50 AG05681, P01 AG03991, R01 AG021910, P50 MH071616, U24 RR021382, R01 MH56584.

Chapter 4

Assessing Individual Decline Parameters

4.1 Models of Aging Brain Structure and Individual Decline - PART B Longitudinal Methods

Gabriel Ziegler[1], Robert Dahnke[1], Christian Gaser[1,2], and the Alzheimer's Disease Neuroimaging Initiative[3]

1 Structural Brain Mapping Group, Department of Psychiatry, Jena University Hospital, Jena, Germany.
2 Department of Neurology, Jena University Hospital, Jena, Germany.
3 Data used in the preparation of this article were obtained from the Alzheimer's Disease Neuroimaging Initiative (ADNI) database (www.loni.ucla.edu/ADNI). As such, the investigators within the ADNI contributed to the design and implementation of ADNI and/or provided data but did not participate in analysis or writing of this report. Complete listing of ADNI investigators available at http://adni.loni.ucla.edu/wp-content/uploads/how_to_apply/ADNI_Authorship_List.pdf.

Type of contribution Research article[1], (published in Ziegler et al., 2012a)

Personal contribution G.Z. conceived and designed the overview framework, adapted and implemented the algorithms for polynomial models, spline models, longitudinal models, preprocessed the data, analyzed the MRI data, and wrote the paper. R.D., C.G. preprocessed a part of the data, R.D. photoshoped the designed figures, C.G. corrected the paper.

[1]In order to improve the structure of this thesis, the original overview article is divided in PART A describing cross-sectional models and PART B describing longitudinal models. PART A is included as introduction to chapter 3 and PART B is included as introduction to chapter 4

4.1.1 Analysis of inter-individual variability in aging brain structure

There is an increasing interest in MR-based neuroimaging methods that allow measuring local neuroantomical variability in healthy populations (for review see Ashburner and Klöppel, 2011). Studies using Voxel-Based Morphometry (VBM) (Ashburner and Friston, 2000) have successfully addressed these inter-individual differences of adult brain structure and have given some insights into the complex relation to behavior and cognitive processing (Eckert, 2011; Kanai and Rees, 2011). Irrespective of their potential to separate age-related change and inter-individual differences, there is still a lack of studies addressing between-subjects neuroanatomical variability in repeated measurement designs. Moreover, the existing longitudinal designs are often restricted to *a-priori* selected regions of interest (ROI). This section addresses the estimation of voxel- or vertex-wise individual neuroanatomical age trajectories, their variability across subjects and promising models to identify correlated changes between neuroanatomy and other levels of the brain-behavior-environment system, e.g., cognitive performance, lifestyle and health parameters, etc.

Longitudinal design

In the field of neuroimaging, a longitudinal design refers to repeated MRI acquisitions of peoples brain, covering a maximum of a few years of the lifespan. This within-subject (or intra-individual) sampling can be more or less time-structured, often taking place at a baseline measurement with 1-4 annual follow-ups. However, most studies do not standardize the subjects ages at baseline and thus the between-subject (or inter-individual) sampling also covers a certain age range. Owing to the number of follow-ups, the effort to organize sampling and MRI acquisitions increases enormously. In addition to the high costs and efforts of longitudinal design, these studies often face selection bias and late selective dropouts (Lindenberger et al., 2002; Raz et al., 2005). As we intend to demonstrate only the analysis, we begin with preprocessed images (e.g., cortical thickness or grey matter volume) that have been normalized to either a voxel- or surface-based reference template, respectively. Notably, the selection of an appropriate data structure for spatially distributed (or 'quasi-continuous') longitudinal measurements is not trivial. Although the practical implementation of models presented below is much more flexible, for reasons of simplicity, we assume time-structured data with three annual follow-ups to be in the following form: The $\mathbf{Y}^{(k)}$ matrices contain the preprocessed MR-based markers for brain locations $k = 1, \ldots, n$, e.g., voxels or vertices. The entries of $\mathbf{Y}^{(k)}$ are denoted $y_{ij}^{(k)}$ for subject $i = 1, \ldots, m$ at timepoint $j = 1, \ldots, 5$. The corresponding subject ages at baseline measurement are represented by the column vector age. In addition, we use the vector $\mathbf{time} = [0, 1, 2, 3, 4]^T$ to code the intra-individual measurement timing, i.e., baseline, 1st follow-up,..., 4th follow-up.

Modelling change: the individual decline model

Compared to the cross-sectional analysis of age-related differences (i.e., expressed by age covariations), longitudinal data enables analysis of age-related change of brain morphometry. Primarily, this is reflected by taking a within-subject perspective in analysis, modelling brain changes in each subject separately. More specifically, due to the expected between-subjects variations of change, we are particularly interested in individual trajectories $g_i^{(k)}(age, \beta)$ of subject i. There are three reasons that justify the choice of a linear parametric decline model for $g_i^{(k)}(age, \beta)$: Firstly, most studies with longitudinally MRI do not cover more than a few measurements. Thus the low number of follow-ups restricts the complexity (i.e., degrees of freedom) of the intra-individual change model. Secondly, the covered age range of a few years makes the rejection of linearity rather unlikely, even if much more samples were available. Thirdly, the individual MR-based measures on voxel- or vertex level are prone to scanner inhomogeneities, segmentation- and normalization errors. This often results in large errors and residual variance and favors the simplicity of the model to provide robust estimates of change. Consequently, for many longitudinal MR studies it is reasonable to apply the following linear approximation of the individual decline curves:

$$y_{ij} \quad = \quad b_{i0} + b_{i1} time_j + \epsilon_{ij}, \quad \epsilon_{ij} \sim \mathcal{N}(0, \sigma_\epsilon^2) \tag{4.1}$$

Since longitudinal MR-data intrinsically varies due to space, time and persons, symbolic description requires triple indexing. To avoid confusion, we omit the space index (indicating voxels- and vertices k) in all models of intra-individual change though we reintroduce the brain locations in the final prediction models of brain change. Assuming the independence and homoscedasticity of errors, the OLS minimization provides unbiased estimates of the individual change parameters namely the initial status b_{i0} and the slope or annual rate of decline b_{i1} for each subject (Singer and Willett, 2003). The general linear model (GLM) facilitates the effective 'whole-brain' implementation of the individual decline model. The resulting images of determination coefficient R^2 and residual variance can vary substantially over voxels or vertices and subjects, depending on the success of morphometric preprocessing. Figure 4.1 depicts an application of the linear decline model to longitudinal voxel-based morphometry data in a sample of healthy elderly. Importantly, Willet (1998) revealed the following relation about the reliability of the slope estimates using the above individual decline model (for balanced designs and i.i.d. errors):

$$Rel(b_{.1}) \quad = \quad \frac{\sigma^2_{TrueSlope}}{\sigma^2_{TrueSlope} + \dfrac{\sigma^2_\epsilon}{CSST}} \tag{4.2}$$

Thus the reliability of the slope estimates depends on the true variation of the slopes $\sigma^2_{TrueSlope}$, the error variance σ^2_ϵ and the corrected sum of squares of the time variable $CSST$ (see illustration in Figure 4.2). Moreover, this has substantial implications for future studies using longitudinal designs. The key point is that the reliability of estimated annual rates substantially increases with

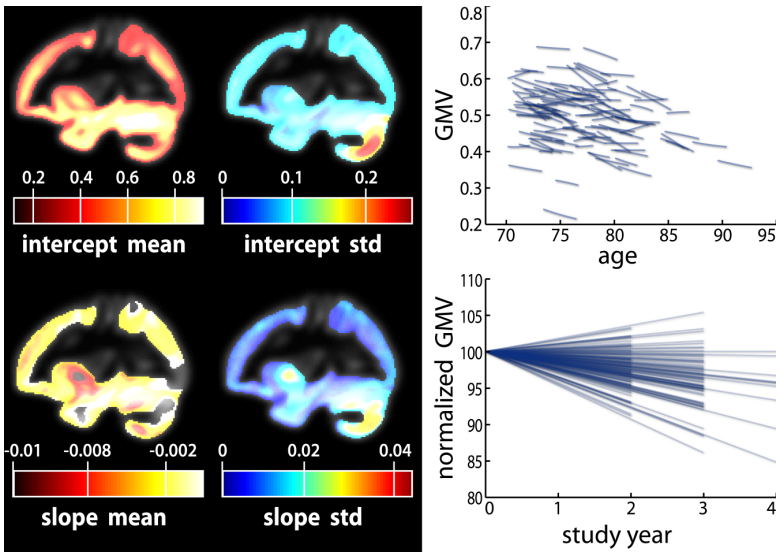

Figure 4.1: Application of a linear decline model to a longitudinal sample of voxel-based morphometry data. The individual grey matter intercept and slope parameters were estimated using 572 MRI scans of 123 healthy subjects with ages 70 to 90 at baseline. Number of follow-ups varied from 2-4. Local mean and standard deviation of intercept and slope parameters (left). Longitudinal individual linear decline models of a right hemisphere hippocampus voxel (right top). Normalized decline models showing percent grey matter change relative to baseline (right bottom). Figure and legend modified from Ziegler et al. (2012a).

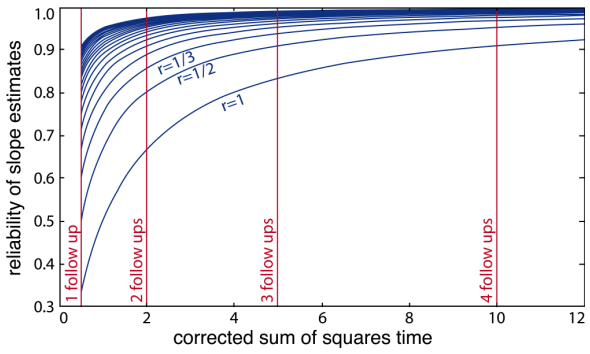

Figure 4.2: Illustration of the reliability of ordinary least squares slope parameter estimates and its dependency on the corrected sum of squares of time variable ($CSST$). Nonlinear functions depict the expected increase of reliability with CSST for different ratios $r = 1/h$ of (error variance)/(true slope variance) for $h = 1, 2, \ldots, 10$. The vertical lines indicate values of $CSST$ for 1, 2, 3 and 4 annual follow-up measurements in a longitudinal MRI design. Figure and legend from Ziegler et al. (2012a).

the temporal spread of longitudinal measurements in terms of $CSST$. Importantly, this can be achieved by adding follow-ups or placing them out of the center of the time variable. For instance with $\sigma_\epsilon^2 = \frac{1}{2}\sigma_{TrueSlope}^2$, using 3 instead of 1 annual follow-ups increases the reliability from 50% to 91%. However, the fitted linear OLS trajectories are rather convenient for exploratory purposes than for making inference about inter-individual differences of age-related change (Singer and Willet, 2003). Using OLS, the between-subject variations of the error variance are not taken into account. Instead of fitting the individual decline separately, multi-level models of change have been suggested to estimate error-free latent change parameters (McArdle, 2009).

Separating variability in elderly using multi-level models

The within-subject structural decline and the between-subject variations can also be combined in a single statistical model. In general the aim is achieved by hierarchical modelling that includes both levels of variation (see also Friston et al., 2002). We here apply a multi-level (or mixed-effects) model (Bryk and Raudenbush, 1987) to local neuroanatomical changes in elderly people. The first level submodel embodies the linear approximation of intra-individual brain change $g_i^{(k)}(age, \beta)$ similar to the fitted OLS trajectories:

$$y_{ij} = \alpha_{0i} + \alpha_{1i} time_j + \epsilon_{ij} \tag{4.3}$$

In addition, there is a second level sub-model that further specifies the inter-individual relations of the first level change parameters. For our purpose, the second level simply models the subject's deviation from the initial status β_{00} and slope β_{10} parameters in the population:

$$\alpha_{0i} = \beta_{00} + \zeta_{0i} \tag{4.4}$$

$$\alpha_{1i} = \beta_{10} + \zeta_{1i} \tag{4.5}$$

Furthermore, the multi-level model assumes zero mean Gaussian distributions for the first level residual ϵ_{ij} and second level residuals ζ_{0i} and ζ_{1i}:

$$\epsilon_{ij} \sim \mathcal{N}(0, \sigma_\epsilon^2), \begin{bmatrix} \zeta_{0i} \\ \zeta_{1i} \end{bmatrix} \sim \mathcal{N}\left(\begin{bmatrix} 0 \\ 0 \end{bmatrix}, \begin{bmatrix} \sigma_0^2 & \sigma_{01} \\ \sigma_{10} & \sigma_1^2 \end{bmatrix} \right) \tag{4.6}$$

The first level residuals ϵ_{ij} account for erroneous variations around the individual linear decline model. Age effects and multidirectionality can be tested via parameters β_{00} and β_{10}, that are often called fixed effects. However, the idea here is to study inter-individual differences of aging morphology by analysis of the random effects α_{0i} and α_{1i}, i.e., the variation of the individual decline parameters around the population means. According to the second level sub-model, this deviation is explicitly represented by the residuals ζ_{0i} (for the initial status) and ζ_{1i} (for the slopes). In order to estimate the fixed and random effects, many implementations apply maximum likelihood (ML), generalized least squares (GLS) (Raudenbush and Bryk, 2002; Singer

and Willett, 2003), or Bayesian methods with expectation maximization (Friston et al., 2002; Schmid et al., 2009). We denote the local second level residuals (or centered random effects) with $\zeta_{0i}^{(k)}$ and $\zeta_{1i}^{(k)}$ for subject i and voxel or vertex k. For reasons of simplicity, we arrange the centered random effects to the following matrices for initial status $\mathbf{I}_0$ and slope $\mathbf{S}$:

$$\mathbf{I}_0 = \{t_{ik}\}, t_{ik} = \zeta_{0i}^{(k)}, \mathbf{S} = \{s_{ik}\}, s_{ik} = \zeta_{1i}^{(k)}, i = 1, \ldots, m, k = 1, \ldots, n \tag{4.7}$$

In particular, rows of **S**include the subjects' images of annual rates of decline during the study period. In conclusion, the linear approximation of local individual trajectories $g_i^{(k)}(age, \beta)$ and multi-level modelling condenses the whole longitudinal dataset to two matrices containing the intra-individual change parameters. Notably, there are some limitations and caveats of repeated measures MRI data in general and multi-level modelling in particular. Firstly, longitudinal MR-based morphometry is prone to artifacts due to scanner inhomogeneities, registration inconsistency, and subtle age-related deformations of the brains. Thus it needs highly sophisticated preprocessing pipelines in order to detect the changes of interest and achieve unbiased results (Reuter et al., 2010; Reuter and Fischl, 2011). Secondly, a related issue is that the multi-level analysis of longitudinal changes in voxel- or vertex-wise neuroanatomical markers requires high retest-reliability of local structural measures. A few existing evaluation studies on this topic provide promising results for voxel-based morphometry and cortical thickness (Dickerson et al., 2008; Schnack et al., 2010). Thirdly, on the one hand, multi-level modelling is capable of missing scans and unbalanced designs (i.e, between-subject variations of the follow-up times). On the other hand, it is a large sample procedure, which is limited by enormous costs and efforts of this particular study design. Fourthly, the intra-individual change models are seriously affected by correlated residuals due to repeated preprocessing errors over follow-ups (Singer and Willett, 2003). One can account for this by explicit modelling of autocorrelations in the first level residual covariances (see Friston et al., 2002). Finally, the application of multi-level models in a 'mass-univariate' manner, i.e., for voxel- or vertex-wise analysis of age-related decline, can be computationally expensive. This limitation can be overcome by using efficient implementations and algorithms (Pinheiro and Bates, 2000).

Explaining inter-individual variability in structural aging

A large variety of studies address potential modifiers of structural decline in older ages. On one hand there is evidence that hypertension (Raz and Rodrigue, 2006), obesity and diabetes (Luchsinger and Gustafson, 2009), and high plasma homocysteine concentrations (Oulhaj et al., 2010) increase the individual risk for brain deterioration and dementia. In addition, the lifestyle factors such as vascular and aerobic fitness (Erickson and Kramer, 2009; Erickson et al., 2009, 2011), and healthy nutrition (Féart et al., 2010; Frisardi et al., 2010) are discussed as promising protective factors in order to maintain the structural integrity in old age. On the other hand, psychometric tests of cognitive abilities and intelligence are also potential covariates of structural change (Fjell and Walhovd, 2010). However, the complex interactions of aging brain structure

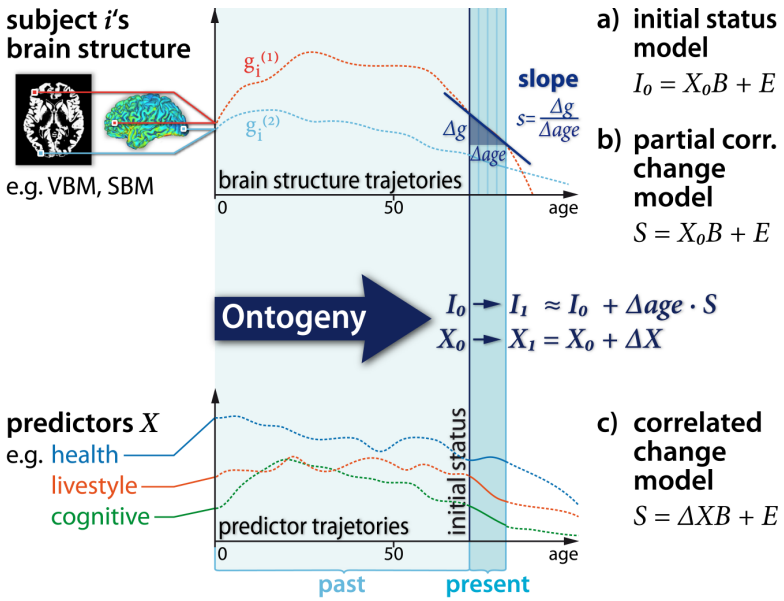

Figure 4.3: Illustration of analysis of inter-individual variability in longitudinal structural brain imaging studies. Brain level (top): We show the individual subject's local lifespan trajectories and the longitudinal sampling with baseline MRI and 4 annual follow-ups. A linear approximation of the trajectories reveals individual change parameters, namely the initial status $\mathbf{I}_0$ and slope/annual rate of decline $\mathbf{S}$. Predictor level (bottom): Here we depict hypothetical trajectories of predictors and covariates for structural brain changes. The baseline predictors are called $\mathbf{X}_0$ and predictor change across the study is $\Delta\mathbf{X}$. (a), (b), and (c) are suggested linear prediction models for individual change parameters (right). Figure and legend from Ziegler et al. (2012a).

with cognitive functioning are still not completely resolved (Raz and Kennedy, 2009; Salthouse, 2011c).

Predictor models: past differences vs. present changes Studying the aging brain structure in relation to covariates from other levels of the brain-behavior-environment system is a methodologically challenging task (Lindenberger et al., 2006). At first, we assume a set of multiple predictors (e.g., memory performance subscales) that were acquired at baseline MR measurement $\mathbf{X}_0$ and again at the last follow-up $\mathbf{X}_1$ (containing predictor subscales in columns and observation in rows). The predictors can be twofold (a) person-specific attributes that are highly stable, e.g., genes, total brain intracranial volume, etc. (i.e., $\mathbf{X}_0 \approx \mathbf{X}_1$) or (b) variables that exhibit developmental changes during the study period, e.g., depression symptoms (i.e., $\Delta\mathbf{X} = \mathbf{X}_1 - \mathbf{X}_0$). Figure 4.3 illustrates the situation faced in a typically MR longitudinal setting with predictors. It depicts three hypothesized regional age trajectories $g_i^{(k)}(age)$ from a single subject before, during and after the study. Moreover, it embodies this particular subject's linear decline model including the initial status $\mathbf{I}_0$, the slopes $\mathbf{S}$, and the interpolation to the age with the last MRI follow up $\mathbf{I}_1$. In order to identify potential modifiers and correlates of brain aging we briefly review three models that afford testing their local effects on aging and age-related differences in brain structure (see also Salthouse, 2011c):

Predicting the initial status: In this first model we use the baseline predictors $\mathbf{X}_0$ to predict the inter-individual differences in the estimated baseline brain structure $\mathbf{I}_0$. The model is similar to a typical cross-sectional analysis of effects of the covariates. However, the initial status does not reflect the intra-individual changes during the study period. Thus predicting the initial status equals the analysis of brain development and aging before the study onset. In particular, correlations of $\mathbf{X}_0$ and $\mathbf{I}_0$ characterize the cumulative effects of all predictor-brain interactions during the subject's past including gestation. For instance significant effects of lifestyle predictors on the initial status can reflect lifestyle-brain interactions that occurred at 1, 10, or even 60 years before the first MR-measurement. Thus because these effects are not necessarily related to the process of aging, the conclusions derived from this model are strongly restricted by its lack of specificity.

Partial correlated change: In contrast, this model predicts subjects' intra-individual change parameters $\mathbf{S}$ using the baseline predictors $\mathbf{X}_0$. Thus the between-subjects differences are used to forecast the within-subject structural brain decline during the study. For instance subjects with higher memory capacity at study onset may reveal a less negative annual rate of change. Practically, this is often applied if the predictors are not expected to change, e.g., genetic information or if predictor follow-ups are not available. Notably, because the baseline predictors may be similar to earlier ages in life, the predictor-brain interaction could have started long before the study (Salthouse, 2011c). However, the partial correlated change model gives evidence about the brain changes that take place during the particular study period. Therefore it might provide specific insights about the modifiers and correlates of structural brain aging.

Correlated change: This model additionally requires (at least) one follow-up measurement of the predictors and accounts for their change $\Delta\mathbf{X}$ during the study. Then, the predictor change is tested for correlations with brain change in terms of slope differences $\mathbf{S}$. For instance Murphy et al. (2010) found that elderly subjects with stronger longitudinal decline in fusiform gyrus thickness also exhibited stronger decline in memory tests. In contrast to the partial correlated change model, this model additionally exploits temporal specificity of the ongoing age-related changes on the predictor level. However, it is often unknown which (latent) processes underlie the interactions of the brain-behavior-environment system. This is especially true for exact time lags and delays of this interaction. Therefore, the conclusions from the above predictor models are restricted to correlations and do not afford causal inferences (for details see Gollob and Reichardt, 1987; Salthouse, 2011c). Otherwise, studying these temporal aspects is a promising approach to disentangle the mechanisms of structural decline in changing contexts of lifestyle, nutrition, and 'cognitive environment'.

The majority of the recent studies that have explored inter-individual differences and modifiers of age-related brain structural changes have either focused on global brain parameters (Schmidt et al., 2005; Charlton et al., 2010) or an *a-priori* selection of regions of interest (ROI) (Du et al., 2006; Kramer and Erickson, 2007; Raz et al., 2008; Murphy et al., 2010; Raz et al., 2010). Therefore, the (partial) correlated change models are often separately applied to global- or local ROI measures (e.g., hippocampus volume). On one hand, this univariate approach is advantageous

because it affords the application of sophisticated structural equation models (SEM) for the purpose of intra-individual change analysis (for review see McArdle, 2009). For instance recent studies by Raz et al. (2005, 2008, 2010) successfully applied latent difference models (LDM) to explore contributors to ROI-based intra-individual decline of brain volume. However, the univariate ROI-based approach (1) does not fully account for regional variability of age-related differences and (2) often neglects the inter-regional dependencies of age-related effects in terms of distributed structural patterns of change. Therefore, we address the implementation of the (partial) correlated change for voxel- or surface-based analysis taking the advantage of univariate and multivariate approaches.

Univariate generative model: local prediction of decline

Due to its computational efficiency, usability and straightforward statistics the general linear model (GLM) is a predestined approach to analyze local change parameters. It enables assessment of linear effects of predictors $\mathbf{X}_0$ or $\Delta\mathbf{X}$ on individual local rates of decline $\mathbf{S}$. A straightforward GLM implementation of the above slope prediction models is:

$$s_{ik} = \sum_{r=1}^{p} x_{ir}\beta_{rk} + \epsilon_{ik}, \quad \epsilon_{ik} \sim \mathcal{N}(0, \sigma_k^2),$$

i.e., $\mathbf{S} = \mathbf{XB} + \mathbf{E}$ using a design matrix $\mathbf{X}$ containing p predictors in columns, the parameter matrix $\mathbf{B}$ with entries β_{rk}, and the matrix $\mathbf{E}$ with errors ϵ_{ik}. In order to implement the 'partial correlated change' model we detect the effects of baseline predictors (i.e., $\mathbf{X} = \mathbf{X}_0$) and for a 'correlated change' model the effects of the predictor change (i.e., $\mathbf{X} = \Delta\mathbf{X}$). Notably, if the longitudinal design includes subjects from different ages (at baseline measurement), the individual change parameters $\mathbf{I}_0$ and $\mathbf{S}$ are not supposed to be free of age effects. In particular, testing for age effects on subjects' slopes can reveal age dependent differences in the rates of decline, e.g., due to nonlinear local age trajectories $g^{(k)}(age, \beta)$. Thus the subjects' ages can be included in the design matrix as well as other covariates, e.g., $\mathbf{X} = [\Delta\mathbf{X}, \mathbf{age}, \mathbf{ticv}]$. If the predictors are supposed to show multicollinearity, the confidence of parameter estimates is improved by precedent orthogonalization of the design matrix. Unfortunately, strong correlations of the predictors might also limit the interpretability of effects. This is especially true for collections of psychometric tests which often show substantial intercorrelations.

As recently pointed out by (Salthouse, 2011c), multivariate analysis techniques might improve the analysis of aging structure in relation to covariates and predictors such as cognitive abilities. On one hand, studies have successfully demonstrated the inter-regional dependencies of age effects in brain structure using multivariate methods (Alexander et al., 2006; Brickman et al., 2007, 2008; Ecker et al., 2009; Bergfield et al., 2010). On the other hand, the shared variance of predictors can be used to define composite scores or latent factors that improve reliability (Penke and Deary, 2010). Moreover, in a recent study this 'aggregation' on the brain- and the predictor side revealed sophisticated insights in the relation of brain structure and information

processing in elderly (Penke et al., 2010b).

Multivariate generative model: predictive patterns of decline

The partial least squares correlation (PLSC) technique was initially introduced into the field of functional neuroimaging to relate brain activity data to experimental design matrices and it evolved to a powerful tool for various applications (Krishnan et al., 2011). To account for the above mentioned caveats of GLM we apply a PLSC to identify more general commonalities of individual structural decline $\mathbf{S}$ and the set of predictors $\mathbf{X}$ (i.e., $\mathbf{X}_0$ or $\Delta\mathbf{X}$). We suppose matrices $\mathbf{S}$ and $\mathbf{X}$ to be centered and normalized (e.g., z-scores). Then, the idea of PLSC is to detect important patterns in the correlations of local slopes and predictors, i.e., $\mathbf{R} = \mathbf{X}^T\mathbf{S}$. In particular, this is performed by a singular value decomposition (SVD) of the correlation matrix:

$$\boldsymbol{R} = \boldsymbol{X}^T\boldsymbol{S} = \boldsymbol{U}\Delta\,\boldsymbol{V}^T = \sum_{l=1}^{r} \sigma_l \boldsymbol{u}_l \boldsymbol{v}_l \tag{4.8}$$

Formally, the SVD results in pairs of left and right singular vectors $\mathbf{u}_l$ and $\mathbf{v}_l$, also called saliences. The saliences $\mathbf{u}_l$ and $\mathbf{v}_l$ represent weighting patterns of the predictors- and the slopes respectively. For instance, if $\mathbf{X}$ contains elderly subjects' health parameters we can think of $\mathbf{u}_l$ as a specific health profile. The $\mathbf{v}_l$ saliences for slopes $\mathbf{S}$ represent voxel- or vertex-wise brain images. Technically, PLSC determines the saliences that maximize the covariance of weighted predictors and slopes (for exact constraints see Krishnan et al., 2011):

$$\max_{\mathbf{u},\mathbf{v}} \quad Cov(\boldsymbol{X}\boldsymbol{u}, \boldsymbol{S}\boldsymbol{v}) \tag{4.9}$$

The resulting covariance of salience-weighted predictors $\mathbf{X}\mathbf{u}_l$ and slopes $\mathbf{S}\mathbf{v}_l$ is given by the singular values σ_l indicating the magnitude of explained covariation in the data. Finally, the obtained pairs of brain regional patterns and predictor profiles in a sample can be generalized to population level by the use of permutation tests (McIntosh and Lobaugh, 2004). In addition, bootstrapping techniques allow assessment of confidence intervals for patterns and profiles. In conclusion, PLSC provides a multivariate approach to simultaneously analyze multiple contributing factors (or predictors) to local intra-individual rates of structural decline. Its implicit search for weighting patterns and profiles accounts for inter-regional and inter-predictor correlations. Figure 4.4 illustrates the partial least squares approach to analyze inter-individual variability in change parameters. Alternatively, other multivariate models, e.g., canonical variates analysis (CVA) have been suggested to analyze distributed patterns of brain parameters in relation to experimental designs and predictors (Worsley et al., 1997).

4.1.2 Limitations

Some caveats of the presented framework have to be mentioned. Firstly, a general issue for all presented modelling approaches is the assumption of an age-unbiased preprocessing, in particular

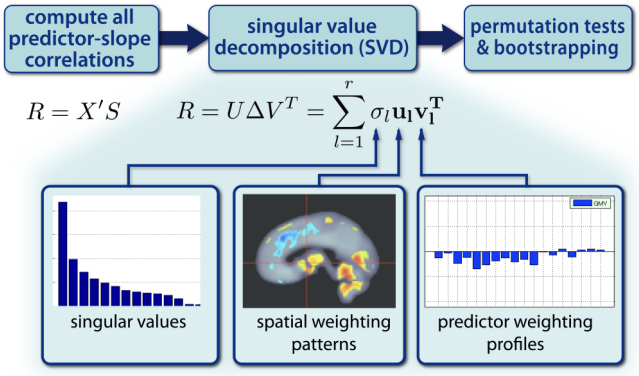

Figure 4.4: Partial least squares correlation (PLSC) approach for analysis of inter-individual variability of decline parameters. PLSC decomposes the correlation structure of change parameters **S** and predictors **X** using singular value decomposition (SVD). This reveals pairs of spatial weighting patterns and predictor profiles. Figure and legend from Ziegler et al. (2012a).

for samples including higher ages, i.e., in which there will inevitably be higher levels of atrophy. Age-bias in segmentation, registration and normalization could be misleadingly identified as region-specific age effects in subsequent analyses. In part, this limitation might be overcome by applying prior-free segmentation approaches in studies with a large age range. In addition, the normalization might be optimized by generation of average shaped tissue templates (Ashburner and Friston, 2009). Secondly, a main limitation of the above models is that they are based upon an observational design, which does not conform to a randomized experimental design. The former does not allow inference about causality of potential interactions between predictors and brain levels. Thirdly, the approaches do not explicitly address multidimensionality of aging brain structure in terms of multiple MR-based modalities obtained from the same brain region. However, a recent unsupervised learning method called Link ICA was suggested to jointly analyze their covariations (Groves et al., 2011). Fourthly, most of the generative models of age were presented from a classical 'mass-univariate' statistical perspective allowing voxelwise inference. This often requires Gaussian smoothing with *a-priori* chosen filter width and decorrelation of noise terms in advance. Notably, Bayesian modelling has become a promising alternative for multivariate analysis of neuroimaging data (Friston et al., 2008). It provides a flexible approach to multi-level and hierarchical models (Friston et al., 2002) including biophysical priors on age-related processes, adaptive spatial regularization (Penny et al., 2005; Groves et al., 2009), and model comparisons (Penny et al., 2007).

There is an ongoing discussion about limitations of cross-sectional and longitudinal design to study aging brain structure (Fjell and Walhovd, 2010; Raz and Lindenberger, 2011). One critical issue is that cross-sectional studies in principle merge age independent inter-individual differences and age-related effects risking a biased sample composition over ages with unknown hidden covariates. In addition, the sensitivity for the detection of age-related effects varies with the amount of inter-individual differences of brain structure and sample size. Some studies observe deviations in the estimated annual decline rates derived by either a cross-sectional

or a longitudinal approach (e.g. see Raz et al., 2005). As recently reviewed, cross-sectional decline estimators sometimes underestimate the longitudinal decline (Fjell and Walhovd, 2010). However, apart from artifacts due to cohort effects, secular trends, and age-biased sampling, there are other factors that also contribute to deviating results obtained from different study designs. There are substantial differences in the preprocessing pipelines of cross-sectional and longitudinal brain structural images, which are either optimized for accurate intra-individual registration or inter-individual normalization, respectively. The statistical models that define the estimators for local change rates often vary across studies and designs. In addition, if the true lifespan trajectories of aging brain structure are expected to be nonlinear, differences in the age range of the sample, the mean age, and the age distribution influence the estimated annual decline rates obtained from either longitudinal or cross-sectional studies. Thus in order to estimate age effects on brain structure, the differences due to study design should be interpreted with caution. As also reviewed by Fjell and Walhovd (2010), the cross-sectional age effects on brain structure in large sample studies using semi-automated methods were similar to those obtained in longitudinal studies.

A related issue is that longitudinal studies seldom span more than 5 years, limited by routine scanner upgrades or replacement. Being aware of the immense methodological advantages of longitudinal designs, the analysis of pure intra-individual age variations in MR-based markers does not allow exploring lifespan brain differences and accelerated aging over decades. For this particular purpose, longitudinal and cross-sectional studies require the analysis of effects due to age variations on the between-subjects level which are susceptible to sampling-bias and trends. As pointed out by (Raz et al., 2005) in an important longitudinal study, by using only a restricted age range (at baseline) the observed nonlinear age effects on brain structure would simply be missed. Thus under careful inspection of sample characteristics, the inter-individual age variations in cross-sectional and longitudinal designs can provide insights in long term age differences not accessible with repeated measures MRI. In addition, the availability of cross-sectional compared to longitudinal MR data in research practice is expected to stay much higher. Further studies on methods and structural aging should account for this asymmetry and emphasize valid and critical aspects of cross-sectional analysis.

Notably, our framework did not address the issue of cross-sectional mediation models (for introduction see Baron and Kenny, 1986). In contrast to the typical cross-sectional analysis of age-structure covariation, a mediation model is more complex because it additionally introduces a covariate, e.g., cognitive abilities. Then, a mediation analysis aims at testing alternative scenarios of indirect statistical effects between age, brain structure, and the covariate, e.g., whether normative age-related brain structural decline mediates cognitive decline (for review see Salthouse, 2011c). Some studies point out that cross-sectional sampling (i.e., observing only inter-individual differences) of subjects' ages, brain structure, and cognitive abilities is inappropriate to solve complex questions regarding their mutual interaction as a process of aging (Shrout and Bolger, 2002; Penke and Deary, 2010; Raz and Lindenberger, 2011). In particular, recent statistical modelling revealed the fact that substantial indirect effects in cross-sectional

studies might be observed even if the true longitudinal mediation is completely absent (Maxwell and Cole, 2007; Maxwell et al., 2011). Thus, longitudinal designs observing both intra- and inter-individual variations of structure and cognition seem to be more promising to disentangle different hypotheses about mediation of cognitive decline (Salthouse, 2011c).

4.1.3 Summary and perspectives

Here we presented analytical approaches to age-related differences and aging in MR-based markers of brain morphometry. All reviewed models afford whole brain analysis of voxel- or surface-based neuroimaging data. We focused on the detection of age effects, the estimation of population mean trajectories and individual decline. In particular, we assumed that aging might vary across brain regions (i.e. space), lifespan phases (i.e. time), and subjects. Accounting for these sources of variability would have increased model complexity in terms of numbers of parameters and degrees of freedom. Each of these 'extensions' might provide sophisticated insights into the process of structural development and aging in future studies.

Emergent properties in regional patterns: Recent studies have emphasized that there is a consistent pattern of inter-regional covariance of brain structure (Lerch et al., 2006; Colibazzi et al., 2008; Nosarti et al., 2011; Eyler et al., 2011). Other studies have explicitly related these covariance patterns to age differences (Alexander et al., 2006; Brickman et al., 2007; Bergfield et al., 2010). The joint variation of local neuroanatomy across subjects raises the question, which latent factors 'orchestrate' regional structural development and aging? Moreover, these covariations define structural developmental networks with potentially differential age-related trajectories and specific modifiers or contributors.

Age trajectories and structural plasticity: The reviewed parametric and nonparametric models allow the detection and estimation of region-specific nonlinearities of lifespan brain structural trajectories (Ziegler et al., 2012b). Interestingly, studies on learning-induced structural plasticity have revealed localized brain changes after intense training of motor skills or acquisition of abstract knowledge (Draganski et al., 2004, 2006; Boyke et al., 2008; Scholz et al., 2009; Engvig et al., 2010). Then the concept of structural plasticity can be embedded in the above framework of development and aging. Plasticity can be thought of as event-related, short-term disturbances of the structural age trajectories $g(age)$. As a consequence of the training, the directions of local trajectories exhibit changes (e.g., quadratic $\ddot{g}(age) \neq 0$) during a comparable short period of weeks or a few months (see also Taubert et al., 2010). However, it is still unknown how the local age trajectories and change parameters (e.g., $\mathbf{I}_0$ and $\mathbf{S}$) before and after the training period are related to the quantitative characteristics of induced short-term structural change.

Individual prediction of structural change: In order to estimate the structural trajectories in cross-sectional samples, we supposed smooth functions of age. Interestingly, the supposed temporal smoothness (or autocorrelation) of trajectories $g_i^{(k)}(age)$ applied to the within-subject level might allows individual predictions of prospective brain changes.

Acknowledgments

Data collection and sharing for this project was funded by the Alzheimer's Disease Neuroimaging Initiative (ADNI) (National Institutes of Health Grant U01 AG024904). ADNI is funded by the National Institute on Aging, the National Institute of Biomedical Imaging and Bioengineering, and through generous contributions from the following: Abbott; Alzheimer's Association; Alzheimer's Drug Discovery Foundation; Amorfix Life Sciences Ltd.; AstraZeneca; Bayer HealthCare; BioClinica, Inc.; Biogen Idec Inc.; Bristol-Myers Squibb Company; Eisai Inc.; Elan Pharmaceuticals Inc.; Eli Lilly and Company; F. Hoffmann-La Roche Ltd and its affiliated company Genentech, Inc.; GE Healthcare; Innogenetics, N.V.; Janssen Alzheimer Immunotherapy Research & Development, LLC.; Johnson & Johnson Pharmaceutical Research & Development LLC.; Medpace, Inc.; Merck & Co., Inc.; Meso Scale Diagnostics, LLC.; Novartis Pharmaceuticals Corporation; Pfizer Inc.; Servier; Synarc Inc.; and Takeda Pharmaceutical Company. The Canadian Institutes of Health Research is providing funds to support ADNI clinical sites in Canada. Private sector contributions are facilitated by the Foundation for the National Institutes of Health (www.fnih.org). The grantee organization is the Northern California Institute for Research and Education, and the study is coordinated by the Alzheimer's Disease Cooperative Study at the University of California, San Diego. ADNI data are disseminated by the Laboratory for Neuro Imaging at the University of California, Los Angeles. The Open Access Series of Imaging Studies (OASIS) is supported by grants P50 AG05681, P01 AG03991, R01 AG021910, P50 MH071616, U24 RR021382, R01 MH56584.

4.2 Bayesian Decline Modelling

Gabriel Ziegler[1], Robert Dahnke[1], Christian Gaser[1,2], and the Alzheimers Disease Neuroimaging Initiative[3]

1 Structural Brain Mapping Group, Department of Psychiatry, Jena University Hospital, Jena, Germany.

2 Department of Neurology, Jena University Hospital, Jena, Germany.

3 Data used in the preparation of this article were obtained from the Alzheimer's Disease Neuroimaging Initiative (ADNI) database (www.loni.ucla.edu/ADNI). As such, the investigators within the ADNI contributed to the design and implementation of ADNI and/or provided data but did not participate in analysis or writing of this report. Complete listing of ADNI investigators available at http://adni.loni.ucla.edu/wp-content/uploads/how_to_apply/ADNI_Authorship_List.pdf.

Type of contribution Manuscript based on conference abstract "Individual Change Patterns in Elderly and the Structural Covariance of Decline", presented at the Annual Meeting of Human Brain Mapping, 2012, Beijing, China.

Personal contribution G.Z. conceived and designed the study, adapted algorithms for Bayesian decline modelling, implemented PLSC for decline parameters, preprocessed the MRI data, analyzed the MRI data, and wrote the manuscript. R.D., C.G. helped to preprocess the data, R.D. supported server administration for calculations.

4.2.1 Abstract

What can a single MRI scan tell us about the ongoing speed of structural decline in elderly people ? In order to explore this question, we aimed at the variability and the covariance of individual decline parameters in healthy and pathological brain aging using repeated measurements MRI. For this purpose we used voxel-based morphometry (VBM) to investigate 3-7 scans of 616 elderly subjects between 57-92 years of age from the ADNI longitudinal MRI dataset. This included 193 healthy elderly, 295 subjects with Mild Cognitive Impairment (MCI) and 128 subjects with Alzheimer's Disease (AD). Using two level Bayesian decline modelling we estimated the current structural state, the rate of decline and the rate of accelerated shrinkage of voxelwise grey matter volume. Finally, we explored predictive patterns of decline by application of multivariate partial least squares analysis in healthy aging and MCI subjects.

4.2.2 Introduction

Age-related decline of brain structure is a highly individual spatiotemporal process which is accessible with Magnetic Resonance Imaging (MRI) (Fjell and Walhovd, 2010; Raz and Kennedy, 2009). Unfortunately, the majority of studies restrict their focus on the general course of regional atrophy using either cross-sectional or longitudinal methods (Raz et al., 2010). However, a single subject's local tissue volume at a certain age can be characterized more specifically. Thus, we here exploit the concept of a 'state space' of structural aging, which represents the states of the individual brain structure as a process of healthy or pathological aging. Using taylor expansion around a particular age, each subject's trajectory g can be approximated with the following parameters (Figure 4.5A). The first parameter is the current structural state $g(age)$ which reflects the results of its precedent development. This involves the cumulative effects of maturation, plasticity and previous age-related structural loss. Independent of the state, the brain is characterized by the current rate of decline $\dot{g}(age)$ in the very same age. This rate represents the severity of the ongoing atrophic process. Moreover, the rate of decline itself can undergo changes indicated by the third decline parameter, the current rate of acceleration $\ddot{g}(age)$. These accelerations might indicate effects of the 'driving forces' underlying development and aging which includes the contributions of protective as well as risk inducing factors in the joint system of genes, behavior and environment (Baltes et al., 2006). Consequently, each subject is characterized by generalized decline coordinates $G(age) = [g, \dot{g}, \ddot{g}, \dots]$ which are spatially multivariate, and refer to the whole regional patterns of a neuroanatomical marker, e.g., local grey matter volume. Importantly, subjects are supposed to differ with respect to their lifespan trajectories, and thus each subject has its unique set of brain parameters of decline (Figure 4.5B). Here we investigate individual decline parameters $g, \dot{g}, \ddot{g}$ on a local voxelwise level in healthy and pathological aging and explore the covariance of $[g, \dot{g}]$ in the 'state space'.

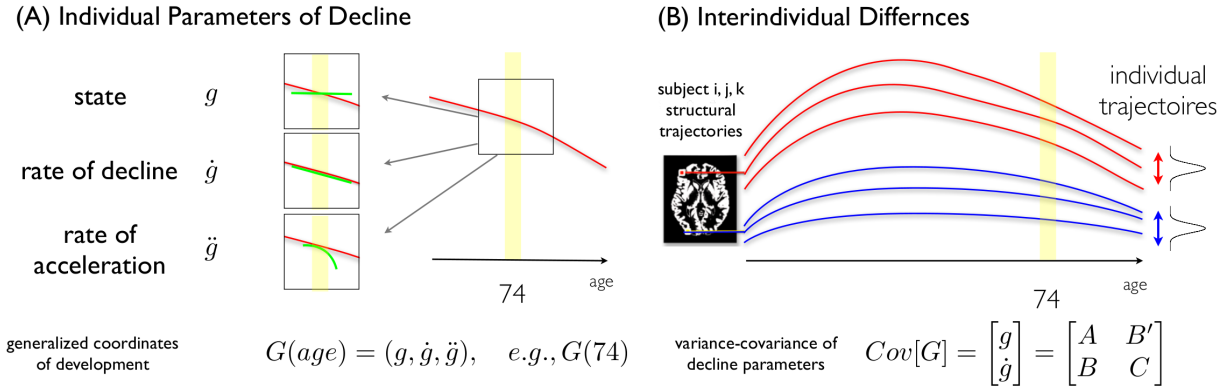

Figure 4.5: Overview of individual parameters of structural decline. (A) Introduction of generalized coordinates of decline using taylor expansion of the structural trajectory around a certain age, e.g., 74. The states, rates of decline, rates of acceleration characterize the individual subject's brain at a certain age. (B) Individual differences of lifespan structural trajectories can be analyzed in terms of variance-covariance of decline parameters.

4.2.3 Two level Bayesian models

In order to obtain individual decline parameters $G_i(age) = [g, \dot{g}, \ddot{g}]$, we follow the multilevel Bayesian framework described by Friston et al. (2002) for the special case of two levels accounting for variations across time and subjects. Due to limitations of computational load in the large sample ADNI application with 616 subjects and 2907 scans, a spatial level is not included and a univariate voxelwise Bayesian estimation on pre-smoothed data is applied. Generally, the Bayesian approach has some advantages for the analysis of structural aging on the single subject level. Firstly, it circumvents limitations of classical inference, e.g., the sample size dependent differences of testing power (see e.g. Friston et al., 2002). Secondly, it directly allows to estimate the distribution of decline parameters given the data, including probabilistic measures of confidence. Thirdly, the hierarchical Bayesian framework directly affords modelling of inter-individual differences of intra-individual change parameters. In particular, the subjects' voxelwise grey matter volume observations $\mathbf{y}$ have been modelled using the following two levels

$$\mathbf{y} = \mathbf{X}^{(1)}\mathbf{G} + \boldsymbol{\epsilon}^{(1)} \tag{4.10}$$

$$\mathbf{G} = \mathbf{X}^{(2)}\boldsymbol{\theta} + \boldsymbol{\epsilon}^{(2)} \tag{4.11}$$

with the matrix of first level individual decline parameters $\mathbf{G}$, second level group decline parameters $\boldsymbol{\theta}$ and the gaussian errors $\boldsymbol{\epsilon}^{(i)} \sim \mathcal{N}(\mathbf{0}, \mathbf{C}_\epsilon^{(i)}), i = 1, 2$. The first level models individual states $g(age)$, rates of decline $\dot{g}(age)$ and rate of acceleration $\ddot{g}(age)$ as within-subjects effects of time (Figure 4.6A). The second level models group expectations and individual differences of decline parameters specific for healthy and pathological aging (Figure 4.6B). The further advantage of the multilevel Bayesian decline modelling framework is that higher levels serve as priors for the

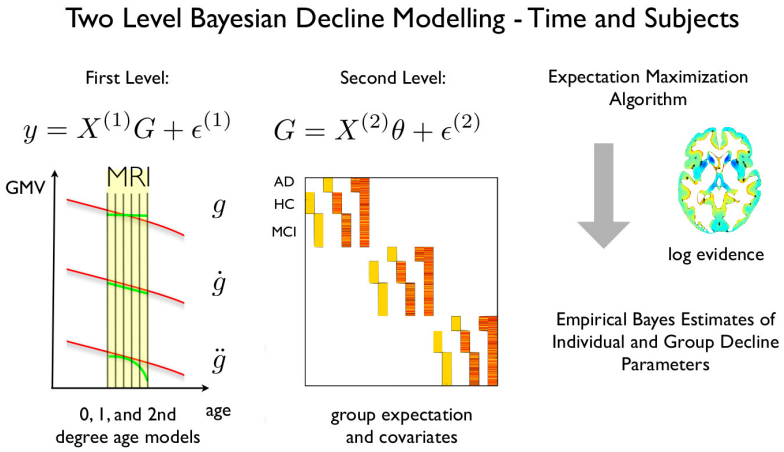

Figure 4.6: Bayesian two level decline modelling to analyze 2907 grey matter segments of 616 subjects from the ADNI database with ages 57-92. The first level models the individual effects of time in terms of centered zero, first and second order polynomials of time (left). The regressors have been orthogonalized. The second level models the individual differences of first level decline parameters separate for the groups HC, MCI, and AD (middle). Age, gender, and ticv have been additionally entered as covariates. The final log evidence obtained from expectation-maximization (EM) is shown (right).

lower level parameters which can be useful for noisy and artifact-prone longitudinal MRI series:

$$E(\mathbf{G}) = \mathbf{X}^{(2)}\boldsymbol{\theta} \tag{4.12}$$

$$Cov(\mathbf{G}) = \mathbf{C}_{\epsilon}^{(2)} \tag{4.13}$$

The group parameters of the second level are treated as *a-priori* unknown to implement a parametric empirical bayes (PEB) estimation (for details see Friston et al., 2002). This is achieved by setting their covariance to infinity, i.e., $Cov\{\boldsymbol{\theta}\} = \infty$, and thus the flat priors impose no constraints on the data. Then the aim of the Bayesian estimation is the conditional probability of the individual and group parameters given the local brain data, i.e., the posterior densities $P(\mathbf{G}|\mathbf{y})$ and $P(\boldsymbol{\theta}|\mathbf{y})$ respectively. Under the assumption of gaussian errors, the posterior is fully characterized by its expectation and its covariance for both levels. The further estimation of covariance components is based on the parametrization of the covariances $C_{\epsilon}^{(i)} = \sum \lambda_j^{(i)} Q_j^{(i)}$, with hyperparameters λ_j and covariances models Q_j. As covariance constraints we here applied the identity matrix for the first level, and group specific variances for either the states g, the rates of decline $\dot{g}$, and the rates of accelerations $\ddot{g}$ respectively for the second level. Finally, the full decline model estimation was performed using expectation maximization as implemented in SPM8 (Wellcome Trust Centre for Neuroimaging, London, UK, SPM Webpage). It estimates parameters and hyperparameters using and E-step, that finds the conditional expectation of the parameters, holding the hyperparameters fixed and a M-step, that updates the maximum likelihood estimate of the hyperparameters, for fixed parameters (Friston et al., 2002).

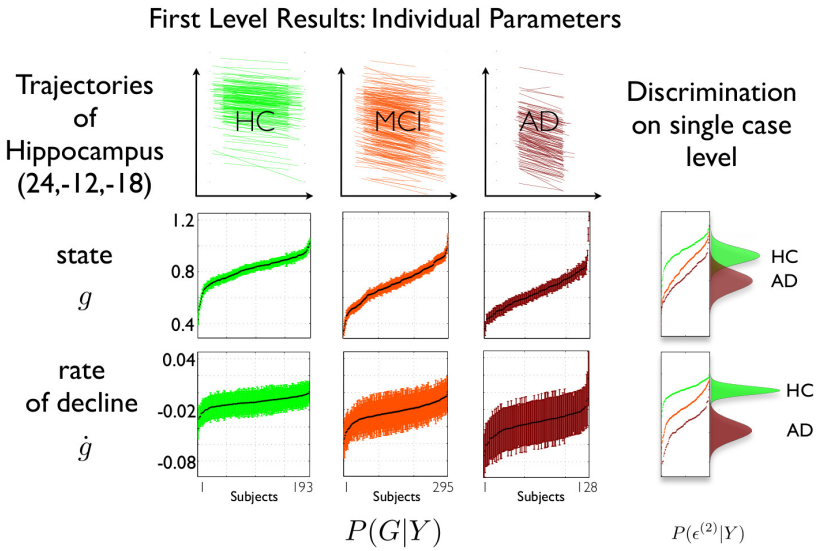

Figure 4.7: Individual grey matter decline trajectories from Bayesian two level modelling for a single hippocampus voxel (24,-12,-18) mm MNI is shown (upper row). Age was standardized for visualization. Expectations of individual decline states and rates of decline are shown in ascending order (middle and bottom row). In addition the $\mu \pm 1.96\sigma$ confidence intervals of the posterior distribution is attached. Between-subjects distributions of individual decline parameters for HC and AD groups are depicted on the right.

First Level Individual Parameters

The results of a two level Bayesian decline model estimation in 616 ADNI subjects is depicted for a single hippocampus voxel (Figure 4.7). Here we restricted the within-subjects model to simple linear effects of time. The corresponding individual decline trajectories clearly revealed the severe effects of pathological aging in subjects with mild cognitive impairment (MCI) and Alzheimer's Disease (AD). Also depicted are the conditional subject parameters $E(\mathbf{G}|\mathbf{y})$ attached with its $\mu \pm 1.96\sigma$ interval of the variances $Var(\mathbf{G}|\mathbf{y})$. The latter served as a useful measure of confidence and substantially varies with preprocessing errors and the number of follow-up measurements. Moreover, the individual differences of structural brain aging are reflected by between-subjects distributions of decline parameters (Figure 4.7 right). Interestingly, even only inspecting a single voxel, we observed almost non-overlapping individual rates of decline in healthy aging vs. Alzheimer's Disease, which indicates that the current speed of atrophy might serve as a promising marker for pathological aging using multivariate analysis.

Second Level Group Parameters

In addition, the two level Bayesian models revealed the conditional expectation and variances of healthy and pathological group decline parameters given the ADNI sample. We first inspected the local rates of atrophy in the healthy aging group (Figure 4.8 and 4.9). Under correction of age differences, the Bayesian estimates of second level local rates of decline $\dot{g}$ clearly emphasized the ongoing atrophy in elderly subject's bilateral putamen, the nucleus caudatus, thalamus, the

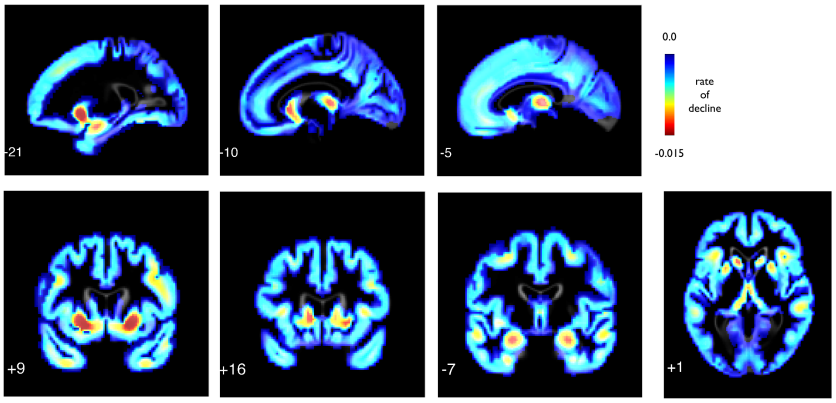

Figure 4.8: Second level decline parameters from Bayesian two level modelling of the ADNI sample: Expectation $E(\dot{g}|Y)$ of the local decline rates of grey matter volume for 193 healthy elderly subjects (mean $\pm$ std of age: 76.5 ± 5.6 years). Atrophy rates were found to be higher in fronto-temporal cortical regions and strongest in subcortical grey matter.

medial and lateral temporal lobe, the anterior insula and to a lesser degree further fronto-parietal cortex regions. Thus, the shrinkage in the subcortical structures was found to be predominant in healthy aging during the 7th to 9th decade (Figure 4.8). Moreover, individual differences of local rates of atrophy exhibited a highly similar pattern (Figure 4.9). Our sample of 193 healthy elderly subjects indicated that the individual differences of intra-individual change of local grey matter are strongest in striatal, hippocampal, and thalamus regions. Notably, the log model evidence of the Bayesian decline model was found to be comparable low in basal ganglia and thalamus, indicating worse fit and erroneous influences (Figure 4.6).

Furthermore, we additionally compared states g and rates of decline $\dot{g}$ in healthy and pathological aging groups (Figure 4.10). Healthy aging structural states (for a comparable age) of regional grey matter volumes were found to be higher in widespread cortical and subcortical regions. Thus these existing differences indicate a differential development in the groups even before the first MRI measurement. Moreover, the group rates of decline exhibited substantially increased rates of local atrophy in the pathological aging groups. We observed up to 4 times higher annual decline in subjects with Alzheimer's Disease, in particular in the frontal-temporal cortex and the medial temporal lobe grey matter.

Nonlinearities and Accelerated Aging

Furthermore, we explored whether there is evidence for late life acceleration of structural decline, as suggested by the cross-sectional analysis of the IXI adult lifespan sample. On the between-subjects level, we observed steeper grey matter decline for older subjects in lateral and medial temporal lobe, the insular cortex and thalamus (Figure 4.11A) Moreover, we also assessed the within-subjects rate of acceleration in a narrow-age band subsample around 74 years. On the local ROI level, the decline parameter confirmed substantial accelerated decline within medial temporal lobe and the insula (Figure 4.11B)

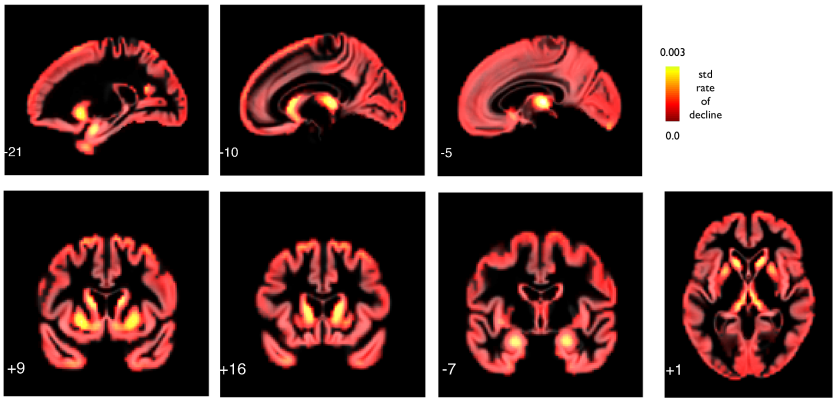

Figure 4.9: Second level decline parameters from Bayesian two level modelling of the ADNI sample: Variance in terms of $Var(\dot{g}|Y))^{1/2}$ of the local decline rates of grey matter volume for 193 healthy elderly subjects. Variability on the second level indicates individual differences of local rates of decline $\dot{g}$ which are not due to differences of age, ticv, and gender.

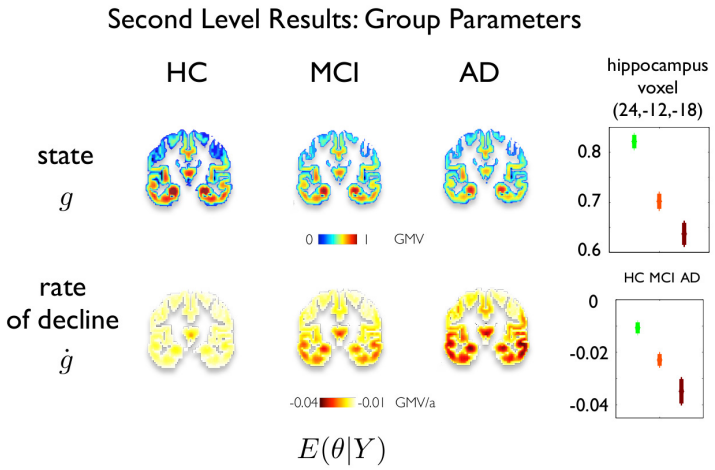

Figure 4.10: Second level decline parameters from Bayesian two level modelling of the ADNI sample. Expectation of states (top row) and rates of decline (bottom row) in healthy controls (HC), subjects with mild cognitive impairment (MCI), and with Alzheimer's disease (AD). Hippocampus voxel (24,-12,-18) mm MNI comparison of effects (right). Observed differences are independent of differences of age, ticv, and gender.

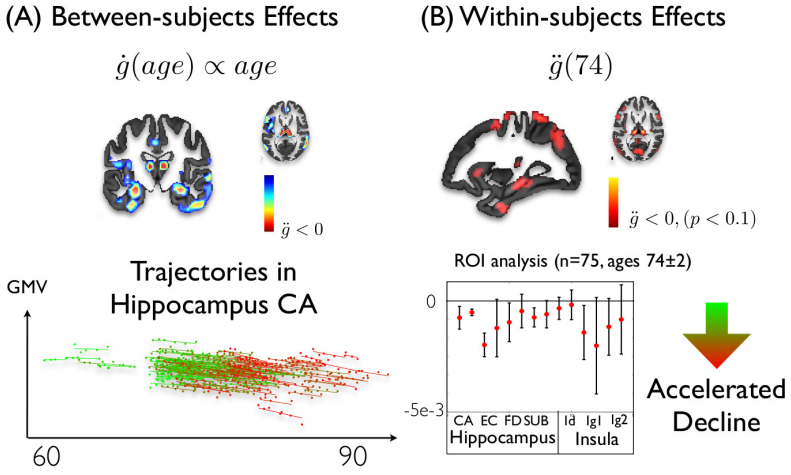

Figure 4.11: Analysis of late life accelerated decline of local grey matter volume. (A) Between-subjects effects in the 193 healthy subjects of the ADNI sample: Depicted are regional correlations of rates of decline with subject's age. Regional atrophy rates are found to be increased in elderly subjects, particularly in medial and lateral temporal lobe, insula and the thalamus. (B) Within-subjects effects of a narrow age band sample of elderly subjects with ages 74 ± 2 years: Shown are the parameter estimates of $\ddot{g}$. ROI analysis revealed accelerated aging-related decline of local grey matter volume in hippocampus and insula ROIs.

4.2.4 PLSC analysis of the covariance of decline parameters

Finally, we explored whether a single MRI scan is informative about the ongoing speed or rate of structural decline in elderly people. Many cross-sectional aging studies assess individual brain differences in relation to lifestyle and behavior. However, the cross-sectional MRI is only restricted to measure the current structural state of the brain. Because it is still unknown whether the states also reflect the rate of decline or speed of atrophy, we here explored the cross-covariance of decline parameters (Figure 4.12). In order to avoid spurious correlations induced by age differences we focussed on a narrow-age band sample of 75 healthy and 67 MCI subjects. Individual states with ages 74 ± 2. The states $g(74)$ and rates of decline $\dot{g}(74)$ were obtained from independent models in the same subjects, which avoids covariation due to modelling artefacts. Then the whole spatial pattern of decline parameters was analyzed using partial least squares correlation (PLSC, see chapter 2 for an introduction). This multivariate analysis technique was adapted to identify the spatial weightings u and v that maximize the covariances of states and rates of decline across subjects respectively, i.e.,

$$s_1 = \max_{||u||=||v||=1} Cov(gu, \dot{g}v). \tag{4.14}$$

Figure 4.13A depicts the PLSC modelling results for 75 healthy elderly subjects. Permutation testing revealed two significant latent variables (LV1 and LV2, $p < 0.05$) which contributed to the covariance of states and rates of decline in elderly subjects. Importantly, LV1's weighting patterns indicated that subjects' state of grey matter volume in medial cortex regions, precuneus,

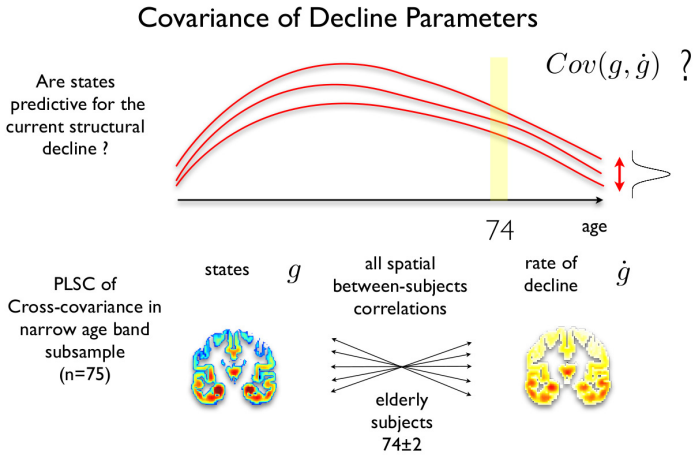

Figure 4.12: Motivation and approach to analysis of covariance of decline parameters $Cov(g, \dot{g})$. We aimed to assess the predictive potential of single MRI scans (i.e., a cross-sectional estimate) for the current rate of structural decline $\dot{g}$ (i.e., a longitudinal estimate). In order to avoid spurious effects of age, the analysis focussed on a narrow age band sample with ages 74 ± 2 years. A multivariate partial least squares correlation (PLSC) approach was chosen to provide high sensitivity and allow for distributed patterns of covariation.

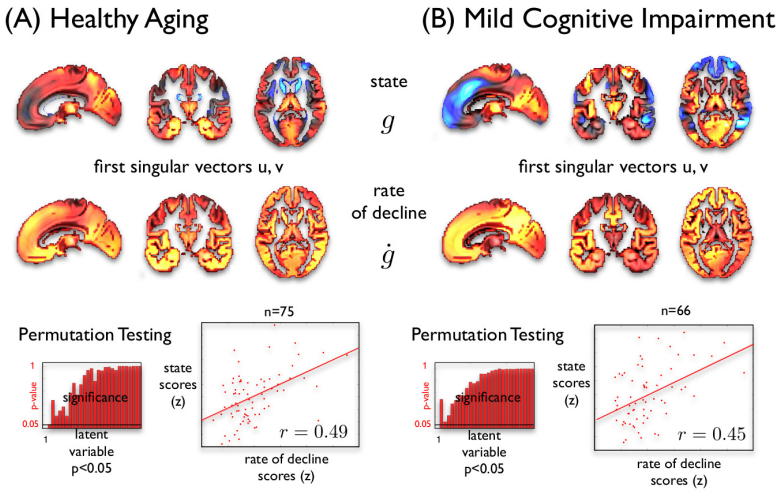

Figure 4.13: Results of the partial least squares correlation (PLSC) analysis of the spatial covariance of decline parameters $Cov(g, \dot{g})$ in 75 healthy aging subjects (ages 74 ± 2 years) and 67 subjects with mild cognitive impairment (MCI). The first and significant ($p < 0.05$) latent variable is depicted for both clinical groups. The top row shows the PLSC result for the spatial weighting pattern of states g which exhibits maximal covariation $Cov(gu, \dot{g}v)$ with the rates of decline $\dot{g}$ using the weighting pattern in the bottom row. The direction of covariation was found to be positive in widespread cortical regions in healthy aging.

the thalamus, the temporal lobe and especially hippocampal regions predicted subjects' individual rate of decline in widespread cortical regions. The observed latent variable LV1 exhibited a correlation of 0.49 explaining almost 25% of the individual differences of grey matter atrophy rates. Stated otherwise, the atrophy rates were found to be lower for subjects with higher initial grey matter volume states at the same age. This finding is in line with the hypothesis of a neural or brain reserve and indicates the continuity of person specific contributing factors to preceding and ongoing development. Interestingly, this pattern of 'reserve' was found to be substantially altered in MCI subjects (Figure 4.13B). We observed similar weightings for local rates of decline but the weightings for states were found to be completely reversed in fronto-parietal regions of cognitive impaired subjects. In conclusion, Bayesian decline modelling longitudinal MRI revealed valid estimates of decline parameters which specifically characterize each subject's aging trajectory. Considering these generalized decline parameters allowed us to identify individual differences in healthy and pathological structural aging. Finally, further analysis indicated that a substantial amount of variance in rates of decline are explained by existing differences in states of narrow-age band samples. Further studies might focus on underlying genetic and behavioral factors which contribute to this pattern of reserve and continuity.

Acknowledgments

This work was supported by BMBF grant 01EV0709. Data collection and sharing for this project was funded by the Alzheimer's Disease Neuroimaging Initiative (ADNI) (National Institutes of Health Grant U01 AG024904). ADNI is funded by the National Institute on Aging, the National Institute of Biomedical Imaging and Bioengineering, and through generous contributions from the following: Abbott; Alzheimer's Association; Alzheimer's Drug Discovery Foundation; Amorfix Life Sciences Ltd.; AstraZeneca; Bayer HealthCare; BioClinica, Inc.; Biogen Idec Inc.; Bristol-Myers Squibb Company; Eisai Inc.; Elan Pharmaceuticals Inc.; Eli Lilly and Company; F. Hoffmann-La Roche Ltd and its affiliated company Genentech, Inc.; GE Healthcare; Innogenetics, N.V.; Janssen Alzheimer Immunotherapy Research & Development, LLC.; Johnson & Johnson Pharmaceutical Research & Development LLC.; Medpace, Inc.; Merck & Co., Inc.; Meso Scale Diagnostics, LLC.; Novartis Pharmaceuticals Corporation; Pfizer Inc.; Servier; Synarc Inc.; and Takeda Pharmaceutical Company. The Canadian Institutes of Health Research is providing funds to support ADNI clinical sites in Canada. Private sector contributions are facilitated by the Foundation for the National Institutes of Health (www.fnih.org). The grantee organization is the Northern California Institute for Research and Education, and the study is coordinated by the Alzheimer's Disease Cooperative Study at the University of California, San Diego. ADNI data are disseminated by the Laboratory for Neuro Imaging at the University of California, Los Angeles.

Chapter 5

General Discussion

The general scope of this thesis is the development of computational models and methods to study major aspects of lifespan brain structural development using MRI data. The framework of lifespan psychology provides the conceptual basis and a guideline to explore: (a) *multiple dimensions* in terms of brain regions and cognitive abilities, (b) *multiple directions* in terms of decline rates and nonlinearities of lifespan trajectories and (c) the *individual differences* of development by assessing subject-specific parameter changes. The following discussion aims at condensing the methodological aspects and empirical findings to draw conclusions and describe future research possibilities in the field of lifespan computational neuroscience.

5.1 Covariance of Brain Structure and Cognitive Abilities in Early Lifespan

The first part of this thesis focusses on individual differences in brain morphology in early lifespan, namely in children and adolescents. Partial least squares correlation (PLSC) was used to extend the common psychometric factor modelling of multiple cognitive abilities tests to explore the covariation with local GM patterns obtained from VBM. Because cognitive abilities are not sufficiently represented by a single score (Jensen, 1998), a multivariate approach was applied to account for the multidimensionality of the covariance in brain structure and cognitive abilities. Using latent variable modelling, it was demonstrated that Spearman (1904)'s 'positive manifold of cognitive abilities' can be linked directly to macrostructural differences of cortical and subcortical networks without using an explicit representation of the g-factor or factor analysis. The identified dominant direction of maximum covariance of local GM patterns and the abilities of general intelligence and executive functions revealed predominantly positive weightings across all tests and brain regions. Thus, the estimated structure-cognition covariance at the transition between the first and second decade of life (mean age 11.7 years) extends the positive manifold to magnetic resonance (MR)-based measures of local GM volume. An abundance of studies in neurodevelopmental imaging have revealed brain structural correlates of cognitive abilities in early lifespan (Shaw et al., 2006; Wilke et al., 2003; Lange et al., 2010; Karama et al., 2009,

2011; Frangou et al., 2004; Tamnes et al., 2010c, 2011; Østby et al., 2011, 2012; Porter et al., 2011; Pangelinan et al., 2011), early and middle adulthood (Amat et al., 2008; Choi et al., 2008; Gunning-Dixon and Raz, 2003; Hartberg et al., 2010; Gong et al., 2005; Colom et al., 2006; Haier et al., 2005, 2010; Narr et al., 2007; Hulshoff Pol et al., 2006; Burzynska et al., 2012) and late lifespan (MacLullich et al., 2002; Raz et al., 2008; Reuben et al., 2011; Schretlen et al., 2000; Elderkin-Thompson et al., 2008; Gunning-Dixon and Raz, 2003; Burzynska et al., 2012). Focussing on regional volumes, voxel-based GM volume or cortical thickness estimates, studies on late childhood and early adolescence reveal predominately positive associations of intelligence quotient (IQ) or g-factor scores in the fronto-temporo-parietal cortex regions (Shaw et al., 2006; Wilke et al., 2003; Lange et al., 2010; Karama et al., 2009, 2011; Frangou et al., 2004; Pangelinan et al., 2011). These univariate analysis results are consistent with the observed pattern for the dominant latent variable in the age-corrected multivariate PLSC models. However, consistency within existing studies is restricted by their obvious heterogeneity with respect to the spatial distribution and the directions of the observed effects. Potential influences and factors contributing to these variations in the regional networks correlate with cognitive abilities and general intelligence, and will be discussed further.

5.1.1 Regional Distribution of Covariance

It is expected that studies using either voxel-based or surface-based measures would show correlated but likely different results due to the fundamentally different approaches of the methods to local cortical properties (Hutton et al., 2009; Mietchen and Gaser, 2009). This may cause a slight bias in the reported GM networks due to intelligence differences between individuals in diverse studies. However, the PLSC finding of a considerable involvement of subcortical medial temporal lobe and striatum GM volume to individual differences in multiple cognitive abilities that is presented in this thesis would be missed using a purely surface-based approach.

Studies vary considerably with respect to their treatment of potential confounders of individual brain differences, especially global brain measures. In early lifespan studies, global brain measures are sometimes included as covariates (Wilke et al., 2003; Karama et al., 2011; Pangelinan et al., 2011) or they are not even mentioned in the statistical analysis (Shaw et al., 2006; Frangou et al., 2004; Tamnes et al., 2011; Østby et al., 2011). At the same time, Karama et al. (2011) clearly demonstrated the changes of observed region-specific g-factor effects on cortical thickness by inclusion of measures of total brain volume. Unfortunately, the authors argued against a 'full correction' procedure in order to observe more widespread effects. However, there is a consistent finding of a positive relationship between global brain parameters and individual differences in intelligence (McDaniel, 2005; Rushton and Ankney, 2009). These are likely to be driven by more elementary biological processes such as biological growth factors and hormones, which influence body height and brain development (Taki et al., 2012). According to the parieto-frontal integration theory (P-FIT) of intelligence, individual differences reflect variability of neuronal processing in a distributed network of brain regions (Jung and Haier,

2007). In order to differentiate subtle and distributed differences of structural brain networks from a global growth process, it is clearly preferable to include body- or brain-scale in terms of additive or multiplicative effects. Then, multivariate approaches might provide the required sensitivity to detect the fine-grained and localised residual covariation with general intelligence or more specific cognitive domains. In the above PLSC analysis the applied partialling of global brain parameters increases the number of significant latent variables of the covariance models, allowing more focal effects of cognitive tests to be detected.

A further issue in the spatial distribution of effects using univariate analysis is the psychometric property of the cognitive predictor. Most studies use the full scale IQ or IQ composite scores directly(Wilke et al., 2003; Karama et al., 2009; Misaki et al., 2012; Pangelinan et al., 2011), whereas others obtain g-factors from structural equation modelling (SEM) or factor analysis (Colom et al., 2006; Karama et al., 2011). The latter focusses explicitly on modelling the shared variance of many cognitive subtests to identify the common abstract source of individual differences, independent of materials or domains (Lubinski, 2004; Jensen, 1998). This results in specific loading patterns across cognitive subtests, which is often unaccounted for in the IQ composite scores. Although there are high correlations of IQ and g-factor, the resulting cognitive construct and neuronal substrates are supposed to differ. Although eye movements and attentional, executive and working memory operations are required for many domains of cognitive abilities, there is still a lack of specificity of the proposed P-FIT theory for the involved sets of cognitive processes (see comments Jung and Haier, 2007). Impressively, Colom et al. (2006) showed that the number of regional clusters with significant effects increased with the g-factor correlations of a particular subtest. Therefore, hypothesis-driven studies focussing on higher levels of abstractness are expected to provide more heterogeneous and distributed results with lower predictability (Noveck & Prado comment Jung and Haier, 2007). In contrast to the hypothesis-driven studies using IQ, g-factor or specific subtests, the presented PLSC model weightings for the subtests are determined using the maximum covariance principle, i.e., in a data-driven manner. As expected, the brain-based subtest weightings obtained in the PLSC models differ substantially from typical g-factor loadings of the Wechsler abbreviated scale of intelligence (WASI) subtests (e.g., high g-loading block and vocabulary vs. low g-loading similarities) (see also Colom et al., 2006).

5.1.2 Direction of Structure-Cognition Covariance

The dominant latent variable observed in the PLSC models echoes previously published results indicating *positive associations* of local volume or cortical thickness to measures of intelligence in late childhood and adolescence (Wilke et al., 2003; Karama et al., 2009, 2011; Lange et al., 2010; Frangou et al., 2004). However, the consistency of regional volume with cognitive ability relationships is generally weak (see also Petten, 2004; Raz and Rodrigue, 2006). The plausibility of a 'bigger is better' hypothesis, notwithstanding the above PLSC analysis and the empirical evidence (e.g. Shaw et al., 2006), suggests more complex models of associations in childhood

and adolescence. This becomes even more true if one aims at exploring the covariance across the entire human lifespan (Petten, 2004). If one focusses strictly on the direction (i.e., the sign) of the major cortical effects of studies on a volume/thickness-cognitive abilities relationship, the following association has been observed, i.e., positive (+) or negative (−) (ordered with an increasing mean of the particular investigated (sub-) sample): (−) early-middle childhood (Shaw et al., 2006), (+) late childhood (Shaw et al., 2006; Pangelinan et al., 2011; Wilke et al., 2003; Karama et al., 2009, 2011), (−) adolescence (Tamnes et al., 2010c, 2011; Østby et al., 2011, 2012; Porter et al., 2011), (+) early adulthood (Choi et al., 2008; Burzynska et al., 2012; Haier et al., 2004, 2010; Hulshoff Pol et al., 2006; Narr et al., 2007), (+) middle adulthood (Hartberg et al., 2010; Gong et al., 2005; Colom et al., 2006), (+) late adulthood and elderly (MacLullich et al., 2002; Schretlen et al., 2000; Elderkin-Thompson et al., 2008; Gunning-Dixon and Raz, 2003; Burzynska et al., 2012). In the work of this thesis, observed subcortical effects (e.g. Frangou et al., 2004; Pangelinan et al., 2011) and medial temporal lobe regions (for review see Petten, 2004) were explicitly excluded, since other studies have begun to elucidate a slightly differential role for these effects in cognitive abilities. This summary of empirical evidence advocates the hypothesis of an alternating lifespan pattern of the structure-cognition covariance, i.e. $(-), (+), (-), (+), (+), (+)$. Moreover, it clearly suggests the chronological age as a fundamental covariate in order to account for the apparent dynamic changes during the human lifespan.

This thesis presents an analysis of 286 healthy children and adolescents, whereby the 'age-corrected' PLSC model estimated the covariance specifically for the mean age of approximately 11 years. The dominant latent variable (LV1) supported the second (+) of the empirical chain of directions for late childhood. Furthermore, the negative stability in the age-group PLSC model lends preliminary support for Shaw et al. (2006)'s finding of an inversion of the direction of association between early and late adulthood, i.e., the first (−). Notably, the data-driven latent cognitive scores obtained from the PLSC analysis presented in this thesis are correlated but not identical to IQ-related individual differences in the analysis by Shaw et al. (2006). In contrast to the above outlined studies, the PLSC stability coefficients of LV1 presented in this thesis did not reveal any evidence for an additional inversion to the negative associations observed in samples with mean age in adolescence (e.g. Tamnes et al., 2011). However, a second latent variable (LV2) was observed, exhibiting negative weightings in cortical regions and lending support to the finding of a negative direction in adolescents. Apart from basic methodological variations in surface-based vs. voxel-based preprocessing, a different modelling of global covariates and the potential influences for biased direction of effects will be further analysed and discussed. The work of this thesis will argue that the consistency of effects in studies on structure-cognition covariance is reduced strongly by the interaction of two factors: (a) the complexity/nonlinearity of the underlying developmental trajectories and (b) the almost exclusive application of cross-sectional sampling of these structural dynamics.

Complexity of Early Lifespan Structural Trajectories

MRI studies on human brain maturation provide insights into the complexity and differences of growth trajectories across brain regions and tissue types (Lenroot and Giedd, 2006; Giedd and Rapoport, 2010; Raznahan et al., 2011). These studies identify inverted-U shaped and curvilinear trajectories of local GM volume, i.e., further denoted by $g(age)$ (Gogtay et al., 2004; Lenroot et al., 2007) and cortical thickness (Shaw et al., 2006; Shaw, 2008; Sowell et al., 2004), and temporally continuous increases of WM volume into early adulthood (Ostby et al., 2009; Tamnes et al., 2010c).

In particular, longitudinal studies report the age of maximum GM in cortical regions between 7-13 years (Lenroot et al., 2007) and 7.5-11 years (Shaw, 2008). As outlined in (Brain Development Cooperative Group, 2012) and from the present cross-sectional analysis, the NIH sample suggested mainly monotone decreasing GM volume trajectories. However, the work presented in this thesis also observed a few prefrontal, temporal and parietal regions with slightly prolonged development and maxima between the ages of 6 and 10 years. In a groundbreaking study Shaw et al. (2006) found evidence that a prolonged development in frontal regions (i.e., delayed maxima of $g(age)$) might be related to higher measures of general intelligence. However, the underlying neurobiological processes of these early increases and subsequent continuous decline of cortical GM volume during the second decade of life are not completely understood. Apoptosis, synaptic pruning, dendritic branching, reduction of the neuropil and increases in axonal size and myelination are presumably involved in the macroanatomical changes (Huttenlocher, 1990; Huttenlocher and Dabholkar, 1997; Gogtay et al., 2004; Shaw, 2008; Tamnes et al., 2010c). Moreover, studies have begun to elucidate the complex gene-environment interactions in healthy brain maturation (Lenroot et al., 2009; Lenroot and Giedd, 2011). The complex structural maturation process is accompanied by a steady increase in cognitive abilities (Waber et al., 2007; Luna et al., 2004). During subsequent discussion, we further denote the cognitive developmental trajectories using functions $c(age)$ (with the temporal derivative denoted by $\dot{c}(age)$).

Contributors to Covariance in Cross-Sectional Studies

The P-FIT theory of intelligence suggests that individual differences of cognitive abilities might be due to a differential information processing which is related to macroanatomical variations in the underlying GM networks and their connectivity (Jung and Haier, 2007). Moreover, as emphasised by (Tamnes et al., 2011; Petten, 2004), the structure-cognition covariance might, at least in part, be due to subtle differences in the individual biological maturational status of these networks. This idea can be formalised using subtle biological age differences Δage_i, causing subtle gains (or losses) in brain variables $\Delta g_i = \dot{g}(age)\Delta age_i$ and cognitive variables $\Delta c_i = \dot{c}(age)\Delta age_i$ relative to the mean trajectory across all individuals $g(age)$ and $c(age)$, respectively. Consequently, even for a fixed chronological age, this 'model of accelerated development' predicts children to be more or less developed in *both* brain structure and cognitive variables, i.e., $g_i(age) \approx g(age) + \Delta g_i$ and $c_i(age) \approx c(age) + \Delta c_i$. The model implies the follow-

ing structure-cognition covariance across subjects for a particular age: $Cov(\Delta\mathbf{g}, \Delta\mathbf{c})(age)$. One can easily observe that the direction of the covariance directly depends on the direction of the developmental growth or decline process, in particular the following sign: $sign(\dot{g}(age)\dot{c}(age))$. The 'model of accelerated development' is in line with findings of a negative covariance in adolescents due to cortical thickness reductions and concurrent increases in cognitive abilities (see e.g. Tamnes et al., 2010c, 2011; Østby et al., 2011, 2012; Porter et al., 2011). As mentioned above, LV2 in our PLSC models also supports these findings by indicating negative cortical weightings with positive weights on most WASI and CANTAB test scores. In addition, the positive covariance observed in most late-life studies also lends support to this idea of 'accelerated development' (MacLullich et al., 2002; Schretlen et al., 2000; Elderkin-Thompson et al., 2008; Gunning-Dixon and Raz, 2003; Burzynska et al., 2012). However, the model contradicts the findings of (Shaw et al., 2006) and the positive covariance findings of most studies of early adulthood (Choi et al., 2008; Burzynska et al., 2012; Haier et al., 2004, 2010; Hulshoff Pol et al., 2006; Narr et al., 2007). These discrepant findings suggest there are additional contributors to the structure-cognition covariance, independent of slightly accelerated and decelerated development of individual subjects (as also discussed by Tamnes et al., 2011).

In the context of the complexity and nonlinearity of early lifespan trajectories, it is important to note the shortcomings of cross-sectional sampling to analyse lifespan dynamics of the structure-cognition covariance. Firstly, cross-sectional samples with age ranges that include non-monotonic structural and cognitive trajectories are prone to a bias due to the pooling of effects with different directions. Secondly, the underlying assumption of the 'accelerated development model' (and other cross-sectional analysis approaches) is that individual differences are only due to different 'biological' ages on the *same* general developmental courses. In contrast, lifespan developmental theory (Baltes et al., 2006; Quartz and Sejnowski, 1997) and longitudinal evidence (Shaw et al., 2006; Raz et al., 2010) strongly suggest substantial intersubject variability of lifespan brain and cognitive trajectories. Thus, as outlined in Chapter 4 of this thesis, continuous individual trajectories of local brain structure $g_i(age)$ and cognitive ability $c_i(age)$ of subject i will be further supposed. Using the linear Taylor expansion of these trajectories around age_0, with $age = age_0 + \Delta age$, i.e., $g_i(age) \approx g_i(age_0) + g_i'(age_0)\Delta age$ and $c_i(age) \approx c_i(age_0) + c_i'(age_0)\Delta age$, a more sufficient representation of the structure-cognition covariance across subjects is derived:

$$\begin{aligned} Cov(\mathbf{g}, \mathbf{c})(age) &\approx Cov(\mathbf{g}(age_0) + \mathbf{g}'(age_0)\Delta age, \mathbf{c}(age_0) + \mathbf{c}'(age_0)\Delta age) \\ &= Cov(\mathbf{g}, \mathbf{c})(age_0) + Cov(\mathbf{g}'(age_0)\Delta age, \mathbf{c}'(age_0)\Delta age) + Cov_{cross} \\ &= Cov(\mathbf{g}, \mathbf{c})(age_0) + Cov(\Delta\mathbf{g}, \Delta\mathbf{c})(age_0) + Cov_{cross} \\ &= Cov_{previous} + Cov_{present} + Cov_{cross} \end{aligned}$$

Consequently, by assuming individual growth or decline trajectories of brain structure and cognitive abilities, three contributors to the covariance at a particular age are observed. The first

term, $Cov_{previous}$, is the covariance due to existing differences and cumulative effects of previous development, genes, plasticity, environment, etc. The second term, $Cov_{present}$, is similar to that derived from the above 'accelerated development model' and indicates the variability due to the small accelerations and decelerations of individual subjects compared to the general or average course of development at age_0.

As a result, the applied PLSC approach to morphometric substrates of cognitive abilities, as well as to other cross-sectional studies, are inherently unable to distinguish between directions of effects established during earlier or later developmental phases of the sample age range, e.g.brain growth in early childhood and pruning-related volume decline in adolescents. With the exception of the study by (Shaw et al., 2006), the alternating early lifespan developmental pattern $(-), (+), (-)$ is observed mainly in cross-sectional studies and might be biased by cumulative effects of the previous development of explored subjects. Bearing these caveats in mind, one can only speculate that the observed dominant LV1 with positive widespread volume effects on cognitive abilities stems from an early and more unspecific maturation effect that causes the observed early inversion of the covariance. Moreover, the cortical negative weightings of LV2 might be related to pruning or ongoing myelination and the concurrent increases in WASI and CANTAB scores during adolescence (see also Tamnes et al., 2011). Thus, the age-group PLSC stability coefficients provide at least some support for the hypothesis of an alternating early lifespan pattern (i.e., $(-), (+), (-)$) of the direction of the covariance. Longitudinal analysis of the multivariate structure-cognition covariance might further strengthen the validity of these findings. Moreover, application of the above concepts to adulthood and late-life decline might reveal the unknown contribution of the developmental processes in each lifespan phase (in terms of $Cov_{present}$) to the substantial heterogeneity observed in healthy elderly subjects (Raz et al., 2010).

5.1.3 Conclusion

Using VBM and latent variable modelling in healthy children and adolescents, the results presented in this thesis reveal that early lifespan brain structure shows substantial variation amongst individuals of the same age. Moreover, on average 11% (with up to 35%) of the between-subject variance of local GM volume in fronto-temporo-parietal networks was explained by profiles of cognitive abilities from the domains of general intelligence and executive functions. The observed individual differences in cognitive abilities might be due to differential information processing related to macroanatomical variations in the GM networks (Jung and Haier, 2007). Moreover, there were indications of dynamic changes of the association that might be due to processes of early lifespan brain maturation.

5.2 Structural Decline in Adulthood and Later Life

As already observed, early lifespan individual differences of brain morphology occur during maturation and are closely linked to cognitive development. This suggests that structural decline in later life might be involved in commonly observed decreases in cognitive ability in elderly subjects (Fjell and Walhovd, 2010; Raz and Rodrigue, 2006; Hedden and Gabrieli, 2004). The middle and later lifespan structural trajectories of brain morphometry, variability across subjects and the differences in healthy and pathological ageing between individuals present many remaining challenges for neuroimaging research. The second part of this thesis is, therefore, focussed on cross-sectional modelling of large-sample VBM data, the general course of age-related decline, the nonlinearities due to accelerated structural ageing, lifespan variability of local brain structure and longitudinal modelling of individual decline parameters.

5.2.1 Early Cognitive Reserve for Late Lifespan

According to lifespan biocultural co-constructivism, early lifespan differences might be expected to 'initialise', and therefore influence, brain structural and cognitive development in later life (Baltes et al., 2006). As emphasised by (Deary et al., 2009a), individual differences in cognitive capacities during the early lifespan are a major source of late-life variability in cognitive abilities. Longitudinal lifespan evidence suggests that even at around 80 years old at least 50% of the variance might be explained by childhood intelligence and cognitive capacity (Deary et al., 2009b). In addition, these studies revealed that low childhood intelligence, in terms of a stable lifelong trait (Deary et al., 2004), is a predictor of health variables and health risk factors (e.g., vascular failures) which might increase the likelihood for structural and cognitive decline in middle and old age (see also Raz et al., 2008). Indeed, research studies have explored the hypothesis that childhood intelligence represents a passive reserve capacity for late life cognitive development (Salarirad et al., 2011).

Methodologically, the distinction of previous and concurrent developmental processes is crucial for the hypothesis of an early cognitive reserve. While previous development is mainly reflected by intercepts of developmental trajectories, concurrent development is captured in the rates of change. Longitudinal lifespan samples reveal that childhood intelligence can be used specifically to explain the variability of fluid intelligence abilities and WM integrity in the elderly, but that childhood intelligence is not predictive for the future rate of decline in an individual (Salarirad et al., 2011). The exact cause of these correlations is not completely understood and is often mistakenly interpreted as 'reverse causation' in cross-sectional studies Deary et al. (2009a). It has been shown that early lifespan intelligence levels are predictive of maximum educational attainment during adulthood (Deary, 2012). Higher levels of intelligence in the early lifespan may mediate the effects of strong cognitive reserve for late life cognitive abilities and provide protection against dementia (Murray et al., 2011). Moreover, lifespan cognitive trajectories have been associated to differential cortical maturation patterns in terms of complexity of cortex shape (Mustafa et al., 2012). Other findings indicate that lower intelligence in early lifespan and

increased rates of cognitive decline in late life might be related to individual differences in iron deposits in the brain, often observed in basal ganglia; these deposits increase continuously during the process of ageing (Penke et al., 2010a). In line with this hypothesis, the work presented in this thesis showed a substantial involvement of GM volume differences in the striatum in early lifespan cognitive abilities (e.g. PLSC latent variable LV2).

5.2.2 General Course of Age-Related Structural Decline

MRI studies of the macroanatomy of the brain throughout the adult human lifespan have observed substantial regional variations in age-related trajectories (Fjell and Walhovd, 2010; Raz and Kennedy, 2009). Establishing these 'heterochronic' regional trajectories in healthy subjects is also an important step in understanding the diverse pathological forms of ageing. In contrast to the majority of published studies, the work of this thesis aimed to estimate age trajectories $g(age)$ for the whole brain and on a voxel-by-voxel basis, also taking into account the computational load of large-sample analysis. After diffeomorphic normalisation (Ashburner, 2007) 'quasi-continuous' measurement allowed *a priori* identification of unknown GM lifespan dynamics and nonlinearities in unattended subfields. The application of diverse developmental modelling techniques to the cross-sectional IXI sample of 547 subjects and the Alzheimer's Disease Neuroimaging Initiative (ADNI) longitudinal sample with 616 subjects generally corroborated earlier longitudinal findings from manual volumetry (Raz et al., 2003, 2005, 2010; Du et al., 2006), voxel-based analysis (Driscoll et al., 2009; Resnick et al., 2003; Taki et al., 2011) and surface-based analysis (Fjell et al., 2009b; Rettmann et al., 2006; Thambisetty et al., 2010). Although there are considerable methodological concerns regarding cross-sectional analysis (see e.g. Raz et al., 2005), there is considerable agreement between the findings presented in this thesis and the results from large-sample cross-sectional multicentre studies (e.g. Walhovd et al., 2011). Using parametric (e.g., polynomial) and nonparametric (e.g., smoothing spline- and Gaussian process-based) decline models, it was observed that the general course of adult lifespan GM volume in most neocortical regions is approximated coarsely by a linear function of age. This is supported by cross-sectional evidence (Walhovd et al., 2011) but comparable longitudinal studies on a voxel or vertex basis are still to be undertaken. The corresponding rates of decline in fronto-parietal regions indicate stronger age-related atrophy compared to lateral temporal and occipital lobe regions. The current findings generally support the hypothesis of a 'structural ageing gradient' of brain GM from anterior to posterior and superior to inferior, similar to observations in WM studies (Madden et al., 2009). Although the focus of this work was on approaches to healthy brain ageing and its variability, the ADNI sample findings also support earlier work on pathological ageing in subjects with mild cognitive impairment (MCI) and Alzheimer's disease (AD) (Thompson et al., 2004; Mosconi et al., 2007; McEvoy et al., 2009; Fennema-Notestine et al., 2009; Holland et al., 2012; McDonald et al., 2009; Fjell et al., 2010a).

An important finding from the current cross-sectional and longitudinal analysis is the existence of substantial nonlinearities in ageing trajectories of particular local GM regions, especially

in the medial temporal lobe hippocampus and adjacent regions. This is consistent with the literature (Fjell and Walhovd, 2010; Raz and Kennedy, 2009); specifically, the strongest support for lifespan age-related increases of atrophy rates comes from studies using manual region of interest (ROI) analysis (Raz et al., 2005) and cross-sectional studies using other semi-automated methods (Walhovd et al., 2011, 2005a). Notably, further nonlinearities are suggested by the current results (in particular in the striatum, cerebellum, parietal operculum, orbitofrontal cortex, etc.) and in longitudinal studies (Driscoll et al., 2009; Thambisetty et al., 2010; Raz et al., 2005), but their consistency across studies is much weaker. This might be related, in part, to the sample size dependency of sensitivity in classical inference, which allows detection of subtle effects using larger samples and can be overcome using Bayesian inference (Friston et al., 2002). It is worth mentioning that lifespan nonlinearities do not necessarily indicate accelerated atrophy. In most studies, age-related nonlinearities are detected in one of the following three ways: (a) cross-sectional evidence indicating significant $\ddot{g}(age) < 0$ (e.g. Walhovd et al., 2005a, 2011), (b) longitudinal evidence for $\dot{g}(age) \propto age$ at the between-subject level (e.g Taki et al., 2012; Raz et al., 2005; Fjell et al., 2009b) and (c) within-subject acceleration of atrophy, i.e, a significant $g_i''(age) < 0$ from the within-subject level of a mixed-effects model (e.g. Raz et al., 2010; Driscoll et al., 2009). Evidence (a) and (b) in large age range lifespan samples are more unspecific indications for the lifespan multi-directionality of brain structural development which might be due to an unknown combination of early adult increase in brain volume, adulthood preservation of brain volume or late-life acceleration of atrophy. However, the shape of this approximative general (or average) course of lifespan trajectories is highly uncertain due to the expected variations in individual trajectories $g_i(age)$. Therefore, the current finding of (a) in the IXI lifespan sample and (b) in the late-life ADNI sample in hippocampal regions is strongly suggestive of accelerated ageing, and the ROI-based observations of (c) in the ADNI sample is conclusive evidence of late-age accelerated decline in the medial temporal lobe.

Future longitudinal analysis might more firmly establish the existence of nonlinearities by increasing the sensitivity and reliability under spatial regularisation of decline parameters in the Bayesian multilevel framework, i.e, across time, subjects and space. The underlying neurobiological mechanisms of nonlinearities in local volume changes with age and changes in the rate of atrophy are still poorly understood. As noted by Raz et al. (2005), such nonlinearities might be due to an interaction between the cumulative and progressive effects of certain risk factors for structural ageing, such as in the case of hypertension. More generally, nonlinearities might be further explored in relation to age- or disease-dependent changes in the equilibrium of protective as well as risk-inducing 'forces' of development: i.e., $\ddot{g}(age) \propto F_{pro}/F_{risk}$ (genes, lifestyle, etc.). Notably, because the region-specific effects are focussed on the medial temporal lobe, further studies should also take into account regional variables, e.g., adjacent WM processes of late myelination (Baumann and Pham-Dinh, 2001) or changes in the WM/GM contrast (Salat et al., 2009, 2011).

In order to establish the general course of adult lifespan brain changes in clinically healthy subjects, the work of this thesis also explored the rates of atrophy in the ADNI sample for

subjects in their 7th to 10th decades. The large-sample longitudinal findings in elderly subjects indicated a clearly different pattern from the adult lifespan IXI analysis of subjects in their 3rd to 9th decades. In contrast, the IXI analysis revealed predominantly fronto-parietal cortex decline, insular age effects and almost preserved ventral and posterior regions, whereas the ADNI subjects exhibited the most severe atrophy in the subcortical putamen region, caudate nucleus, thalamus and the medial temporal lobe, while fronto-temporal cortical regions were affected to a lesser extent. This finding is supported by lifespan cross-sectional studies (Walhovd et al., 2005a, 2011) and agrees with adult lifespan and late-life longitudinal evidence using semi-automated and manual methods (Fjell et al., 2009b; Raz et al., 2003, 2005, 2010). In contrast to the current findings, the comparable age-range longitudinal study of Fjell et al. (2009b) reported the highest rates of decline in the hippocampus and the amygdala as well as substantial cortical effects. These deviations suggest that, even for samples with similar age ranges, the general course of decline is rather specific to the applied segmentation and preprocessing pipeline, i.e., VBM8 and Freesurfer, respectively. Moreover, other sample characteristics, selection of IQ, Socioeconomic Status (SES) and selective dropout might be involved.

The findings from both of the current analyses of IXI and ADNI are consistent with the idea of specific regional lifespan nonlinearities. Both the hippocampus and neostriatum exhibited an acceleration of volume loss after early and middle adulthood in the adult lifespan IXI sample, while the neocortex exhibited a continuous and linear decline in volume. Consistently, the late-life decline pattern of ADNI revealed a more substantial rate of decline in the neostriatum (especially the putamen) and the hippocampus in the elderly subjects, while the cortical regions showed a comparably lower rate of decline. In line with these subcortical nonlinearities an age-correlated increase of striatum and thalamus rates of decline, similar to the hippocampus, was also observed. This is, at least in part, supported by other findings for the striatum (Raz et al., 2010; Taki et al., 2012). Therefore, taking the advantage of VBM to perform concurrent automatic subcortical *and* cortical analysis, substantial nonlinearities were observed in the medial temporal lobe as well as further indications of late-life accelerated decline of the striatum and thalamus. These lifespan nonlinearities are likely to contribute to the pronounced late-life subcortical atrophy in the 7th to 10th decades. Notably, a major consequence of regional heterochronic decline and nonlinearities is a reduction in local trajectory redundancies. Consequently, patterns of local GM volume, e.g., $\mathbf{y} = [g^{(MTL)}(age), g^{(PFC)}(age), g^{(ITG)}(age)]^T$ become more informative about the developmental stage or disease progression of an individual. This increases the efficiency of decoding models such as, e.g., $age = R(\mathbf{y}, \beta) + \epsilon$ and affords pattern-based analysis in developmental neuroimaging.

5.2.3 Encoding and Decoding Model Nonlinearities

The above described results regarding local nonlinearities of the brain morphometric ageing trajectories have several implications for the purpose of encoding and decoding models in the context of developmental neuroimaging. In addition to classical inferences regarding age-related effects through the application of standard encoding models (e.g., polynomials), recent studies

have focussed on decoding disease progression (e.g., in terms of mini mental state examination (MMSE) scores) in dementia and on decoding of the developmental status of individuals (e.g., in terms of chronological age). These approaches (sometimes implicitly) make assumptions about the general (or average) course of regional structural decline, which substantially influences the validity of the results and the ability to make generalisable predictions.

Firstly, decline parameter estimates from small-sample cross-sectional and longitudinal studies (i.e., from encoding models) are expected to vary substantially with the sample age range and distribution. Subtle nonlinearities in lateral temporal cortex regions, even below the threshold in the IXI adult lifespan sample, might explain the finding of a stronger fronto-temporal decline in healthy elderly subjects (Fjell et al., 2009a). Apart from the basic morphometric methodology (Hutton et al., 2009), global covariate confounders (Peelle et al., 2012), appropriate vs. inappropriate age models (Fjell et al., 2010b) and the fundamental flaws in cross-sectional designs (Raz et al., 2005), these nonlinearities are expected to be the major source of the immense heterogeneity observed in structural ageing studies (Fjell and Walhovd, 2010). As successfully demonstrated by Walhovd et al. (2011), this limitation can be overcome by taking advantage of pooling, multicentre studies and semi-automated processing of publically available data (see also Fjell and Walhovd, 2010). In addition, more consistent findings can be obtained by averaging across hidden age-confounded variables that otherwise bias the sample selection procedure.

Secondly, recent studies have indicated that nonlinearities and accelerated ageing might be predictors of disease progression in preclinical and pathological ageing (Davatzikos et al., 2008; Franke et al., 2010). The nonlinearities of structural trajectories of individual subject, i.e., $g_i''(age) < 0$, might indicate short-term deviations from the normal ageing and atrophic process. A recent study by McDonald et al. (2009) suggested that these disease-related accelerations in medial temporal lobe regions are specific for the earlier phases of MCI. With increasing symptom severity the atrophic pattern seems to spread from Medial Temporal Lobe (MTL) to the neocortical areas. For the purpose of a highly valuable early MR-based diagnosis and disease monitoring system one might, therefore, aim at comparing the rate of atrophy $\dot{g}_i(age)$ of an individual patient to the atrophy expected from the general course of decline, i.e., the derivative $\dot{g}(age)$. Unfortunately, this would require follow-up measurement(s) for a particular patient, which are often not available at prodromal stages of disease. However, according to (McDonald et al., 2009) there is spatial specificity of the early disease progression in patients with MCI and, thus, it is promising to apply pattern-based decoding of disease states by only using the spatial pattern of a patient's initial GM volume $g_i(age)$ as input (Filipovych et al., 2011a,b; Misra et al., 2009). As pointed out by Dukart et al. (2011), to successfully apply decoding models (e.g., Support Vector Machine (SVM)) for disease status, one should, beforehand, account for age differences in healthy structural brain ageing. Supposing that the disease onset of MCI and dementia might be in the 6th to 9th decades, the current results suggest that the reference models $g(age)$ should account for the substantial accelerations of *healthy* decline in medial temporal lobe regions.

Thirdly, a related issue is the recent application of multivariate decoding to predict the

brain age of an individual given the general course of structural change in a large training sample of adult and elderly subjects (Franke et al., 2010). Given the current findings about late-life accelerations of structural decline, the average spatial pattern of subtle structural atrophy $\Delta\mathbf{y}$, which optimally predicts the true underlying positive age difference Δage, is expected to focus strongly on subcortical compared to cortical regions in later life. Therefore, the accuracy of pattern-based decoding of the developmental status of an individual might be considerably increased by inclusion of explicit nonlinear mapping of brain features $\Phi(\mathbf{y})$, e.g., implementing the prediction $age = R(\mathbf{y}, \beta) + \epsilon$ with a linear Bayesian scheme $R = \sum \Phi(\mathbf{y})^T \boldsymbol{\omega}$, with $\Phi(\mathbf{y}) = [\Phi^T_{lin}(\mathbf{y}), \Phi^T_{nonlin}(\mathbf{y})]^T$ and appropriate spatial priors $\mathbf{w} \sim \mathcal{N}(\mathbf{0}, \boldsymbol{\Sigma}_p)$. The model selection for highly efficient brain-predictor mappings or decoding models might be realised in a multivariate variational Bayes (MVB) framework (Friston et al., 2008).

5.2.4 Variance and Covariance of Decline Parameters

In addition to studying the general course of age-related structural decline (in terms of first-order statistics), the work of this thesis also aimed at elucidating individual differences of the brain structural trajectories on a voxel-by-voxel basis. This focus on the normal between-subject variance (or second-order statistics) of macroanatomy in ageing brains is essential in order to address a number of important issues in developmental neuroimaging. Firstly, the relative contribution and interdependencies of potential modifiers (i.e., protective as well as risk-inducing factors) of individual decline parameters were explored using generative (or encoding) models of brain ageing. Secondly, brains were characterised as developing normally or as being explicitly affected by pathology using recognition (or decoding) models. Thirdly, the contribution of structural brain variability to age-related increases of heterogeneity and de-differentiation observed in cognitive ageing was evaluated (Lindenberger et al., 2008; de Frias et al., 2007).

Unfortunately, as recently emphasised by Raz et al. (2010), the majority of longitudinal studies report mean changes of decline parameters without measuring their variance. A few exceptional studies by Raz et al. (2005, 2010) used SEM to study variances of latent change variables based on manual volumetric ROIs. At the same time, studies addressing voxel- or surface-based between-subject anatomical variability (for review see Ashburner and Klöppel, 2011) often do not model age-related differences at either the inter-individual or the intra-individual level. Taking the lifespan perspective of this thesis, the common basis of both approaches is the analysis of variance of generalised coordinates of development $G(age) = [g, \dot{g}]$, focussing on either spatial patterns of states g or local rates of change $\dot{g}$, respectively. After a short discussion of the current variance modelling results for g and $\dot{g}$ respectively, the concluding finding will demonstrate that g and $\dot{g}$ are substantially inter-related in late life.

Structural Variability in Healthy Adults

In order to assess macroanatomical variability in healthy adults and elderly subjects, a Gaussian process (GP)-based generative lifespan model was first estimated using GM segments of 1338

subjects (age range: 18-94 years). The obtained adult lifespan GP models the general course of decline and its variability in terms of a distribution over functions. Individual differences in local brain structure were supposed to be reflected by random fluctuations around a common decline function, i.e., $y = g(\mathbf{x}, \boldsymbol{\theta}) + \epsilon$, in terms of an error variance. The error of the generative model of the adult lifespan exhibited particularly high variability in the putamen, caudate nucleus and thalamus and was slightly less variable in the fronto-temporal cortex, medial occipital and inferior parietal GM. Interestingly, this variability was found to be more pronounced in subcortical regions compared to the NIH sample of children and adolescents. The analysis of the latter exhibited rather similar variances in cortical and subcortical regions, with an R^2 of up to one-third explained by latent variables of cognitive abilities in posterior cingulate cortex regions. Notably, the measured error in the generative lifespan model is only a proxy measure for the amount of brain structural variability due to individual differences because it is cross-sectional in nature, i.e., it includes measurement error variance and the variance due to age-related secular trends across the seven decades in the sample. However, a comparison of the initial state variability using the ADNI longitudinal two-level modelling revealed a very similar pattern, indicating strong subcortical variability in healthy elderly subjects. One can only speculate that the variability in the generative adult lifespan model was driven strongly by the sub-sample of 216 healthy, elderly ADNI subjects. It is important to mention the limitation of the current GP approach, which did not allow for heteroscedasticity, i.e., age-related changes in the residual variance. Visual inspection of the distributions did not support the hypothesis of age-related increases in the heterogeneity observed in cognitive ageing (Lindenberger et al., 2008; de Frias et al., 2007) and heteroscedasticity modelling extensions of the GP framework should be implemented in further studies (see e.g. Kersting et al., 2007).

A further potential application of the Bayesian framework and GPs was demonstrated by making predictions in single cases with regional pathological ageing patterns. Given the GP representation of healthy ageing and its variability, it was possible to evaluate the predictive distributions in MCI subjects. Exceptional decreases in local likelihoods were observed, especially in lateral and medial temporal lobe regions. The applied principle of capturing the healthy variance of individual structural ageing parameters and assessing the likelihood of subjects deviating from the general course of decline might be promising for longitudinal MRI datasets. In addition to considering states of individual subjects $g(age)$ from cross-sectional datasets, this framework of analysis of individual differences might be extended to generalised coordinates of decline $G(age) = [g, \dot{g}]$. This would be especially valuable for the prodromal stages of pathological ageing, when brain decline is expected to accelerate but the local GM patterns remain in the normal range of variability. Moreover, spatial regularisation of the generative model (Flandin and Penny, 2007; Friston and Penny, 2003; Harrison and Green, 2010) might improve its validity and the generalisability of predictions in clinical case-based scenarios.

Variability in Rate of Late Life Decline

Bayesian multilevel decline modelling in healthy elderly individuals also provided insights into the variability of individual rates of GM atrophy $\dot{g}(age)$. The decline variability was found to be strongest in the neostriatum, thalamus and hippocampus. The only reference study by Raz et al. (2010) also reported significant individual differences in shrinkage rates of manual ROI volumes in the hippocampus, caudate and putamen. However, in this particular study no average putamen decline or substantial lateral prefrontal cortex shrinkage variability was reported. Generally, the current findings from VBM indicate a regional specificity of late-life subcortical GM change with respect to the most prominent annual decline and individual differences. The latter might be due to the effects of commonly discussed risk factors for structural decline, e.g., genes, vascular risk factors, gender and education (Raz and Rodrigue, 2006). Although there is a subcortical genetic factor that contributes jointly to individual differences in the basal ganglia and the thalamus (Eyler et al., 2011), the support for subcortical specificity of general vascular health and hypertension is rather limited (Raz et al., 2010, 2003, 2007, 2005; Burgmans et al., 2010; Jennings et al., 2012; Gianaros et al., 2006).

As suggested recently, the observed subcortical variability in the rates of decline might be mediated by microbleeds, which are small focal microhaemorrhages that leave residual iron deposits (Harder et al., 2008). These local iron deposits are expected to increase in number across the human lifespan and are more frequently observed in brain regions with high metabolism, particularly in the basal ganglia (Haacke et al., 2005). There is evidence that iron accumulation might be involved in local neurodegeneration and demyelination (Zecca et al., 2004; Bartzokis et al., 2007, 2011) or increased inflammation (Rosidi et al., 2011) and it has been found to be increased in patients with Alzheimer's disease (Rombouts et al., 2007). MRI magnetic susceptibility imaging in elderly subjects has revealed that local iron levels in the basal ganglia and thalamus are associated with macroanatomical volumes (Sullivan et al., 2009; Rodrigue et al., 2011) and reduced cognitive capacities (Rodrigue et al., 2012; Penke and Deary, 2010). These studies are mainly cross-sectional and, thus, future longitudinal studies should focus on the hypothesis of an iron-level mediation of local ageing-related decline differences. Notably, the factors that contribute to variability in local rates of decline may also differ across brain regions, e.g., medial temporal lobe and basal ganglia.

It is worth mentioning that the observed individual differences of healthy structural ageing might also be a consequence of the applied image preprocessing steps. Although validated procedures have been applied for segmentation (Ashburner and Friston, 2005) and normalisation (Ashburner, 2007), the former might be sensitive to GM/WM contrast variations, especially in the basal ganglia regions and the thalamus (Fischl et al., 2002). Ashburner and Friston (2009) pointed out that the lower GM/WM contrast in thalamus GM might increase the spurious influence of non-uniformity artefacts. Additionally, the GM/WM contrast in cortical and medial temporal lobe regions has been found to change with increasing age (Salat et al., 2009, 2011), which might have biased the age-related declines of local GM volumes in these regions. The cur-

rent finding of a low subcortical marginal likelihood (or model evidence) of both the lifespan GP regression and the Bayesian decline models indicate stronger influences of unmodelled sources of variance such as noise.

5.3 Conclusions and Perspectives

An important contribution of this work is the conceptual refinement and adaption of univariate and multivariate statistical approaches to support future studies in the field of lifespan developmental neuroscience.

The first finding of this work on methodology is that individual differences observed in brain and behavioural variables can be effectively represented in multivariate feature spaces, especially taking advantage of kernel-based embeddings. This has been demonstrated for structure-ability mappings during early lifespan and might be also promising for other parameters in the 'biocultural co-constructivism' framework with potentially nonlinear relationships, e.g., dopaminergic neuromodulation of behaviour.

The second finding of this work is that it is promising to characterise individual differences in change in terms of generalised coordinates of brain development $G = [g, \dot{g}]$. This physical concept brings both structural brain states g and the current rate of change $\dot{g}$ in a joint framework: a 'state-space' or flow field of trajectories. As demonstrated using a longitudinal VBM sample, g and $\dot{g}$ exhibit substantial positive inter-correlations of GM networks, indicating a brain reserve and continuity of contributing factors to development in late life. The 'state-space' concept is potentially highly useful for future characterisation of normative variability in general and to explore the inner dynamics of developmental trajectories in particular. Moreover, it again raises the question of the degrees of freedom (plasticity) of neurobehavioural development, i.e.,'where can you go?'. The framework also has considerable impact for developmental pathology in late life. Future studies might consider that the first steps towards disease pathology (in terms of $\dot{g}$) can be variable according to the patient age and their initial brain state $g(age)$.

The third finding of the work of this thesis is that the normative variability of development observed in large-sample morphometry data can be captured effectively using Bayesian models and GPs. This perspective is especially promising for longitudinal data with available estimates of generalised coordinates G. Similar to the presented approach with structural brain states g, these Bayesian methods might be promising for use in the detection of subtle deviations from healthy ageing patterns in early stages of disease pathology in the brain.

Acknowledgements

First of all, I would like to thank my PhD supervisor Christian Gaser for the excellent open-minded support and for giving me the freedom to develop independent thoughts. There have been countless opportunities to learn from his tremendous expertise, his scientific skills and importantly how to finally translate ideas into scientific practice. Moreover, his international orientation and supporting me to attend worldwide conferences helped to develop a much broader perspective far beyond the PhD. I would like to thank Prof. Lutz Jäncke for his excellent supervision, and making it possible to attend to the University of Zürich and for getting through the trouble of regulations due to the external graduation. For me personally, it was a valuable experience to get in touch with the excellent educational environment at the University Zürich. I would like to particularly thank the former and current members of the Structural Brain Mapping Group and the Center of Neuroimaging Jena, especially Robert Dahnke for critical discussions about almost everything, collaboration, and not stopping to explain technical details in preprocessing algorithms, 'Adobe'-ing the imaginable, freezing, etc. and Katja Franke for her kind support, reminding and a lot of patience, Ali Winkler for valuable feedback, Raka Maitra for very funny discussions. Last but not least, I am deeply grateful to my parents Sigrid and Frank, my whole family and also my good friends, especially Martin Rudloff, Richie Richnow, and Meffen Goldau, all of whom provided unconditional support, always trying to ground myself, a lot of distraction, and very thoughtful inspiration.

References

Ackerman, P. L., Beier, M. E., and Boyle, M. O. (2005). Working memory and intelligence: the same or different constructs? *Psychol Bull*, 131(1):30–60.

Alexander, G. E., Chen, K., Merkley, T. L., Reiman, E. M., Caselli, R. J., Aschenbrenner, M., Santerre-Lemmon, L., Lewis, D. J., Pietrini, P., Teipel, S. J., Hampel, H., Rapoport, S. I., and Moeller, J. R. (2006). Regional network of magnetic resonance imaging gray matter volume in healthy aging. *Neuroreport*, 17(10):951–6.

Allen, J. S., Bruss, J., Brown, C. K., and Damasio, H. (2005). Normal neuroanatomical variation due to age: the major lobes and a parcellation of the temporal region. *Neurobiology of aging*, 26(9):1245–60; discussion 1279–82.

Almli, C. R., Rivkin, M. J., McKinstry, R. C., and Brain Development Cooperative Group (2007). The nih mri study of normal brain development (objective-2): newborns, infants, toddlers, and preschoolers. *Neuroimage*, 35(1):308–25.

Altaye, M., Holland, S. K., Wilke, M., and Gaser, C. (2008). Infant brain probability templates for mri segmentation and normalization. *Neuroimage*, 43(4):721–30.

Amat, J. A., Bansal, R., Whiteman, R., Haggerty, R., Royal, J., and Peterson, B. S. (2008). Correlates of intellectual ability with morphology of the hippocampus and amygdala in healthy adults. *Brain Cogn*, 66(2):105–14.

Amunts, K., Kedo, O., Kindler, M., Pieperhoff, P., Mohlberg, H., Shah, N. J., Habel, U., Schneider, F., and Zilles, K. (2005). Cytoarchitectonic mapping of the human amygdala, hippocampal region and entorhinal cortex: intersubject variability and probability maps. *Anat Embryol*, 210(5-6):343–52.

Amunts, K., Malikovic, A., Mohlberg, H., Schormann, T., and Zilles, K. (2000). Brodmann's areas 17 and 18 brought into stereotaxic space-where and how variable? *Neuroimage*, 11(1):66–84.

Andrade, A., Paradis, A. L., Rouquette, S., and Poline, J. B. (1999). Ambiguous results in functional neuroimaging data analysis due to covariate correlation. *Neuroimage*, 10(4):483–6.

Antal, A., Baudewig, J., Paulus, W., and Dechent, P. (2008). The posterior cingulate cortex and planum temporale/parietal operculum are activated by coherent visual motion. *Vis Neurosci*, 25(1):17–26.

Ardila, A., Pineda, D., and Rosselli, M. (2000). Correlation between intelligence test scores and executive function measures. *Arch Clin Neuropsychol*, 15(1):31–6.

Ashburner, J. (2007). A fast diffeomorphic image registration algorithm. *Neuroimage*, 38(1):95–113.

Ashburner, J. (2009). Computational anatomy with the spm software. *Magnetic resonance imaging*, 27(8):1163–74.

Ashburner, J. and Friston, K. J. (1999). Nonlinear spatial normalization using basis functions. *Human brain mapping*, 7(4):254–66.

Ashburner, J. and Friston, K. J. (2000). Voxel-based morphometry–the methods. *Neuroimage*, 11(6 Pt 1):805–21.

Ashburner, J. and Friston, K. J. (2001). Why voxel-based morphometry should be used. *Neuroimage*, 14(6):1238–43.

Ashburner, J. and Friston, K. J. (2005). Unified segmentation. *Neuroimage*, 26(3):839–51.

Ashburner, J. and Friston, K. J. (2009). Computing average shaped tissue probability templates. *Neuroimage*, 45(2):333–41.

Ashburner, J. and Klöppel, S. (2011). Multivariate models of inter-subject anatomical variability. *Neuroimage*, 56(2):422–39.

Assaf, Y. and Pasternak, O. (2008). Diffusion tensor imaging (dti)-based white matter mapping in brain research: a review. *J Mol Neurosci*, 34(1):51–61.

Balleine, B. W., Delgado, M. R., and Hikosaka, O. (2007). The role of the dorsal striatum in reward and decision-making. *J Neurosci*, 27(31):8161–5.

Baltes, P. B. (1987). Theoretical propositions of life-span developmental psychology: On the dynamics between growth and decline. *Developmental psychology*, 23:611–626.

Baltes, P. B., Reese, H., and Lipsitt, L. P. (1980). Life-span developmental psychology. *Annual review of psychology*, 31:65–110.

Baltes, P. B., Reuter-Lorenz, P. A., and Rösler, F. (2006). *Lifespan Development and the Brain: The Perspective of Biocultural Co-Constructivism*. Cambridge University Press.

Baltes, P. B. and Staudinger, U. (1999). Lifespan psychology: Theory and application to intellectual functioning. *Annual Review of Psychology*, 50:471–507.

Barbey, A. K., Colom, R., Solomon, J., Krueger, F., Forbes, C., and Grafman, J. (2012). An integrative architecture for general intelligence and executive function revealed by lesion mapping. *Brain*, 135(Pt 4):1154–64.

Baron, R. M. and Kenny, D. A. (1986). The moderator-mediator variable distinction in social psychological research: conceptual, strategic, and statistical considerations. *J Pers Soc Psychol*, 51(6):1173–82.

Bartholomew, D. (2004). *Measuring intelligence: Facts and fallacies*. Cambridge Univ Pr.

Bartzokis, G., Lu, P. H., Tingus, K., Peters, D. G., Amar, C. P., Tishler, T. A., Finn, J. P., Villablanca, P., Altshuler, L. L., Mintz, J., Neely, E., and Connor, J. R. (2011). Gender and iron genes may modify associations between brain iron and memory in healthy aging. *Neuropsychopharmacology*, 36(7):1375–84.

Bartzokis, G., Tishler, T. A., Lu, P. H., Villablanca, P., Altshuler, L. L., Carter, M., Huang, D., Edwards, N., and Mintz, J. (2007). Brain ferritin iron may influence age- and gender-related risks of neurodegeneration. *Neurobiol Aging*, 28(3):414–23.

Baumann, N. and Pham-Dinh, D. (2001). Biology of oligodendrocyte and myelin in the mammalian central nervous system. *Physiol Rev*, 81(2):871–927.

Belaroussi, B., Milles, J., Carme, S., Zhu, Y. M., and Benoit-Cattin, H. (2006). Intensity non-uniformity correction in mri: existing methods and their validation. *Med Image Anal*, 10(2):234–46.

Bergfield, K. L., Hanson, K. D., Chen, K., Teipel, S. J., Hampel, H., Rapoport, S. I., Moeller, J. R., and Alexander, G. E. (2010). Age-related networks of regional covariance in mri gray matter: reproducible multivariate patterns in healthy aging. *Neuroimage*, 49(2):1750–9.

Blakemore, S.-J. and Choudhury, S. (2006). Development of the adolescent brain: implications for executive function and social cognition. *J Child Psychol Psychiatry*, 47(3-4):296–312.

Bookstein, F. L. (2001). "voxel-based morphometry" should not be used with imperfectly registered images. *Neuroimage*, 14(6):1454–62.

Borga M., Landelius T., K. H. (1992). A unified approach to pca, pls, mlr and cca. Technical report, ISY.

Boyke, J., Driemeyer, J., Gaser, C., Büchel, C., and May, A. (2008). Training-induced brain structure changes in the elderly. *J Neurosci*, 28(28):7031–5.

Braddick, O., Atkinson, J., and Wattam-Bell, J. (2003). Normal and anomalous development of visual motion processing: motion coherence and 'dorsal-stream vulnerability'. *Neuropsychologia*, 41(13):1769–84.

Brain Development Cooperative Group (2012). Total and regional brain volumes in a population-based normative sample from 4 to 18 years: the nih mri study of normal brain development. *Cereb Cortex*, 22(1):1–12.

Bray, S., Chang, C., and Hoeft, F. (2009). Applications of multivariate pattern classification analyses in developmental neuroimaging of healthy and clinical populations. *Front Hum Neurosci*, 3:32.

Brickman, A. M., Habeck, C., Ramos, M. A., Scarmeas, N., and Stern, Y. (2008). A forward application of age associated gray and white matter networks. *Human brain mapping*, 29(10):1139–46.

Brickman, A. M., Habeck, C., Zarahn, E., Flynn, J., and Stern, Y. (2007). Structural mri covariance patterns associated with normal aging and neuropsychological functioning. *Neurobiology of aging*, 28(2):284–95.

Bryk, A. S. and Raudenbush, S. W. (1987). Application of hierarchical linear models to assessing change. *Psychol Bull*, 101:147–158.

Buades, A., Coll, B., and Morel, J. (2005). A non local algorithm for image denoising. *IEEE Computer Vision and Pattern Recognition*, 2:60–65.

Bukach, C. M., Gauthier, I., and Tarr, M. J. (2006). Beyond faces and modularity: the power of an expertise framework. *Trends Cogn Sci (Regul Ed)*, 10(4):159–66.

Burgmans, S., van Boxtel, M. P. J., Gronenschild, E. H. B. M., Vuurman, E. F. P. M., Hofman, P., Uylings, H. B. M., Jolles, J., and Raz, N. (2010). Multiple indicators of age-related differences in cerebral white matter and the modifying effects of hypertension. *Neuroimage*, 49(3):2083–93.

Burke, S. N. and Barnes, C. A. (2006). Neural plasticity in the ageing brain. *Nat Rev Neurosci*, 7(1):30–40.

Burzynska, A. Z., Nagel, I. E., Preuschhof, C., Gluth, S., Bäckman, L., Li, S.-C., Lindenberger, U., and Heekeren, H. R. (2012). Cortical thickness is linked to executive functioning in adulthood and aging. *Human brain mapping*, 33(7):1607–1620.

Carroll, J. (1993). *Human Cognitive Abilities: A Survey of Factor-Analytic Studies*. Cambridge University Press.

Chaddock, L., Erickson, K. I., Prakash, R. S., VanPatter, M., Voss, M. W., Pontifex, M. B., Raine, L. B., Hillman, C. H., and Kramer, A. F. (2010). Basal ganglia volume is associated with aerobic fitness in preadolescent children. *Dev Neurosci*, 32(3):249–56.

Chaddock, L., Hillman, C. H., Pontifex, M. B., Johnson, C. R., Raine, L. B., and Kramer, A. F. (2012). Childhood aerobic fitness predicts cognitive performance one year later. *J Sports Sci*, 30(5):421–30.

Chan, R. C. K., Shum, D., Toulopoulou, T., and Chen, E. Y. H. (2008). Assessment of executive functions: review of instruments and identification of critical issues. *Arch Clin Neuropsychol*, 23(2):201–16.

Charlton, R. A., Schiavone, F., Barrick, T. R., Morris, R. G., and Markus, H. S. (2010). Diffusion tensor imaging detects age related white matter change over a 2 year follow-up which is associated with working memory decline. *J Neurol Neurosurg Psychiatr*, 81(1):13–9.

Chen, J., Myerson, J., and Hale, S. (2002). Age-related dedifferentiation of visuospatial abilities. *Neuropsychologia*, 40(12):2050–6.

Cherubini, A., Péran, P., Caltagirone, C., Sabatini, U., and Spalletta, G. (2009). Aging of subcortical nuclei: microstructural, mineralization and atrophy modifications measured in vivo using mri. *Neuroimage*, 48(1):29–36.

Choi, Y. Y., Shamosh, N. A., Cho, S. H., DeYoung, C. G., Lee, M. J., Lee, J.-M., Kim, S. I., Cho, Z.-H., Kim, K., Gray, J. R., and Lee, K. H. (2008). Multiple bases of human intelligence revealed by cortical thickness and neural activation. *J Neurosci*, 28(41):10323–9.

Cleveland, W. S. (1979). Robust locally weighted regression and smoothing scatterplots. *J. Amer. Statist. Assoc.*, 74(368):829–836.

Cleveland, W. S., Devlin, S. J., and Grosse, E. (1988). Regression by local fitting. methods, properties, and computational algorithms. *J. Econometrics*, 37(1):87–114.

Cleveland, W. S. and Grosse, E. (1991). Computational methods for local regression. *Statistics and Computing*, 1(1):47–62.

Colibazzi, T., Zhu, H., Bansal, R., Schultz, R. T., Wang, Z., and Peterson, B. S. (2008). Latent volumetric structure of the human brain: Exploratory factor analysis and structural equation modeling of gray matter volumes in healthy children and adults. *Hum Brain Mapp*, 29(11):1302–12.

Colom, R., Jung, R. E., and Haier, R. J. (2006). Distributed brain sites for the g-factor of intelligence. *Neuroimage*, 31(3):1359–65.

Colom, R., Jung, R. E., and Haier, R. J. (2007). General intelligence and memory span: evidence for a common neuroanatomic framework. *Cognitive neuropsychology*, 24(8):867–78.

Colom, R., Karama, S., Jung, R. E., and Haier, R. J. (2010). Human intelligence and brain networks. *Dialogues Clin Neurosci*, 12(4):489–501.

Cools, R. (2008). Role of dopamine in the motivational and cognitive control of behavior. *Neuroscientist*, 14(4):381–95.

Cools, R. (2011). Dopaminergic control of the striatum for high-level cognition. *Curr Opin Neurobiol*, 21(3):402–7.

Craven, P. and Wahba, G. (1978). Smoothing noisy data with spline functions. estimating the correct degree of smoothing by the method of generalized cross-validation. *Numer. Math.*, 31(4):377–403.

Cuadra, M. B., Cammoun, L., Butz, T., Cuisenaire, O., and Thiran, J. P. (2005). Comparison and validatiaon of tissue modelization and statistical classification methods in t1-weighted mr brain images. *IEEE transactions on medical imaging*, 24:1548–1565.

Dale, A. M., Fischl, B., and Sereno, M. I. (1999). Cortical surface-based analysis. i. segmentation and surface reconstruction. *Neuroimage*, 9(2):179–94.

Davatzikos, C. (2004). Why voxel-based morphometric analysis should be used with great caution when characterizing group differences. *Neuroimage*, 23(1):17–20.

Davatzikos, C., Bhatt, P., Shaw, L. M., Batmanghelich, K. N., and Trojanowski, J. Q. (2011). Prediction of mci to ad conversion, via mri, csf biomarkers, and pattern classification. *Neurobiol Aging*, 32(12):2322.e19–27.

Davatzikos, C., Fan, Y., Wu, X., Shen, D., and Resnick, S. M. (2008). Detection of prodromal alzheimer's disease via pattern classification of magnetic resonance imaging. *Neurobiology of aging*, 29(4):514–23.

Davatzikos, C., Genc, A., Xu, D., and Resnick, S. M. (2001). Voxel-based morphometry using the ravens maps: methods and validation using simulated longitudinal atrophy. *Neuroimage*, 14(6):1361–9.

de Frias, C. M., Lövden, M., Lindenberger, U., and Nilsson, L. G. (2007). Revisiting the dedifferentiation hypothesis with longitudinal multi-cohort data. *Intelligence*, 35:381–392.

Deary, I. J. (2012). Intelligence. *Annual review of psychology*, 63:453–82.

Deary, I. J., Corley, J., Gow, A. J., Harris, S. E., Houlihan, L. M., Marioni, R. E., Penke, L., Rafnsson, S. B., and Starr, J. M. (2009a). Age-associated cognitive decline. *Br Med Bull*, 92:135–52.

Deary, I. J., Penke, L., and Johnson, W. (2010). The neuroscience of human intelligence differences. *Nat Rev Neurosci*, 11(3):201–11.

Deary, I. J., Whalley, L. J., and Starrr, J. M. (2009b). *A Lifetime of Intelligence: Follow-up Studies of the Scottish mental Surveys of 1932 and 1947.* Washington, DC: American Psychological Association.

Deary, I. J., Whiteman, M. C., Starr, J. M., Whalley, L. J., and Fox, H. C. (2004). The impact of childhood intelligence on later life: following up the scottish mental surveys of 1932 and 1947. *J Pers Soc Psychol*, 86(1):130–47.

Deboer, T., Wu, Z., Lee, A., and Simon, T. J. (2007). Hippocampal volume reduction in children with chromosome 22q11.2 deletion syndrome is associated with cognitive impairment. *Behav Brain Funct*, 3:54.

DeFelipe, J. (2006). Brain plasticity and mental processes: Cajal again. *Nat Rev Neurosci*, 7(10):811–7.

Deichmann, R., Good, C. D., Josephs, O., Ashburner, J., and Turner, R. (2000). Optimization of 3-d mp-rage sequences for structural brain imaging. *Neuroimage*, 12(1):112–27.

der Maaten, V., Postma, E. O., and van den Herik, H. J. (2008). Dimensionality reduction: A comparative review. Technical report, MICC, Maastricht University, The Netherlands.

Dickerson, B. C., Fenstermacher, E., Salat, D. H., Wolk, D. A., Maguire, R. P., Desikan, R., Pacheco, J., Quinn, B. T., der Kouwe, A. V., Greve, D. N., Blacker, D., Albert, M. S., Killiany, R. J., and Fischl, B. (2008). Detection of cortical thickness correlates of cognitive performance: Reliability across mri scan sessions, scanners, and field strengths. *Neuroimage*, 39(1):10–8.

Dosenbach, N. U. F., Nardos, B., Cohen, A. L., Fair, D. A., Power, J. D., Church, J. A., Nelson, S. M., Wig, G. S., Vogel, A. C., Lessov-Schlaggar, C. N., Barnes, K. A., Dubis, J. W., Feczko, E., Coalson, R. S., Pruett, J. R., Barch, D. M., Petersen, S. E., and Schlaggar, B. L. (2010). Prediction of individual brain maturity using fmri. *Science*, 329(5997):1358–61.

Dotson, V. M., Zonderman, A. B., Davatzikos, C., Kraut, M. A., and Resnick, S. M. (2009). Frontal atrophy and attention deficits in older adults with a history of elevated depressive symptoms. *Brain Imaging Behav*, 3(4):358.

Draganski, B., Ashburner, J., Hutton, C., Kherif, F., Frackowiak, R. S. J., Helms, G., and Weiskopf, N. (2011). Regional specificity of mri contrast parameter changes in normal ageing revealed by voxel-based quantification (vbq). *Neuroimage*, 55(4):1423–34.

Draganski, B., Gaser, C., Busch, V., Schuierer, G., Bogdahn, U., and May, A. (2004). Neuroplasticity: changes in grey matter induced by training. *Nature*, 427(6972):311–2.

Draganski, B., Gaser, C., Kempermann, G., Kuhn, H. G., Winkler, J., Büchel, C., and May, A. (2006). Temporal and spatial dynamics of brain structure changes during extensive learning. *J Neurosci*, 26(23):6314–7.

Driscoll, I., Davatzikos, C., An, Y., Wu, X., Shen, D., Kraut, M., and Resnick, S. M. (2009). Longitudinal pattern of regional brain volume change differentiates normal aging from mci. *Neurology*, 72(22):1906–13.

Du, A.-T., Schuff, N., Chao, L. L., Kornak, J., Jagust, W. J., Kramer, J. H., Reed, B. R., Miller, B. L., Norman, D., Chui, H. C., and Weiner, M. W. (2006). Age effects on atrophy rates of entorhinal cortex and hippocampus. *Neurobiology of aging*, 27(5):733–40.

Dukart, J., Schroeter, M. L., Mueller, K., and Alzheimer's Disease Neuroimaging Initiative (2011). Age correction in dementia–matching to a healthy brain. *PLoS One*, 6(7):e22193.

Ebisch, S. J., Perrucci, M. G., Mercuri, P., Romanelli, R., Mantini, D., Romani, G. L., Colom, R., and Saggino, A. (2012). Common and unique neuro-functional basis of induction, visualization, and spatial relationships as cognitive components of fluid intelligence. *Neuroimage*, 62(1):331–42.

Ecker, C., Stahl, D., Daly, E., Johnston, P., Thomson, A., and Murphy, D. G. M. (2009). Is there a common underlying mechanism for age-related decline in cortical thickness? *Neuroreport*, 20(13):1155–60.

Eckert, M. A. (2011). Slowing down: age-related neurobiological predictors of processing speed. *Front Neurosci*, 5:25.

Efron, B. and Tibshirani, R. J. (1994). *An Introduction to the Bootstrap*. Chapman and Hall.

Eickhoff, S. B., Amunts, K., Mohlberg, H., and Zilles, K. (2006a). The human parietal operculum. ii. stereotaxic maps and correlation with functional imaging results. *Cereb Cortex*, 16(2):268–79.

Eickhoff, S. B., Heim, S., Zilles, K., and Amunts, K. (2006b). Testing anatomically specified hypotheses in functional imaging using cytoarchitectonic maps. *Neuroimage*, 32(2):570–82.

Eickhoff, S. B., Paus, T., Caspers, S., Grosbras, M.-H., Evans, A. C., Zilles, K., and Amunts, K. (2007). Assignment of functional activations to probabilistic cytoarchitectonic areas revisited. *Neuroimage*, 36(3):511–21.

Eickhoff, S. B., Schleicher, A., Zilles, K., and Amunts, K. (2006c). The human parietal operculum. i. cytoarchitectonic mapping of subdivisions. *Cereb Cortex*, 16(2):254–67.

Eickhoff, S. B., Walters, N. B., Schleicher, A., Kril, J., Egan, G. F., Zilles, K., Watson, J. D. G., and Amunts, K. (2005). High-resolution mri reflects myeloarchitecture and cytoarchitecture of human cerebral cortex. *Human brain mapping*, 24(3):206–15.

Elderkin-Thompson, V., Ballmaier, M., Hellemann, G., Pham, D., and Kumar, A. (2008). Executive function and mri prefrontal volumes among healthy older adults. *Neuropsychology*, 22(5):626–37.

Engvig, A., Fjell, A. M., Westlye, L. T., Moberget, T., Sundseth, Ø., Larsen, V. A., and Walhovd, K. B. (2010). Effects of memory training on cortical thickness in the elderly. *Neuroimage*, 52(4):1667–76.

Erickson, K. I., Boot, W. R., Basak, C., Neider, M. B., Prakash, R. S., Voss, M. W., Graybiel, A. M., Simons, D. J., Fabiani, M., Gratton, G., and Kramer, A. F. (2010). Striatal volume predicts level of video game skill acquisition. *Cereb Cortex*, 20(11):2522–30.

Erickson, K. I. and Kramer, A. F. (2009). Aerobic exercise effects on cognitive and neural plasticity in older adults. *Br J Sports Med*, 43(1):22–4.

Erickson, K. I., Prakash, R. S., Voss, M. W., Chaddock, L., Hu, L., Morris, K. S., White, S. M., Wójcicki, T. R., McAuley, E., and Kramer, A. F. (2009). Aerobic fitness is associated with hippocampal volume in elderly humans. *Hippocampus*, 19(10):1030–9.

Erickson, K. I., Voss, M. W., Prakash, R. S., Basak, C., Szabo, A., Chaddock, L., Kim, J. S., Heo, S., Alves, H., White, S. M., Wojcicki, T. R., Mailey, E., Vieira, V. J., Martin, S. A., Pence, B. D., Woods, J. A., McAuley, E., and Kramer, A. F. (2011). Exercise training increases size of hippocampus and improves memory. *Proc Natl Acad Sci U S A*, 108(7):3017–22.

Evans, A. C., Collins, D. L., Mills, S. R., Brown, E. D., Kelly, R. L., and Peters, T. M. (1993). 3D statistical neuroanatomical models from 305 MRI volumes. In *1993 IEEE Conference Record Nuclear Science Symposium and Medical Imaging Conference*, pages 1813–1817. IEEE.

Evans, A. C. and Group, B. D. C. (2006). The nih mri study of normal brain development. *Neuroimage*, 30(1):184–202.

Eyler, L. T., Prom-Wormley, E., Fennema-Notestine, C., Panizzon, M. S., Neale, M. C., Jernigan, T. L., Fischl, B., Franz, C. E., Lyons, M. J., Stevens, A., Pacheco, J., Perry, M. E., Schmitt, J. E., Spitzer, N. C., Seidman, L. J., Thermenos, H. W., Tsuang, M. T., Dale, A. M., and Kremen, W. S. (2011). Genetic patterns of correlation among subcortical volumes in humans: Results from a magnetic resonance imaging twin study. *Hum Brain Mapp*, 32(4):641–53.

Féart, C., Samieri, C., and Barberger-Gateau, P. (2010). Mediterranean diet and cognitive function in older adults. *Curr Opin Clin Nutr Metab Care*, 13(1):14–8.

Fennema-Notestine, C., Hagler, Jr, D. J., McEvoy, L. K., Fleisher, A. S., Wu, E. H., Karow, D. S., Dale, A. M., and Alzheimer's Disease Neuroimaging Initiative (2009). Structural mri biomarkers for preclinical and mild alzheimer's disease. *Hum Brain Mapp*, 30(10):3238–53.

Filipovych, R., Resnick, S. M., and Davatzikos, C. (2011a). Semi-supervised cluster analysis of imaging data. *Neuroimage*, 54(3):2185–97.

Filipovych, R., Wang, Y., and Davatzikos, C. (2011b). Pattern analysis in neuroimaging: Beyond two-class categorization. *Int J Imaging Syst Technol*, 21(2):173–178.

Fischl, B., Salat, D. H., Busa, E., Albert, M., Dieterich, M., Haselgrove, C., van der Kouwe, A., Killiany, R., Kennedy, D., Klaveness, S., Montillo, A., Makris, N., Rosen, B., and Dale, A. M. (2002). Whole brain segmentation: automated labeling of neuroanatomical structures in the human brain. *Neuron*, 33(3):341–55.

Fischl, B., Sereno, M. I., and Dale, A. M. (1999). Cortical surface-based analysis. ii: Inflation, flattening, and a surface-based coordinate system. *Neuroimage*, 9(2):195–207.

Fjell, A. M. and Walhovd, K. B. (2010). Structural brain changes in aging: courses, causes and cognitive consequences. *Reviews in the neurosciences*, 21(3):187–221.

Fjell, A. M., Walhovd, K. B., Fennema-Notestine, C., McEvoy, L. K., Hagler, D. J., Holland, D., Brewer, J. B., and Dale, A. M. (2009a). One-year brain atrophy evident in healthy aging. *J Neurosci*, 29(48):15223–31.

Fjell, A. M., Walhovd, K. B., Fennema-Notestine, C., McEvoy, L. K., Hagler, D. J., Holland, D., Brewer, J. B., Dale, A. M., and Initiative, A. (2010a). Csf biomarkers in prediction of cerebral and clinical change in mild cognitive impairment and alzheimer's disease. *J Neurosci*, 30(6):2088–101.

Fjell, A. M., Walhovd, K. B., Reinvang, I., Lundervold, A., Salat, D., Quinn, B. T., Fischl, B., and Dale, A. M. (2006). Selective increase of cortical thickness in high-performing elderly–structural indices of optimal cognitive aging. *Neuroimage*, 29(3):984–94.

Fjell, A. M., Walhovd, K. B., Westlye, L. T., Østby, Y., Tamnes, C. K., Jernigan, T. L., Gamst, A., and Dale, A. M. (2010b). When does brain aging accelerate? dangers of quadratic fits in cross-sectional studies. *Neuroimage*, 50(4):1376–83.

Fjell, A. M., Westlye, L. T., Amlien, I., Espeseth, T., Reinvang, I., Raz, N., Agartz, I., Salat, D. H., Greve, D. N., Fischl, B., Dale, A. M., and Walhovd, K. B. (2009b). High consistency of regional cortical thinning in aging across multiple samples. *Cereb Cortex*, 19(9):2001–12.

Fjell, A. M., Westlye, L. T., Amlien, I., Espeseth, T., Reinvang, I., Raz, N., Agartz, I., Salat, D. H., Greve, D. N., Fischl, B., Dale, A. M., and Walhovd, K. B. (2009c). Minute effects of sex on the aging brain: a multisample magnetic resonance imaging study of healthy aging and alzheimer's disease. *J Neurosci*, 29(27):8774–83.

Flandin, G. and Penny, W. D. (2007). Bayesian fmri data analysis with sparse spatial basis function priors. *Neuroimage*, 34(3):1108–25.

Flood, D. G. (1991). Region-specific stability of dendritic extent in normal human aging and regression in alzheimer's disease. ii. subiculum. *Brain Res*, 540(1-2):83–95.

Flood, D. G., Buell, S. J., Defiore, C. H., Horwitz, G. J., and Coleman, P. D. (1985). Age-related dendritic growth in dentate gyrus of human brain is followed by regression in the 'oldest old'. *Brain Res*, 345(2):366–8.

Flood, D. G., Buell, S. J., Horwitz, G. J., and Coleman, P. D. (1987a). Dendritic extent in human dentate gyrus granule cells in normal aging and senile dementia. *Brain Res*, 402(2):205–16.

Flood, D. G., Guarnaccia, M., and Coleman, P. D. (1987b). Dendritic extent in human ca2-3 hippocampal pyramidal neurons in normal aging and senile dementia. *Brain Res*, 409(1):88–96.

Fox, J. (2008). *Applied regression analysis and generalized linear models*. Thousand Oaks: Sage Publications Inc.

Frangou, S., Chitins, X., and Williams, S. C. R. (2004). Mapping iq and gray matter density in healthy young people. *Neuroimage*, 23(3):800–5.

Franke, K., Ziegler, G., Klöppel, S., Gaser, C., and Initiative, A. D. N. (2010). Estimating the age of healthy subjects from t1-weighted mri scans using kernel methods: exploring the influence of various parameters. *Neuroimage*, 50(3):883–92.

Fray, P. J. and Robbins, T. W. (1996). Cantab battery: proposed utility in neurotoxicology. *Neurotoxicol Teratol*, 18(4):499–504.

Friedman, N. P., Miyake, A., Corley, R. P., Young, S. E., Defries, J. C., and Hewitt, J. K. (2006). Not all executive functions are related to intelligence. *Psychol Sci*, 17(2):172–9.

Friedman, N. P., Miyake, A., Young, S. E., Defries, J. C., Corley, R. P., and Hewitt, J. K. (2008). Individual differences in executive functions are almost entirely genetic in origin. *J Exp Psychol Gen*, 137(2):201–25.

Frisardi, V., Panza, F., Seripa, D., Imbimbo, B. P., Vendemiale, G., Pilotto, A., and Solfrizzi, V. (2010). Nutraceutical properties of mediterranean diet and cognitive decline: possible underlying mechanisms. *J Alzheimers Dis*, 22(3):715–40.

Friston, K. J. and Ashburner, J. (2004). Generative and recognition models for neuroanatomy. *Neuroimage*, 23(1):21–4.

Friston, K. J., Chu, C., Mourao-Miranda, J., Hulme, O., Rees, G., Penny, W. D., and Ashburner, J. (2008). Bayesian decoding of brain images. *Neuroimage*, 39(1):181–205.

Friston, K. J., Glaser, D. E., Henson, R. N. A., Kiebel, S., Phillips, C., and Ashburner, J. (2002). Classical and bayesian inference in neuroimaging: applications. *Neuroimage*, 16(2):484–512.

Friston, K. J., Harrison, L., and Penny, W. (2003). Dynamic causal modelling. *Neuroimage*, 19(4):1273–302.

Friston, K. J., Holmes, A., and Worsley, K. J. (1995). Statistical parametric maps in functional imaging: a general linear approach. *Human brain mapping*, 2:189–210.

Friston, K. J. and Penny, W. (2003). Posterior probability maps and spms. *Neuroimage*, 19(3):1240–9.

Geladi, P. (1988). Notes on the history and nature of partial least squares (pls) modelling. *Chemometrics*, 2(4):231–246.

Geyer, S., Schleicher, A., and Zilles, K. (1999). Areas 3a, 3b, and 1 of human primary somatosensory cortex. *Neuroimage*, 10(1):63–83.

Gianaros, P. J., Greer, P. J., Ryan, C. M., and Jennings, J. R. (2006). Higher blood pressure predicts lower regional grey matter volume: Consequences on short-term information processing. *Neuroimage*, 31(2):754–65.

Giedd, J. N. and Rapoport, J. L. (2010). Structural mri of pediatric brain development: what have we learned and where are we going? *Neuron*, 67(5):728–34.

Gioia, G. A. and Isquith, P. K. (2004). Ecological assessment of executive function in traumatic brain injury. *Developmental Neuropsychology*, 25(1-2):135–58.

Gioia, G. A., Isquith, P. K., Kenworthy, L., and Barton, R. M. (2002a). Profiles of everyday executive function in acquired and developmental disorders. *Child Neuropsychol*, 8(2):121–37.

Gioia, G. A., Isquith, P. K., Retzlaff, P. D., and Espy, K. A. (2002b). Confirmatory factor analysis of the behavior rating inventory of executive function (brief) in a clinical sample. *Child Neuropsychol*, 8(4):249–57.

Gioia, G. A., Kenworthy, L., and Isquith, P. K. (2010). Executive function in the real world: Brief lessons from mark ylvisaker. *J Head Trauma Rehabil*, 25(6):433–9.

Giorgio, A., Watkins, K. E., Chadwick, M., James, S., Winmill, L., Douaud, G., Stefano, N. D., Matthews, P. M., Smith, S. M., Johansen-Berg, H., and James, A. C. (2010). Longitudinal changes in grey and white matter during adolescence. *Neuroimage*, 49(1):94–103.

Gläscher, J., Rudrauf, D., Colom, R., Paul, L. K., Tranel, D., Damasio, H., and Adolphs, R. (2010). Distributed neural system for general intelligence revealed by lesion mapping. *Proc Natl Acad Sci U S A*, 107(10):4705–9.

Gogtay, N., Giedd, J. N., Lusk, L., Hayashi, K. M., Greenstein, D., Vaituzis, A. C., Nugent, T. F., Herman, D. H., Clasen, L. S., Toga, A. W., Rapoport, J. L., and Thompson, P. M. (2004). Dynamic mapping of human cortical development during childhood through early adulthood. *Proc Natl Acad Sci USA*, 101(21):8174–9.

Golarai, G., Liberman, A., Yoon, J. M. D., and Grill-Spector, K. (2010). Differential development of the ventral visual cortex extends through adolescence. *Front Hum Neurosci*, 3:80.

Gollob, H. F. and Reichardt, C. S. (1987). Taking account of time lags in causal models. *Child Dev*, 58(1):80–92.

Gong, Q.-Y., Sluming, V., Mayes, A., Keller, S., Barrick, T., Cezayirli, E., and Roberts, N. (2005). Voxel-based morphometry and stereology provide convergent evidence of the importance of medial prefrontal cortex for fluid intelligence in healthy adults. *Neuroimage*, 25(4):1175–86.

Good, C. D., Johnsrude, I. S., Ashburner, J., Henson, R. N., Friston, K. J., and Frackowiak, R. S. J. (2001). A voxel-based morphometric study of ageing in 465 normal adult human brains. *Neuroimage*, 14(1 Pt 1):21–36.

Grady, C. L., Maisog, J. M., Horwitz, B., Ungerleider, L. G., Mentis, M. J., Salerno, J. A., Pietrini, P., Wagner, E., and Haxby, J. V. (1994). Age-related changes in cortical blood flow activation during visual processing of faces and location. *J Neurosci*, 14(3 Pt 2):1450–62.

Grieve, S. M., Clark, C. R., Williams, L. M., Peduto, A. J., and Gordon, E. (2005). Preservation of limbic and paralimbic structures in aging. *Human brain mapping*, 25(4):391–401.

Grill-Spector, K., Golarai, G., and Gabrieli, J. (2008). Developmental neuroimaging of the human ventral visual cortex. *Trends Cogn Sci*, 12(4):152–62.

Grön, G., Wunderlich, A. P., Spitzer, M., Tomczak, R., and Riepe, M. W. (2000). Brain activation during human navigation: gender-different neural networks as substrate of performance. *Nat Neurosci*, 3(4):404–8.

Groves, A. R., Beckmann, C. F., Smith, S. M., and Woolrich, M. W. (2011). Linked independent component analysis for multimodal data fusion. *Neuroimage*, 54(3):2198–217.

Groves, A. R., Chappell, M. A., and Woolrich, M. W. (2009). Combined spatial and non-spatial prior for inference on mri time-series. *Neuroimage*, 45(3):795–809.

Groves, A. R., Smith, S. M., Fjell, A. M., Tamnes, C. K., Walhovd, K. B., Douaud, G., Woolrich, M. W., and Westlye, L. T. (2012). Benefits of multi-modal fusion analysis on a large-scale dataset: life-span patterns of inter-subject variability in cortical morphometry and white matter microstructure. *Neuroimage*, 63(1):365–80.

Gunn, A., Cory, E., Atkinson, J., Braddick, O., Wattam-Bell, J., Guzzetta, A., and Cioni, G. (2002). Dorsal and ventral stream sensitivity in normal development and hemiplegia. *Neuroreport*, 13(6):843–7.

Gunning-Dixon, F. M., Brickman, A. M., Cheng, J. C., and Alexopoulos, G. S. (2009). Aging of cerebral white matter: a review of mri findings. *International journal of geriatric psychiatry*, 24(2):109–17.

Gunning-Dixon, F. M. and Raz, N. (2003). Neuroanatomical correlates of selected executive functions in middle-aged and older adults: a prospective mri study. *Neuropsychologia*, 41(14):1929–41.

Haacke, E. M., Cheng, N. Y. C., House, M. J., Liu, Q., Neelavalli, J., Ogg, R. J., Khan, A., Ayaz, M., Kirsch, W., and Obenaus, A. (2005). Imaging iron stores in the brain using magnetic resonance imaging. *Magn Reson Imaging*, 23(1):1–25.

Haier, R. J., Jung, R. E., Yeo, R. A., Head, K., and Alkire, M. T. (2004). Structural brain variation and general intelligence. *Neuroimage*, 23(1):425–33.

Haier, R. J., Jung, R. E., Yeo, R. A., Head, K., and Alkire, M. T. (2005). The neuroanatomy of general intelligence: sex matters. *Neuroimage*, 25(1):320–7.

Haier, R. J., Schroeder, D. H., Tang, C., Head, K., and Colom, R. (2010). Gray matter correlates of cognitive ability tests used for vocational guidance. *BMC Res Notes*, 3:206.

Harder, S. L., Hopp, K. M., Ward, H., Neglio, H., Gitlin, J., and Kido, D. (2008). Mineralization of the deep gray matter with age: a retrospective review with susceptibility-weighted mr imaging. *AJNR Am J Neuroradiol*, 29(1):176–83.

Harrison, L. M. and Green, G. G. R. (2010). A bayesian spatiotemporal model for very large data sets. *Neuroimage*, 50(3):1126–41.

Hartberg, C. B., Lawyer, G., Nyman, H., Jönsson, E. G., Haukvik, U. K., Saetre, P., Bjerkan, P. S., Andreassen, O. A., Hall, H., and Agartz, I. (2010). Investigating relationships between cortical thickness and cognitive performance in patients with schizophrenia and healthy adults. *Psychiatry Res*, 182(2):123–33.

Hasan, K. M., Sankar, A., Halphen, C., Kramer, L. A., Brandt, M. E., Juranek, J., Cirino, P. T., Fletcher, J. M., Papanicolaou, A. C., and Ewing-Cobbs, L. (2007). Development and organization of the human brain tissue compartments across the lifespan using diffusion tensor imaging. *Neuroreport*, 18(16):1735–9.

Haxby, J. V., Grady, C. L., Horwitz, B., Ungerleider, L. G., Mishkin, M., Carson, R. E., Herscovitch, P., Schapiro, M. B., and Rapoport, S. I. (1991). Dissociation of object and spatial visual processing pathways in human extrastriate cortex. *Proc Natl Acad Sci U S A*, 88(5):1621–5.

Hedden, T. and Gabrieli, J. D. E. (2004). Insights into the ageing mind: a view from cognitive neuroscience. *Nat Rev Neurosci*, 5(2):87–96.

Hoeft, F., McCandliss, B. D., Black, J. M., Gantman, A., Zakerani, N., Hulme, C., Lyytinen, H., Whitfield-Gabrieli, S., Glover, G. H., Reiss, A. L., and Gabrieli, J. D. E. (2011). Neural systems predicting long-term outcome in dyslexia. *Proc Natl Acad Sci U S A*, 108(1):361–6.

Hoeskuldsson, A. (1988). Pls regression methods. *Chemometrics*, 2(3):211–228.

Hof, P. R. and Morrison, J. H. (2004). The aging brain: morphomolecular senescence of cortical circuits. *Trends Neurosci*, 27(10):607–13.

Holland, D., Desikan, R. S., Dale, A. M., McEvoy, L. K., and for the Alzheimer's Disease Neuroimaging Initiative (2012). Rates of decline in alzheimer disease decrease with age. *PLoS One*, 7(8):e42325.

Hulshoff Pol, H. E., Schnack, H. G., Posthuma, D., Mandl, R. C. W., Baaré, W. F., van Oel, C., van Haren, N. E., Collins, D. L., Evans, A. C., Amunts, K., Bürgel, U., Zilles, K., de Geus, E., Boomsma, D. I., and Kahn, R. S. (2006). Genetic contributions to human brain morphology and intelligence. *J Neurosci*, 26(40):10235–42.

Huttenlocher, P. R. (1990). Morphometric study of human cerebral cortex development. *Neuropsychologia*, 28(6):517–27.

Huttenlocher, P. R. and Dabholkar, A. S. (1997). Regional differences in synaptogenesis in human cerebral cortex. *J Comp Neurol*, 387(2):167–78.

Hutton, C., Draganski, B., Ashburner, J., and Weiskopf, N. (2009). A comparison between voxel-based cortical thickness and voxel-based morphometry in normal aging. *Neuroimage*, 48(2):371–80.

Jennings, J. R., Mendelson, D. N., Muldoon, M. F., Ryan, C. M., Gianaros, P. J., Raz, N., and Aizenstein, H. (2012). Regional grey matter shrinks in hypertensive individuals despite successful lowering of blood pressure. *J Hum Hypertens*, 26(5):295–305.

Jensen, A. (1998). *The g factor: The science of mental ability*. Praeger Westport, CT.

Jernigan, T. L. and Gamst, A. C. (2005). Changes in volume with age–consistency and interpretation of observed effects. *Neurobiol Aging*, 26(9):1271–1278.

Jung, R. E. and Haier, R. J. (2007). The parieto-frontal integration theory (p-fit) of intelligence: converging neuroimaging evidence. *Behav Brain Sci*, 30(2):135–87.

Jurado, M. B. and Rosselli, M. (2007). The elusive nature of executive functions: a review of our current understanding. *Neuropsychol Rev*, 17(3):213–33.

Kanai, R. and Rees, G. (2011). The structural basis of inter-individual differences in human behaviour and cognition. *Nat Rev Neurosci*, 12(4):231–42.

Karama, S., Ad-Dab'bagh, Y., Haier, R., and Deary, I. J. (2009). Erratum to "positive association between cognitive ability and cortical thickness in a representative us sample of healthy 6 to 18 year-olds". *Intelligence, 10.1016/j.intell.2008.09.006.*

Karama, S., Colom, R., Johnson, W., Deary, I. J., Haier, R., Waber, D. P., Lepage, C., Ganjavi, H., Jung, R., Evans, A. C., and Group, B. D. C. (2011). Cortical thickness correlates of specific cognitive performance accounted for by the general factor of intelligence in healthy children aged 6 to 18. *Neuroimage*, 55(4):1443–53.

Kennedy, K. M., Erickson, K. I., Rodrigue, K. M., Voss, M. W., Colcombe, S. J., Kramer, A. F., Acker, J. D., and Raz, N. (2009). Age-related differences in regional brain volumes: a comparison of optimized voxel-based morphometry to manual volumetry. *Neurobiology of aging*, 30(10):1657–76.

Kersting, K., Plagemann, C., Pfaff, P., and Burgard, W. (2007). Most likely heteroscedastic gaussian process regression. In *Proceedings of the 24th international conference on Machine learning*, pages 393–400. ACM.

Kherif, F., Poline, J.-B., Flandin, G., Benali, H., Simon, O., Dehaene, S., and Worsley, K. J. (2002). Multivariate model specification for fmri data. *Neuroimage*, 16(4):1068–83.

Klein, A., Andersson, J., Ardekani, B. A., Ashburner, J., Avants, B., Chiang, M.-C., Christensen, G. E., Collins, D. L., Gee, J., Hellier, P., Song, J. H., Jenkinson, M., Lepage, C., Rueckert, D., Thompson, P. M., Vercauteren, T., Woods, R. P., Mann, J. J., and Parsey, R. V. (2009). Evaluation of 14 nonlinear deformation algorithms applied to human brain mri registration. *Neuroimage*, 46(3):786–802.

Klempin, F. and Kempermann, G. (2007). Adult hippocampal neurogenesis and aging. *Eur Arch Psychiatry Clin Neurosci*, 257(5):271–80.

Klöppel, S., Stonnington, C. M., Barnes, J., Chen, F., Chu, C., Good, C. D., Mader, I., Mitchell, L. A., Patel, A. C., Roberts, C. C., Fox, N. C., Jack, C. R., Ashburner, J., and Frackowiak, R. S. J. (2008). Accuracy of dementia diagnosis: a direct comparison between radiologists and a computerized method. *Brain*, 131(Pt 11):2969–74.

Koutsouleris, N., Gaser, C., Bottlender, R., Davatzikos, C., Decker, P., Jäger, M., Schmitt, G., Reiser, M., Möller, H.-J., and Meisenzahl, E. M. (2010). Use of neuroanatomical pattern regression to predict the structural brain dynamics of vulnerability and transition to psychosis. *Schizophr Res*, 123(2-3):175–87.

Kramer, A. F. and Erickson, K. I. (2007). Capitalizing on cortical plasticity: influence of physical activity on cognition and brain function. *Trends Cogn Sci (Regul Ed)*, 11(8):342–8.

Kravitz, D. J., Saleem, K. S., Baker, C. I., and Mishkin, M. (2011). A new neural framework for visuospatial processing. *Nat Rev Neurosci*, 12(4):217–30.

Kriegeskorte, N., Simmons, W. K., Bellgowan, P. S. F., and Baker, C. I. (2009). Circular analysis in systems neuroscience: the dangers of double dipping. *Nat Neurosci*, 12(5):535–40.

Krishnan, A., Williams, L. J., McIntosh, A. R., and Abdi, H. (2011). Partial least squares (pls) methods for neuroimaging: A tutorial and review. *Neuroimage*, 56(2):455–75.

La Joie, R., Fouquet, M., Mézenge, F., Landeau, B., Villain, N., Mevel, K., Pélerin, A., Eustache, F., Desgranges, B., and Chételat, G. (2010). Differential effect of age on hippocampal subfields assessed using a new high-resolution 3t mr sequence. *Neuroimage*, 53(2):506–14.

Lange, N., Froimowitz, M. P., Bigler, E. D., Lainhart, J. E., and Group, B. D. C. (2010). Associations between iq, total and regional brain volumes, and demography in a large normative sample of healthy children and adolescents. *Developmental Neuropsychology*, 35(3):296–317.

Lenroot, R. K. and Giedd, J. N. (2006). Brain development in children and adolescents: insights from anatomical magnetic resonance imaging. *Neuroscience and biobehavioral reviews*, 30(6):718–29.

Lenroot, R. K. and Giedd, J. N. (2011). Annual research review: Developmental considerations of gene by environment interactions. *J Child Psychol Psychiatry*, 52(4):429–41.

Lenroot, R. K., Gogtay, N., Greenstein, D. K., Wells, E. M., Wallace, G. L., Clasen, L. S., Blumenthal, J. D., Lerch, J. P., Zijdenbos, A. P., Evans, A. C., Thompson, P. M., and Giedd, J. N. (2007). Sexual dimorphism of brain developmental trajectories during childhood and adolescence. *Neuroimage*, 36(4):1065–73.

Lenroot, R. K., Schmitt, J. E., Ordaz, S. J., Wallace, G. L., Neale, M. C., Lerch, J. P., Kendler, K. S., Evans, A. C., and Giedd, J. N. (2009). Differences in genetic and environmental influences on the human cerebral cortex associated with development during childhood and adolescence. *Human brain mapping*, 30(1):163–74.

Lerch, J. P., Worsley, K. J., Shaw, W. P., Greenstein, D. K., Lenroot, R. K., Giedd, J. N., and Evans, A. C. (2006). Mapping anatomical correlations across cerebral cortex (macacc) using cortical thickness from mri. *Neuroimage*, 31(3):993–1003.

Li, S.-C. (2003). Biocultural orchestration of developmental plasticity across levels: the interplay of biology and culture in shaping the mind and behavior across the life span. *Psychol Bull*, 129(2):171–94.

Lindenberger, U., Li, S.-C., and Bäckman, L. (2006). Delineating brain-behavior mappings across the lifespan: substantive and methodological advances in developmental neuroscience. *Neuroscience and biobehavioral reviews*, 30(6):713–7.

Lindenberger, U., Nagel, I. E., Chicherio, C., Li, S.-C., Heekeren, H. R., and Bäckman, L. (2008). Age-related decline in brain resources modulates genetic effects on cognitive functioning. *Front Neurosci*, 2(2):234–44.

Lindenberger, U., Singer, T., and Baltes, P. B. (2002). Longitudinal selectivity in aging populations: separating mortality-associated versus experimental components in the berlin aging study (base). *J Gerontol B Psychol Sci Soc Sci*, 57(6):P474–82.

Lubinski, D. (2004). Introduction to the special section on cognitive abilities: 100 years after spearman's (1904) "'general intelligence,' objectively determined and measured". *J Pers Soc Psychol*, 86(1):96–111.

Luchsinger, J. A. and Gustafson, D. R. (2009). Adiposity, type 2 diabetes, and alzheimer's disease. *J Alzheimers Dis*, 16(4):693–704.

Luciana, M. (2003). Practitioner review: computerized assessment of neuropsychological function in children: clinical and research applications of the cambridge neuropsychological testing automated battery (cantab). *J Child Psychol Psychiatry*, 44(5):649–63.

Luders, E., Gaser, C., Narr, K. L., and Toga, A. W. (2009a). Why sex matters: brain size independent differences in gray matter distributions between men and women. *J Neurosci*, 29(45):14265–70.

Luders, E., Narr, K. L., Bilder, R. M., Szeszko, P. R., Gurbani, M. N., Hamilton, L., Toga, A. W., and Gaser, C. (2008). Mapping the relationship between cortical convolution and intelligence: effects of gender. *Cereb Cortex*, 18(9):2019–26.

Luders, E., Narr, K. L., Bilder, R. M., Thompson, P. M., Szeszko, P. R., Hamilton, L., and Toga, A. W. (2007). Positive correlations between corpus callosum thickness and intelligence. *Neuroimage*, 37(4):1457–64.

Luders, E., Narr, K. L., Thompson, P. M., Rex, D. E., Woods, R. P., Deluca, H., Jancke, L., and Toga, A. W. (2006). Gender effects on cortical thickness and the influence of scaling. *Human brain mapping*, 27(4):314–24.

Luders, E., Narr, K. L., Thompson, P. M., and Toga, A. W. (2009b). Neuroanatomical correlates of intelligence. *Intelligence*, 37(2):156–163.

Luders, E., Thompson, P. M., Narr, K. L., Zamanyan, A., Chou, Y.-Y., Gutman, B., Dinov, I. D., and Toga, A. W. (2011). The link between callosal thickness and intelligence in healthy children and adolescents. *Neuroimage*, 54(3):1823–30.

Luna, B., Garver, K. E., Urban, T. A., Lazar, N. A., and Sweeney, J. A. (2004). Maturation of cognitive processes from late childhood to adulthood. *Child Dev*, 75(5):1357–72.

Lupien, S. J., Evans, A. C., Lord, C., Miles, J., Pruessner, M., Pike, B., and Pruessner, J. C. (2007). Hippocampal volume is as variable in young as in older adults: implications for the notion of hippocampal atrophy in humans. *Neuroimage*, 34(2):479–85.

MacLullich, A. M. J., Ferguson, K. J., Deary, I. J., Seckl, J. R., Starr, J. M., and Wardlaw, J. M. (2002). Intracranial capacity and brain volumes are associated with cognition in healthy elderly men. *Neurology*, 59(2):169–74.

Madden, D. J., Bennett, I. J., and Song, A. W. (2009). Cerebral white matter integrity and cognitive aging: contributions from diffusion tensor imaging. *Neuropsychol Rev*, 19(4):415–35.

Magnusson, D., editor (1996). *The lifespan development of individuals: Behavioral, neurobiological and psychosocial perspectives: A synthesis.* Cambridge, UK: Cambridge University Press.

Maguire, E. A., Burgess, N., Donnett, J. G., Frackowiak, R. S., Frith, C. D., and O'Keefe, J. (1998). Knowing where and getting there: a human navigation network. *Science*, 280(5365):921–4.

Maldjian, J. A., Laurienti, P. J., Kraft, R. A., and Burdette, J. H. (2003). An automated method for neuroanatomic and cytoarchitectonic atlas-based interrogation of fmri data sets. *Neuroimage*, 19(3):1233–9.

Malikovic, A., Amunts, K., Schleicher, A., Mohlberg, H., Eickhoff, S. B., Wilms, M., Palomero-Gallagher, N., Armstrong, E., and Zilles, K. (2007). Cytoarchitectonic analysis of the human extrastriate cortex in the region of v5/mt+: a probabilistic, stereotaxic map of area hoc5. *Cereb Cortex*, 17(3):562–74.

Marcus, D. S., Fotenos, A. F., Csernansky, J. G., Morris, J. C., and Buckner, R. L. (2010). Open access series of imaging studies: longitudinal mri data in nondemented and demented older adults. *J Cogn Neurosci*, 22(12):2677–84.

Margulies, D. S., Vincent, J. L., Kelly, C., Lohmann, G., Uddin, L. Q., Biswal, B. B., Villringer, A., Castellanos, F. X., Milham, M. P., and Petrides, M. (2009). Precuneus shares intrinsic functional architecture in humans and monkeys. *Proc Natl Acad Sci U S A*, 106(47):20069–74.

Maxwell, S. E. and Cole, D. A. (2007). Bias in cross-sectional analyses of longitudinal mediation. *Psychol Methods*, 12(1):23–44.

Maxwell, S. E., Cole, D. A., and Mitchell, M. A. (2011). Bias in cross-sectional analysis of longitudinal mediation: Partial and complete mediation under an autoregressive model. *Multivariate Behavioral Research*, 46:1–26.

McArdle, J. J. (2009). Latent variable modeling of differences and changes with longitudinal data. *Annual review of psychology*, 60:577–605.

McDaniel, M. A. (2005). Big-brained people are smarter: a meta-analysis of the relationship between in vivo brain volume and intelligence. *Intelligence*, 33:337–346.

McDonald, C. R., McEvoy, L. K., Gharapetian, L., Fennema-Notestine, C., Hagler, Jr, D. J., Holland, D., Koyama, A., Brewer, J. B., Dale, A. M., and Alzheimer's Disease Neuroimaging Initiative (2009). Regional rates of neocortical atrophy from normal aging to early alzheimer disease. *Neurology*, 73(6):457–65.

McEvoy, L. K., Fennema-Notestine, C., Roddey, J. C., Hagler, Jr, D. J., Holland, D., Karow, D. S., Pung, C. J., Brewer, J. B., Dale, A. M., and Alzheimer's Disease Neuroimaging Initiative (2009). Alzheimer disease: quantitative structural neuroimaging for detection and prediction of clinical and structural changes in mild cognitive impairment. *Radiology*, 251(1):195–205.

McIntosh, A. R., Bookstein, F. L., Haxby, J. V., and Grady, C. L. (1996). Spatial pattern analysis of functional brain images using partial least squares. *Neuroimage*, 3(3 Pt 1):143–57.

McIntosh, A. R., Chau, W. K., and Protzner, A. B. (2004). Spatiotemporal analysis of event-related fmri data using partial least squares. *Neuroimage*, 23(2):764–75.

McIntosh, A. R. and Lobaugh, N. J. (2004). Partial least squares analysis of neuroimaging data: applications and advances. *Neuroimage*, 23 Suppl 1:S250–63.

Mendes, M., Silva, F., Simões, L., Jorge, M., Saraiva, J., and Castelo-Branco, M. (2005). Visual magnocellular and structure from motion perceptual deficits in a neurodevelopmental model of dorsal stream function. *Brain research Cognitive brain research*, 25(3):788–98.

Mietchen, D. and Gaser, C. (2009). Computational morphometry for detecting changes in brain structure due to development, aging, learning, disease and evolution. *Front Neuroinform*, 3:25.

Milan, L. and Whittaker, J. (1995). Applications of the parameteric bootstrap to models that incorporate a singular value decomposition. *Journal of the Royal Statistical Society. Series C (Applied Statistics)*, 44(1):31–49.

Misaki, M., Wallace, G. L., Dankner, N., Martin, A., and Bandettini, P. A. (2012). Characteristic cortical thickness patterns in adolescents with autism spectrum disorders: Interactions with age and intellectual ability revealed by canonical correlation analysis. *NeuroImage*, 60(3):1890–1901.

Misra, C., Fan, Y., and Davatzikos, C. (2009). Baseline and longitudinal patterns of brain atrophy in mci patients, and their use in prediction of short-term conversion to ad: results from adni. *Neuroimage*, 44(4):1415–22.

Mitchell, D. J. and Cusack, R. (2008). Flexible, capacity-limited activity of posterior parietal cortex in perceptual as well as visual short-term memory tasks. *Cereb Cortex*, 18(8):1788–98.

Monti, M. M. (2011). Statistical analysis of fmri time-series: A critical review of the glm approach. *Front Hum Neurosci*, 5:28.

Mora, F., Segovia, G., and del Arco, A. (2007). Aging, plasticity and environmental enrichment: structural changes and neurotransmitter dynamics in several areas of the brain. *Brain research reviews*, 55(1):78–88.

Morosan, P., Rademacher, J., Schleicher, A., Amunts, K., Schormann, T., and Zilles, K. (2001). Human primary auditory cortex: cytoarchitectonic subdivisions and mapping into a spatial reference system. *Neuroimage*, 13(4):684–701.

Mosconi, L., Brys, M., Glodzik-Sobanska, L., De Santi, S., Rusinek, H., and de Leon, M. J. (2007). Early detection of alzheimer's disease using neuroimaging. *Exp Gerontol*, 42(1-2):129–38.

Murphy, E. A., Holland, D., Donohue, M., McEvoy, L. K., Hagler, D. J., Dale, A. M., Brewer, J. B., and Initiative, A. D. N. (2010). Six-month atrophy in mtl structures is associated with subsequent memory decline in elderly controls. *Neuroimage*, 53(4):1310–7.

Murray, A. D., Staff, R. T., McNeil, C. J., Salarirad, S., Ahearn, T. S., Mustafa, N., and Whalley, L. J. (2011). The balance between cognitive reserve and brain imaging biomarkers of cerebrovascular and alzheimer's diseases. *Brain*, 134(Pt 12):3687–96.

Mustafa, N., Ahearn, T. S., Waiter, G. D., Murray, A. D., Whalley, L. J., and Staff, R. T. (2012). Brain structural complexity and life course cognitive change. *Neuroimage*, 61(3):694–701.

Narr, K. L., Woods, R. P., Thompson, P. M., Szeszko, P., Robinson, D., Dimtcheva, T., Gurbani, M., Toga, A. W., and Bilder, R. M. (2007). Relationships between iq and regional cortical gray matter thickness in healthy adults. *Cereb Cortex*, 17(9):2163–71.

Nosarti, C., Mechelli, A., Herrera, A., Walshe, M., Shergill, S. S., Murray, R. M., Rifkin, L., and Allin, M. P. G. (2011). Structural covariance in the cortex of very preterm adolescents: a voxel-based morphometry study. *Hum Brain Mapp*, 32(10):1615–25.

Østby, Y., Tamnes, C. K., Fjell, A. M., and Walhovd, K. B. (2011). Morphometry and connectivity of the fronto-parietal verbal working memory network in development. *Neuropsychologia*, 49(14):3854–62.

Østby, Y., Tamnes, C. K., Fjell, A. M., and Walhovd, K. B. (2012). Dissociating memory processes in the developing brain: the role of hippocampal volume and cortical thickness in recall after minutes versus days. *Cereb Cortex*, 22(2):381–90.

Ostby, Y., Tamnes, C. K., Fjell, A. M., Westlye, L. T., Due-Tønnessen, P., and Walhovd, K. B. (2009). Heterogeneity in subcortical brain development: A structural magnetic resonance imaging study of brain maturation from 8 to 30 years. *J Neurosci*, 29(38):11772–82.

Oulhaj, A., Refsum, H., Beaumont, H., Williams, J., King, E., Jacoby, R., and Smith, A. D. (2010). Homocysteine as a predictor of cognitive decline in alzheimer's disease. *International journal of geriatric psychiatry*, 25(1):82–90.

Pangelinan, M. M., Zhang, G., VanMeter, J. W., Clark, J. E., Hatfield, B. D., and Haufler, A. J. (2011). Beyond age and gender: relationships between cortical and subcortical brain volume and cognitive-motor abilities in school-age children. *Neuroimage*, 54(4):3093–100.

Park, D. C., Polk, T. A., Park, R., Minear, M., Savage, A., and Smith, M. R. (2004). Aging reduces neural specialization in ventral visual cortex. *Proc Natl Acad Sci U S A*, 101(35):13091–5.

Peelle, J. E., Cusack, R., and Henson, R. N. A. (2012). Adjusting for global effects in voxel-based morphometry: Gray matter decline in normal aging. *Neuroimage*, 60(2):1503–16.

Penke, L. and Deary, I. J. (2010). Some guidelines for structural equation modelling in cognitive neuroscience: the case of charlton et al.'s study on white matter integrity and cognitive ageing. *Neurobiology of aging*, 31(9):1656–1666.

Penke, L., Hernandéz, M. C. V., Maniega, S. M., Gow, A. J., Murray, C., Starr, J. M., Bastin, M. E., Deary, I. J., and Wardlaw, J. M. (2010a). Brain iron deposits are associated with general cognitive ability and cognitive aging. *Neurobiology of aging*.

Penke, L., Maniega, S. M., Murray, C., Gow, A. J., Hernández, M. C. V., Clayden, J. D., Starr, J. M., Wardlaw, J. M., Bastin, M. E., and Deary, I. J. (2010b). A general factor of brain white matter integrity predicts information processing speed in healthy older people. *J Neurosci*, 30(22):7569–74.

Penny, W., Flandin, G., and Trujillo-Barreto, N. (2007). Bayesian comparison of spatially regularised general linear models. *HBM*, 28(4):275–93.

Penny, W. D., Trujillo-Barreto, N. J., and Friston, K. J. (2005). Bayesian fmri time series analysis with spatial priors. *Neuroimage*, 24(2):350–62.

Pereira, A. C., Huddleston, D. E., Brickman, A. M., Sosunov, A. A., Hen, R., McKhann, G. M., Sloan, R., Gage, F. H., Brown, T. R., and Small, S. A. (2007). An in vivo correlate of exercise-induced neurogenesis in the adult dentate gyrus. *Proc Natl Acad Sci U S A*, 104(13):5638–43.

Peters, A., Morrison, J. H., Rosene, D. L., and Hyman, B. T. (1998). Feature article: are neurons lost from the primate cerebral cortex during normal aging? *Cereb Cortex*, 8(4):295–300.

Petten, C. V. (2004). Relationship between hippocampal volume and memory ability in healthy individuals across the lifespan: review and meta-analysis. *Neuropsychologia*, 42(10):1394–413.

Pinheiro, J. C. and Bates, D. M. (2000). *Mixed-Effects Models in S and S-PLUS*. New York: Springer.

Porter, J. N., Collins, P. F., Muetzel, R. L., Lim, K. O., and Luciana, M. (2011). Associations between cortical thickness and verbal fluency in childhood, adolescence, and young adulthood. *Neuroimage*, 55(4):1865–77.

Quartz, S. R. and Sejnowski, T. J. (1997). The neural basis of cognitive development: a constructivist manifesto. *Behav Brain Sci*, 20(4):537–96.

Rajapakse, J. C., Giedd, J. N., and Rapoport, J. L. (1997). Statistical approach to segmentation of single-channel cerebral mr images. *IEEE Trans Med Imaging*, 16(2):176–86.

Ramsden, S., Richardson, F. M., Josse, G., Thomas, M. S. C., Ellis, C., Shakeshaft, C., Seghier, M. L., and Price, C. J. (2011). Verbal and non-verbal intelligence changes in the teenage brain. *Nature*, 479(7371):113–6.

Rasmussen, C. E. and Williams, C. K. I. (2006). *Gaussian processes for machine learning*. MIT Press.

Raudenbush, S. W. and Bryk, A. S. (2002). *Hierarchical Linear Models: Applications and Data Analysis Methods*. Newbury Par: Sage, 2nd edition.

Raz, N., Ghisletta, P., Rodrigue, K. M., Kennedy, K. M., and Lindenberger, U. (2010). Trajectories of brain aging in middle-aged and older adults: regional and individual differences. *Neuroimage*, 51(2):501–11.

Raz, N., Gunning-Dixon, F., Head, D., Rodrigue, K. M., Williamson, A., and Acker, J. D. (2004a). Aging, sexual dimorphism, and hemispheric asymmetry of the cerebral cortex: replicability of regional differences in volume. *Neurobiology of aging*, 25(3):377–96.

Raz, N. and Kennedy, K. M. (2009). A systems approach to age-related change: neuroanatomical changes, their modifiers and cognitive correlates. In Jagust, W. J. and D'Esposito, M., editors, *Imaging the Aging Brain*, pages 43–70. New York: Oxford University Press.

Raz, N. and Lindenberger, U. (2011). Only time will tell: Cross-sectional studies offer no solution to the age-brain-cognition triangle: Comment on salthouse (2011). *Psychol Bull*, 137(5):790–5.

Raz, N., Lindenberger, U., Ghisletta, P., Rodrigue, K. M., Kennedy, K. M., and Acker, J. D. (2008). Neuroanatomical correlates of fluid intelligence in healthy adults and persons with vascular risk factors. *Cereb Cortex*, 18(3):718–26.

Raz, N., Lindenberger, U., Rodrigue, K. M., Kennedy, K. M., Head, D., Williamson, A., Dahle, C., Gerstorf, D., and Acker, J. D. (2005). Regional brain changes in aging healthy adults: general trends, individual differences and modifiers. *Cereb Cortex*, 15(11):1676–89.

Raz, N. and Rodrigue, K. M. (2006). Differential aging of the brain: patterns, cognitive correlates and modifiers. *Neuroscience and biobehavioral reviews*, 30(6):730–48.

Raz, N., Rodrigue, K. M., and Haacke, E. M. (2007). Brain aging and its modifiers: insights from in vivo neuromorphometry and susceptibility weighted imaging. *Ann N Y Acad Sci*, 1097:84–93.

Raz, N., Rodrigue, K. M., Head, D., Kennedy, K. M., and Acker, J. D. (2004b). Differential aging of the medial temporal lobe: a study of a five-year change. *Neurology*, 62(3):433–8.

Raz, N., Rodrigue, K. M., Kennedy, K. M., Head, D., Gunning-Dixon, F., and Acker, J. D. (2003). Differential aging of the human striatum: longitudinal evidence. *AJNR American journal of neuroradiology*, 24(9):1849–56.

Raznahan, A., Shaw, P., Lalonde, F., Stockman, M., Wallace, G. L., Greenstein, D., Clasen, L., Gogtay, N., and Giedd, J. N. (2011). How does your cortex grow? *J Neurosci*, 31(19):7174–7.

Resnick, S. M., Pham, D. L., Kraut, M. A., Zonderman, A. B., and Davatzikos, C. (2003). Longitudinal magnetic resonance imaging studies of older adults: a shrinking brain. *J Neurosci*, 23(8):3295–301.

Rettmann, M. E., Kraut, M. A., Prince, J. L., and Resnick, S. M. (2006). Cross-sectional and longitudinal analyses of anatomical sulcal changes associated with aging. *Cereb Cortex*, 16(11):1584–94.

Reuben, A., Brickman, A. M., Muraskin, J., Steffener, J., and Stern, Y. (2011). Hippocampal atrophy relates to fluid intelligence decline in the elderly. *J Int Neuropsychol Soc*, 17(1):56–61.

Reuter, M. and Fischl, B. (2011). Avoiding asymmetry-induced bias in longitudinal image processing. *Neuroimage*, 57(1):19–21.

Reuter, M., Rosas, H. D., and Fischl, B. (2010). Highly accurate inverse consistent registration: a robust approach. *Neuroimage*, 53(4):1181–96.

Rodrigue, K. M., Daugherty, A. M., Haacke, E. M., and Raz, N. (2012). The role of hippocampal iron concentration and hippocampal volume in age-related differences in memory. *Cereb Cortex*, 23(7):1533–41.

Rodrigue, K. M., Haacke, E. M., and Raz, N. (2011). Differential effects of age and history of hypertension on regional brain volumes and iron. *Neuroimage*, 54(2):750–9.

Rombouts, S. A. R. B., Scheltens, P., Kuijer, J. P. A., and Barkhof, F. (2007). Whole brain analysis of t2* weighted baseline fmri signal in dementia. *Hum Brain Mapp*, 28(12):1313–7.

Rosidi, N. L., Zhou, J., Pattanaik, S., Wang, P., Jin, W., Brophy, M., Olbricht, W. L., Nishimura, N., and Schaffer, C. B. (2011). Cortical microhemorrhages cause local inflammation but do not trigger widespread dendrite degeneration. *PLoS One*, 6(10):e26612.

Rosipal, R. (2001). Kernel partial least squares regression in reproducing kernel hilbert space. *Journal of Machine Learning Research*, 2:97–123.

Rosipal, R. (2003). Kernel partial least squares for nonlinear regression and discrimination. *Neural Network World*, 13(3):291–300.

Rosipal R, Krämer, N. (2006). Overview and recent advances in parital least squares. In Saunders, C., Grobelnik, M., Gunn, S., and Shawe-Taylor, J., editors, *Subspace, Latent Structure and Feature Selection Techniques*. Springer.

Rottschy, C., Eickhoff, S. B., Schleicher, A., Mohlberg, H., Kujovic, M., Zilles, K., and Amunts, K. (2007). Ventral visual cortex in humans: cytoarchitectonic mapping of two extrastriate areas. *Human brain mapping*, 28(10):1045–59.

Rushton, J. P. and Ankney, C. D. (2009). Whole brain size and general mental ability: a review. *Int J Neurosci*, 119(5):691–731.

Salarirad, S., Staff, R. T., Fox, H. C., Deary, I. J., Whalley, L., and Murray, A. D. (2011). Childhood intelligence and brain white matter hyperintensities predict fluid intelligence age 78-81 years: a 1921 aberdeen birth cohort study. *Age Ageing*, 40(5):562–7.

Salat, D. H., Buckner, R. L., Snyder, A. Z., Greve, D. N., Desikan, R. S. R., Busa, E., Morris, J. C., Dale, A. M., and Fischl, B. (2004). Thinning of the cerebral cortex in aging. *Cereb Cortex*, 14(7):721–30.

Salat, D. H., Chen, J. J., van der Kouwe, A. J., Greve, D. N., Fischl, B., and Rosas, H. D. (2011). Hippocampal degeneration is associated with temporal and limbic gray matter/white matter tissue contrast in alzheimer's disease. *Neuroimage*, 54(3):1795–802.

Salat, D. H., Lee, S. Y., van der Kouwe, A. J., Greve, D. N., Fischl, B., and Rosas, H. D. (2009). Age-associated alterations in cortical gray and white matter signal intensity and gray to white matter contrast. *Neuroimage*, 48(1):21–8.

Salmond, C. H., Ashburner, J., Vargha-Khadem, F., Connelly, A., Gadian, D. G., and Friston, K. J. (2002). Distributional assumptions in voxel-based morphometry. *Neuroimage*, 17(2):1027–30.

Salthouse, T. A. (2011a). All data collection and analysis methods have limitations: Reply to rabbitt (2011) and raz and lindenberger (2011). *Psychol Bull*, 137(5):796–9.

Salthouse, T. A. (2011b). Cognitive correlates of cross-sectional differences and longitudinal changes in trail making performance. *J Clin Exp Neuropsychol*, 33(2):242–8.

Salthouse, T. A. (2011c). Neuroanatomical substrates of age-related cognitive decline. *Psychol Bull*, 137(5):753–84.

Salthouse, T. A., Atkinson, T. M., and Berish, D. E. (2003). Executive functioning as a potential mediator of age-related cognitive decline in normal adults. *J Exp Psychol Gen*, 132(4):566–94.

Scahill, R. I., Frost, C., Jenkins, R., Whitwell, J. L., Rossor, M. N., and Fox, N. C. (2003). A longitudinal study of brain volume changes in normal aging using serial registered magnetic resonance imaging. *Arch Neurol*, 60(7):989–94.

Scheperjans, F., Eickhoff, S. B., Hömke, L., Mohlberg, H., Hermann, K., Amunts, K., and Zilles, K. (2008). Probabilistic maps, morphometry, and variability of cytoarchitectonic areas in the human superior parietal cortex. *Cereb Cortex*, 18(9):2141–57.

Schmid, V. J., Whitcher, B., Padhani, A. R., Taylor, N. J., and Yang, G.-Z. (2009). A bayesian hierarchical model for the analysis of a longitudinal dynamic contrast-enhanced mri oncology study. *Magnetic resonance in medicine : official journal of the Society of Magnetic Resonance in Medicine / Society of Magnetic Resonance in Medicine*, 61(1):163–74.

Schmidt, R., Ropele, S., Enzinger, C., Petrovic, K., Smith, S., Schmidt, H., Matthews, P. M., and Fazekas, F. (2005). White matter lesion progression, brain atrophy, and cognitive decline: the austrian stroke prevention study. *Annals of neurology*, 58(4):610–6.

Schmithorst, V. J. (2009). Developmental sex differences in the relation of neuroanatomical connectivity to intelligence. *Intelligence*, 37(2):164–173.

Schnack, H. G., van Haren, N. E. M., Brouwer, R. M., van Baal, G. C. M., Picchioni, M., Weisbrod, M., Sauer, H., Cannon, T. D., Huttunen, M., Lepage, C., Collins, D. L., Evans, A. C., Murray, R. M., Kahn, R. S., and Pol, H. E. H. (2010). Mapping reliability in multicenter mri: voxel-based morphometry and cortical thickness. *Human brain mapping*, 31(12):1967–82.

Schölkopf, B. and Smola, A. J. (2002). *Learning with Kernels: Support Vector Machines, Regularization, Optimization, and Beyond*. MIT Press.

Scholz, J., Klein, M. C., Behrens, T. E. J., and Johansen-Berg, H. (2009). Training induces changes in white-matter architecture. *Nat Neurosci*, 12(11):1370–1.

Schretlen, D., Pearlson, G. D., Anthony, J. C., Aylward, E. H., Augustine, A. M., Davis, A., and Barta, P. (2000). Elucidating the contributions of processing speed, executive ability, and frontal lobe volume to normal age-related differences in fluid intelligence. *J Int Neuropsychol Soc*, 6(1):52–61.

Schumann, C. M., Hamstra, J., Goodlin-Jones, B. L., Kwon, H., Reiss, A. L., and Amaral, D. G. (2007). Hippocampal size positively correlates with verbal iq in male children. *Hippocampus*, 17(6):486–93.

Seber, G. A. F. (2007). *A Matrix Handbook for Statisticians*. Wiley-Interscience.

Shaw, L. M. (2008). Penn biomarker core of the alzheimer's disease neuroimaging initiative. *Neurosignals*, 16(1):19–23.

Shaw, P., Greenstein, D., Lerch, J. P., Clasen, L., Lenroot, R., Gogtay, N., Evans, A. C., Rapoport, J., and Giedd, J. N. (2006). Intellectual ability and cortical development in children and adolescents. *Nature*, 440(7084):676–9.

Shawe-Taylor, J. and Cristianini, N. (2004). *Kernel methods for pattern analysis*. Cambridge University Press.

Shelton, J. T., Elliott, E. M., Hill, B. D., Calamia, M. R., and Gouvier, W. D. (2009). A comparison of laboratory and clinical working memory tests and their prediction of fluid intelligence. *Intelligence*, 37(3):283.

Shrout, P. E. and Bolger, N. (2002). Mediation in experimental and nonexperimental studies: new procedures and recommendations. *Psychol Methods*, 7(4):422–45.

Silverman, B. W. (1985). Some aspects of the spline smoothing approach to nonparametric regression curve fitting. *J. Roy. Statist. Soc. Ser. B*, 47(1):1–52.

Simić, G., Kostović, I., Winblad, B., and Bogdanović, N. (1997). Volume and number of neurons of the human hippocampal formation in normal aging and alzheimer's disease. *J Comp Neurol*, 379(4):482–94.

Singer, J. D. and Willett, J. B. (2003). *Applied longitudinal data analysis: modeling change and event occurrence*. Oxford University Press.

Sled, J. G., Zijdenbos, A. P., and Evans, A. C. (1998). A nonparametric method for automatic correction of intensity nonuniformity in mri data. *IEEE Trans Med Imaging*, 17(1):87–97.

Smith, C., Chebrolu, H., Wekstein, D., and Schmitt, F. (2007). Age and gender effects on human brain anatomy: a voxel-based morphometric study in healthy elderly. *Neurobiology of aging*, 28(7):1075–1087.

Smith, S. M. (2002). Fast robust automated brain extraction. *Hum Brain Mapp*, 17(3):143–55.

Sowell, E. R., Peterson, B. S., Kan, E., Woods, R. P., Yoshii, J., Bansal, R., Xu, D., Zhu, H., Thompson, P. M., and Toga, A. W. (2007). Sex differences in cortical thickness mapped in 176 healthy individuals between 7 and 87 years of age. *Cereb Cortex*, 17(7):1550–60.

Sowell, E. R., Thompson, P. M., and Toga, A. W. (2004). Mapping changes in the human cortex throughout the span of life. *The Neuroscientist : a review journal bringing neurobiology, neurology and psychiatry*, 10(4):372–92.

Spearman, C. (1904). General intelligence objectively determined and measured. *Am. J. Psychol.*, 15:201–93.

Squire, L. R. (2004). Memory systems of the brain: a brief history and current perspective. *Neurobiol Learn Mem*, 82(3):171–7.

Squire, L. R. (2009). Memory and brain systems: 1969-2009. *J Neurosci*, 29(41):12711–6.

Stern, Y. (2009). Cognitive reserve. *Neuropsychologia*, 47(10):2015–28.

Sullivan, E. V., Adalsteinsson, E., Rohlfing, T., and Pfefferbaum, A. (2009). Relevance of iron deposition in deep gray matter brain structures to cognitive and motor performance in healthy elderly men and women: Exploratory findings. *Brain Imaging Behav*, 3(2):167–175.

Sullivan, E. V., Marsh, L., Mathalon, D. H., Lim, K. O., and Pfefferbaum, A. (1995). Age-related decline in mri volumes of temporal lobe gray matter but not hippocampus. *Neurobiology of aging*, 16(4):591–606.

Sullivan, E. V., Marsh, L., and Pfefferbaum, A. (2005). Preservation of hippocampal volume throughout adulthood in healthy men and women. *Neurobiol Aging*, 26(7):1093–8.

Sullivan, E. V., Rosenbloom, M., Serventi, K. L., and Pfefferbaum, A. (2004). Effects of age and sex on volumes of the thalamus, pons, and cortex. *Neurobiol Aging*, 25(2):185–92.

Taki, Y., Hashizume, H., Sassa, Y., Takeuchi, H., Asano, M., Asano, K., Kotozaki, Y., Nouchi, R., Wu, K., Fukuda, H., and Kawashima, R. (2012). Correlation among body height, intelligence, and brain gray matter volume in healthy children. *Neuroimage*, 59(2):1023–7.

Taki, Y., Kinomura, S., Sato, K., Goto, R., Wu, K., Kawashima, R., and Fukuda, H. (2011). Correlation between baseline regional gray matter volume and global gray matter volume decline rate. *Neuroimage*, 54(2):743–9.

Tamnes, C. K., Fjell, A. M., Ostby, Y., Westlye, L. T., Due-Tønnessen, P., Bjørnerud, A., and Walhovd, K. B. (2011). The brain dynamics of intellectual development: Waxing and waning white and gray matter. *Neuropsychologia*, 49(13):3605–11.

Tamnes, C. K., Ostby, Y., Fjell, A. M., Westlye, L. T., Due-Tønnessen, P., and Walhovd, K. B. (2010a). Brain maturation in adolescence and young adulthood: regional age-related changes in cortical thickness and white matter volume and microstructure. *Cereb Cortex*, 20(3):534–48.

Tamnes, C. K., Østby, Y., Walhovd, K. B., Westlye, L. T., Due-Tønnessen, P., and Fjell, A. M. (2010b). Intellectual abilities and white matter microstructure in development: a diffusion tensor imaging study. *Hum Brain Mapp*, 31(10):1609–25.

Tamnes, C. K., Østby, Y., Walhovd, K. B., Westlye, L. T., Due-Tønnessen, P., and Fjell, A. M. (2010c). Neuroanatomical correlates of executive functions in children and adolescents: a magnetic resonance imaging (mri) study of cortical thickness. *Neuropsychologia*, 48(9):2496–508.

Tarr, M. J. and Gauthier, I. (2000). Ffa: a flexible fusiform area for subordinate-level visual processing automatized by expertise. *Nat Neurosci*, 3(8):764–9.

Tau, G. Z. and Peterson, B. S. (2010). Normal development of brain circuits. *Neuropsychopharmacology*, 35(1):147–68.

Taubert, M., Draganski, B., Anwander, A., Müller, K., Horstmann, A., Villringer, A., and Ragert, P. (2010). Dynamic properties of human brain structure: learning-related changes in cortical areas and associated fiber connections. *J Neurosci*, 30(35):11670–7.

Thambisetty, M., Wan, J., Carass, A., An, Y., Prince, J. L., and Resnick, S. M. (2010). Longitudinal changes in cortical thickness associated with normal aging. *Neuroimage*, 52(4):1215–23.

Thompson, P. M., Hayashi, K. M., De Zubicaray, G. I., Janke, A. L., Rose, S. E., Semple, J., Hong, M. S., Herman, D. H., Gravano, D., Doddrell, D. M., and Toga, A. W. (2004). Mapping hippocampal and ventricular change in alzheimer disease. *Neuroimage*, 22(4):1754–66.

Tipping, M. (2001). Sparse bayesian learning and the relevance vector machine. *The Journal of Machine Learning Research*, 1:211–244.

Todd, J. J. and Marois, R. (2004). Capacity limit of visual short-term memory in human posterior parietal cortex. *Nature*, 428(6984):751–4.

Toga, A. W. and Thompson, P. M. (2003). Temporal dynamics of brain anatomy. *Annu Rev Biomed Eng*, 5:119–45.

Tohka, J., Zijdenbos, A., and Evans, A. (2004). Fast and robust parameter estimation for statistical partial volume models in brain mri. *Neuroimage*, 23(1):84–97.

van Schouwenburg, M. R., den Ouden, H. E. M., and Cools, R. (2010). The human basal ganglia modulate frontal-posterior connectivity during attention shifting. *J Neurosci*, 30(29):9910–8.

van Schouwenburg, M. R., O'Shea, J., Mars, R. B., Rushworth, M. F. S., and Cools, R. (2012). Controlling human striatal cognitive function via the frontal cortex. *J Neurosci*, 32(16):5631–7.

Waber, D. P., De Moor, C., Forbes, P. W., Almli, C. R., Botteron, K. N., Leonard, G., Milovan, D., Paus, T., Rumsey, J., and Brain Development Cooperative Group (2007). The nih mri study of normal brain development: performance of a population based sample of healthy children aged 6 to 18 years on a neuropsychological battery. *J Int Neuropsychol Soc*, 13(5):729–46.

Wahba, G. (1990). *Spline models for observational data*, volume 59. SIAM.

Walhovd, K. B., Fjell, A. M., Reinvang, I., Lundervold, A., Dale, A. M., Eilertsen, D. E., Quinn, B. T., Salat, D., Makris, N., and Fischl, B. (2005a). Effects of age on volumes of cortex, white matter and subcortical structures. *Neurobiology of aging*, 26(9):1261–70; discussion 1275–8.

Walhovd, K. B., Fjell, A. M., Reinvang, I., Lundervold, A., Dale, A. M., Quinn, B. T., Salat, D., Makris, N., and Fischl, B. (2005b). Neuroanatomical aging: Universal but not uniform. *Neurobiology of Aging*, 26(9):1279–1282.

Walhovd, K. B., Westlye, L. T., Amlien, I., Espeseth, T., Reinvang, I., Raz, N., Agartz, I., Salat, D. H., Greve, D. N., Fischl, B., et al. (2011). Consistent neuroanatomical age-related volume differences across multiple samples. *Neurobiology of aging*, 32(5):916–932.

Wechsler, D. (1991). *Wechsler Intelligence Scale for Children*. New York: Psychological Corporation, 3rd edition.

Wechsler, D. (1997). *Wechsler Adult Intelligence Scale*. San Antonio, TX: The Psychological Corporation.

Wechsler, D. (1999). *Wechsler Abbreviated Scale of Intelligence*. New York: Psychological Corporation.

Wegelin, J. A. (2000). A survey of partial least squares (pls) methods, with emphasis on the two-block case. Technical report, Department of Statistics, University of Washington.

West, M. J., Coleman, P. D., Flood, D. G., and Troncoso, J. C. (1994). Differences in the pattern of hippocampal neuronal loss in normal ageing and alzheimer's disease. *Lancet*, 344(8925):769–72.

Westlye, L. T., Grydeland, H., Walhovd, K. B., and Fjell, A. M. (2011). Associations between regional cortical thickness and attentional networks as measured by the attention network test. *Cerebral Cortex*, 21(2):345–356.

Westlye, L. T., Walhovd, K. B., Dale, A. M., Bjørnerud, A., Due-Tønnessen, P., Engvig, A., Grydeland, H., Tamnes, C. K., Østby, Y., and Fjell, A. M. (2010). Differentiating maturational and aging-related changes of the cerebral cortex by use of thickness and signal intensity. *Neuroimage*, 52(1):172–85.

Westman, E., Cavallin, L., Muehlboeck, J.-S., Zhang, Y., Mecocci, P., Vellas, B., Tsolaki, M., Kłoszewska, I., Soininen, H., Spenger, C., Lovestone, S., Simmons, A., Wahlund, L.-O., and AddNeuroMed consortium (2011). Sensitivity and specificity of medial temporal lobe visual ratings and multivariate regional mri classification in alzheimer's disease. *PLoS One*, 6(7):e22506.

Wilke, M., Holland, S. K., Altaye, M., and Gaser, C. (2008). Template-o-matic: a toolbox for creating customized pediatric templates. *Neuroimage*, 41(3):903–13.

Wilke, M., Sohn, J.-H., Byars, A. W., and Holland, S. K. (2003). Bright spots: correlations of gray matter volume with iq in a normal pediatric population. *Neuroimage*, 20(1):202–15.

Willet, J. B. (1998). Some results on reliability for the longitudinal measurement of change: Implications for the design of studies of individual growth. *Educational and Psychological Measurement*, 49(3):587–602.

Wold, H. (1975). Path models with latent variables: the nipals approach. In Blalock, H. M., editor, *Quantitative sociology: international perspectives on mathematical and statistical modeling.*, pages 307–357. Academic.

Wold, H. (1982). Soft modeling: the basic design and some extensions. In Jöreskog, K. G., editor, *Systems under indirect observation: causality, structure, prediction, Part II*. Amsterdam: North Holland Publishing Company.

Worsley, K. J., Poline, J.-B., Friston, K. J., and Evans, A. (1997). Characterizing the response of pet and fmri data using multivariate linear models. *NeuroImage*, 6(4):305–319.

Zecca, L., Youdim, M. B. H., Riederer, P., Connor, J. R., and Crichton, R. R. (2004). Iron, brain ageing and neurodegenerative disorders. *Nat Rev Neurosci*, 5(11):863–73.

Ziegler, G., Dahnke, R., Gaser, C., and Alzheimer's Disease Neuroimaging Initiative (2012a). Models of the aging brain structure and individual decline. *Front Neuroinform*, 6:3.

Ziegler, G., Dahnke, R., Jäncke, L., Yotter, R. A., May, A., and Gaser, C. (2012b). Brain structural trajectories over the adult lifespan. *Hum Brain Mapp*, 33(10):2377–89.

Ziegler, G., Dahnke, R., Winkler, A., and Gaser, C. (2013). Partial least squares correlation of multivariate cognitive abilities and local brain structure in children and adolescents. *NeuroImage*, 82:284–294.

Curriculum Vitae

Gabriel Ziegler

Education

PhD Student Exam Psychology, University of Zürich, October, 2012, Thesis: *Lifespan Brain Structural Trajectories and Individual Differences of Growth and Decline*, "summa cum laude"

B.S. Mathematics, University of Jena, 2011, Thesis: *Phase Information and Independent Component Analysis*, "very good".

Diploma Degree Psychology, University of Jena, 2007, "excellent with distinction"

PreDiploma Degree Physics, University of Jena, 2001, "very good".

Employment

Additional affiliation to the Translational Imaging Group at the *Center of Medical Image Computing*, University College London, UK.

PostDoc researcher in the Computational Anatomy and Genetics Group (John Ashburner) and SPM Methods Group (Karl Friston), Wellcome Trust Centre for Neuroimaging, Institute of Neurology, University College London, April 2013 – present

PostDoc researcher in Structural Brain Mapping Group (C. Gaser), Department of Psychiatry, Jena University Hospital, November 2012 – March 2013.

PhD Student in Structural Brain Mapping Group (C. Gaser), Department of Psychiatry, Jena University Hospital, September 2008 – September 2012.

Research Assistant, Autonomic Function Group (K.-J. Baer), Department of Psychiatry, Jena University Hospital, April 2007 – September 2008.

Fields of Research Interest

Lifespan brain development and aging

Analysis of individual differences of brain morphology

Multivariate modelling of brain-behavior relationships

Mixed-effects modelling of developmental trajectories

Encoding and decoding models of age

Multivariate analysis and Gaussian processes in neuroimaging

Bayesian inference and hierarchical models

Research

Working Papers

G. Ziegler, W. Penny, G. Ridgway, S. Ourselin, K. Friston, Estimation of Individual Structural Trajectories using Bayesian Mixed-Effects Modelling, (submitted).

G. Ziegler, G. R. Ridgway, R. Dahnke, C. Gaser (2014). Individualized Gaussian process-based prediction and detection of local and global gray matter abnormalities in elderly subjects, *Neuroimage*, http://dx.doi.org/10.1016/j.neuroimage.2014.04.018, (in press).

G. Ziegler, R. Dahnke, C. Gaser (2013). Partial Least Squares Correlation of Multivariate Cognitive Abilities and Local Brain Morphology in Children and Adolescents, *Neuroimage*, 82, 284-294

G. Ziegler, R. Dahnke, C. Gaser (2012). Models of the Aging Brain Structure and Individual Decline, *Frontiers in Neuroinformatics*, 6, pp 3.

G. Ziegler, R. Dahnke, L. Jaencke, R. A. Yotter, A. May, C. Gaser (2012). Brain Structural Trajectories over the Adult Lifespan, *Human Brain Mapping*, 33, 2377-2389.

R. A. Yotter, I. Nenadic, G. Ziegler, P. M. Thompson, C. Gaser (2011). Local cortical surface complexity maps from spherical harmonic reconstructions, *Neuroimage*, 56 (3), 961-73.

K. Franke, G. Ziegler, S. Kloeppel, C. Gaser (2010). Estimating the age of healthy subjects from T1-weighted MRI scans using kernel methods: exploring the influence of various parameters, *Neuroimage*, 50 (3), 883-92.

G. Ziegler, R. Dahnke, V. K. Yeragani, K. J. Baer (2009). The relation of ventromedial prefrontal cortex activity and heart rate fluctuations at rest, *Eur J Neurosci*, 30 (11), 2205-10.

Talks, Conferences, Symposia, and Workshops

Attendance to the "MPS-UCL Symposium and Advanced Course on Computational Psychiatry and Ageing Research", September, 2014, Ringberg Castle, Germany.

Attendance to the Workshop on "Development of Brain Image Banks and Age-Specific Normative Human Brain Atlases", August, 2014, Royal Society of Edinburgh, UK.

Poster presentation "Gaussian-Process based Model for Individual Rates of Local Atrophy in Aging and Dementia", June, 2014, *OHBM Annual Meeting*, Hamburg, Germany.

Invited Speaker about "Estimation of Individual Structural Trajectories using Bayesian Mixed-Effects Modelling and Serial MRI", May, 2014, *Translational Imaging Group at the Center of Medical Image Computing*, University College London, UK.

Attendance to the "Pronto Course on Pattern Recognition for Neuroimaging", May, 2013, *Machine Learning and Neuroimaging Lab*, Computer Science Department, University College London, UK.

Invited Speaker about the "Lifespan Structural Trajectories and Individual Differences of Growth and Decline", December, 2012, *Max Planck Institute for Human Development*, Berlin, Germany.

Invited Speaker about "Structural Trajectories Models and Individual Differences of Growth and Decline", November, 2012, *Wellcome Trust Centre for Neuroimaging, Institute of Neurology*, University College London, UK.

Attendance to the "MPS-UCL Symposium and Advanced Course on Computational Psychiatry and Ageing Research", September, 2012, Ringberg Castle, Germany.

Attendance to the "INAPIC Fall Workshop on Longitudinal Methods to Analyze Brain-Behavior Relationships", September, 2012, University of Zürich, Switzerland.

Attendance to the Workshop on "Modern Methods for the Analysis of Change", June, 2012, *University of Zürich*, Switzerland.

Poster presentation "Gaussian Confidence Maps for Detection of Structural Alterations on the Single Subject Level", June, 2012, *OHBM Annual Meeting*, Beijing, China.

Invited Speaker about the "Individual Change Patterns in Elderly and the Structural Covariance of Decline", June, 2012, *OHBM Annual Meeting*, Beijing, China.

Invited Speaker about the "Models of Structural Brain Ageing and Variability", December, 2011, *Max Planck Institute for Human Cognitive and Brain Sciences*, Leipzig, Germany.

Poster presentation of the "Multivariate Realtion of Brain Structure and Cognitive Performance in Healthy Children", June, 2011, *OHBM Annual Meeting*, Quebec City, Canada.

Talk and Poster on "Preservation Effects and Hippocampal Increases of Grey Matter During

Healthy Adulthood", November, 2010, *DGPA Autumn School*, Oppurg, Germany.

Invited Speaker and Poster about "Preservation Effects and Hippocampal Increases of Grey Matter During Healthy Adulthood", June, 2010, *OHBM Annual Meeting*, Barcelona, Spain.

Teaching

University College London

Statistical Parametric Mapping (SPM) Short Course, Demo and Practical Sessions on Voxel-Based Morphometry, May, 2014, *Wellcome Trust Centre for Neuroimaging*, University College London, UK.

Statistical Parametric Mapping (SPM) Short Course, Voxel-Based Morphometry - Practical sessions, October, 2013, *Wellcome Trust Centre for Neuroimaging*, University College London, UK.

Statistical Parametric Mapping (SPM) Short Course, Voxel-Based Morphometry - Practical sessions, May, 2013, *Wellcome Trust Centre for Neuroimaging*, University College London, UK.

University of Jena

Special Methods of Medical Imaging Processing: Multivariate Analysis in Neuroimaging (B.S. Informatics, Computational Neuroscience), Spring 2012.

Special Methods of Medical Imaging Processing: Multivariate Analysis in Neuroimaging (B.S. Informatics, Computational Neuroscience), Spring 2011.

Special Methods of Medical Imaging Processing: Multivariate Methods and Machine Learning (B.S. Informatics, Computational Neuroscience), Spring 2010.

Professional Activities

Reviewer for *Neuroimage*

Reviewer for *Neuroimage Clinical*

Reviewer for *Human Brain Mapping*

Reviewer for *Computeres in Biology and Medicine*

Reviewer for *Archives of General Psychiatry*

Reviewer for *Journal of Intellectual Disability*

Reviewer for *Neuroinformatics*

Grant Reviewer for the CSO of Experimental and Translational Medicine Research Committee, Scotland

Awards

Trainee Abstract Travel Award at the OHBM annual meeting, 2012, Beijing.

Best Research Proposal Award at the MPS-UCL Symposium and Advanced Course on Computational Psychiatry and Ageing Research, September, 2012, Ringberg Castle, Germany.

Last updated: August 26, 2014

Selbständigkeitserklärung

Hiermit erkläre ich, dass ich die Arbeit selbstständig angefertigt und nur die angegebenen Quellen verwendet habe.

Jena, 27.9.2012